

University of Hertfordshire

School of Physics, Engineering and Computer Science

MICROPOWER GENERATION USING BUCKLING PIEZOELECTRIC ELEMENTS

Nathan Alan Counsell

Submitted to the University of Hertfordshire in partial fulfilment of the requirement of the
degree of Doctor of Philosophy

The programme of research was carried out in the School of Engineering and Computer
Science at the University of Hertfordshire

July 2020

Abstract

In recent years, piezoelectric materials and structures have gained significant attention for energy harvesting purposes. This attention can be attributed to the enhancement of low-power electronics and the high energy density of piezoelectric materials compared to other forms of energy conversion and transduction. This work explores the recent contributions to the field of piezoelectric energy harvesting, contributing two novel methods that can be implemented to improve the power output and efficiency of a single piezoelectric element.

The methods that have been investigated in this thesis are based on the buckling of piezoelectric material. The initial method examines a diaphragm preformed piezoelectric element, where numerical and simulation model has been carried out. This work has then been validated through experimentation, where empirical data has been collected verifying the COMSOL model and future optimising the manufacturing process of the diaphragm. This work contributes to a peer-reviewed paper **“Powering lights with Piezoelectric energy-harvesting floors” published in the journal Energy Technology**. This work shows that employed a diaphragm structure can increase both efficiency and power output with an increase of efficiency from 0.522% to 3.765%. The observed power output increase from 191.686 μ J to 644.16 μ J.

The second method investigates a preloaded piezoelectric curved structure with elastic walls. The use of nonlinear materials is critical to the development of a buckling structure, allowing

energy to be stored upon actuation while reducing input stresses. The result of this is a reduced buckling force, with an increased energy output and efficiency for the whole system. The findings of this work demonstrate that efficiency can be increase from 0.522% to 16.813% while achieving a greater power output from 191.686 μ J to 208.577 μ J. Furthermore, this work identifies that a monostable structure as opposed to a bi or multi-stable structure can significantly produce higher power outputs than conventional methods, whilst achieving long life within a small compact area. A COMSOL simulation of the mechanical behaviour coupled with the constitutive equations has been developed to enable future optimises to structure and design and validated using the empirical data. In additional, two equations have been developed using empirical data to aid in selection of buckling force and power output for an energy harvester. This is to enable developers of low-power electronics to select the optimised system for their application reducing the need for primary batteries within electrical devices.

This work contributes to a peer-reviewed paper **“Powering lights with piezoelectric energy-harvesting floors”** published in **Energy Technology** and one world patent **WO2020095064A1: Improvements in or relating to energy generation in a piezoelectric switch**. Published in May 2021 with a Priority date 09-11-2018.

Dedication

To those who have advised and guided me, thank you.

To my wife, Angela, thank you for putting up with the late nights, the stress and frustration. I love you dearly.

To Nancy, I would not be here without you.

Acknowledgements

With thanks to the following people who have advised and guidance throughout this project and beyond.

Associate Professor Mohammad Reza Herfatmanesh

Principal Supervisor

Professor Yong Kang Chen

Second Supervisor

This work has been made possible with the guidance and knowledge of Reza and Yong. Thank you for the time and effort that you have provided.

Thank you to the School of Physics, Engineering and Computer Science at the University of Hertfordshire for the financial support, equipment and software provided to enable this research work.

Table of Contents

Abstract	1
Dedication.....	3
Acknowledgements	4
Table of Contents	5
List of Figures	9
List of Tables	14
Nomenclature	15
Chapter 1 – Introduction	1
Summary	1
1.1 Background.....	2
1.2 Aim and Objectives.....	10
1.3 Thesis Structure.....	11
1.4 Novel contributions to knowledge.....	12
Chapter 2 – Literature Review	14
Summary	14
2.1 History of Energy Harvesting.....	15
2.2 A Brief History of Piezoelectricity.....	16

2.3 Energy Harvesting Structures Using Piezoelectric Materials	20
2.4 Unmodified Piezoelectric Energy Harvesting Structures	20
2.5 Cantilevered Piezoelectric Energy Harvesters	33
2.6 Bistable Piezoelectric Energy Harvesters	40
2.7 Mono-stable Energy Harvesters.....	47
2.8 Piezoelectric Polymer	50
2.9 Lead Zirconate Titanate.....	60
2.10 Lead-Free Ceramics	65
2.11 Electronics	66
2.12 Conclusion	75
Chapter 3 – Methodology.....	76
Summary	76
3.1 Mechanical – Buckling Introduction.....	77
3.2 Mechanical – Buckling Critical Load	79
3.3 Piezoelectricity – Introduction	89
3.4 Piezoelectricity – Important Constants and Terms.....	90
3.5 Piezoelectricity – The Poling Process	98
3.6 Piezoelectricity – Identification	99
Chapter 4 – Energy Harvesting Circuit.....	102
Summary	102

4.1 Introduction.....	103
4.2 Method.....	106
4.3 Results: Open Circuit Full Wave Bridge Rectifier	111
4.4 Results: Full Wave Bridge Rectifier and Voltage Doubler Circuit with Storage Capacitor	113
4.5 Discussion and Conclusion	117
Chapter 5 – Buckling Piezoelectric Elements	118
Summary	118
5.1 Introduction.....	119
5.2 Material identification.....	119
5.3 Manufacture.....	121
5.3.1 Preformed Piezoelectric Element.....	121
5.3.2 Preloaded Piezoelectric Element.....	125
5.4 Theoretical Calculations	128
5.4.1 Preformed Buckling Element.....	128
5.4.2 Preloaded Buckling Element.....	135
5.5 Numerical Simulation	141
5.5.1 Preformed Piezoelectric Element.....	143
5.5.2 Preloaded Piezoelectric Element.....	147
5.6 Experimental – Introduction	157
5.6.1 Preformed Piezoelectric Element.....	158
5.6.2 Preloaded Piezoelectric Element.....	163

5.7 Results	168
5.7.1 Unmodified Piezoelectric Element	168
5.7.2 Preformed Piezoelectric Element	172
5.7.3 Preloaded Piezoelectric Element	177
Chapter 6 – Conclusion.....	195
Summary	195
6.1 Concluding remarks.....	196
Chapter 7 – Recommendations	200
References	201
Appendices	233

List of Figures

Figure 1-1 Keeling curve of CO ₂ (Parts Per Million) versus time (Years) [1]	2
Figure 1-3 Global CO ₂ emissions from fuel combustion [2]	3
Figure 2-1 Industrial PVDF stretching and poling [70]	54
Figure 2-2 Langmuir-Blodgett technique [94]	56
Figure 2-3 Vibration-based hybrid energy harvester [133]	34
Figure 2-4 Hybrid energy harvester Choi et al. [134]	33
Figure 2-5 Starner's approximation of human energy [149]	21
Figure 2-6 Howells novel method of generating power from a heel strike [150]	35
Figure 2-7 Gupta and Sharma Piezoelectric energy harvesting shoe [144]	23
Figure 2-8 Xie and Cai's novel V shaped harvester [142]	36
Figure 2-9 Shape's assembled cymbal transducer [129]	25
Figure 2-10 Leg mounted piezoelectric energy harvester [37]	41
Figure 2-11 Method of reducing natural frequency [167]	39
Figure 2-12 Artery cuff energy harvester [177]	30
Figure 2-13 Energy in situ on the bovine heart [179]	31
Figure 2-14 Double- well bi-stable a) inner-well oscillations b) chaotic multi-well oscillations c) inter-well oscillations [186]	43
Figure 2-15 Cottone et al. novel bi-stable energy harvesting system [36]	44
Figure 2-16 Energy transfer in a piezoelectric energy harvester	67
Figure 2-17 One-way valve operation	69

Figure 2-18 P-N Junction Diode	70
Figure 2-19 Diode Characteristics	71
Figure 2-20 SBR structure [223]	72
Figure 3-1 First buckling mode for a perfect beam	77
Figure 3-2 Ideal column structure for a perfect beam	78
Figure 3-3 demonstration of the equation where θ is assumed to be small.	82
Figure 3-4 Perovskite structure for piezoelectric Lead Zirconate Titanate	89
Figure 3-5 A. Piezoelectric material with a compressive load applied. B. Piezoelectric material with a tensile load applied.....	90
Figure 3-6 Constant Direction Diagram by APC International Ltd [224].....	91
Figure 3-7 Relationship between Dielectric, Piezoelectric, Pyroelectric and Ferroelectric classification.....	100
Figure 4-1 Impedance vs Dissipated Power	104
Figure 4-2 Half-wave rectifier	105
Figure 4-3 Voltage Doubler	105
Figure 4-4 Full Wave Bridge Rectifier	106
Figure 4-5 MOSFET Full Wave Rectifier	106
Figure 4-6 Signal from 100 Actuations of BPB, silicon rectifier circuit	109
Figure 4-7 Average Peaks with Standard Deviation A Single Actuation of BPB, silicon rectifier circuit	110
Figure 4-8 Full Wave Rectifier Test Circuit.....	111
Figure 4-9 Voltage Doubler Test Circuit.....	111
Figure 4-10 Peak One Open Circuit.....	113
Figure 4-11 Peak 2 Open Circuit	113

Figure 4-12 Bridge and voltage doubler comparison	115
Figure 4-13 Storage Voltage	116
Figure 5-1 D33 meter by Sinocera	120
Figure 5-2 Scanning electron microscope image and material identification of brass substrate for the piezoelectric energy harvester	121
Figure 5-3 Piezoelectric transducer dimensions.....	122
Figure 5-4 Punch and die setup	125
Figure 5-5 Pre (left) and the post-forming (right) piezoelectric element.....	125
Figure 5-6 Manufacture of preloaded piezoelectric elements.....	126
Figure 5-7 Preload piezoelectric element using solid walls to create a buckled transducer. [236].....	126
Figure 5-8 a. Buckling test equipment b. The power unit (25mm by 35mm and 3mm thick)	127
Figure 5-9 Simplified diaphragm design and geometry.....	131
Figure 5-10 Diaphragm second moment of area assumption and breakdown.....	132
Figure 5-11 Buckling modes (1,2 and 3) for a perfect slender beam	135
Figure 5-12 Hinged- Hinged In-Plane loading of a shallow arch.....	138
Figure 5-13 Points and lines for the buckling piezoelectric element	144
Figure 5-14 Full revolved model of a preformed buckling element	144
Figure 5-15 Boundary conditions for the preformed piezoelectric element	146
Figure 5-16 CATIA V5 modelling of the arc with reference dimensions and controlled dimensions.....	148
Figure 5-17 Extruded quarter model, creating a complete curved arch.....	148
Figure 5-18 Imported model of buckling arc with boundary conditions applied.....	151

Figure 5-19 Demonstration of buckling force related to the stiffness of the structure. High stiffness increased the buckling force, resulted in a bi-stable system, however with silicone clamping the system is transformed into a mono-stable system.152

Figure 5-20 Mesh optimisation for buckling preloaded piezoelectric square element a. 12.5mm b. 2.5mm c. 0.625mm d. 0.4167mm155

Figure 5-21 Mesh convergence study results for a buckling beam piezoelectric energy harvester.157

Figure 5-22 Tensile machine testing equipment158

Figure 5-23 Punch and die set up on tensile machine ready for forming159

Figure 5-24 Die layout for clamping the piezoelectric element159

Figure 5-25 a. Clamped piezoelectric element b. unclamped piezoelectric element160

Figure 5-26 Punch heads used to press piezoelectric elements into monostable structures a. original punch head with a missing notch to prevent solder damage b. male and female forming cup c. two-notch symmetric punch head d. Three-notch symmetric punch head e. Sloped punch head162

Figure 5-27 Pinned-pinned initial buckling setup using a bespoke holder and point load ...164

Figure 5-28 Preloaded piezoelectric element clamping device for evaluation of curvature on structural stiffness and power output.166

Figure 5-29 Flat piezoelectric element force vs displacement169

Figure 5-30 Open circuit voltage for ten unmodified piezoelectric elements171

Figure 5-31 Linear buckling analysis of a preformed piezoelectric element.....174

Figure 5-32 Buckling force for preformed piezoelectric elements.....174

Figure 5-33 Open circuit voltage for the preformed piezoelectric elements.....176

Figure 5-34 Initial buckling force averaged over 20 elements178

Figure 5-35 Comparison of initial buckling with and without silicone walls	178
Figure 5-36 COMSOL Multiphysics results for 0.8mm arch preloaded piezoelectric element	180
Figure 5-37 Buckling stress of a 0.8mm arch height preloaded piezoelectric element	180
Figure 5-38 Simulation results compared to experimental results from COMSOL simulation of the preloaded piezoelectric element.....	182
Figure 5-39 Experimental force vs displacement data of mono-stable buckling structures with different arch heights	184
Figure 5-40 Predicted force vs displacement of preloaded piezoelectric element buckling structures with different arch heights.....	186
Figure 5-41 Plots of force vs displacement 1 st derivative for mono-stable buckling structures with different arch heights	187
Figure 5-42 Voltage output of different arch heights for a preloaded piezoelectric element	191

List of Tables

Table 2-1 DSC test procedures and associated crystalline peaks	57
Table 2-3 Review of critical peaks within PVDF	58
Table 4-1 Diode Properties	110
Table 4-2 Full-wave bridge rectifier results.	112
Table 4-3 Bridge and Doubler Results.....	114
Table 4-4 Storage Energy	116
Table 5-1 Piezoelectric Transducer Properties	123
Table 5-2 Hinged- hinged in-plane loading of a shallow arch	139
Table 5-3 Fixed-fixed in-plane loading of a shallow arch	140
Table 5-4 Energy output of the preloaded buckling piezoelectric transducer	141
Table 5-5 Preformed piezoelectric element diaphragm height and buckling behaviour.....	161
Table 5-6 Preloaded buckling piezoelectric element parameter optimisation arch height..	167
Table 5-7 Buckling and return force calculations for the preloaded buckling element with different arch heights	188
Table 5-8 Comparison of the predicted and measured buckling and return forces	189
Table 5-9 Input energy calculations for preloaded piezoelectric elements of varying arch heights.....	190
Table 5-10 Preloaded piezoelectric element voltage and energy output	192
Table 5-11 Preloaded piezoelectric element energy efficiency	193
Table 5-12 System efficiency and power output	194

Nomenclature

<u>Acronyms</u>	<u>Description</u>
AC	Alternating Current
Ag-NWs	Silver Nanowires
Bit	A Unit of Digital Information
BPE	Buckling Piezoelectric Element
BWS	Battery-Less Wireless Switch
Byte	A Unit of Digital Information
CFCs	Chlorofluorocarbons
CNT	Carbon Nanotubes
CO ₂	Carbon Dioxide
D	Electric Displacement
DC	Direct Current
DMF	Dimethylformamide
DSC	Digital Scanning Calorimeter
E	Electric Field
EPR	Extended Producer Responsibility
FTIR	Fourier Transform Infrared Spectrometer
GDP	Gross Domestic Product
GPS	Global Positioning System
GTP	Glass Transition Point
HFCs	Hydrofluorocarbons

HSEH	Heel-Strike Energy Harvesting
IR	Infrared
LED	Light Emitting Diodes
MEK	Methyl Ethyl Ketone
MgO	Magnesium Oxide
MPB	Morphotropic Phase Boundary
MPPT	Maximum Power Point Tracking
MtCO ₂ e	Million Tonnes of Carbon Dioxide Equivalent
MWCNTs	Multi-Walled Carbon Nanotubes
NTIPS	Non-Solvent Thermal Induced Phase Separation
OECD	Organisation for Economic Co-operation
P(VDF-TrFE)	Poly (vinylidene fluoride trifluoroethylene)
PDMS	Polydimethylsiloxane
PEH	Piezoelectric Energy Harvester
PFCs	Perfluorocarbons
P-N	Positively and Negatively Doped
PPV	Piezo-Photovoltaic
PVDF	Polyvinylidene Fluoride
PZT	Lead Zirconate Titanate
RF	Radio Frequency
RFID	Radio Frequency Identification
TIPS	Thermally Induced Phase Separation
UNFCCC	United Nations Framework Convention on Climate Change

UV	Ultraviolet
VIPS	Vapour Induced Phase Separation
ZnO-NWs	Zinc Oxide Nanowires
ZTO	Zirconate Titanate
α phase	A Crystalline Form in Which PVDF Crystals are Stable
β phase	A Crystalline Form in Which Piezoelectric Crystals Form in PVDF
γ phase	A Crystalline Form in Which Piezoelectric Crystals Form in PVDF
δ phase	A Crystalline Form in Which Piezoelectric Crystals Form in PVDF

<u>Symbols</u>	<u>Description</u>	<u>Units</u>
b	Breadth	m
C	Capacitance	F
CH ₄	Methane	-
d	Depth	m
d ₃₃	Piezoelectric Dielectric Coefficient	C/N
E	Young's Modulus	N/m ²
F	Force	N
H	Enthalpy	J/kg
I	Second Moment of Area	m ⁴
Joules	A Unit of Energy	J

k	Spring Constant	N/m
Kilograms	A Unit of Mass	kg
L	Unit of Length	m
M	Moment	Nm
NO _x	Nitrogen Oxides	-
q	Load	N
Q	Charge	Coulombs
R	A Unit of Resistance	Ω
SF ₆	Sulphur Hexafluoride	-
v	Deflection	m
wt%	Percentage Weight	-
Z	Impedance	Ω
ε	Permittivity	F/m
ε ₀	The permittivity of a Vacuum	F/m
ε _r	Relative Permittivity	F/m
θ	A Unit of Angular Rotation	°
π	Pi	-
ρ	Density	kg/m ³
σ	Stress	N/mm ²
ω	Angular Velocity	Rad/s
r	Radius of Gyration	m
η	The efficiency of a System	%

Chapter 1 – Introduction

Summary

This chapter consists of three sections: the first section provides a clear argument for the need for this research, through addressing the need to reduce carbon emissions and electronic waste. The second section outlines the aim and objectives of this research to ensure timely completion to the highest standard. Finally, the thesis structure will be discussed, highlighting the novel contributions that have been discovered.

1.1 Background

In the late 19th century, a Swedish chemist named Svante Arrhenius put forward the notion of climate change that is due to more significant amounts of solar energy absorbed by gases in the atmosphere, leading to increased global temperatures. However, it was not until the 1960s, where scientists identified the trend between Carbon Dioxide (CO₂) concentrations within the atmosphere and global temperatures, this data when plotted, Figure 1-1, is known as the Keeling curve [1]. The solid line depicts the average amount of CO₂ measured in the atmosphere per year.

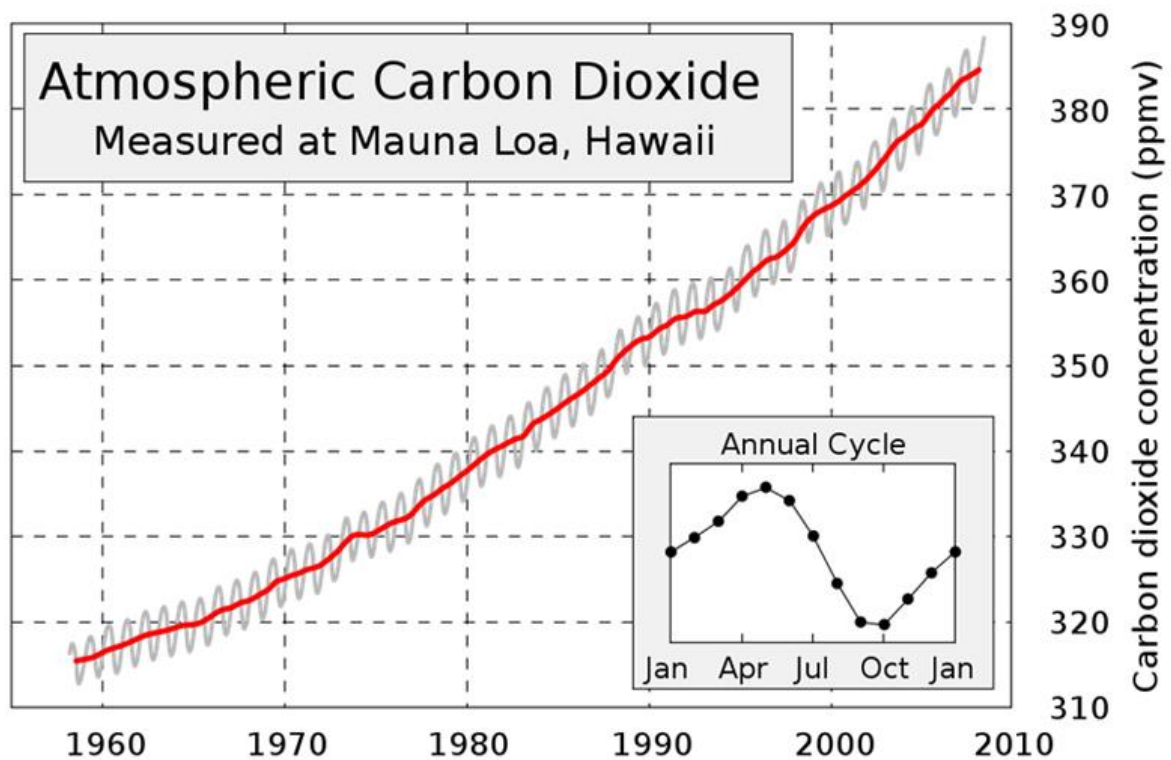


Figure 1-1 Keeling curve of CO₂ (Parts Per Million) versus time (Years) [1]

The increasing level of CO₂ within the atmosphere can be attributed to a range of factors. These include; growing population, Gross Domestic Product (GDP), and demand for energy. These factors are closely linked, with the demand for energy being increased through either population growth or increased GDP. Conversely, through an industrial revolution, the need for energy increases, resulting in more CO₂ production. However, it enables the population to grow and increase GDP, creating a knock-on effect where the increased population demands more energy and as a result, more CO₂ is produced. This effect can be observed in countries such as Brazil, India and China. Therefore, research must be performed to change how energy is generated to break this cycle and dependence on fossil fuels. Figure 1-2 demonstrates the amount of CO₂ emitted by Organisation for Economic Co-operation and Development (OECD) countries, Non-OECD countries and the combined global emissions. The results show that non-OECD nations currently produce over 61% of the world's CO₂.

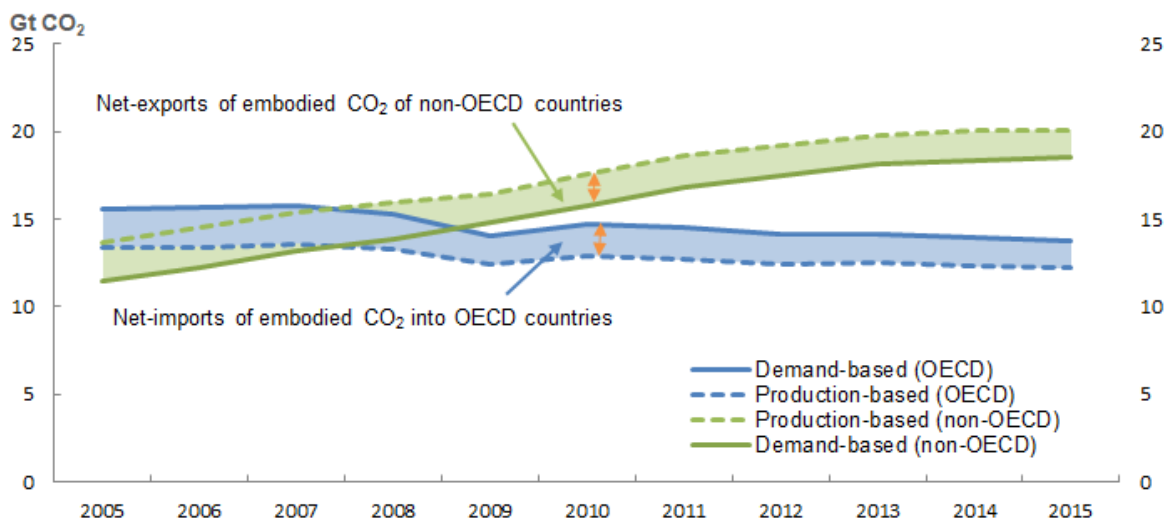


Figure 1-2 Global CO₂ emissions from fuel combustion [2]

It was not until the 1990s that an environmental stance was taken by politicians, a key factor to the development of renewable energy sources. This change in policymaking can be attributed to the concern about Chlorofluorocarbons (CFCs) in the atmosphere that depletes the Ozone (O₃) layer. This concern for the environment has continued to influence governmental policies with the focus expanding to include climate change and waste reduction.

The first factor in the development of renewable energy technology to be discussed is the increased political pressure to reduce heat-trapping gas emissions such as; CO₂, Methane (CH₄), Nitrous Oxides (NO_x), Hydrofluorocarbons (HFCs), Perfluorocarbons (PFCs) and Sulphur Hexafluoride (SF₆). Currently, these gases are released to the atmosphere at a higher rate than they can be removed [3], leading to increased global temperatures and accelerated climate change [4-6]. Furthermore, climate change increases the likelihood of catastrophic weather events such as; flooding, wildfires, droughts and famine [4-7]. This physical change has led to the development of multiple environmental policies. The Climate Change Act of 2008 by the UK government was introduced to reduce greenhouse emissions and to increase public awareness of climate change. The legislation states that by 2050 the UK shall have reduced its annual emissions by at least 100% compared to the levels produced in 1990 [8].

According to the Office for National Statistics and the Department of Energy and Climate Change, in the 2013 government report UK Greenhouse Gas Emissions, the total greenhouse gas emissions are specified to be 777.6 million tonnes of carbon dioxide equivalent (MtCO₂e)

in 1990 [9]. A 100% saving would mean that by 2050 only 388 MtCO₂e in emissions should be produced by the UK each year. Alongside the climate change act of 2008, there are other legislation and incentives to increase the research, production, and employment of renewable energy technologies. An example of this would be the promotion of the use of energy from renewable source regulations 2011, which aims for the renewable energy sector to gain at least 15% of the energy market share by 2020 [10].

On a global scale, the United Nations Framework Convention on Climate Change (UNFCCC) has set up the Kyoto Protocol in which, 192 parties across the globe have agreed to reduce the emissions produced to combat the effect of climate change [11]. The most recent and notable climate change act is the Paris Agreement. The agreement has been used to increase the contribution of all countries, to reduce climate change, keeping global temperatures below a 2°C increase on pre-industrial temperatures. Furthermore, the agreement is designed to help developing countries implement low emission sources of energy, increase the carbon captured through reservoirs and distribute knowledge, technology and finance. Currently, the targets set are well within reach and are expected to be reduced further, thus, achieve a more significant reduction of greenhouse gas emissions.

Due to government incentives and research funding attributed to renewable energy, another factor for moving to renewable energy sources is simply the cost savings. When economists discuss climate change, the transition from fossil fuel-based energy generation to renewable energy generation, and the phrase 'backstop technology' is introduced. Backstop technology

can be explained as the point where the cost of extracting and processing fossil fuels rises beyond the cost of implementing renewable technology [12]. It is at this point, a snowball effect will occur, causing exponential investment in research, production and application of renewable energy technologies. In turn, this will continue to drive down the costs of renewable energy, causing fossil fuels to cease to be used for energy generation.

Energy harvesting captures the energy that otherwise would be lost to the environment, with power generation in the nano to microwatt region. Therefore, it would not be suitable to be implemented for grid power generation. However, with the development of ultra-low-power electronic components [13, 14], it is now possible to develop electronics that require no batteries, a significant step into reducing electronic waste and CO₂ from the production and end of life recycling of batteries.

To further reduce the CO₂ produced by the European Union (EU), a directive (2018/84) relating to single-use batteries and electronic waste has been introduced. Cells contain rare earth and heavy metals, which contaminate soil when they leak, where contamination may inevitably enter waterways and aquifers, causing damage to wildlife and ecosystems. The directive aims to minimise the number of single-use batteries and electronic waste through reusing, repurposing and recycling. However, more research and implementation need to be performed to reduce this waste further. In 2016, 214,000 tonnes of batteries were sold in the EU, and only 93,000 tonnes were recycled with the remainder ending up in landfill sites. Additionally, with the rise of the Extended Producer Responsibility (EPR), product

manufacturers are having to take responsibility for the lifetime of their products, including its carbon footprint and recyclability, creating a niche for energy harvesting devices in modern electronics as a power source.

There are three methods of energy harvesting that can be used to create battery-less devices; electromagnetic, electrostatic and piezoelectric [15, 16]. Although piezoelectric energy harvesters are often selected for generating energy due to the high energy density and simplicity of circuitry [17], they produce very high voltages, thus, requiring an external power management circuit to condition the output signal.

The development of high-efficiency piezoelectric harvesters has been an area of investigation for many researchers where optimising the geometry of a vibration harvester, added proof masses and magnets to the tip of the harvester have resulted in increased power output [16, 18-24]. These techniques reduce the natural frequency of the harvester to be closer to the excitation frequency, thus increasing the power output. Although these methods produce more energy than a natural cantilever system, it is often found that these devices do not have a low natural frequency.

Another method of piezoelectric energy harvesting is the use of a bi-stable system [16, 24-26]. A bi-stable structure has two states such that when a threshold input force is achieved, the device will rapidly switch to the other state. A promising area of research is bi-stable piezoelectric energy harvesting as these systems can achieve much higher output electrical

energies than conventional piezoelectric energy harvesting methods such as cantilevers [22, 27-32]. As previously mentioned, bi-stable systems have two stable states; in between these positions, the structure is chaotic, creating a snapping motion. This rapid motion results in higher internal forces and reduces the impulse time within the piezoelectric material's structure. There are three methods in which a bi-stable system is formed; magnetic repulsion [33-37], beam buckling [38-41] and inverted pendulum buckling [42-44].

Having performed a literature review on piezoelectric energy harvesters and acknowledged the research landscape, it has been identified that buckling of ceramic piezoelectric elements has very little research. This has been attributed to the difficulty of ensuring that the piezoelectric ceramic does not fail after a single or few actuations. Following the investigation into bi-stable, buckling beam and formed harvesters, bistable systems appear to be the most effective method to produce a system that could have commercial appeal. This is due to the compact nature of the system, the simplicity of the structures and the high energy outputs. However, for these methods to be employed for piezoelectric ceramics bi-stable systems cannot be used, simply the forces involved in these systems are too great and are better suited for piezoelectric polymers such as PVDF and its copolymers. Instead, a proposal of work that investigates monostable buckling has been performed. Monostable buckling although generates less energy when compared to equivalent bistable systems. The forces involved are sufficiently lower, this will protect the ceramic and ensure longevity of the power source. Furthermore, when comparing the charge developed from an applied force perpendicular to the polarisation field (d_{33}) the piezoelectric polymers observed in monostable and bistable piezoelectric energy harvesters can be observed to have 20 times less power output unit of

force, when compared to piezoelectric ceramics. This work has potential to enable the replacement of primary batteries (coin cells) in low power electrics.

The basis of a mono-stable system forms around the idea of a bi-stable system. However, instead of two stable states in-which the structure snaps between, only a single stable state is achieved. The single stable state results in highly chaotic behaviour for more extended periods, thus generating more electrical energy. A single stable state can be achieved through two methods; the first is reducing the energy in the systems so that the structure cannot achieve the energy to escape the first energy well and create a second stable state. In this case, the system is more linear, comparable to a fixed cantilever. Another method is to create a system that has excess energy. This excess means that although a second stable state can be achieved, excess energy causes the systems to return to its original position. This is the better option for energy harvesting. However, with an increase in energy comes undesirable effects, like the failure of piezoelectric ceramics because of excessive stress.

The work used three methods to validate the work performed, first is a theoretical approach, coupling buckling and piezoelectric theory, it is possible to predict the power output for a buckling piezoelectric structure. Secondly, COMSOL Multiphysics was used to simulated the proposed designs and to validate theoretical values and gain an more representative models and gain insight into the systems' behaviour. Following this, an experimental approach will be taken to validate the models and create a numerical equation that can be employed to calculate the power output.

1.2 Aim and Objectives

This study has investigated buckling piezoelectric energy harvesting structures for micropower generation applications, which can be used to power low-power battery-operated electronics such as RF communication devices. The main objectives of this investigation are to:

- Perform an extensive literature review of fundamentals, theories and techniques used within the field of piezoelectric energy harvesting and sensing;
- Identify techniques and knowledge that can be used to improve the power output of piezoelectric energy harvesters;
- Experimentally investigate the different methods of energy harvesting to increase power output, efficiency, reliability and reduce size;
- Investigate piezoelectric energy harvesting circuits and its effect on the overall system performance;
- Develop a simulation model capable of accurate prediction of buckling piezoelectric characteristics;
- Develop a buckling piezoelectric energy harvester for micropower generation applications;
- Conduct experimental tests to optimise the power output, efficiency and reliability of the buckling micropower generator;
- Develop empirical models for the optimisation of buckling piezoelectric energy harvesters.

1.3 Thesis Structure

This thesis presents the research and work, which has been performed by the author on behalf of the University of Hertfordshire, from October 2015 through to June 2020. Chapter 1 provides background information on energy demand, energy security and global warming, justifying the need for the presented research work.

Chapter 2 presents a detailed literature review of piezoelectricity that includes; the history of piezoelectricity, manufacturing methods, types of piezoelectric materials, and piezoelectric energy harvesting techniques. This reviews will critically evaluate the previous work performed by other researchers within the field, allowing for identification of new research that can be used to develop knowledge further.

Chapter 3 describes the methodology used for this research to ensure reliability and repeatability of all experiments, simulations and theoretical models. Methods that have been used to numerically define the behaviour are based around buckling theory such as Euler-Bernoulli's equation and Timoshenko.

Chapter 4 investigates the effect of energy harvesting circuitry which has later been used to validate the power output of the proposed novel energy harvesting structures and technology.

Chapter 5 involves experimental testing of a pre-formed buckling piezoelectric harvester, where the resulting power output is compared to existing harvesters to evaluate the effect of the differing structures. Also included is the effect of a buckled beam piezoelectric energy harvester, where simulation and experimentation of a single buckling beam have been performed and evaluated.

Chapter 6 reports on the conclusion of the research work where the novel claims are highlighted and recommendations for future work are presented.

1.4 Novel contributions to knowledge

This section of the thesis highlights the novel contributions to knowledge that has been achieved from the presented research work.

- Development of two novel buckling piezoelectric energy harvesting methods, which increases the energy output, efficiency and reliability of piezoelectric energy harvesters.
- One patent for piezoelectric energy harvesters, based on the buckling energy harvester method. **WO2020095064A1: Improvements in or relating to energy generation in a piezoelectric switch.** Published in May 2021 with a Priority date 09-11-2018.
- Two analytical models that can be used to optimise the structure of a buckling piezoelectric harvester and predict its power output.

- One paper: “Powering lights with piezoelectric energy-harvesting floors.” Published in Energy Technology (Wiley)

Chapter 2 – Literature Review

Summary

Within this chapter, an in-depth review of the existing literature has been performed in the area of piezoelectric energy harvesting. The review initiates with a history of energy harvesting which follows piezoelectricity until the late 1990s. From there, the investigation moves into the fundamentals of piezoelectric where characteristics, materials, manufacturing techniques, constants and constitutive equations are discussed, creating a solid foundation for the work performed. Following this, energy harvesting applications has been investigated to identify harvesting techniques that yield high energy outputs.

2.1 History of Energy Harvesting

The use of energy harvesting is not a new phenomenon; in fact, energy harvesting was one of the first forms of energy conversion. Forms of energy harvesting date back to as early as 5000BC, where ancient Egyptians used the wind to power their boats along the river Nile [45]. In 200BC, there were windmills located in China used to pump water from the ground and to grind grain [46]. In the Middle East during the 11th-century, windmills were widely used, and were introduced to Europe a few centuries later, by Dutch merchants [45]. The Dutch improved on the designs brought back from the Middle East and used them to pump water, freeing land in the marshes around the river Rhine. In the 19th-century windmills transitioned to wind turbines. In America, rural parts that were not connected to the National grid had to produce electricity from other methods. This method was done through the use of a Direct Current (DC) generator being connected to a windmill. In the 1930s, most of America was connected to the grid, making the need to generate electricity irrelevant [45]. However, due to increasing fossil fuel prices, the return of wind turbines as energy generators has increased.

An energy harvesting device can be defined as a tool to convert energy from one medium to another; in most cases, it is used to create electricity. Typical forms of macro energy harvesting are wind turbines, photovoltaic (solar) panels, nuclear reactors and geothermal power plants. Due to more focus on renewable technology and the development of smart low-power energy devices, research into micro energy harvesting is becoming a more popular field of study.

2.2 A Brief History of Piezoelectricity

Within this chapter, a review of the history of piezoelectricity, pyroelectricity and ferroelectricity has been performed. These three phenomena have been reviewed together as they are closely related. There has been a recent influx of interest and development of piezoelectric materials for energy harvesting purposes; however, for this to have happened, scientists from the 19th and 20th century played a vital part in the development and application of piezoelectric materials.

Pyroelectricity was first observed over 2000 years ago. The Greek philosopher Theophrastus, the successor to Aristotle, is believed to have written the earliest observation. A material referred to as lyngourion showed signs of attraction to straws, bits of wood and even small bits of copper and iron [47]. Sidney B. Lang states “Those attractions were no doubt the effects of electrostatic charges produced by temperature changes” [48].

In 1717, Louis Lemery described pyroelectricity; however, it was Carl von Linné, who was the first to relate pyroelectricity to a material referred to as tourmaline. This material was known for its ability to attract materials without being magnetic. Tourmaline was further studied throughout the 18th century with significant contributors to the field such as Franz Ulrich Theodor Aepinus, Johann Karl Wilcke, Benjamin Wilson, Joseph Priestly, John Canton, and Torben Bergman [48]. In 1824 David Brewster was the first author to use the term pyroelectricity. This was due to his work with the material Rochelle salt.

Piezoelectricity was first postulated by Charles-Augustin de Coulomb when he theorised that material would be able to produce an electrical charge from an applied force [49]. It was this work that inspired other scientists such as René Just Haüy and Antonie César Becquerel to individually conduct experiments to prove this theory and both their experiments noted an electrical charge being produced. Results were, however, inconclusive and it could not be determined if the charge had been produced due to piezoelectricity or friction [50]. Ballato goes on to say “Becquerel did make a prescient remark in respect to charges occasioned by stretching rubber; he conjectured that experiments with crystalline minerals might show effects due to their anisotropy” [50]. This allowed for Haüy to theorise integrated molecules, that laid the building blocks for piezoelectricity.” [51].

On August the 2nd 1880, the Curie brothers identified a method for producing electricity when Rochelle salt was subjected to a pressure [52]. It should be noted that the Curie brothers were trying to perform experiments on pyroelectric materials when they discovered piezoelectricity. “In 1881, Hermann Hankel suggested the name ‘Piezoelectricity’ this name had been derived from the Greek word ‘Piezen’ meaning ‘to press’” [49]. This name was widely accepted by the scientific community; thus, it was adopted. Later that year, Gabriel Lippmann used mathematical models, using fundamental laws of thermodynamics, to predict that application of an electric field to a piezoelectric material would cause deformation of the material [53]. This process is known as converse or indirect piezoelectric effect. This prediction was subsequently proven by the Curie brothers through their experimentation.

In 1893, Lord Kelvin produced work on piezoelectricity that has proven to be the basis of the modern understanding of piezoelectricity. This was done through an atomic model to describe the piezoelectric effect [49]. From this model the field of piezoelectricity was established, drawing in more curious scientists. However, it was not until 1910 when Woldemar Voigt showed the relationships between electromechanical and piezoelectricity. This then became the standard reference guide in the field of piezoelectricity [51].

By 1915 interest in piezoelectricity was gaining momentum and was becoming a widely studied area for physicists. Two of these physicists were Ernest Rutherford and Paul Langevin. The two physicists were enlisted by England and France, respectively, to develop devices to detect enemy submarines. They both identified piezoelectric materials as the best method to detect submarines; however, that is where their similarities in work ended. Rutherford alongside Albert Wood and Harrold Gerrard developed a system to monitor noise from enemy submarines similar to an underwater phone. This led to the application and development of hydrophones. Langevin, on the other hand, had more extensive knowledge of piezoelectricity compared to Rutherford. This allowed him to push further into applications. Langevin used his knowledge to focus on problems with emitting and receive signals which ultimately led to the development and application of ultrasonic sonar. This technology paved the way for later technologies such as; modern medical scanners, frequency control and quartz clocks [54].

In 1920, Joseph Valasek further studied the properties of Rochelle salt and discovered that the material was ferroelectric [48]. During the 1940s the field started to gather momentum,

due to the development of piezoelectric ceramics; Barium Oxide and Titanium Oxide. These materials were found to exhibit dielectric constants that were ten times larger than that of single crystals such as quartz and Rochelle salt [55]. Subsequent research on the Barium group resulted in a new class of ferroelectric materials. Later it was discovered that the method of applying a high voltage would cause spontaneous polarisation of the ceramics [55]. This poling technique showed an increase in the dielectric properties of the materials. The increase in dielectric properties led to the development of more powerful sonar along with piezoelectric igniters and phonographs [53].

In 1946 Cady published a book titled "Piezoelectricity: an introduction to the theory and applications of electromechanical phenomena in crystals" [56], which comprehensively explains the early history of piezoelectricity which has become the field's primary reference book.

During the Second World War, pyroelectric materials were further investigated for applications such as infrared detectors, yet no results were published. It was not until 1962, where J Cooper analysed the behaviour of IR detectors made from Barium Titanate [48].

In 1969 Kawai discovered large piezoelectric constants with poled Polyvinylidene Fluoride (PVDF) with results comparable to that of some piezo-ceramics. This led to research into other ferroelectric polymers and copolymers. In 1991, copolymers of PVDF such as Poly (vinylidene fluoride trifluoroethylene) P (VDF-TrFE) and nylons were developed due to a greater

understanding of the Curie point [57]. These discoveries have led to an increasing interest in the field of piezoelectric polymers. This is mainly due to their elastic nature which results in excellent fatigue performance and the ability to be formed into flexible sensors and actuators. Furthermore, they contain non-toxic and biocompatible materials, allowing for a higher number of applications compared to piezoelectric ceramics.

2.3 Energy Harvesting Structures Using Piezoelectric Materials

Piezoelectric Energy Harvesters (PEH) can be used to harvest energy from vibration. However, to harness the large amounts of energy, the PEH must be placed in high-stress (i.e. high vibration) environments. This section investigates different applications of PEHs, highlighting the limitations of the piezoelectric materials and the energy output.

2.4 Unmodified Piezoelectric Energy Harvesting Structures

Heel Strikes Energy Harvesting (HSEH) is the most common method of energy harvesting [136-148]. The development of such devices can be attributed to the large amounts of energy produced from a heel strike. The energy available from human motion was first discussed by Starner in 1996 [149]. It was suggested that 67W could be produced from heel strikes when walking at the speed of 2m/s. This is a significant amount of energy compared to other forms of movement, such as the expansion of the diaphragm when breathing, which only produces 0.83W. Figure 2-1 depicts Starner's prediction on available sources of human energy. With heel strikes producing 67W and occurring frequently, it is apparent why researchers are producing heel strike generators. However, the predictions by Starner have been

contradicted by Niu et al. [141]. They suggest that with a shoe-mounted PEH, the shoe would absorb most of the force with only 2W of useful energy being available. The power suggested by Niu et al. coincides with a large number of design results, where most devices have an efficiency between 1-10%. Therefore, the available energy suggested by Niu et al. appears to be more reliable. Furthermore, Gonzalez, Rubio and Moll [138] concur with Niu et al., reporting that the energy available from walking in their study was approximately 1.265W.

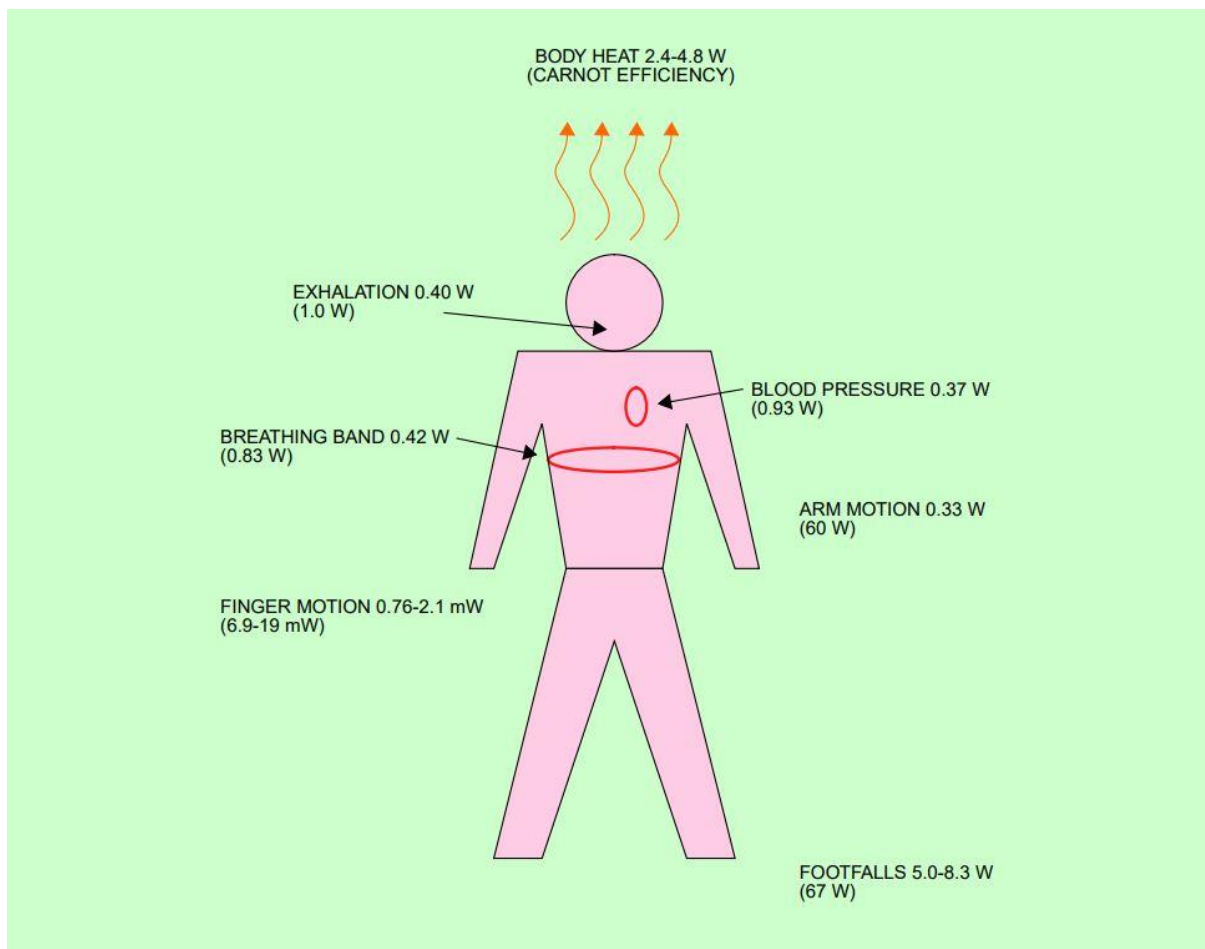


Figure 2-1 Starner's approximation of human energy [149]

Contrary to Howell's cam design, Shenck and Paradiso [143] developed an energy harvesting shoe insole. Two designs are purposed and investigated: the first is a hexagonal sole made from two stacks of eight 28 μ m thick PVDF encapsulating a 2 mm flexible epoxy; the second is

a PZT dimorph [143]. The latter is made from a PZT layer applied to sprung metal and attached to a metal plate. A second spring is applied to the opposite side of the plate. Design one and two both work by being compressed as the user walks, converting the mechanical to electrical energy. The two designs are developed for different shoe types. The PVDF design was applied to a pair of sports shoes, keeping weight to a minimum while maintaining comfort for the user.

On the other hand, the PZT design was applied to a sturdy military boot since a durable heel was needed. The PZT dimorph is actuated on heel strikes, converting the mechanical to electrical energy. The results of the testing show that the PVDF sole would generate approximately 1.3mW of power when walking at the frequency of 0.9Hz, while the PZT design produced 8.4mW at the same impact frequency [143]. The PZT design produces less than 10% of the power output of the Howells's design. However, Shenck and Paradiso's design is more compact and therefore, more comfortable to implement.

Shenck and Paradiso investigated the use of a small low power circuit to power a Radio Frequency Identification (RFID) communication system, which could be used for keyless entry to a motor vehicle. The system transmits a short-range 12-bit wireless signal that can be picked up by a receiver. The circuit uses a rectifier to change the polarity of the negative voltage peaks from the piezoelectric dimorph. This signal is then used to charge a capacitor which powers the RFID transmitter circuit, resulting in a wireless signal being generated and picked up by a receiver [143]. This design has many applications which could be very beneficial to modern living such as smart housing, temperature controls and vehicle settings. Shenck

and Paradiso's work may be old; however, it is still relevant especially as the use of low power electronics is now an established area of research and smart housing is becoming a highly desired area to produce technology. Further research should be put into implementing bi-stable or fan PZT generators into shoe soles. This has been suggested as research shows that the use of these designs results in more significant amounts of output energy.

More recently, Gupta and Sharma [144] developed a shoe insert with a single piezoelectric element made of PZT, shown in Figure 2-2. This single element was then used to identify the location of the point at which maximum mechanical to electrical energy conversion occurs. The sensor was positioned in four places; the heel, the sole, the toes, and between toes and sole. The results indicated that the area with the maximum energy output was the toes, closely followed by the heel. When designing energy harvesting from shoes, these two areas should be considered to obtain a higher efficiency PEH.

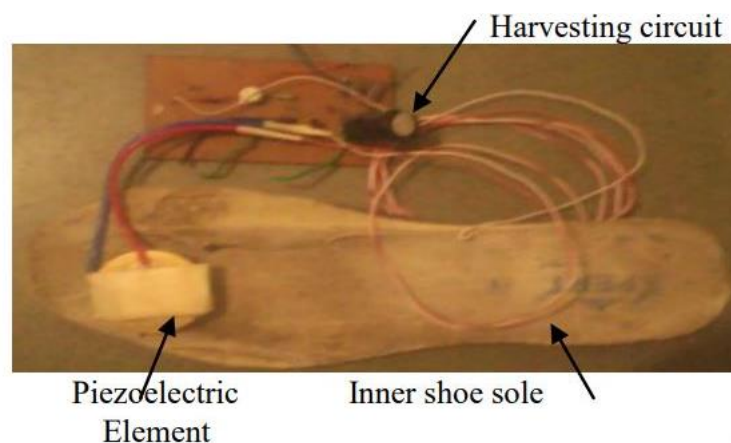


Figure 2-2 Gupta and Sharma Piezoelectric energy harvesting shoe [144]

Alghisi et al. [145] developed a piezoelectric energy transducer used to harvest energy from pre-fabricated piezoelectric buzzers. The pre-fabricated buzzers are mounted into a cube, in which a steel ball bearing is placed. As the user walks the ball bearing moves, striking the

piezoelectric buzzers. The impact results in an electric pulse being generated by the buzzer. The ball bearing then ricochets off the buzzers striking yet another. This method of energy harvesting has been chosen in this investigation since linear actuators previously developed by other researchers are only efficient when they operate at their resonant frequency which is usually significantly higher than the naturally occurring frequencies such as walking. Alghisi et al. furthered this research by optimising the power management that is used to power a temperature sensor. A voltage doubler is chosen for this design since energy losses are lower compared to a full bridge rectifier.

Furthermore, the use of a voltage doubler allows for more voltage to be stored in the capacitor. For smart energy management, a trigger circuit has been used, which allows voltage to be stored to a certain threshold. However, once this threshold is achieved, the circuit closes, allowing for the energy to be used in another circuit. Once the voltage drops to the lower threshold the circuit opens, allowing for the charge to accumulate where the process starts over again. It was found that with the user running at 7km/h a peak power of 16mW was generated and that over 260s of walking at 2km/h enough energy was stored to power the temperature sensor and to read and transmit the data.

Integrating PEHs into shoes is an advantageous method of powering personal electronics. However, another form of converting heel strike energy into electricity is to embed PEHs into flooring. Bobby et al. [5] developed a PEH tile that integrates a PZT element mounted to a brass substrate into the flooring to reduce the size of the device. Using more than one PZT component and point load actuator allowed for an increase in the amount of electricity

produced from a user walking over the tile. It was found that a combination of series and parallel PZT layout allowed for an optimum amount of energy to be harvested. With the device producing a maximum of 0.09W with a user with a mass of 75kg. Removing all mechanical actuators has resulted in the reduced thickness of the flooring tile. This, however, leads to the power produced from the tiles being dependent on the user's mass which may affect the amount of electrical energy produced by the device. It is suggested that a mechanical actuator should be used to increase the voltage output and give a more reproducible power output.

Sharpes et al. [137] designed a PEH floor tile that transmits a signal to smart enabled devices. In this case, a signal was sent to a light, which turned it on and off. The tile works using four cymbal transducers. Sheets of steel were pressed into a near oval shape and bonded together with the PZT transducers located in the centre of the tile, as shown in Figure 2-3.

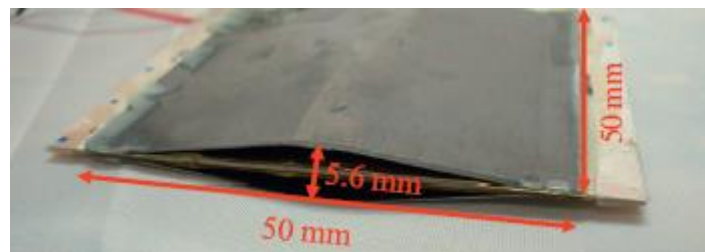


Figure 2-3 Shape's assembled cymbal transducer [129]

The PEH works by inducing a strain in the d_{31} direction of the PZT, through the compression of the curved sheets. These transducers were mounted into a tile so that all four could be activated simultaneously. The peak energy harvested from the tile was $2.57\mu\text{J}/\text{N}$, which was not sufficient to transmit a wireless signal; thus, a storage circuit was used along with a Schottky bridge rectifier. However, it was identified that the diode bridge had a high leakage

current above 15V. Using an optimised storage capacitor of 10 μ F, the energy stored would accumulate to the point where a signal could be sent and turn the lighting on and off.

Won et al. [152] developed a wearable energy harvester using poly(vinylidene fluoride trifluoroethylene) (P (VDF-TrFE)). P (VDF-TrFE) due to its biocompatibility and ability to form stable β phase crystals as opposed to PVDF where α phase crystals are the stable crystalline form. The material was synthesised using solution spin coating. This method involved dissolving PVDF and TrFE granules into a solvent; in this case, methyl ethyl ketone (MEK). Subsequently, the solution was heated and spun through a nozzle while being subjected to a high electric field. The solution was then deposited onto paper substrates. To achieve high crystallisation, annealing was used, it was stated that annealing close to the melting point allowed for high crystallisation; however, slow cooling resulted in a porous structure. It was found that quenching the material on chilled steel prevented a porous structure from forming, resulting in dense piezoelectric material. The P (VDF-TrFE) and cellulose paper were then attached to the back of a glove and tested. Under the excitation of 0.25Hz and 2Hz, the single harvester produced 0.4V and 0.6V, respectively. To further improve upon this design, the use of a rectangular square should be investigated. Furthermore, the use of thin fibres would increase the amount of stress, resulting in more significant amounts of energy to be harvested.

Song and Yun [153] investigated the use of flexible PVDF to harvest energy from wearable energy harvesters. The design that was investigated was of PVDF through silicone thread. The system produces energy through stretching the PVDF over the silicone thread. When the

device was stretched, the silicone treads created local stress on the PVDF, leading to larger amounts of energy to be harvested. It was found that the thickness and amount of the PVDF stripes highly affect the output of the device and that the optimum thickness was 3mm which resulted in the power output of $425\mu\text{W}$ at the excitation frequency of 6Hz. This is a very high power output even compared to PZT based energy harvesters. This high power output could be attributed to the time at which the device was actuated, in reality, the device would only be actuated at frequencies below 1Hz which would provide a more accurate assumption of the power the device would produce in real-world applications.

Yoon et al. [154] have also investigated generating electricity from a skin mounted P (VDF-TrFE) to harvest energy from an arterial pulse. Simply, stretching of P (VDF-TrFE) from the low forces of an arterial pulse would not generate much energy, however, through the use of an innovative window technique the theoretical energy generated was increased 45% when compared to a sheet P (VDF-TrFE) generator. Furthermore, the use of the windows reduced the bending stiffness of the harvesters, increasing the sensitivity of the harvester. The window technique works by increasing localised stress at the edges of the window, resulting in larger energy output.

Yang et al. [155] have investigated the use of PEHs for battery-less wireless switch (BWS) applications. They developed a harvester that produced $220\mu\text{J}$ of energy. This was achieved using a single actuation, meaning that there were two pulses, a positive and negative signal. However, using smart power management $160\mu\text{J}$ was delivered to the RF transmitter, which was enough to transmit a 4 - byte signal over 10m.

Tan et al. [157] investigated the implementation of a low-power and low-cost wireless sensor. This was achieved using a pushbutton piezoelectric igniter. Results show that the igniter produces 67.61 μ J of energy per actuation which was used to transmit two 12-bit signals. It was suggested that the use of a hybrid system would be more suitable for an energy harvesting switch. However, this would involve using a battery storage system. This introduces maintenance into the system that is not desirable. Therefore, an investigation into using other materials or actuation methods was suggested.

Ferrari et al. [158] investigated energy harvesting from ambient vibrations to charge a battery for wireless switch applications. Energy harvesting from ambient vibrations appears to be desirable; however, other methods of energy harvesting such as thermoelectric and photovoltaic are widely available and generate more energy. This said the harvester is to be placed in an environment where it is monitoring vibration. It was found that using two passive sensors, and a signal can be sent intermittently. Through further optimisation of the circuit, the harvester was able to transmit data wirelessly without decreasing the effectiveness of the harvesters.

Paradiso and Feldmeier [159] used a piezoelectric striker to produce energy to power an ID radio transmission. This was then applied to a push-button; however, it was found that the striker applied too much force to the harvesters, causing micro-cracks to form in the ceramic. The force was reduced, and different actuation methods were investigated, including

hydraulics. However, it was found that this would not produce enough energy to transmit a signal. It was suggested that using multiple strikers would achieve a successful transmission.

In 2008 Potkay and Brooks [171] produced a prototype piezoelectric energy harvesting artery cuff [177]. The device is a cut cylinder that wraps around an artery, as shown in Figure 2-4. The expansion and contraction of the artery as a result of blood being pumped around the body causes stress on the piezoelectric material, generating an electrical output. The prototype cuff was designed considering its final application. It was designed out of biocompatible materials to ensure medical approval. Unlike other researchers, the piezoelectric material was chosen based on the need to be biocompatible, and this led to the use of PVDF. The cuff was made out of silicone on which the PVDF was bonded to using medical grade epoxy. It was then sealed using more silicone to ensure there were no exposed electrodes. To achieve the curl, the silicone was stretched during curing. This device was tested externally using a pressurised pipe, simulating an artery. It was found that the device produces a peak power of 16nW. This was very little compared to other forms of energy harvesting; however, the non-intrusive and straightforward design may allow for larger devices of similar design to be implemented into the body to increase the power output to match the 1 μ W needed to power a pacemaker. Furthermore, due to arteries being found around the body, the location of the cuff is not limited to powering a pacemaker, it could also be used to power insulin monitors which can be located in the lower abdomen.

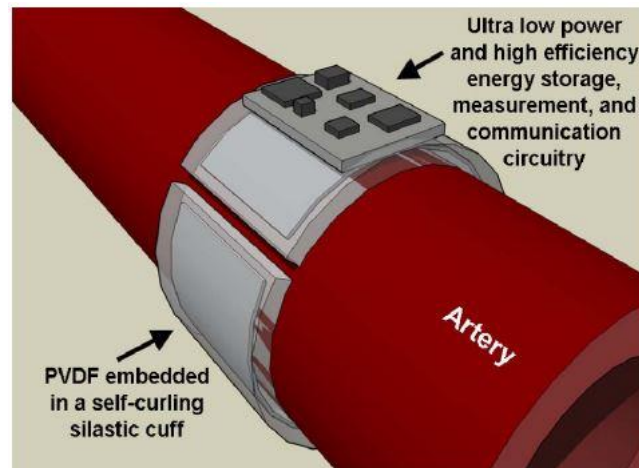


Figure 2-4 Artery cuff energy harvester [177]

In 2009 Qi et al. [178] investigated biocompatible and flexible PZTs. It was identified that the piezoelectric efficiencies of PVDF would not be enough to power implantable energy harvesters. Efforts were then made to make a biocompatible and flexible PZT composite. This was achieved through the use of polydimethylsiloxane (PDMS). The process involved depositing PZT onto MgO and then etching using sulphuric acid after annealing. This process was used to loosen the PZT from the MgO surface. A thin sheet of PDMS was then transferred into contact with the loose PZT and rapidly removed. This resulted in the PZT staying in contact with the PDMS as a result of Van Der Waals forces. The PZT was then poled for 12 hours at 100KV/cm, resulting in a d_{33} coefficient of 101pm/V. It should be noted that this is half of the coefficient of pure PZT piezoelectric material. However, this d_{33} is still four times larger than that of PVDF. A further suggestion of this work would be to increase the poling temperature and pressure during polling through the use of hot plates and contact electrodes. These techniques have been shown to produce higher piezoelectric coefficients when optimised.

Zhang et al. [163] have investigated the use of an implantable device to harvest energy from the blood pressure in the aorta. Two tests have been conducted, one in vitro and one in vivo. Simply a piezoelectric PVDF film was wrapped around a silicone tube. The tube was then inflated and deflated using an intra-aortic balloon pump which replicated the pressures of the heart, allowing for accurate measurement of the energy available from the pulsing heart. It was found that maximum power output was 681nW on a resistor of 33M Ω and could charge to 1V after 40 seconds for a 1 μ F capacitor. Following the testing, the system was implanted into a pig to confirm the findings of the first test. The results confirm the power output observed in the initial tests and that the system can charge a 15 μ F capacitor [151].

Dagdeviren et al. [179] have investigated the application of PZT to harvest energy for an internal implant. The authors suggest that aluminium oxide does not generate enough energy to power an implantable device such as a pacemaker. The device was then implanted into both a cow and sheep was found that the device produced a maximum power of 1.2 μ W/cm², which was five times larger than the predicted output of the harvester. Figure 2-5 shows the energy harvesting system during operation on a bovine heart.

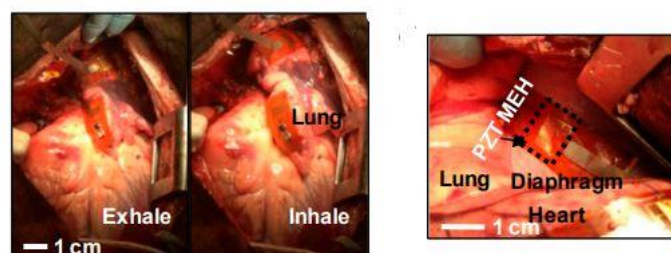


Figure 2-5 Energy in situ on the bovine heart [179]

Lu et al. [170] have investigated the use of PZT on a flexible substrate to harvest the energy from heartbeats. The device was sutured to the heart of a swine and tested. It was found that the device produced a 3V peak to peak under excitation. Although the actual power output of the device is not stated, the authors reported that there is enough energy to power a pacemaker.

Deterre et al. [169] have developed an energy harvesting implant that generates energy from the pressure of the heart. The device harvests energy using a spiral patterned substrate with PZT deposited on its surface. The harvester is placed into an isolated container and is actuated by the compression of bellows. The device is to be placed into the right ventricle of the heart and harvests the energy from the pressure of the blood within the chamber. Experimental testing of the device revealed that the maximum energy of $4.15\mu\text{W}/\text{cm}^3$ could be harvested; this is less than half the predicted output power of $10\mu\text{W}/\text{cm}^3$ [166].

Another form of hybrid energy harvesting investigated is piezo-photovoltaic (PPV) hybrid systems. Solar or photovoltaic systems do not require any mechanical work to harvest energy, unlike the electromagnet method, this allows for different applications, such as flooring. A solar cell can produce a near-constant voltage in the presence of direct and diffuse sunlight, and this energy can be used to charge a circuit. The piezoelectric element can then be used to boost the signal for sensing proposes and efficiency. Choi et al. [134] developed a device that harvests both solar and mechanical energy, as shown in Figure 2-6. The photoactive layer is composed of P3HT: PCBM. In this setup ZnO is used for two primary purposes; the first is to act as the electron transparent layer for the solar part of the device and the other it to generate electricity due to piezoelectric nature of the material. A conductive anode and

cathode are placed on either side of the device to harvest the generated electrical charge. It was reported that the device could power a microcontroller and several Light Emitting Diodes (LEDs). LEDs were used to show the signal from the solar part of the device and two LEDs for the piezoelectric part. The latter LEDs were used to show the amplitude of the force applied as the device is pressed. It was found that the piezoelectric part produces between 20mV and 40mV depending on the force applied and that the solar component would produce an average of 0.546V. Choi et al. suggest that this type of hybrid harvester could be used for mobile touch screen devices to improve battery life.

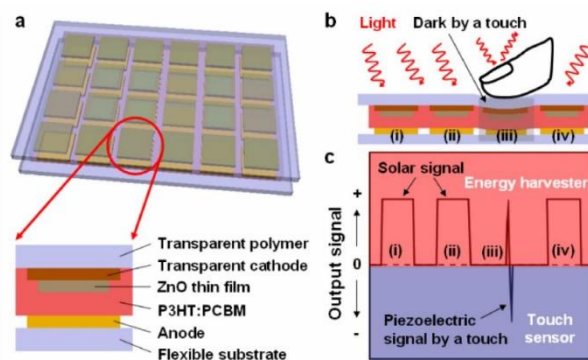


Figure 2-6 Hybrid energy harvester Choi et al. [134]

2.5 Cantilevered Piezoelectric Energy Harvesters

Sang et al. [133] have developed a hybrid piezo-electromagnetic generator. Four designs were produced to implement the hybrid system shown in Figure 2-7. The design chosen utilises a piezoelectric cantilever with a permanent magnet attached to the tip which works as a mass that reduces the natural frequency of the beam. It was found that using the combination of electromagnetic and piezoelectric can increase the efficiency of the energy harvester up to 81.4%. This is a significant increase in the amount of energy harvested.

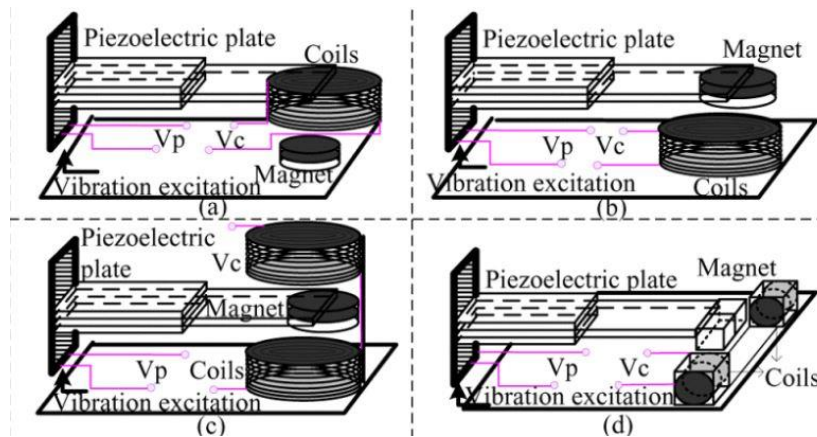


Figure 2-7 Vibration-based hybrid energy harvester [133]

Howells [150], has produced an energy harvesting heel-strike system, which can be attached to shoes. The system uses four PZT bimorphs to convert mechanical energy to electricity, and these transducers are actuated through the use of a star shape cam, as shown in Figure 2-8. When the heel strike generator is compressed, the lead screw causes the cam to rotate which in turn causes the PZT bimorphs to bend following the shape of the cam. This mechanism allows the PZT to convert the linear motion of the heel into useable electricity. This work aimed to produce 0.5 Watts, sufficient to small power electronics such as a GPS receiver. Unfortunately, this was not achieved since on average; the device produced 0.0903W [150]. Although this may not be enough to power a device, it would be enough to extend the life of a portable device such as a pager or a two-way radio. Howells, by not directly actuating the piezoelectric elements from the source stimuli has taken a different approach compared to previous studies. This approach allows for a more controlled period when energy can be harvested and a more consistent amount of energy being produced. However, the major drawback of this system is its size. This device is larger than if the PZT was directly actuated by the heel strike; this is due to the use of the lead screw and cam setup. Unfortunately, the size of the system outweighs any of the benefits achieved by using the cam-actuated system.

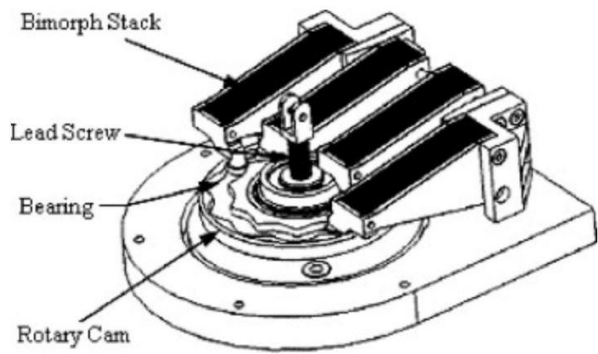
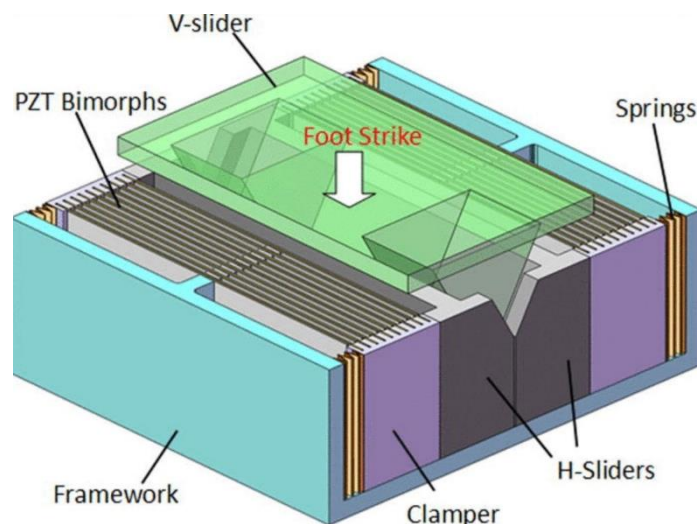


Figure 2-8 Howells novel method of generating power from a heel strike [150]

Xie and Cai [142] reported that an amplification of the force is needed since shoe insoles absorb and dissipate most of the mechanical energy generated during walking. This amplification was achieved by using a triangle jig that forces two trapezoidal plates apart, as shown in Figure 2-9, causing the PZT bimorphs to be displaced. A spring then causes the plates to return to their original position. This results in the PZT bimorphs to vibrate in the horizontal direction. An energy harvesting circuit was used to evaluate the electrical energy produced by a user who weighed 68kg and was 180cm tall. Testing was performed at gaits approximately 1, 1.2 and 1.5Hz. Experiments were conducted to evaluate the effect of the human gait on the performance of the energy harvester, concluding that the device causes a



negligible amount of energy lost during the user's gait. On the other hand, the increased weight of 106g per shoes may lead to increased fatigue.

Figure 2-9 Xie and Cai's novel V shaped harvester [142]

Although many in shoe energy harvesting designs use a beam configuration, the main shortcoming of this design is that the maximum deflection of the beams far exceeds the dimensions of the shoe. Mateu and Moll [140] investigated the optimum beam of PVDF that can be placed in a shoe, to achieve maximum output energy. It was reported that the use of a triangular cantilever is superior to that of a rectangular counterpart, with the rectangular beam producing 25 percent less strain than the triangular beam. Furthermore, it was found that an asymmetric heterogeneous bimorph that is simply supported and is loaded with a distributed force is required for optimum power generation. In addition, it was ascertained that the maximum deflection plays an essential part in the energy generation, the larger the deflection, the greater the output. This knowledge will help identify designs that have the possibility of generating more power than others aiding in the evaluation of the designs purposed.

Moro and Benasciutti [136] performed an investigation into the power harvested from heel strike PEHs. Through the work that was performed, an analytical model and a prototype heel strike energy harvester were developed. The analytical model allowed for acceptable predictions of the power generated compared to experimental results. It should be noted that after 0.3 seconds, the error in the model led to the results being out of phase, however, after this time the voltage attenuated back to zero with the predicted power output being 6% less than the achieved experimental results. Subsequently, modeling variables such as width,

length, thickness and tip mass were evaluated. Using the analytical model combinations of these variables were predicted to optimise the dimensions of the HSEH. It was found that when the single PZT rectangular bimorph's dimensions were optimised, it could produce an average output power of $395\mu\text{W}$, with the only limiting factor being the clamping conditions of the bimorph. This was due to the increased strain at the clamped end, where the tip mass increased.

Furthermore, the natural frequency of the cantilever contributes to the largest effect on the power output of the design. This was observed in simulations where an increase in the tip-mass or length of the cantilever resulted in a peak in power. This peak was attributed to the natural frequency of the beam. Using tip masses and increased beam length, the natural frequency was reduced to the point where the heel strike would cause excess vibrations in the beam, thus improving the output of the harvester. However, increasing the tip mass and length beyond a specific limit resulted in the natural frequency of the beam to fall lower than the excitation frequencies, producing less power. This report has provided an analytical function that can be used to model piezoelectric cantilevers accurately. This is important, as PEH systems can be assessed with minimal prototyping and experimental testing.

Pillatsch et al. developed a rotary piezoelectric energy harvester that produced a peak power output of $43\mu\text{W}$ [152]. This was achieved through the use of a rotating proof mass, permanent magnets and a PZT bimorph. The PZT produced electricity through bending using permanent magnets. This reduces the mechanical wear in the product, extending the harvesters life. Through the development stage, higher outputs were achieved; however, the piezoelectric

element was overstressed and resulted in a dramatic reduction in the output of the harvester. This was resolved by increasing the distance between the two permanent magnets, reducing the repulsion force, thus eliminating the overstressing. The use of a proof mass allowed for energy harvesting over the broad spectrum of frequencies that human motion produces. This is a simple yet effective way to harness linear and rotational energy from human motion. Furthermore, the size of the product allows for it to be worn inconspicuously by the user or incorporated into existing designs which could be used to add extra features such as heart rate monitoring, temperature sensing or as a GPS.

Jeong et al. [156] designed a multi-array energy harvesting switch. The switch produced $324.9\mu\text{J}$ of energy from a single actuation. This was achieved using four piezoelectric transducers (35mm X 35mm) mounted on a substrate (40mm X 50mm). This energy was used to send an infrared signal. The elements were clamped together at one end and separated via a spring at the other, creating a snapping mono-stable structure. This method of actuation increases the output energy while minimising the size of the harvester. However, due to the signals being in opposite phase, full-wave bridge rectifiers are needed for every two elements. Thus the number of transducers are directly proportional to the number of rectifiers, making this method of energy harvesting costly and not comparable to existing methods such as wire push buttons.

Karami and Inman [167] investigated the use of powering a cardiac pacemaker using PZT to convert the vibrations from a heartbeat into usable electrical energy. It was stated that a

pacemaker uses $1\mu\text{W}$ of power, coinciding with the power produced by piezoelectric energy harvesters. In this investigation, a zig-zagged piezoelectric energy harvester, Figure 2-10, was developed and optimised for harvesting energy at 39Hz, which is a regular frequency produced by the heart along with a high amplitude. High amplitude is critical as this produces higher stresses on the PZT, resulting in larger energy yields. The zig-zagged PZT was bonded to a brass substrate using epoxy resin. At this point, it should be noted that neither of the materials is biocompatible and thus must be encased in a biocompatible material. Testing was performed on the mono-stable PEH. When subjected to simulation, the PEH produced $10\mu\text{W}$, which is ten times the energy required to power a pacemaker. It was found that a mono-stable PEH is very dependent upon the input frequency, which is not desired for charging a pacemaker, as heart rates vary affecting the input frequency. Another design was therefore produced utilising magnets to make the structure a bi-stable. A bi-stable design allows for a broad range of frequencies to be harvested, increasing the electrical yield. A bi-stable design, when implemented into a PEH, can produce more electrical energy than a mono-stable PEH since it can be triggered by a broader range of frequencies. The use of magnets increases the complexity of the PEH and increases its size. Therefore these should also be considered when designing the PEH.

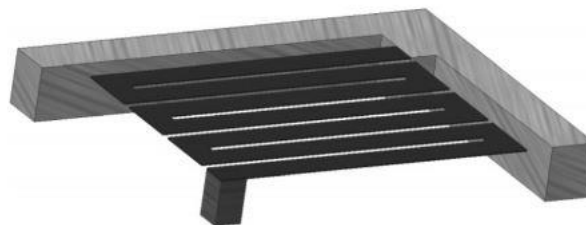


Figure 2-10 Method of reducing natural frequency [167]

Ansari and Karami [180] investigated a technique of harvesting energy for an implantable leadless pacemaker. They used a novel technique of fan-folded piezoelectric beams. The zig-zag system has point masses attached to the end of each beam, the point masses cause a reduction in the natural frequency from 50Hz to 16.18Hz, resulting in possible output power of 10.24 μ W.

2.6 Bistable Piezoelectric Energy Harvesters

Cao et al. [37] investigated the effect of linear, mono-stable and bi-stable piezoelectric energy harvesting devices. To identify the most appropriate energy harvesting technique, a leg mount device was manufactured and tested, as shown in Figure 2-11. The device was used to test the performance characteristics of each energy harvesting method. Their results coincide with that of others where the linear type of harvester produced an average peak power of 3.21 μ W. This was due to the frequency of the linear harvester being tuned to a particular frequency. If the applied frequency is not close to that of the linear harvester, then the energy harvested is minimal. After introducing magnets to the design a mono-stable harvester was produced, this is when the cantilever, much like the linear harvester, returns to one single state after excitation. The magnets amplify the frequency of the cantilever causing high excitation, producing an almost equivalent power output of 18.73 μ W at high operating speeds compared to the 23.2 μ W produced by the bi-stable harvester at the same speeds [37]. However, this was not the case for all other speeds, which is what gives bi-stable designs their advantage for energy harvesting purposes. A bi-stable design has two stable states, and rapid switching will occur when an excitation at any frequency is transferred to the system. This rapid switching causes significant stresses within the cantilever, increasing the voltage output.

Furthermore, the instability of having more than one location to settle causes a reverse damping effect, meaning that it takes longer for the system to reach an equilibrium state, thus increasing the energy output of the system. It is essential to highlight that the energy available is dependent on the swing angle of the user's leg as well as the frequency [37].

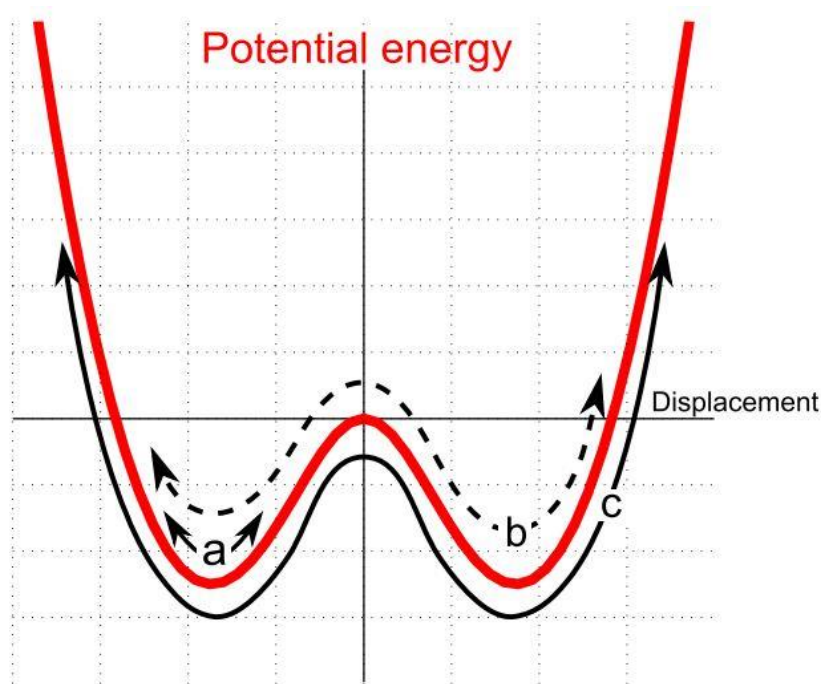


Figure 2-11 Leg mounted piezoelectric energy harvester [37]

Mathieu et al. [172] investigated the use of PVDF to power a pacemaker. In their research, the twisted piezoelectric polymer was used to harvest the energy from blood pressure within the heart, this increased the stress on the material and as a result, produced higher voltage outputs. Testing was done by placing the harvester in a sealed bag to which pressure was applied. The output voltage was rectified using a diode bridge and stored in a capacitor. It was found that 3V could be stored in the capacitor which could supply an LED with a constant supply. However, the time limit for the LED to be illuminated was not stipulated and would

allow for a better assumption on the amount of energy available to charge or power a pacemaker per heartbeat.

A promising area of research is bi-stable piezoelectric energy harvesters; these devices achieve much higher output energy than conventional harvesters such as cantilevers [22, 27-



32]. This is due to that fact that cantilever based harvesters have a narrow excitation band and in most cases need to be directly actuated, which is ideal for applications. However, this is not the case for the majority of vibration-based energy harvesting applications [181, 182, 253-256]. As the name suggests, a bi-stable system has two stable states; however, in-between these two states, the structure is chaotic, creating a snapping motion. This rapid motion results in higher internal forces within an energy harvester; this has been depicted in Figure 2-12. There are three methods by which a bi-stable system can be manufactured; magnetic repulsion [33-37, 183], beam buckling [38-41, 184, 185] and magnetic attraction [42-44].

Figure 2-12 Double- well bi-stable a) inner-well oscillations b) chaotic multi-well oscillations c) inter-well oscillations [186]

As previously stated, there are two important properties that researchers have strived to optimise in piezoelectric energy harvesters; reduction in the natural frequency and increase in the bandwidth of the energy harvesting device. Optimisation of any or both factors results in a significant increase in power output of the harvester. Li et al. [187] produced a bi-resonant system made of two PVDF bimorph cantilevers with natural frequencies of 15Hz and 22Hz. Proof masses were attached at the ends of the cantilevers to reduce the natural frequency of the system. It was reported that this system, when excited between 14Hz and 28Hz, resulted in a power increase of 81% (0.35 μ W). The system vibration collisions between the two beams were observed, spurring the beams to vibrate for longer and with greater amounts of stress [187].

Passive systems have been further investigated, and these are defined by not adapting to changing vibrational inputs [188, 189]. Contrary to this, Lallart et al. [188] performed research on the active turning of piezoelectric energy harvesting beams, where a low power circuit was used to change the structure of the harvester depending on the acceleration and displacement of the system leading to a further increase in output compared to that of a linear system.

A standard method of creating a bistable energy harvester is through the use of magnets. This can be either through repulsion or attraction. Through the use of multiple permanent

magnets, it is possible to create systems of two or more energy wells or stable positions [190-195]. The initial system design was based around a piezoelectric cantilever with a proof mass attached to the end of the beam. The proof mass was then made from a magnetic material. The use of a single magnet of opposite polarity perpendicular to the cantilever would then create two zones in which the beam could come to rest [36]. Cottone et al. [36] were first to investigate this novel form of energy harvesting shown in below Figure 2-13. They reported that the implementation of this system produced 400% to 600% more energy than a traditional cantilever. It was this work that changed the development of energy harvesting and turned the spotlight to piezoelectric energy harvesting over inductive and capacitive energy harvesting techniques.

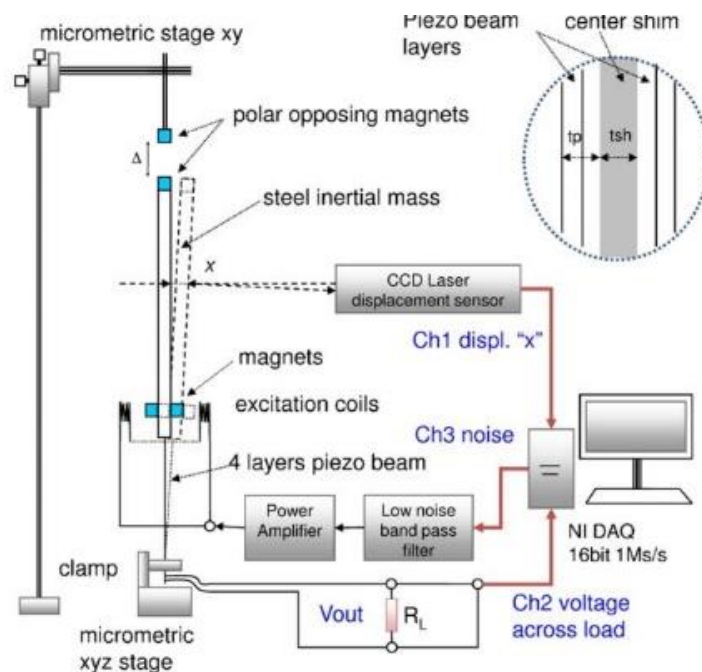


Figure 2-13 Cottone et al. novel bi-stable energy harvesting system [36]

Jiang et al. [25] developed a buckling beam that is driven by magnetic induced buckling, using alternating magnetic poles, a PZT transducer snaps between an attracted and repulsed state. As a result, $0.5\mu\text{W}$ was generated with a load resistance of $3.3\text{M}\Omega$ at 3Hz [25]. Li et al. also

studied the application of magnetic induced buckling to develop a harvester to identify critical parameters to optimise a harvester using stochastic Melnikov theory [196].

An investigation into implementing linear and bi-stable energy harvesters for energy harvesting shoes and bridges have been performed by Green et al. [197]. In their work, they discuss the inaccuracy of using Gaussian white noise, to which realistic data was obtained and used to model the two harvesting techniques. Their results showed that the linear harvesters were more efficient than the proposed bi-stable harvesters. This was attributed to the low energy exerted on the model. The data revealed that there simply was not enough energy to move out of one energy well to the other. In other words, the energy used to excite the piezoelectric cantilever was not sufficient to push through the magnetic field of the permanent magnet to its second state. This was due to the repulsion of the two permanent magnets in the system. However, the implementation of strong magnets into small electronic systems can cause interference. Furthermore, the complexity of the system is increased [39, 198].

The next area of bi-stability to be investigated is the Duffing oscillator, this non-linear system have been studied in detail both experimentally and theoretically for many years. This forms the basis of most bi-stable and mono-stable systems [199-206]. Duffing based energy harvesters show a broad resonance frequency which can be further increased by changing parameters based around; damping, input force, input acceleration, displacement, and nonlinearity strength (magnet strength, spring stiffness or structural stiffness). Changing

these parameters can result in a significant increase in power output for the energy harvester. Furthermore, these resonant frequencies are typically far lower than that of a linear based system, meaning that they have better transference into real-world applications. Characteristically, a duffing bistable system will have a snap through the event during its operation. This is due to the previously discussed energy well. The development of two energy wells means that to switch between states, more energy must be transferred into the system; this extra energy creates more stress in the system. Once the threshold energy is met, the system changes state, expelling the energy as erratic kinetic energy which is then captured by the piezoelectric materials and converted into an electrical charge.

An area that should be focused on is buckling energy harvesters or buckled beam energy harvesters. It is this type of system that has a place in modern-day electronics as it is simple, compact, and develops comparatively large amounts of usable energy [207-213]. Masana and Daqaq [208, 209] have performed a detailed assessment of post-buckled beam energy harvesters. Although they performed far better than a linear device, it was reported that a return system was needed as the energy generated was not significant enough compared to other bi-stable systems. This is due to a single impulse of energy other than a vibration cantilever. As the system can work at very low frequencies, it is possible to use this in more locations, enabling a potentially higher amount of energy that can be harvested. This observation made by Masana and Daqaq appears to concur with other researchers in the field. It was highlighting an area that could be built upon and investigated in more depth.

Eltanany et al. investigated the effect of a PEH based on a buckled beam, with the view to harvesting very-low-frequency vibration from a handshake using two 25mm X 10mm X 0.05mm PZT transducers where 10 μ W of energy was harvested [40].

Although there are demonstrated advantages of bi-stable systems, there is still certainly room for improvement. Erturk and Inman's [201] work illustrated that mechanical shock to the system would help a system stay in a state where a bi-stable system snaps between stable states, generating maximum power output upon a single actuation. The downside of this system is it relies on constant high amplitude actuations that cause detrimental damage to the piezoelectric material, significantly reducing the life of the energy harvesting unit. Sebald et al. [214] proposed an active system that the output impedance changes depending on the input impedance. However, the extra energy is taken to power this active circuit results in a system that produces less power.

2.7 Mono-stable Energy Harvesters

A mono-stable system shows the greatest benefit to modern-day electronics. This is a system that returns to its original position and produces large amounts of energy, however not as much as a bi-stable system. It is of interest as it produces less stress within the piezoelectric element without damaging the material. This means that the system can last longer as a result. From the research performed, it was found that most mono-stable systems are a piezomagnetolectric system, which much like the bi-stable system means that a magnet is used to create a single stable state. The power is extracted via a piezoelectric material [215-

218]. Nasser et al. [215] used two attractive magnets to create a buckling effect in a piezoelectric beam. Their findings suggest that although the power output was lower than that of a bi-stable system, the range of frequencies that could be harvested was found to be much larger. This suggests that a well-placed system could collect power from wind vibrations of all speeds. Similarly, Fan et al. [218] developed a model where their findings showed a 54% increase in bandwidth and a 253% increase in the power output of the system. Hajati and Kim [246] investigated a clamped-clamped beam with a mass in the centre, this caused the beam to sag and create a mono-stable system which when excited with was able to produce double the power output and increased the bandwidth of the systems.

Having performed a literature review on piezoelectric energy harvesters and acknowledged the research landscape, it has been identified that buckling of ceramic piezoelectric elements has very little research. This has been attributed to the difficulty of ensuring that the piezoelectric ceramic does not fail after a single or few actuations. Following the investigation into bi-stable harvesters, buckling beam and formed bistable systems appear to be the most effective method of produce a system that could have commercial appeal. This is due to the compact nature of the system, the simplicity of the structures and the high energy outputs. However, for these methods to be employed for piezoelectric ceramics bi-stable systems cannot be used, simply the forces involved in these systems are too great and are better suited for piezoelectric polymers such as PVDF and it copolymers. Instead, a proposal of work that investigates monostable buckling has been performed. Monostable buckling although generates less energy when compared to equivalent bistable systems. The forces involved are sufficiently lower, this will protect the ceramic and ensure longevity of the power source.

Furthermore, when comparing the charge developed from an applied force perpendicular to the polarisation field (d_{33}) the piezoelectric polymers observed in monostable and bistable piezoelectric energy harvesters can be observed to have 20 times less power per unit of force, when compared to piezoelectric ceramics. This work has potential to enable the replacement of primary batteries (coin cells) in low power electronics.

2.8 Structural Modelling of Piezoelectric Energy Harvesters

Multiple theories have been developed over time for modelling piezoelectric elements, however, two methods are key to the modelling of stresses within beams and plates. The first being Euler-Bernoulli's beam theory, this is typically used to model cantilever type harvesters from this the top surface stresses can be obtained which is then inputted into the piezoelectric equations to find the voltage and charge produced from an actuation. Developing upon this Timoshenko beam theory has been applied this takes into account the deflection of the elements and as a result produces a much more accurate stress, especially with modelling dynamic loads [257 - 266].

Ajitsaria et al [257], a comparison of the two beam methods was investigated, comparing both the models they found an acceptable degree of accuracy with experimental data collected. Using this information, it has been identified that both Euler and Timoshenko's methods are an effective method of determining the voltage and thus the power output of a piezoelectric energy harvester. Throughout this report it was repeatedly highlighted that comparison of buckling beams has been shown minimal attention. This has been attributed to two reasons; the first is piezoelectric energy harvesting is dominated with cantilever harvesters, and the second being the complex modelling of bistable and post-buckling

behaviour that many authors overlook performing buckling on monostable systems through Euler-Bernoulli's and Timoshenko's theories, may be a possible method to extract stresses which can be used to identify the power output of buckling monostable harvesters [267-270].

In addition to Ajitsaria, Ly et al [259], used both Euler and Timoshenko to optimise the shape and resonant frequency of a cantilever, their works employed Hamilton's principle which was computed using the modal decomposition method. Their findings demonstrated that the first modal response was much smaller than the first and generated significantly less power.

2.9 Piezoelectric Polymer

PVDF can be synthesised through multiple methods; hot pressing, extrusion, solution casting, spin casting, Langmuir-Blodgett, NTIPS (Non-Solvent Thermal-Induced Phase Separation), TIPS (Thermally-Induced Phase Separation) and VIPS (Vapour-Induced Phase Separation). These methods produce the desired β phase crystal formation in PVDF. This section will investigate the methods of manufacture to establish areas in which research has not been performed while producing a comprehensive picture of PVDF production.

The first method that will be investigated is hot press; this method involves compressing PVDF powder at extremely high pressures and elevated temperatures. This produces a transparent film with low piezoelectric properties. The reason for the low piezoelectric properties can be attributed to a mixture of α and β crystals being present within the material and that there are no further mechanisms to increase the β phase content or orientate the dipole moment of the polymer chains causing net polarisation of the overall material. Much like the hot press,

extrusion produces similar results. However, other researchers improved upon the first technique by stretching the polymer and applying a high voltage [58-62]. The stretching increased the percentage of α to β conversion [63, 64]. The high voltage across the material caused the dipole orientation resulting in a significant increase in the output. It should be noted that stretching does not result in 100% α to β conversion and that other mechanisms should be investigated such as solution casting. Solution casting is now the most commonly practised method of manufacture; this is attributed to the ease of manufacture, and the higher percentage yield for β crystals [65-69].

Stretching PVDF has been known to increase the yield of β crystal formation. The main variables that have been investigated by researchers are; drawing ratio, drawing speed, and temperature. Stretching has a significant effect on producing β phase polymer chains. This method produces such a high yield due to the structure of the polymer chains. As α phase chains get elongated, a conversion occurs where the trans-gauche trans-gauche (TGTG) chains change to β phase all-trans (TTTT) chains. It was found that once the α chains have been stretched by 20% more than their original length, they will transfer to the β phase.

It should be noted that the optimum stretch is not wholly agreed upon within the research community; however, the consensus is that stretching PVDF at a ratio higher than 4:1 will result in significant α phase conversion. Some researchers believe stretching beyond the ratio mentioned above is ineffective as the change in β crystal content is minimal. In contrast, others suggest that ratios up to 6:1 produce the highest amount of β crystal. Although the optimum drawing ratio is not agreed upon, the other variables such as drawing speed and

temperature have been. The drawing speed is a critical variable to enhance the output of PVDF. The faster the drawing rate, the higher the yield of β phase within the material, slow stretching speeds allow for the chains to move through the material resulting in minimal change in structure. The final variable to be discussed is the temperature at which the material is stretched. To achieve the highest amount of β phase formation the temperature has to be between 60°C and 80°C [64, 66]. The elevated temperature causes the material to become more pliable and soft, allowing it to reach stretching ratios of over 4:1. Temperature is a critical mechanism for PVDF production.

Poling can be described as the orientation of domains within a material. This is achieved through the application of force and high voltage. This process is essential for increasing the output of piezoelectric and ferroelectric materials, allowing for more significant amounts of energy to be converted from mechanical inputs.

The main factors identified affecting the output of a material can be linked to variables during the poling process, these are; mechanical strain applied to the material, poling voltage, poling time, temperature and rate of cooling. These factors differ depending on the material properties.

The poling process can be the same for each classification of material. However, when comparing polymers and ceramics, one vital process differs. For piezoelectric ceramics, the material is usually subjected to a compressive strain, whereas polymers are subjected to

tensile strain. Having said this, no material is the same and tailored poling should always be considered to improve properties.

The literature on PVDF has been reviewed to evaluate what is known about the poling process. This material has been chosen as it processes high piezoelectric constants compared to other materials, is Ultra Violet (UV) resistant and is compatible with organic tissues. These properties make PVDF a desirable piezoelectric energy harvesting material, such that many researchers and academics have investigated the material to harvest energy in a variety of applications.

There are two main manufacturing techniques through which PVDF is produced; from melt or solution. The most common technique for producing PVDF is melt draw. Much like injection moulding, PVDF granules are placed into a hopper, and a lead screw is heated to above the melting point of the PVDF (170°C). The screw compresses, heats and then forces the molten PVDF out of a nozzle. The material is then quenched by blowing ambient air over the material [70]. This technique is simple and effective at producing α phase PVDF on a large scale, as shown in

Figure 2-14; however, the material needs further post-processing to convert α phase crystals to the β phase.

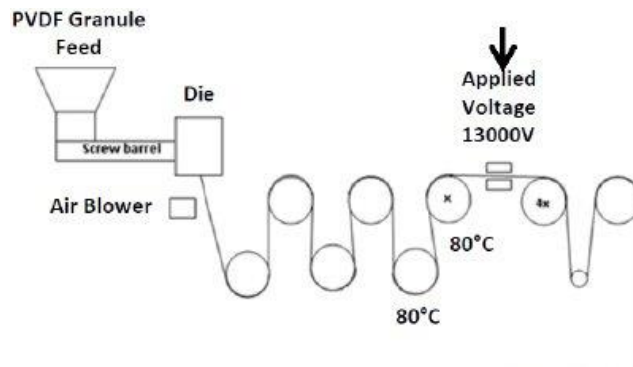


Figure 2-14 Industrial PVDF stretching and poling [70]

The second manufacturing technique is solution base deposition; this technique has many good attributes compared to melt drawing. The method of producing PVDF is achieved by dissolving PVDF granules into a base solution. However, to achieve a material with high amounts of β phase crystals, dimethylformamide (DMF) should be used as the base solution (i.e. solvent) [71]. The solution is deposited on a smooth, clean surface and then annealed to evaporate any moisture and DMF from the solution. Once cooled to room temperature, the remaining PVDF can be observed to be in the β phase. However, results have also shown other crystalline phases such as α , γ , and δ . The crystal formation is dependent on the annealing temperature and cooling rate. Another method of producing β phase PVDF from solution is electrospinning. This method produces the most significant amount of β crystal formation. The PVDF solution is placed in a syringe and spun at high speeds, and a small nozzle allows the solution to escape at very low speeds of 1ml per hour. A high voltage is then applied to the solution. The result is a mat of fibres that possess high β crystal content.

PVDF usually occurs in a stable form; this is known as the α phase. This phase is a non-ferroelectric crystalline form. The α formation is not ferroelectric because the formation is made up of trans-gauche trans-gauche (TGTG) chains [72, 73]. These chains are arranged so that the molecular dipoles cancel each other, with the resultant net polarisation of zero. Piezoelectric characteristics of PVDF can be obtained by transferring from α phase to either of its three other phases; β , δ or γ [63]. This said piezoelectric PVDF could be made up of any combination of these four different crystalline states. To achieve the largest piezoelectric coefficients, PVDF needs to be in its β phase crystal formation. The β phase of PVDF shows the most significant coefficients due to its formation of all-trans (TTTT) molecules [72, 73], this is highly desirable as this formation allows for all dipole moments along the chain to be aligned in the same direction, resulting in large piezoelectric outputs.

Quenching can be described as rapid cooling of a material from an elevated temperature to a lower temperature [58-60, 67, 74-77]. This technique was first used to produce β phase crystals in PVDF when manufactured from melt. The process involves putting PVDF granules into a hopper, and under pressure and temperatures above the melting point, they are turned into a gel. The gel is then extruded from the hopper, where it is immediately quenched into a plastic material using air. However, other methods have been developed that result in an increased piezoelectric output of PVDF, leading to the less frequent use of quenching. Quenching has recently been the focus of several investigations. This is attributed to a better understanding of the Langmuir-Blodgett technique [77-82] where the interaction between water's hydrogen atoms and PVDF's C-F bonds cause the orientation of β phase crystals, resulting in a material that does not require electric polarization [68, 78]. Furthermore, the

NIPS (non-solvent induced phase separation) technique for the production of porous membranes uses quenching [83-93]. This area is new and emerging, where solution cast PVDF can achieve high piezoelectric properties with considerably lower production energy and cost.

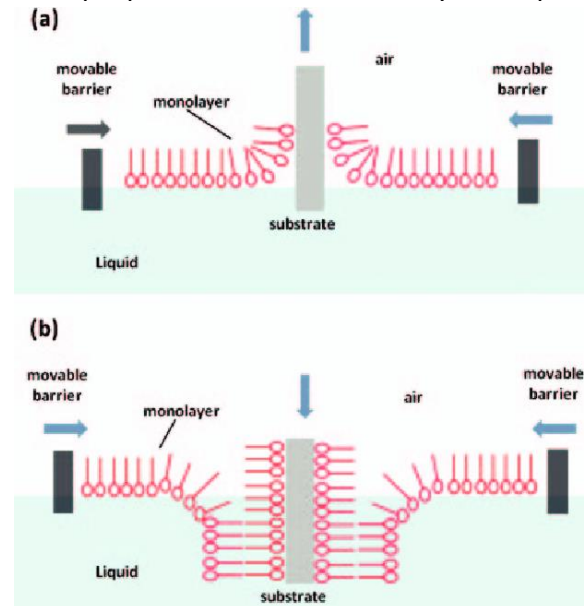


Figure 2-15 Langmuir-Blodgett technique [94]

A Digital Scanning Calorimeter (DSC) is often used to identify crystal formations within materials. A DSC takes a sample and weighs it. It is then heated at a set ramp-rate to a target temperature, held and then cooled. The system measures the weight of the material and the surrounding temperature continuously. This is then used to highlight any endothermic or exothermic peaks indicating crystal growth and crystal melting, respectively. Table 2-1 depicts the test procedures, and associated crystalline formation identified by various authors.

Table 2-1 DSC test procedures and associated crystalline peaks

Digital Scanning Calorimeter					
Author	Heating Rate (°C/min)	Peak Temperature (°C)	α (°C)	β (°C)	γ (°C)
ELmezayyen et al.	10	200	158.7	161	162.8
Ma et al.	10	180	162.6	165.1	
Benz and Euler [95]	10	175	157.9	165	161.3
Zhang et al.	5	200		167	
Mohajir and Heymans [96]	10	227		167	183

Identifying peaks using DSC is a subject in much debate. However, this technique can also be used to identify the degree of crystallinity. This is achieved using equation 2.1, where H_{100} is equal to 103.4 J g^{-1} for β phase crystals in PVDF.

$$\Delta X_c = \frac{\Delta H_f}{\Delta H_{100}} \times 100 \quad 2.1$$

Fourier Transform Infrared Spectrometry (FTIR) is also used to identify crystal formations within materials. Infrared light at different wavelengths are passed through the material; some of these wavelengths are absorbed, while others pass through. A detector then

identifies these wavelengths, depending on the sample's crystal formation, specific wavelengths should be stronger than others. A comparison of literature can then be used to identify not only which crystals are present but also their percentage of the overall structure. Identifying the crystal formations within the polymer samples allows for an accurate prediction of the percentage crystallisation and β phase content. However, there is not a consensus on the exact points where crystals form. Table 2-3 summarises the FTIR and DSC points where α , β and γ crystals form in PVDF.

Table 2-2 Review of critical peaks within PVDF

Fourier Transform Infrared Spectrometer				
Author	Parameter	α Wave Number (cm^{-1})	β Wave Number (cm^{-1})	γ Wave Number (cm^{-1})
Elmezayyen et al. [97]	Absorbance	615, 764, 795, 975	840, 1276, 1433	1433,
Kumar and Viswanath [98]	Transmittance	764, 795, 973, 1183, 1211	840, 1272	
Jia et al. [99]	Intensity	614, 764	510, 840, 1234	840, 1234
Zhang et al. [67]	Reflectance	762, 796, 975, 1210, 1383, 1423	840, 1234, 1275	776, 812, 833, 840, 1234
Sencadas et al. [100]	Transmittance	410, 531, 615, 765, 795, 855, 976	442, 468, 510, 840	

Gregorio and Borges [65]	Transmittance	408, 532, 614, 764, 796	444, 510, 840	431, 512, 770, 812, 833
Wang et al. [101]	Absorbance	796, 764, 614, 532	840, 510	1274
Xiao et al. [89]	Absorbance	1211, 1149, 1069, 975, 854, 794, 763	1275, 840	
Ma et al. [69]	Transmittance	796, 764, 614, 532, 408	840, 510, 445	813, 432
Garain et al. [102]	Absorbance	1212, 976, 764, 614, 532	1276, 841, 510	1236, 841, 510
Benz et al. [103]	Absorbance	1423, 1383, 1210, 974, 762, 532,	1431, 1286	1234
Gregorio [104]	Transmittance	408, 532, 614, 764, 796, 855, 976	445, 510, 840	512, 431, 776, 812, 833, 840
Cui et al. [105]	Transmittance	409, 532, 613, 764, 795, 972	445, 470, 511, 600, 840	431, 512, 776, 812, 833, 840

As shown in Table 2-2-3, the most commonly agreed peaks for β crystals are at 445, 510, 840, and 1275. However, other peaks suggested for α and γ should be considered for testing to identify other crystals within the structure to either improve the piezoelectricity or reduce it.

2.10 Lead Zirconate Titanate

Unlike the piezoelectric polymer PVDF, PZT is a ceramic. This means that production of such materials involves a different approach; the most common difference between the production of a polymer and ceramic is the elevated temperatures ceramics take to form. Most polymers cannot withstand temperatures about 200°C, whereas ceramics due to their excellent thermal capabilities and manufacturing processes can withstand temperatures above 1000°C [106]. Although some ceramics can be produced under melt conditions, most are produced from powder conditions. This can be broken down into four stages; powder preparation, forming, firing and poling [107].

Lead Zirconate Titanate – Solid-state reaction

Mixing of PZT plays an essential part in the production of high piezoelectric and dielectric constants. Simply, poor mixing will result in an inhomogeneous solution where complete perovskite structure is not achieved at later stages of production. To ensure a homogenous mixture is achieved a vigorous motion must be used to break up any aggregates formed prior to and during mixing. It is often recommended to use a ball mill for mixing. The next stage of PZT production is calcination. Calcination is the use of high temperatures to achieve three objectives: removal of moisture, carbonates and volatile impurities; to react the mixture to form a solid solution; and to reduce the proportion of the structure during final firing. Problems with calcination and PZT are the use of volatile materials such as lead oxide in its composition. Calcination at higher temperatures will result in the removal of this core

ingredient to achieve the perovskite structure. However, higher temperatures are needed to ensure reaction and bonding between the substances.

It was found that calcination at set stages reduces the reaction temperature; as a result, this consumes less energy and retains lead oxide. In a single-state reaction, the temperature to bond the three materials is in excess of 800°C, which is too high for lead oxide, thus preventing the formation of the piezoelectric perovskite structure. A two-stage calcination method was introduced, which lowers the calcination temperature from above 800°C to 600°C. The first stage involves the calcination of ZTO, while the second stage results in the calcination of ZTP and PbO. Not only the yield is higher, but it also creates finer powders, requiring less processing. This method is the most common method of PZT manufacture in an industrial setting, due to; low material cost, low energy consumption, relatively high yield of piezoelectric PZT and its simplicity of production.

Lead Zirconate Titanate – Coprecipitation

Coprecipitation is one of the oldest methods of wet deposition, as discussed by Jaffe [55]. The method consists of the preparation of a liquid solution which when a precipitating reagent is introduced, causes the suspended product to be separated from the liquid. This can then be collected via filtering and thermal treatments. Due to the product being suspended in an aqueous solution, it is relatively simple to ascertain the perfect ratio of powders to achieve high purity and small particle size at low cost [108-110].

Lead Zirconate Titanate – Sol-gel

A promising method of PZT production is solution – gel processing. Similar to the coprecipitation method, the sol-gel method involves dissolving the components. However, with this method, they are dissolved into an organic solvent; during this phase of production, an amorphous gel is produced. The continued stirring of the solution results in a homogenous solution. Also, polymerisation starts to occur; this is observed from the cross-linking of the metal oxides and salts, creating a three-dimensional structure [111]. Subsequently, the gel is dried and heated to extract all the organic solvent, leaving only the pure PZT mixture [111-116]. This method of production is excellent for manufacturing thin-film PZT at lower temperatures of 200°C [114].

Methods of forming PZT are the same as other ceramics, including dust pressing, casting, centrifugal casting, extrusion, isostatic pressing and hot pressing [115, 117]. The most common production method is to have the calcined PZT powder mixed with an organic binder which, when heated, will evaporate from the ceramic, yielding pure PZT. Depending on the shape desired, either hot pressing or extrusion can be used.

Sintering is critical to the production process. Which usually occurs at temperatures between 700°C and 1350°C, thus creating a hard ceramic material that can then be finished by polishing, grinding or cutting. Over recent years scientists have investigated methods to reduce the sintering temperature, for two reasons; reduced synthesis energy and the ability

to apply electrodes such as silver during the sintering process. This results in reduced processing time and low resistance electrodes [106, 118].

Doping is essential when producing piezoelectric materials, enhancing the d_{33} and permittivity coefficients, thus resulting in higher charge outputs. Three types of dopants are used when producing piezoelectric materials; isovalent, donor, and acceptor. An isovalent dopant is a dopant that has the same number of cations as the material it is replacing or enhancing, for example; the lead (Pb^{+2}) in PZT can be replaced with Barium (Br^{+2}). This type of doping leads to higher permittivity and a lower Curie temperature [119]. Donor dopants, as the name suggests, have a more significant number of cations, this causes the material to exhibit a larger d_{33} as there are more electrons present in the material. In contrast, the acceptor dopant has fewer cations present, compared to the receptor material. This lowers the permittivity and causes an ion vacancy in the oxygen for perovskite structured piezo-ceramics [119].

It has been identified that poling copolymers of PVDF such as; Poly (vinylidene fluoride trifluoroethylene) or P (VDF-TrFE) require less energy and manufacturing steps to achieve piezoelectricity [120-122]. The TrFE causes the PVDF to align all domains, reducing randomised domain orientation. Consequently, the opposing domain orientation also reduces, further increasing the electrical output of the material. However, the introduction of TrFE alters the structure of the material, resulting in a less efficient mechanical to electrical conversion compared to pure PVDF.

Furthermore, other materials can be added to the ferroelectric polymers to increase the number of β crystals formed from the solution. This reduces the amount of mechanical work needed to induce β phase crystal formation within the polymer as the dopants act as nucleation sites for the β phase crystals.

The conductivity of a piezoelectric material contributes vastly to the piezoelectric properties exhibited. Research has been performed on increasing the conductivity of PVDF through the use of doping with conductive materials such as; Carbon Nanotubes (CNTs), Silver Nanowires (Ag-NWs) and Zinc Oxide Nanowires (ZnO-NWs). Although these are the most common research areas of doping, other areas of doping have been explored.

Yu et al. [123] investigated the effects of doping PVDF, from solution, using Multi-Walled-Carbon-Nano-Tubes (MWCNTs). Samples of PVDF were then produced with 3wt%, 5wt%, 7wt%, and 10wt% MWCNT. Using electrospinning, the solutions were then spin-cast at 18kV. It was found that solutions with 3wt% and 5wt% induce the most substantial amount of β phase formation compared to pure PVDF. Much like TrFE doping, nanotubes act as a catalyst in the formation of β crystals. Moreover, they also cause PVDF to align in a more determined orientation, resulting in the better orientation of the PVDF chains. Therefore, less energy is needed to produce a high piezoelectric response in the material.

Li et al. [124] investigated doping PVDF with Ag-NWs. Much like doping with CNTs, the percentage weight is critical to producing PVDF with more significant amounts of β phase

crystals. Large amounts of dopant results in the PVDF molecules forming a tightly clustered substance; this close packing leads to the formation of straight α phase crystal chains as opposed to the zig-zagged β phase crystal chains. The process of manufacture is similar to that of Li et al., where the material is dissolved and electro-spun. It was found that a high piezoelectric coefficient was achieved with a 1.5wt% solution, 29.8pC/N, this is a 64% increase compared to pure PVDF, 18.1pC/N. This technique yields a piezoelectric response equal to that of P (VDF-TrFE).

The use of dopants can reduce the energy required to produce a high piezoelectric response from PVDF. Another factor that produces a high piezoelectric response is the interactions between the C-F bonds and the dopant. It is suggested that an investigation should be conducted to produce a comparison between different dopants. Furthermore, another investigation should be completed to identify a conductive material, which is cheap and interacts with the C-F bonds in the PVDF to produce a large piezoelectric response.

2.11 Lead-Free Ceramics

The concern for public health has always been paramount. In 2002, the European Union (EU) passed a directive to reduce, remove and replace heavy metals such as mercury, lead and cadmium from electronic parts (EU Directive 2002/95/EC) [125]. This directive was put in place due to the increasing amount of electrical waste produced by the EU, increasing the concerns of heavy metals poisoning the waterways and humans. The directive states that the maximum amount of heavy metals used in a device should be 0.1 wt%. This said, Lead

Zirconate Titanate (PZT) is currently exempt in the EU due to lack of alternative substitutes. However, PZT shall not be allowed to be used when a more suitable material with the same or higher d_{33} becomes available [125, 126]. Therefore, research into lead-free alternative piezoelectric materials has been the subject of many investigations.

A material identified for such a purpose as to replace PZT is (Ba, Ca) (Zr, Ti) O₃ (BCZT). BCZT is a ferroelectric ceramic with a perovskite structure, much like PZT, which under certain poling conditions can achieve a very high d_{33} constant of 620pC/N [127, 128]. This d_{33} is higher than most soft PZT compositions, signifying the importance of this material. To achieve a d_{33} so high, researchers have investigated the effect of the system that sits between two or more ferroelectric-phases. An example of this would be cubic to rhombohedral. The point where two or more changes occur is known as the Morphotropic Phase Boundary (MPB) [55, 127, 129, 130]. The MPB causes instability between different piezoelectric structures; this instability allows for simple orientation of domains within the material, resulting in higher piezoelectric coefficients [127, 131, 132].

2.12 Electronics

Piezoelectric materials are known for producing an electrical charge when an external force is applied to them; the amount of charge produced depends on the material's d constants. For these experiments, PZT (Lead Zirconate Titanate) has been used with a d_{33} of 374 pC/N. A piezoelectric material behaves similarly to a capacitor. When a force is applied, a sharp voltage is achieved; however, over time, the charge will return to zero, even if the force is

kept constant. After removing the force, the structure of the material returns to its original position, resulting in an opposing signal to the applied force. Repetitions of this cycle will result in a sinusoidal wave formation, known as an alternating current (AC). AC power is problematic for piezoelectric energy harvesters since most electrical devices and circuits rely on a constant DC power. Therefore, the signal needs to be converted from AC to DC form; this is achieved through implementing a signal conditioning circuit. This circuit enables the harvester to power electrical circuits and devices. Figure 2-16 shows a flow chart that illustrates the transfer of energy from a mechanical form to an external circuit.

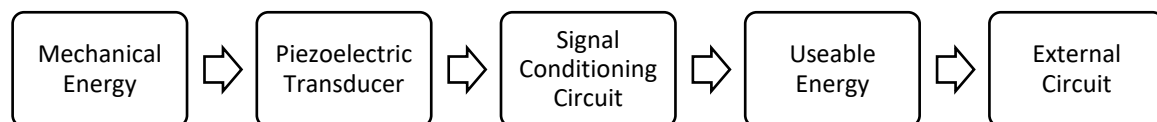


Figure 2-16 Energy transfer in a piezoelectric energy harvester

It should be noted that the implementation of a signal conditioning circuit introduces further losses into the system. Therefore, the efficiency of the circuit is critical for achieving enough usable energy to power external circuits and devices. In this section, an investigation into different methods of signal conditioning has been performed, with the view to reduce the electrical losses, thus increasing the available energy to power external electrical circuits.

Piezoelectric materials typically have a high input impedance, as a result of this, a large variation between the circuit impedance and that of the energy harvester will lead to increased losses of electrical energy. This matching is comparable to the frequency tuning

performed for most cantilever based energy harvesters. The closer the impedance of the loaded circuit and generator are, the smaller the losses of electrical energy. Equation 1.2 demonstrates how to calculate the impedance of the piezoelectric element.

$$Z = \frac{1}{2\pi\omega \times C_0} \quad 2.2$$

Where; Z is the impedance of the piezoelectric energy harvester

ω is the frequency of excitation for the energy harvester

C_0 is the capacitance of the energy harvester

Impedance is measured in ohms (Ω); therefore, to match the two circuits, resistors must be used. Using resistors in series will increase the value of impedance between the two circuits, passively. However, because the frequency of excitation can vary considerably, especially with broadband harvesters, an active system is much more desirable. What is meant by this is when the energy harvester is actuated; the impedance of the load will change with the changing input frequency of the energy harvester [219]. An active method that can be applied to achieve an active system is the use of maximum power point tracking (MPPT). This is an effective method of generating an increased power transfer, but only when the energies generated are more significant than that dissipated by the additional circuit [220]. Trade-offs with using the MPPT system, involve the power consumed by the circuit, the speed at which it reacts to the change in the signal, and the accuracy that it can predict the maximum load. The more accurate the circuit is, the more energy it will consume and dissipate. Therefore, it should be noted that this system does not increase the net energy harvested by the

generator. There are commonly two algorithms that have been investigated; hill climbing and fractional open-circuit voltage. The former relies on a feedback loop that checks if the power output has peaked, if this has not happened it will then increase the resistance further until it starts to drop, upon which the resistance is reduced [221]. The second method, fractional open-circuit voltage, works similarly; however, an open circuit is needed for the period of operation, to ensure that the optimum amount of power is being harvested.

The most common component used in signal conditioning circuits is diodes. Diodes behave similarly to one-way valves. A one-way valve only allows fluid to flow in one direction, as shown in Figure 2-17; however, with enough force, this can be overcome. Furthermore, there is inertia related to the amount of force it takes to open the valve. There are many types of diodes; however, for energy harvesting purposes, three types have been investigated; P-N type, Schottky, and Super-barrier.

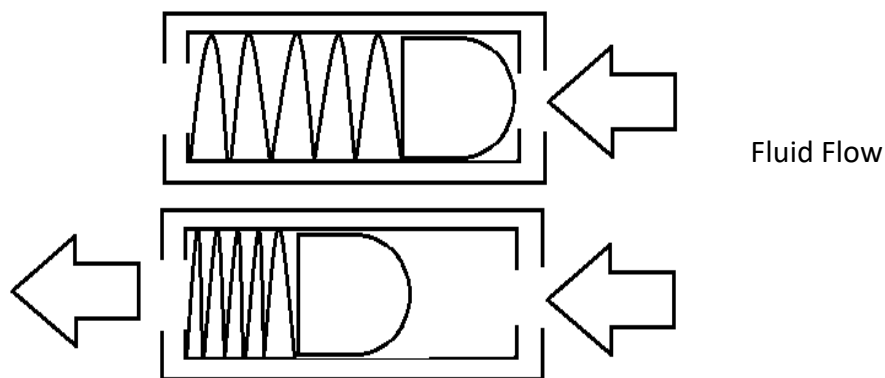


Figure 2-17 One-way valve operation

A P-N diode uses semi-conducting metals that can be doped positively and negatively, producing a positive and negative region in the diode, illustrated in Figure 2-18. The depletion

zone gives this type of diode its properties when no charge is applied the depletion zone acts as an open circuit, preventing any current from flowing. However, when a charge is applied to the anode, electrons build-up reducing the depletion zone. Once a certain amount of charge builds up, the depletion zone disappears, allowing current to flow through the component. This amount of charge is determined by the dopants of the semiconductors. Typically, a silicon diode has a threshold voltage between 0.7-1.2V, whereas a germanium type diode has a lower threshold of approximately 0.3V.

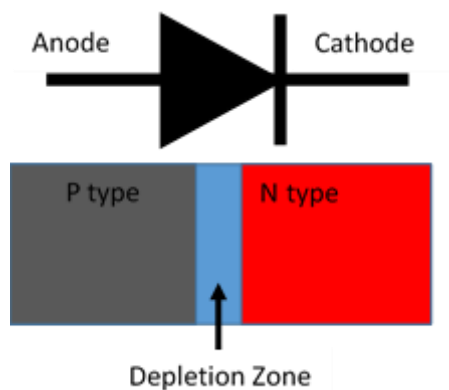


Figure 2-18 P-N Junction Diode

Ideally, a diode will only allow current to pass in one direction, from anode to cathode. However, this is not always the case. When enough current or voltage is applied to the cathode, the depletion zone is once again reduced, creating a closed circuit through the diode. This is known as the reverse breakdown voltage. It should be noted that the line before the reverse breakdown voltage is achieved is not equal to zero. This means that the voltage is being lost before the component fails. A component that does not do this would be ideal to

ensure the maximum amount of energy is harvested. Figure 2-19 illustrates the regions mentioned above.

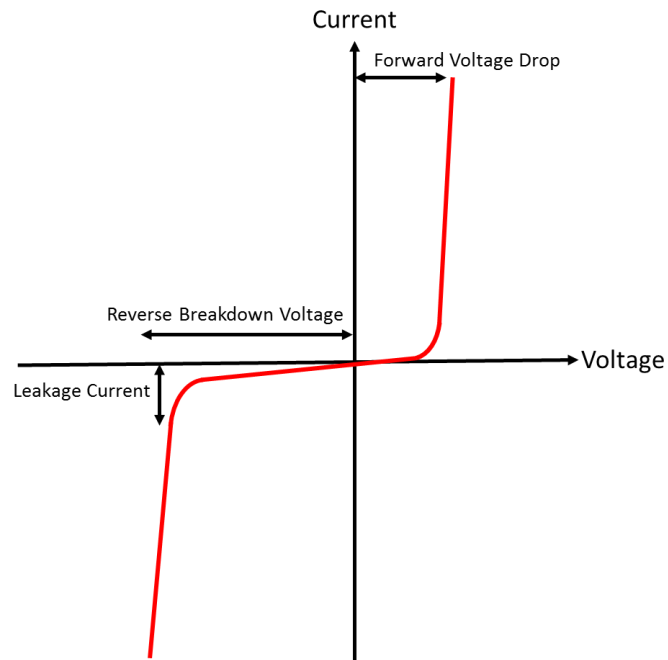


Figure 2-19 Diode Characteristics

Schottky diodes are commonly used in electronics; this is due to their low voltage drop, typically between 0.15 and 0.4 V. Furthermore, these diodes have high switching speeds [222]. These diodes are made with a semiconductor- metal junction. The metal acts as an anode and the semiconductor as the cathode, this reduces the depletion zone and provides the fast switching characteristics. A fast switching diode with low forward voltage is ideal for piezoelectric energy harvesting, as often the energy generated is over a short time and of both positive and negative signs. Of course, these diodes do have drawbacks. A Schottky diode has a low reverse leakage. This means that when loaded in the reverse direction, a Schottky diode would allow more current to pass compared to a silicon diode [223]. This is because the depletion zone in the Schottky diodes is much smaller.

Implementation of a super barrier diode rectifier is an essential step in energy harvesting. Currently, these types of diodes are not being used for energy harvesting purposes. This is because it is a relatively new development. A super barrier rectifier (SBR) is important as it possesses the good characteristics of both Schottky and P-N type diodes, these are; low forward bias, high switching frequencies, high reverse recovery speeds, and high reverse breakdown voltage [223]. This is achieved using the metal oxide semiconductor channel, which is created just below the gate oxide, as shown in Figure 2-20 [223].

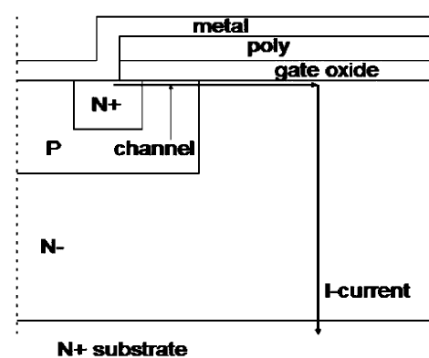


Figure 2-20 SBR structure [223]

For the power generated by the energy harvester to become usable, energy harvesting circuit must be employed. These circuits can be separated into four different areas of research, AC-DC, Two-stage, synchronised switch and synchronous charge extraction. Most commonly used is a fully way bridge rectifier, which relies on diodes to switch negative charge to positive. This then allows for charge to be stored on to the capacitor for later used as a DC source.

As stated previously, a piezoelectric element generates an alternating current (AC), typically low-power electronics depend on direct current (DC) to work. Therefore the first stage of any piezoelectric energy harvesting circuit involves AC-DC rectification [251, 252]. Continued research has led to the development of two-stage piezoelectric energy harvesting circuits. Taking the first principle of rectifying the AC to DC, and then storing the charge generated into a capacitor. Two-stage energy harvesting then utilises a buck converter or step down converter to take the high voltages generated, which are not ideal for logic components, and increase the current. This system allows for better utilisation of the energy generated. This system is limited by three factors; the diodes switching and forward bias, the storage capacitors leakage, and the buck converters conversion efficiency. Therefore when put in a position to select a circuit it can be more efficient to size a capacitor purely for storage which will lead to greater useable energy.

An area of great promise is synchronised switch harvesting on inductor (SSHI) [248, 249, 250]. The energy harvested from a piezoelectric energy harvester can be significantly increased through the use of this non-linear technique. It is based on the resonant circuit created between the capacitor like behaviour of the piezoelectric transducer and an external inductor, this enables the energy, which otherwise would have been lost driving the bridge rectifier to be stored and then captured with a considerable reduction in wasted energy. When compared with a bridge rectifying circuit what can be observed is charge returning to the opposite pole, short circuiting the piezo and reducing the power out of the piezo. The SSHI circuit surmounts this problem in a conventional circuit by using a switch and an inductor. The switch opens when the capacitor voltage reaches maximum in the

opposite polarity, to result in the flipping of the capacitors voltage. This enables the circuit to use the power stored into the capacitor to prime the diodes and enable greater power to be harvested.

There are two methods of employing an switch-inductor circuit that is with them in parallel with the rectifier or in series. It can be observed that both methods increase the power output.

The final circuit to be discussed is the Synchronous electrical charge extraction (SECE) circuit [247]. Unlike the previous method the power generated by this circuit does not rely on the load, meaning that load does not affect the efficiency of the circuit. This said, the used of a control circuit is needed. The system operates when the rectified voltage meets the control circuits threshold, this then opens the gate on a MOSFET allowing the charge to transfer to a coupled inductor, once all of the charge transferred to the inductor, and the control circuits lower threshold it met, the gate is closed. This then allows all of the charge to transfer from the inductor to the storage capacitor. This type of energy harvesting circuit highly depends of the control circuit. Ideally, this circuit will consume very little energy, however, in practice this is not the case and simply is not as efficient as a simple rectifier circuit.

2.13 Conclusion

From all of the work reviewed, a theory has been formed that will allow for large amounts of power to be generated without complex mechanisms, magnets and damage to the piezoelectric element. This will be done through blending mono-stable and bi-stable system thinking and developing a system that buckles in a mono-stable manner with the power output of a bi-stable system.

Chapter 3 – Methodology

Summary

Within this chapter established methodologies relating to buckling and piezoelectric theories are explored and discussed to direct the research and build upon existing theories.

3.1 Mechanical – Buckling Introduction

Buckling has been a long-established area of research. All load-bearing structures will fail, given enough force is applied to the structure. However, this is determined from many characteristics; structure type, load type (dynamic or static), material properties, and boundary conditions (pinned or fixed).

The simplest form of buckling is that of a column that is long and slender, as illustrated in Figure 3-1. When a load is placed in-plane with the structure, the member will compress until a critical load has been achieved. It is at this stage the structure will cease to be horizontal and will bend perpendicular to the axis that the load is applied. The beam has now buckled under the load that has been applied.



Figure 3-1 First buckling mode for a perfect beam

An excellent example of this phenomenon is the buckling of cylindrical drinks cans. When the can has no imperfections, is open and empty, it is possible that the thin walls of the can structure are able to support a force greater than the yield stress of the material, which it is made from. However, when an imperfection is introduced to the wall, the can will collapse and plastically deform. The importance of this observation is that structures can be designed to withstand stresses far beyond a materials yield stress, the point at which a material plastically deforms, causing permeate deformation of the structure. This research has

investigated the effect of buckling structures on piezoelectric energy harvesters, with the view of creating a buckling structure that elastically deforms and returns to its original position, while generating stresses higher than any cantilever system can induce.

To demonstrate an ideal buckling column Figure 3-2 has been produced. As it is made of two rigid bars of equal length that are connected with a pin and rotational spring; it is the spring that the elasticity of the model will be focused. The boundary conditions of the system are then connected to pins with one end fix and the other on a roller bearing. Finally, an in-plane force is then applied to the column. This then causes the column to rotate around the pin; in reality, the beam would be curved; however, this simplified design demonstrates that same principle.

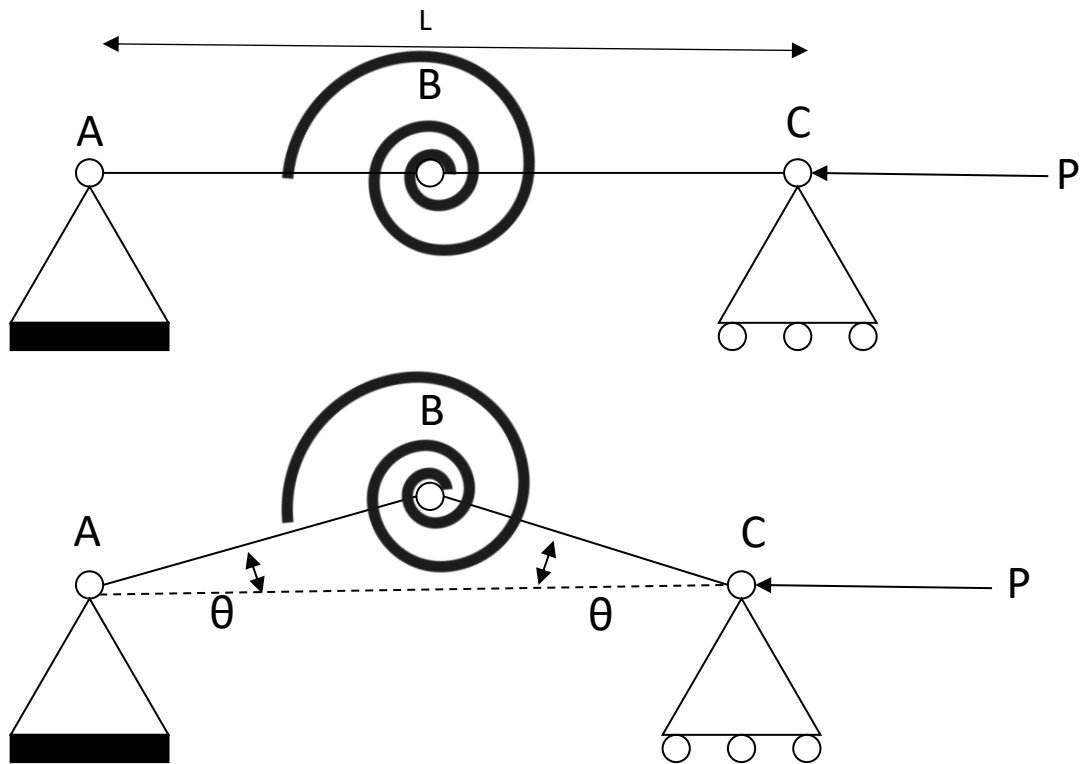


Figure 3-2 Ideal column structure for a perfect beam

Assume that from the buckled position is in equilibrium with the applied force, this creates an angle (θ), in which point B is out-of-plane with points A and C. If the system was to then be subjected to a larger force, a larger θ will be observed. This means that as in-plane force increases, as does the angle of curvature (θ). To meet Newton's third law, a reaction force in the rotational spring will be observed. This creates a moment that resists the curvature increases. If the applied force to the column is reduced, it will tend towards its original position, this is known as a restoring moment. This behaviour can be used to describe stable and unstable conditions. A stable system would be one that when the load is removed from the system, the restoring moment will cause the structure to return to its original position. However, if the in-plane force is too great, then the angle of θ will continue to increase until the structure completely fails, creating an unstable structure, known as lateral buckling.

3.2 Mechanical – Buckling Critical Load

The force at which a system switches from stable to unstable is known as the critical buckling load represented as P_{cr} . The critical buckling load can be found to make a free body diagram of the simplified system.

$$M_{spring} = 2\theta k_{rs} \quad 3.1$$

$$\sum Moments = 0 \quad 3.2$$

Where k is the rotational spring stiffness, θ is the angle of curvature and M is the moment about the centre of curvature for the column. Assuming that the angle of θ is small, the following equation can be used

$$\frac{\theta L}{2}$$

3.3

Where L is the length of the beam. Summing the moments about the centre point will result in the following equation

$$M_B - P \left(\frac{\theta L}{2} \right) = 0$$

3.4

Where P is equal to the reaction force of the beam.

Which is equal to

$$\left(2k_{rs} - \frac{PL}{2} \right) \theta = 0$$

3.5

Therefore, when the angle is equal to zero, there is no observed deflection within the system.

If the above equation was then solved to find P , the critical load could be found with the resulting equation.

$$P_{cr} = \frac{4k_{rs}}{L}$$

3.6

The above equation can then be used to identify the critical buckling load of the system. Simply this is the limit of the stable system if any more force is applied, the system will become unstable and buckle. Through observation of the above formula, it is clear that two factors play a significant part in the critical buckling load; stiffness and length. As the length of the structure increases, the system's buckling load decreases, and the opposite can be observed for the stiffness of the structure.

$$P < P_{cr} = \textit{Stable} \quad 3.7$$

$$P > P_{cr} = \textit{Unstable} \quad 3.8$$

To demonstrate the effect of θ and $\left(2k_{rs} - \frac{PL}{2}\right)$ or P have on the stability of an ideal column the below graph (Figure 3-3) has been produced.

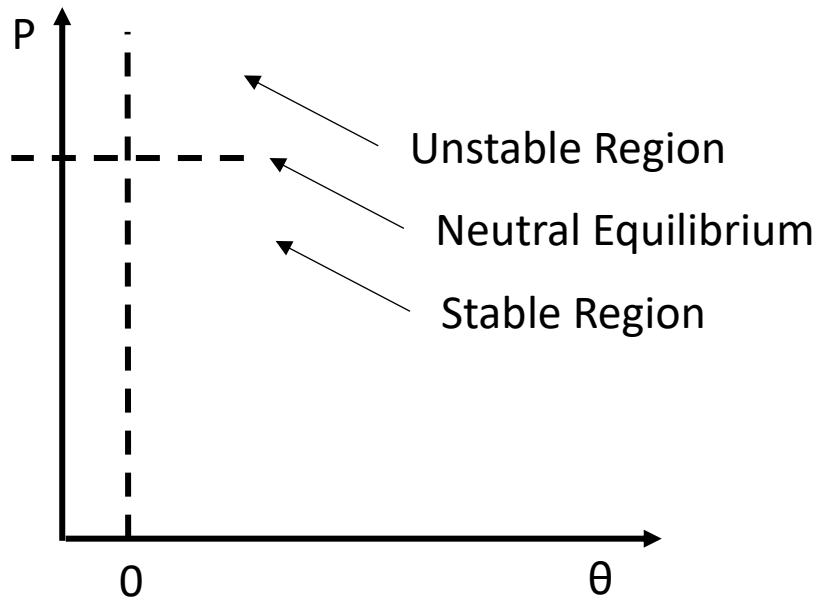


Figure 3-3 demonstration of the equation where θ is assumed to be small.

It can be observed that when $\left(2k_{rs} - \frac{PL}{2}\right)$ is equal to zero a plateau appears, showing the system to be neither stable nor unstable. This point is known as the bifurcation point. Bifurcation can be explained as the point where two or more equilibriums can occur. The bifurcation point occurs at the critical buckling point for structures. It is from this point two outcomes can occur. When force is applied to a structure deformation occurs, as the force reaches the bifurcation point, two equilibriums can occur, either force and be continued to be applied to the structure without change or the structure with chaotically fail. It extends both positively and negatively as the curvature of the beam can curve in any direction. The neutral equilibrium line is limited and can only be satisfied when equation 3-3 θ is equal to zero. In summary, the structure can be in three states; stable, neutral and unstable. A stable state has one singular final position. This position can be likened to a ball being drop into a bowl, and it will always return to its singular settled position at the bottom of the bowl. A neutral system is where the ball in this example is static. However, any input to the system

could cause it to become either state or unstable. It is in this state where the system is extremely chaotic. This behaviour can be likened to the balancing a ball on another ball, where the outcome could be a number of states, for example, does it fall left or right?

To validate these states, the applied force must be compared to the critical buckling load. The simplest method is to evaluate using the below equations; 3.11, 3.12, and 3.13. These relate to the moment, shear force and load to Young's modulus (E), I and deflection

$$E = \frac{\text{Stress}}{\text{Strain}} = \frac{\sigma}{\varepsilon} = \frac{\left(\frac{\text{Force}}{\text{Area}}\right)}{\left(\frac{\text{Change Length}}{\text{Original Length}}\right)} \quad 3.9$$

$$I = \frac{bd^3}{12} \quad 3.10$$

$$EIv'' = M \quad 3.11$$

$$EIv''' = V \quad 3.12$$

$$EIv'''' = -q \quad 3.13$$

The simplest solution can be found using the bending moment equation. Where M is the bending moment, v is the deflection of the beam in the lateral axis, V is the shear force, and q is the load.

Where

$$M + Pv = 0 \therefore M = -Pv \quad 3.14$$

Which is then equal to

$$EIv'' + Pv = 0 \quad 3.15$$

Introducing in a new constant k which is equal to

$$k^2 = \frac{P}{EI} \therefore k = \sqrt{\frac{P}{EI}} \quad 3.16$$

$$v'' + k^2v = 0 \quad 3.17$$

$$v = C_1 \sin kx + C_2 \cos kx \quad 3.18$$

Where C_1 and C_2 are constants from integration that are linked to the boundary conditions of the system. Now evaluating the equation for the deflection is equal to zero. This can only occur at two positions where the column/beam is simply supported.

$$x = 0 \text{ and } x = L \quad 3.19$$

$$v(0) = 0 \text{ and } v(L) = 0 \quad 3.20$$

The first condition this yields C_2 equal to zero, therefore:

$$v = C_1 \sin kx \quad 3.21$$

And the second condition:

$$C_1 \sin kL = 0 \quad 3.22$$

To evaluate these two zero equations two cases will be considered, $C_1=0$ and $\sin kL = 0$.

If the constant C_1 equals zero, then the deflection (v) is also zero given by equation 3.21, and therefore the column has no observable curvature. As a result equation, 3.22 can be any value which is the same for the applied load (P). This is known as the trivial solution which gives the behaviour of an ideal column that is in equilibrium and straight from the compressive load. The second state that satisfies equation 3.22 is known as the buckling equation. This equation identifies the shape in which the ideal beam has buckled.

$$\sin kl = 0 \quad 3.23$$

This equation is only satisfied if it is equal to; $0, \pi, 2\pi$ and so on. When $\sin kl = 0$ the applied load is therefore also equal to 0, and this means that for valid solutions this answer will not be considered and only whole numbers of pi (2, 3, 4...) will be considered.

$$KL = n\pi \quad 3.24$$

Using the previous equation 3.24 and putting this into equation 3.6, the following equation can be written.

$$P = \frac{n^2\pi^2EI}{L^2}$$

3.25

This is the buckling equation that can be used to observe the critical buckling load where

n = to the buckling mode of the structure.

E = Elastic modulus of the column

I = the Second moment of Inertia

L = is the original length of the column

It should be noted that for larger buckling modes to be observed webs or stiffeners must be put into place along the column. This form of buckling is known as Euler buckling, which predicts the critical load for an ideal long/slender beam.

After analysis of the column for its critical load the critical buckling stress can be calculated by dividing the critical buckling load by the cross-sectional area of the column, giving the following equation

$$\sigma_{cr} = \frac{P_{cr}}{A} = \frac{\pi^2EI}{AL^2} \quad 3.26$$

Introducing the radius of gyration, this is the equation which describes that distribution of the cross-sectional area around its central axis.

$$r = \sqrt{\frac{I}{A}} \quad 3.27$$

Where

r = radius of gyration

I = second moment of inertia

A = cross-sectional area of the beam/column

This, when applied to equation 3.26, gives:

$$\sigma_{cr} = \frac{\pi^2 E}{\left(\frac{L}{r}\right)^2} \quad 3.28$$

Where

$$\text{Slenderness ratio} = \frac{L}{r} \quad 3.29$$

The slenderness ratio is a dimensionless ratio that is related to the dimensions of the column/beam. The greater the slenderness ratio, the lower the critical stress for the beam to buckle. Conversely, the lower the slenderness value, the stiffer the beam, thus the greater

the critical stress needed for the beam, note that the elastic limit for a given material is the limit for this buckling theorem.

3.3 Piezoelectricity – Introduction

A basic understanding of piezoelectricity is needed to understand applications for energy harvesting. The word 'piezoelectricity' was derived from the Greek meaning "to press", thus piezoelectricity meaning electricity from pressure [144]. This name was first used to describe this effect by Hermann Hankel in 1881 [49], as stated in the previous chapter.

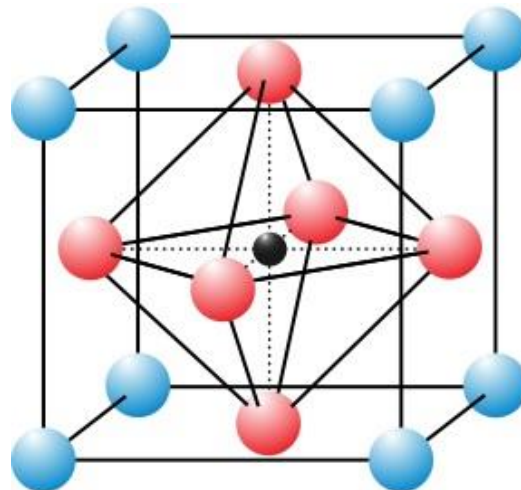


Figure 3-4 Perovskite structure for piezoelectric Lead Zirconate Titanate

What makes the phenomena of piezoelectric materials so intriguing for energy generation is the ability to produce an electric charge when a material subjected to an external force. This is known as the direct piezoelectric effect. It should be noted that the reverse is also possible. Applying an external charge to a piezoelectric material would then cause the structure to deform. This is known as the indirect piezoelectric effect. Figure 3-4 describes the basic characteristics of a piezoelectric material that has no external load applied. From all directions, the material is electrically neutral. This is due to the positively charged atoms and negatively charged atoms being equally distributed throughout the structure Figure 3-5 A; illustrates a piezoelectric material that has an external compressive load applied. It can be noted that under compression, polarisation occurs due to the imbalance of atoms. Figure 3-5

B; displays a piezoelectric material that has an external tensile load applied; this again shows an unbalance of atoms. If electrodes were to be placed on the surfaces perpendicular to the external forces and connected in a closed circuit via a voltmeter, a voltage could be registered. Depending on the composition of the material and load applied the voltage may be seen as positive or negative.

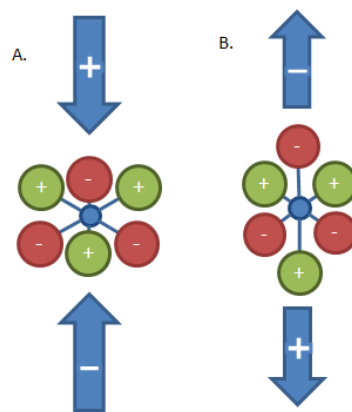


Figure 3-5 A. Piezoelectric material with a compressive load applied. B. Piezoelectric material with a tensile load applied.

3.4 Piezoelectricity – Important Constants and Terms

As with all fields of research, there are constants associated with piezoelectric materials. It is important to understand these constants. Each constant has two subscripts 'i' and 'j'. These subscripts identify the direction of polarisation for the material and the direction of the applied mechanical or electrical force, respectively. It should be noted that polarisation is usually stated to be coincidental with the Z-axis. Figure 3-6 [224] shows that forces in the X, Y and Z direction are denoted as numbers 1, 2, 3, respectively. Torsional forces about the X, Y and Z axis are denoted as 4, 5 and 6 respectively. Understanding this system allows the user

to identify the most appropriate application for a piezoelectric material to optimise the output of a given device depending on which direction a material produces the strongest output.

Permittivity or dielectric constant (ϵ_{ij}). Permittivity is the ability for a dielectric material to polarise under an external electrical voltage. The subscript 'i' identifies the direction of the applied voltage, and the 'j' subscript shows that the material is either in stress or strain [225].

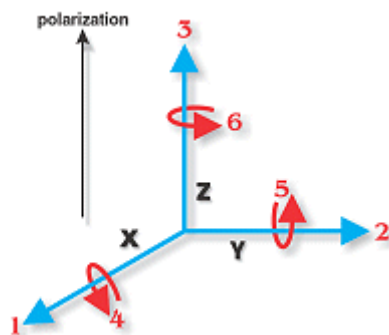


Figure 3-6 Constant Direction Diagram by APC International Ltd [224]

The IEEE defines that PZT is a transversely isotropic material, therefore a piezoelectric material exhibits symmetric the 3-axis, which as previously described is the axis in which the material is poled.

The field variable is the stress components (T_{kl}), strain components (S_{ij}), electric field components (E_k) and the electric displacement components (D_i). It is then possible to evaluate a piezoelectric system with two of the four variables as independent variables. These equations can be written as equations (3.30) and (3.31). Where equation (3.29) is the actuator equation and equation (3.30) is the sensor equation. The latter is of use for this work as it

determines the electrical displacement, dependant on the stress applied to the piezoelectric material.

$$S = s^E \times T + d^t \times E \quad 3.30$$

$$D = d \times T + \varepsilon \times E \quad 3.31$$

Where: S is the strain

s^E is the elastic compliance of the material under a constant electric field

T is the stress applied

d is the dielectric constant

E is the electric field

ε is the complex permittivity

Superscript t is the transpose of that matrix

These equations 3.30 and 3.31 can then be written in matrix form that becomes:

$$\begin{bmatrix} S_1 \\ S_2 \\ S_3 \\ S_4 \\ S_5 \\ S_6 \end{bmatrix} = \begin{bmatrix} s_{11}^E & s_{12}^E & s_{13}^E & 0 & 0 & 0 \\ s_{21}^E & s_{22}^E & s_{23}^E & 0 & 0 & 0 \\ s_{31}^E & s_{32}^E & s_{33}^E & 0 & 0 & 0 \\ 0 & 0 & 0 & s_{44}^E & 0 & 0 \\ 0 & 0 & 0 & 0 & s_{55}^E & 0 \\ 0 & 0 & 0 & 0 & 0 & s_{66}^E \end{bmatrix} \begin{bmatrix} T_1 \\ T_2 \\ T_3 \\ T_4 \\ T_5 \\ T_6 \end{bmatrix} + \begin{bmatrix} 0 & 0 & d_{31} \\ 0 & 0 & d_{32} \\ 0 & 0 & d_{33} \\ 0 & d_{24} & 0 \\ d_{15} & 0 & 0 \\ 0 & 0 & 0 \end{bmatrix} \begin{bmatrix} E_1 \\ E_2 \\ E_3 \end{bmatrix} \quad 3.32$$

3.33

$$\begin{bmatrix} D_1 \\ D_2 \\ D_3 \end{bmatrix} = \begin{bmatrix} 0 & 0 & 0 & 0 & d_{15} & 0 \\ 0 & 0 & 0 & d_{24} & 0 & 0 \\ d_{31} & d_{32} & d_{33} & 0 & 0 & 0 \end{bmatrix} \begin{bmatrix} T_1 \\ T_2 \\ T_3 \\ T_4 \\ T_5 \\ T_6 \end{bmatrix} + \begin{bmatrix} \epsilon_{11} & 0 & 0 \\ 0 & \epsilon_{22} & 0 \\ 0 & 0 & \epsilon_{33} \end{bmatrix} \begin{bmatrix} E_1 \\ E_2 \\ E_3 \end{bmatrix}$$

To simplify the below equation can be used to identify the charge produced by a piezoelectric material.

In the case of this work the force is always applied in the d_{33} direction and therefore no other directions are needed and can be neglected for this work.

$$D = d_{33} \times \sigma \quad 3.34$$

Where: d_{33} is the dielectric constant of a piezoelectric material whose units are C/N.

σ is the applied stress to the piezoelectric materials units N/mm²

To further simplify the electric displacement D can be equated to.

$$\frac{Q}{A} = d_{33} \times \frac{F}{A} \quad 3.35$$

Simplifying further results in.

$$Q = d_{33} \times F \quad 3.36$$

Where the charge produced by the piezoelectric material is equal to the dielectric constant multiplied by force applied. Experimentally charge is difficult to measure and identify. A much

easier method is to measure the voltage produced by the piezoelectric material. Therefore the equation 3.35 can be arranged to break charge down into its respected components which is capacitance multiplied by voltage substituting this into the equation 3.36 results in the below equations.

$$C \times V = d_{33} \times F \quad 3.37$$

$$V = \frac{d_{33} \times F}{C} \quad 3.38$$

If the capacitance was to be turned into its components that final equation can be observed.

$$C = \frac{\varepsilon \times A}{d} \quad 3.39$$

$$\varepsilon = \varepsilon_0 \times \varepsilon_r \quad 3.40$$

$$V = \frac{d_{33}}{\varepsilon} \times \frac{\sigma}{t} \quad 3.41$$

Where:

d_{33} is the tangential piezoelectric charge constant

ε is the relative permittivity of the material

σ is the stress applied to the piezoelectric which in this case is tangential to the polarisation field

t is the thickness of the piezoelectric material

Where $\frac{d_{33}}{\epsilon}$ is equal to another piezoelectric constant g_{33} . The piezoelectric constant g_{33} will be used throughout this work to identify the voltage, thus the power output of the energy harvester.

$$V = g_{33} \times F \quad 3.42$$

The piezoelectric charge constant (d_{ij}) is the most important constant for energy harvesting. This identifies the amount of charge per unit of force a material will produce. The units for this constant are Coulombs per Newton (C/N). However, the amount of Coulombs produced are minute and are known as Pico (10^{-12}) and can be seen in the text as pC/N. There are three main d_{ij} constants used; d_{33} , d_{32} d_{31} . The most common is d_{33} . The subscript identifies induced polarisation parallel to the direction that the material is polarised with mechanical stress being applied in the same direction [225].

$$D = d_{33} \times \sigma \quad 3.43$$

The g coefficient is the voltage constant for piezoelectric materials. It can be defined as the voltage generated per unit of mechanical stress. Much like the other coefficients, g is followed by two subscripts 'i' and 'j', which define the direction of polarisation and the direction of the applied stress to the material.

The k coefficient can be argued the most important factor for energy harvesting. This coefficient defines the efficiency that a piezoelectric material converts mechanical inputs to an electrical output. The k is followed by two subscripts 'i' and 'j' where the first subscript indicates the direction that the electrodes are applied to a material and the second indicates the direction of the applied force to the material.

To identify what material should be used for energy harvesting, the k_{ij} coefficient should be taken into account. This is important as it may make materials with lower d_{ij} coefficients more appropriate to be used when designing energy harvesting devices. An example would be if the input force is low and therefore, a material with a high k coefficient would be more appropriate and that of a material with a high d_{ij} and a low k coefficient. Ultimately a material that possesses a high d_{ij} of 500pC/N and a high k factor would be what is desired for a piezoelectric energy harvester.

A domain can be characterised as a small region within a material where all-electric dipoles follow the same direction. Within a material, there are countless domains, all in varying size and orientation. Due to the randomised nature of domains, it is usually found that a ferroelectric material shows little to no polarity. The effect of no polarity is caused by positive to positive or negative to negative domains. This orientation leads to the cancelling of charges when the material is stressed, with a result of neutral polarity across the material.

As with all materials, ferroelectric materials possess different properties at different temperatures. The most important to acquiring the highest piezoelectric constants would be the ferroelectric stage; in this temperature range, the material possesses the highest possible piezoelectric properties. This range is usually found to start below 0°C and depending on the material over 100°C. This is beneficial for energy harvesting proposes as the materials need not be cooled or heated to harvest optimum amounts of energy, improving the efficiency of the devices.

Following the ferroelectric stage is the paraelectric stage. When a ferroelectric material is in its paraelectric stage, it is still able to polarise spontaneously. However, due to it occurring at higher temperatures, the more internal energy is present in the material, this causes some of the orientation of the domains to reverse resulting in a reduction in the net polarisation of the materials.

The Curie point is the temperature where all ferroelectric materials lose their spontaneous polarization. This is because there is too much energy within the material and causes all domains to become disorganised, leading to the cancellation of charges. The result being zero net polarisation of the material when an applied strain is present.

The glass transition point or (GTP) is a critical temperature where a polymer transfers from a hard, brittle material like glass to a soft, flexible material like rubber. Piezoelectric polymers

need to be heated above this temperature to maintain the desirable characteristics needed to harvest energy.

3.5 Piezoelectricity – The Poling Process

Poling can be described as the orientation of domains within a material. This is achieved by the application of force and application of a high voltage. This process is essential for increasing the output of piezoelectric and ferroelectric materials, thus allowing for larger amounts of energy to be converted from mechanical inputs.

The main factors identified affecting the output of a material can be linked to variables during the poling process, these are; mechanical strain applied to the material, poling voltage, poling time, temperature and rate of cooling. These factors differ depending on material properties. The poling process can be considered to be the same for each classification of material. However, when compared polymers and ceramics, one vital process differs. For piezoelectric ceramics, the material is usually subjected to a compressive strain, whereas polymers are subjected to tensile strain. Having said this, no material is the same and tailored poling should always be considered to improve properties.

3.6 Piezoelectricity – Identification

The relationship between dielectrics, piezoelectricity, pyroelectricity and ferroelectricity can be likened to Matryoshka dolls (Russian nesting dolls) where the largest group contains all other groups. This can be related to dielectrics, as shown by Figure 3-7. The dielectrics group is made up of 32 classes of crystal. The classes can be identified by their; “centre of symmetry, the axis of rotation, mirror planes and multiple combinations of these characteristics.” [226]. The next group is piezoelectricity. The piezoelectric group makes up 21 of the 32 classes of dielectric materials and can be identified by being non-centrosymmetric. In other words, the crystal must not be mirrored through its centre. The next layer is pyroelectricity; only ten crystal types of the 21 non-centrosymmetric crystals show signs of pyroelectricity [226]. The final group is ferroelectricity. Ferroelectric crystals show spontaneous polarization when an external force or charge is applied. Ferroelectricity is a subclass of both piezoelectric and pyroelectric classes because of this; it exhibits both piezo and pyro characteristics [225]. It should be noted that ferroelectric materials exhibit the highest piezoelectric charge coefficient (d_{33}). However, this can only be achieved by orientating the domains of a material.

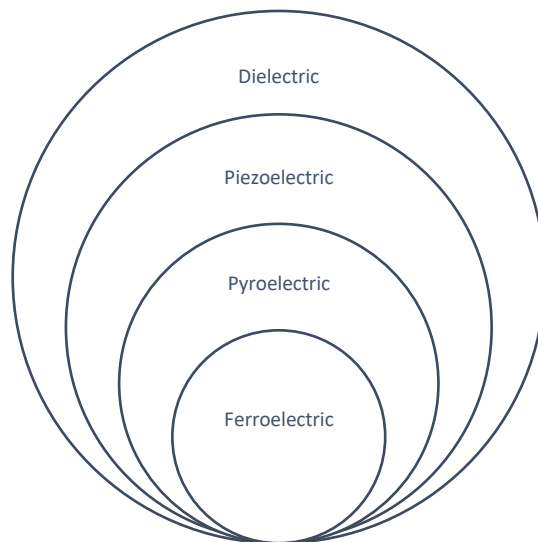


Figure 3-7 Relationship between Dielectric, Piezoelectric, Pyroelectric and Ferroelectric classification.

Having identified that for a material to exhibit piezoelectric properties, it must be non-centrosymmetric, it becomes easier to identify materials that would be piezoelectric by recognising their composition and structure. The first structure to be discussed is the perovskite.

The perovskite group can easily be identified. The perovskite structure generally follows the formula ABO_3 [226], for example, Barium Titanate is a perovskite, and its chemical structure is $BaTiO_3$. Perovskites can be more complicated than just three elements. An example of this is PZT. PZT's chemical formulation is $Pb(Zr-Ti)O_3$, PZT produces a very high piezoelectric constant. Many researchers have tried to increase the output by modifying the composition of the material by altering the ratio of Zr to Ti and doping with other materials. The Perovskite

structure can be observed from the network of 6 oxygen atoms making the shape easily identifiable, as shown in Figure 3-4.

Due to the electromechanical properties of piezoelectric materials, both mechanical and electrical analysis will need to be performed to assess the performance of the proposed systems. To ensure consistency the following chapter 4 will investigate passive signal processing and storage. This circuitry has been used throughout the work to validate the proposed structures.

Chapter 4 – Energy Harvesting Circuit

Summary

In this chapter, the energy harvesting circuit has been investigated. This circuit has been optimised and used in later chapters to validate the power produced by the two novel piezoelectric energy harvesters. This work focuses on two passive energy harvesting circuits, a full wave bridge rectified and a voltage doubler. These have been compared using multiple diode types to achieve the most effective method to extract energy from the piezoelectric energy harvester. Findings show that a full wave bridge rectifier using 1000V Schottky diodes is the most effective circuit to use. Further to this, 10 μ F tantalum capacitor is the most effective form of energy storage; this is due to large amount of energy stored and very low leakage.

4.1 Introduction

A series of tests have been performed to identify the signal conditioning circuit with the lowest energy losses. This is to ensure that the maximum amount of useable energy is extracted, allowing for higher power applications. First, the impedance of the energy harvester must be identified, using a datasheet for the piezoelectric transducers, it was found that the impedance of a single transducer was equal to 800Ω (Table 4-1), as the harvester uses three transducers in series this was multiplied by 3, giving a total impedance of $2,400\Omega$ ($2.4k\Omega$). To confirm this, an impedance analyser (LCR) has been used, producing the following Figure 4-1. This works by calculating the resistance of a circuit through transmitting an AC signal and measuring the change in resistance, which is derived from the voltage and current of the signal.

Figure 4-1 identifies the power dissipated by the resistor. To achieve the maximum power from the harvester, the impedance of both the transducer and conditioning circuit should be equal. To show this, The maximum of the graph identifies the matching input impedance, where the impedance matches and maximum power is achieved. The power dissipated in the load resistor was calculated using the following equation 4.1. Where; R_{load} is the resistance (Ω) of the signal conditioning circuit, and V_{load} is the voltage across the load resistor.

$$Power (W) = \frac{V_{load}^2}{R_{load}} \quad 4.1$$

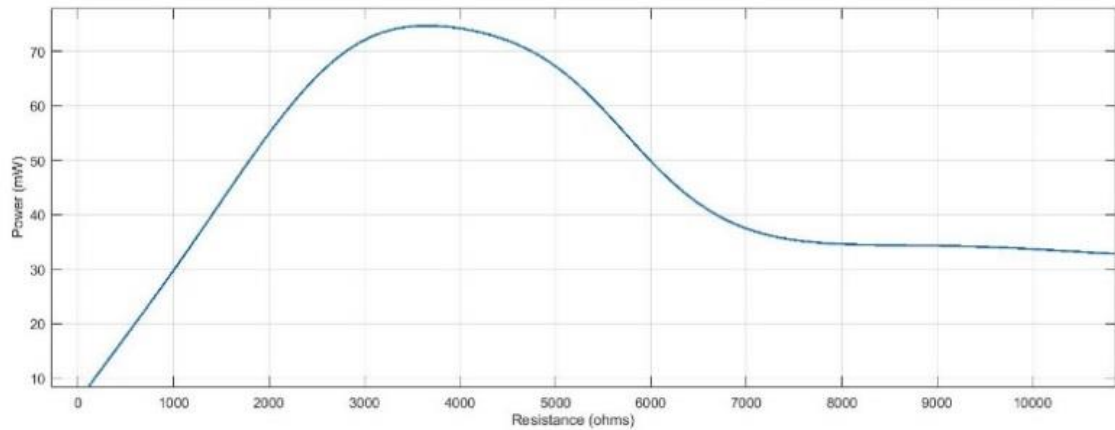


Figure 4-1 Impedance vs Dissipated Power

Following the identification of the ideal load resistor, different passive signal conditioning circuits have been tested both open circuit and with DC smoothing. The following circuits have been identified as passive signal conditioning circuits; half-wave rectifier (Figure 4-2), voltage doubler (Figure 4-3), full-wave bridge rectifier (Figure 4-8) and MOSFET full-wave rectifier (Figure 4-5). Further to this, a comparison of Silicon (P-N), Schottky and super-barrier diodes has been performed for full-wave bridge rectification. Where equation 4.2 was used to identify the efficiency of the conditioning circuit. Where V_{output} is the AC signal observed across the load resistor and V_{Input} is the AC signal generated by the harvester.

$$Efficiency \% (\eta) = \frac{V_{output}(V)}{V_{Input}(V)} \times 100 \quad 4.2$$

However, to identify the efficiency of a circuit that has implemented a storage capacitor. The input voltage must be converted to an RMS (root mean square) value. This is done through the following equation 4.3, which can be simplified to equation 4.4.

$$V_{RMS} = \sqrt{\frac{1}{T} \int_0^T x(t)^2 dt} \quad 4.3$$

$$V_{RMS} = \frac{V_{peak}}{\sqrt{2}} \quad 4.4$$

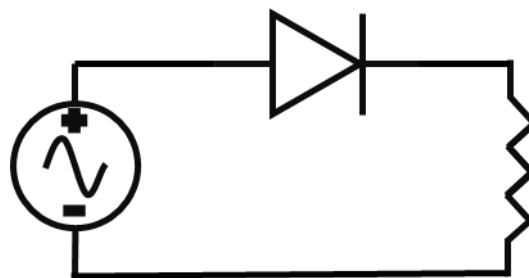


Figure 4-2 Half-wave rectifier

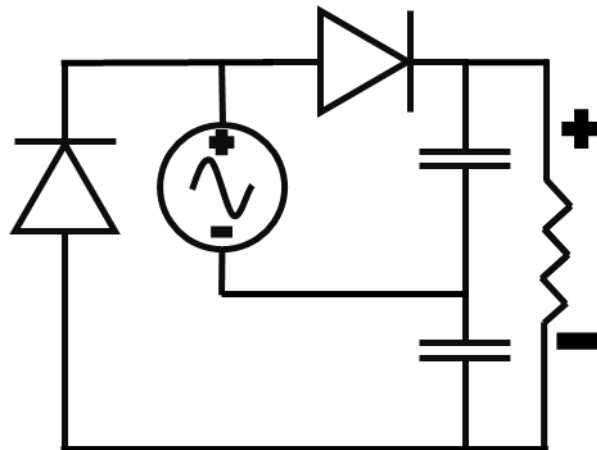


Figure 4-3 Voltage Doubler

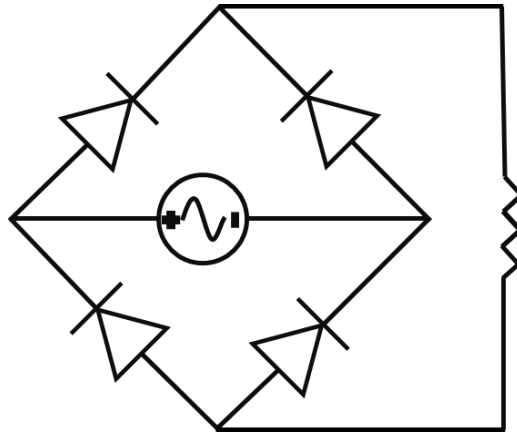


Figure 4-4 Full Wave Bridge Rectifier

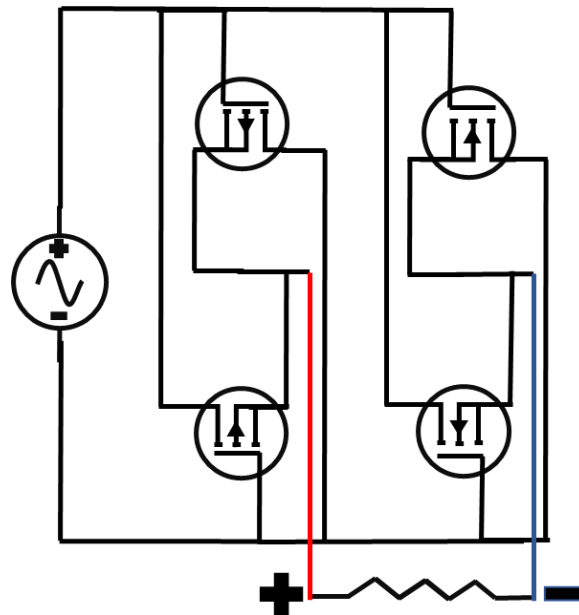


Figure 4-5 MOSFET Full Wave Rectifier

4.2 Method

Six diode bridges have been tested to optimise the energy harvesting circuit; these are;

1N4148 Switching Diode, Fairchild 1N4003, Germanium, Bourns CD2320-B11000, 100v

Schottky chip and a Vishay B2M-E3/45. The details of the diodes have been displayed in Table

4-2. A buckling piezoelectric buzzer (BPB) was used as the source of energy, which was actuated by hand. Therefore, to remove any statistical anomalies, each circuit was tested with a minimum of 100 actuations of the BPB as shown by Figure 4-6 with a signal shape displayed in Figure 4-7. Furthermore, the circuit was tested with and without two 10 μ F series storage capacitors.

Schottky diodes are commonly used in energy harvesting; this is because of the low voltage drop, typically between 0.15 and 0.4 V. Furthermore, these diodes have high switching speeds [222]. These diodes are made with a semiconductor metal junction. The metal acts as an anode and the semiconductor the cathode; this reduces the depletion zone and provides the fast switching characteristics. A fast switching diode with low forward voltage is ideal for energy harvesting using piezoelectric materials, as often the energy generated is over a short time and of both positive and negative sign. Of course, these diodes do have drawbacks. A Schottky diode has a low reverse leakage. This means that when loaded in the reverse direction, a Schottky diode would allow more current to pass when compared to a silicon diode [223]. The depletion zone in the Schottky diodes are much smaller, meaning that less reverse voltage is needed until voltage can flow. Therefore, they should only be used in low power situations.

A full-wave bridge rectifier is commonly used to harvest energy for piezoelectric devices. This device is made of four diodes in the shape of a diamond. A full-wave bridge rectifier corrects a sinusoidal waveform into only positive peaks [227]. This, when used in conjunction with a

capacitor, can provide a smoothed DC voltage, which in turn can be used to power circuits. For this part of the experiment, Schottky diodes have been chosen for the full-wave bridge rectifier for the high reverse voltage, quick switching and low forward bias.

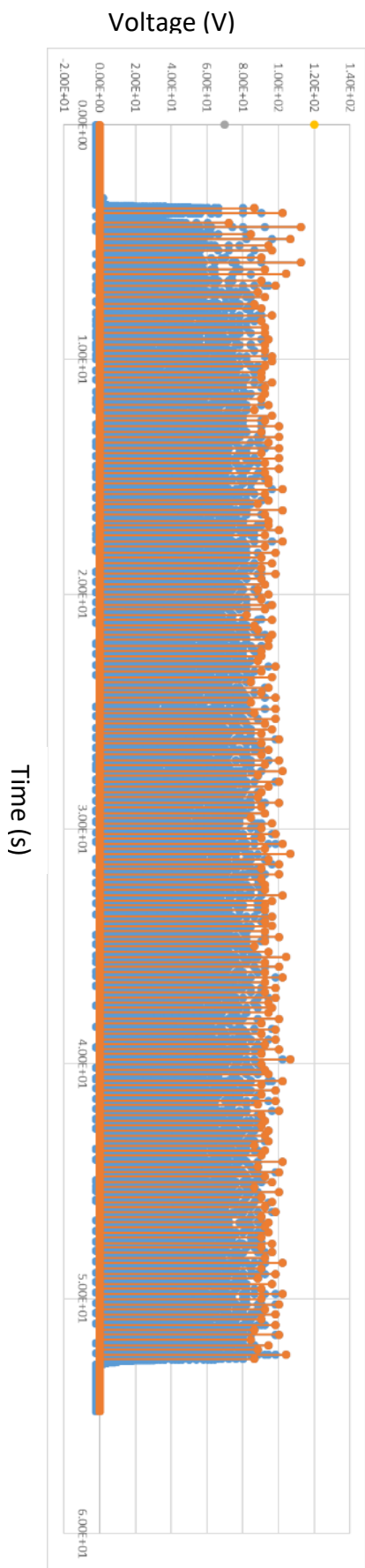


Figure 4-6 Signal from 100 Actuations of BPT, silicon rectifier circuit

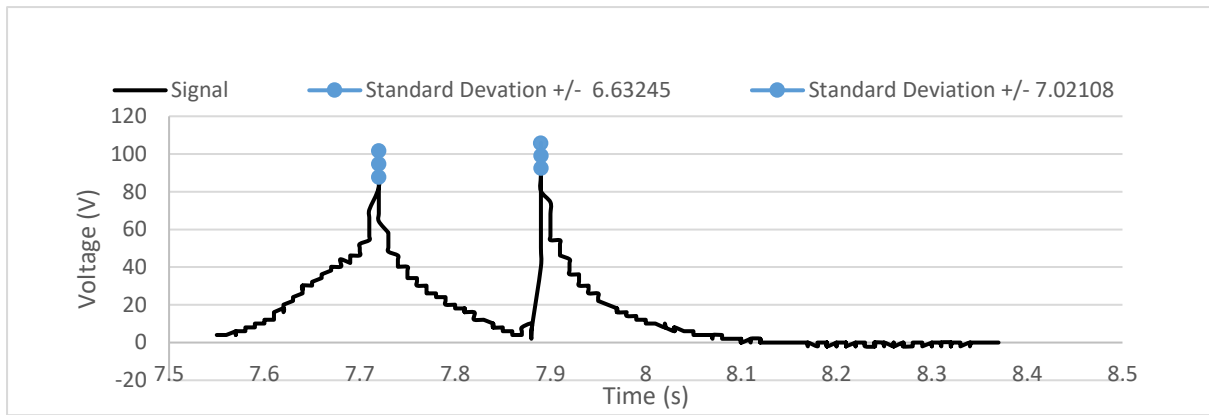


Figure 4-7 Average Peaks with Standard Deviation for Single Actuation of BPB, silicon rectifier circuit

Table 4-2 Diode Properties

Diode Name	Diode Type	Peak Forward Voltage (V_f) @ 200mA	Maximum Reverse Peak Voltage (V_{RRM})
1N4148	Silicon	1	100
1N4003	Schottky	0.8	200
	Germanium		
CD2320-B11000	Schottky Chip	0.8	1000
	Schottky Chip		
Vishay B2M-E3/45	Silicon	0.85	200

To compare, a bridge rectifier circuit to a voltage circuit, storage capacitors must be used. The voltage doubler circuit uses two capacitors in series. Therefore, testing will be completed with two 10 μ F capacitors in series for both the full-wave bridge rectifier and voltage doubler

circuits. A single buckling piezoelectric transducer has been actuated and the energy stored in two storage capacitors for the P-N, Schottky and Germanium full-wave bridge rectifiers (Figure 4-8). The results of which will confirm the best choice of diodes for a harvesting circuit as well as a comparison to the voltage doubler (Figure 4-9).

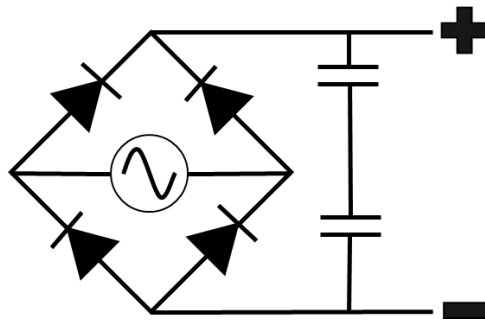


Figure 4-8 Full Wave Rectifier Test Circuit

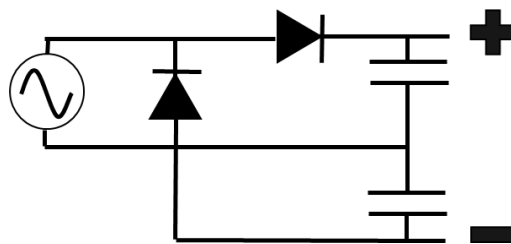


Figure 4-9 Voltage Doubler Test Circuit

4.3 Results: Open Circuit Full Wave Bridge Rectifier

A piezoelectric material has similar characteristics, much like a capacitor. Therefore, to analyse the open circuit energy, produced by the buckling piezoelectric transducer (BPT), equation 4.5 must be used. 'C' is the capacitance of the material, in the case of the BPT this is 40nF, and 'V' is the maximum voltage produced. The results shown in Table 4-3, Figure 4-10 and Figure 4-11 suggest that the silicon signal diode has the highest efficiency as it produced

the largest amount of energy. This has been attributed to a lower forward voltage than the other bridges that have been tested. However, when a comparison between the P-N type and Schottky type rectifiers, it is found that the Schottky rectifiers allow for more energy to be captured.

$$E = \frac{C \times V^2}{2}$$

4.5

Table 4-3 Full-wave bridge rectifier results.

Diode type	Peak One Voltage (V)	Standard Deviation	Energy (μJ)	Peak Two Voltage (V)	Standard Deviation	Energy (μJ)	Total Energy (μJ)
Silicon	93.64	6.35	175	93.07	7.25	173	348
Schottky	93.23	4.68	174	93.25	4.17	173	347
Germanium	90.12	3.68	162	91.87	3.81	169	331
Silicon Chip	88.39	1.90	156	92.39	2.57	170	326
1000V Schottky	93.25	3.95	174	94.12	3.74	177	351
Schottky chip	91.49	3.96	167	94.00	3.45	177	344

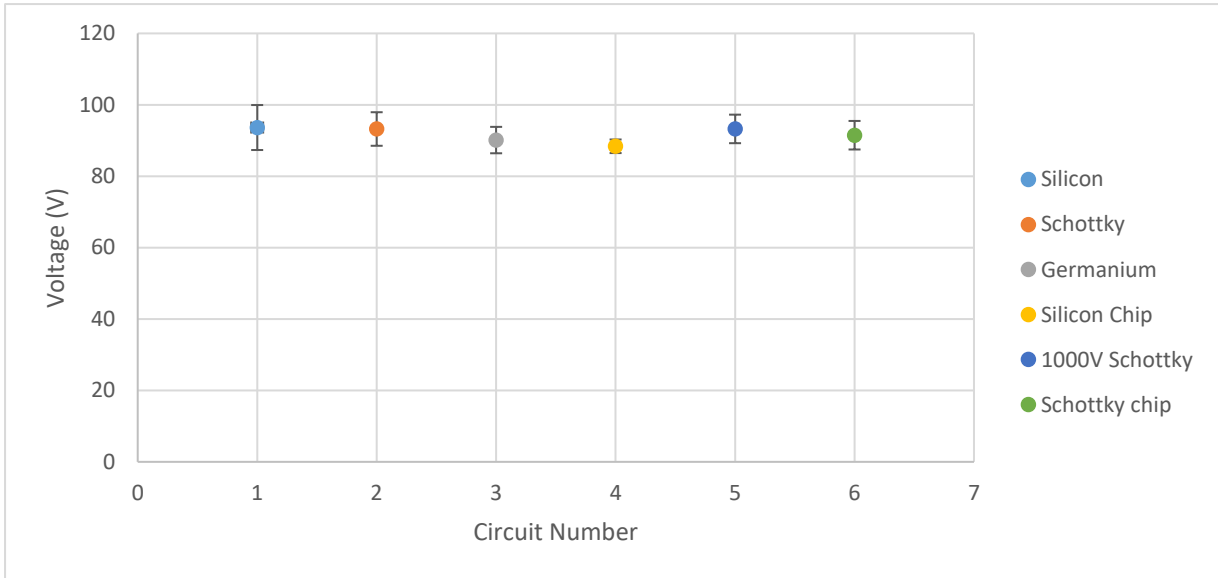


Figure 4-10 Peak One Open Circuit

Error has been obtained from one standard deviation of the average voltage measured.

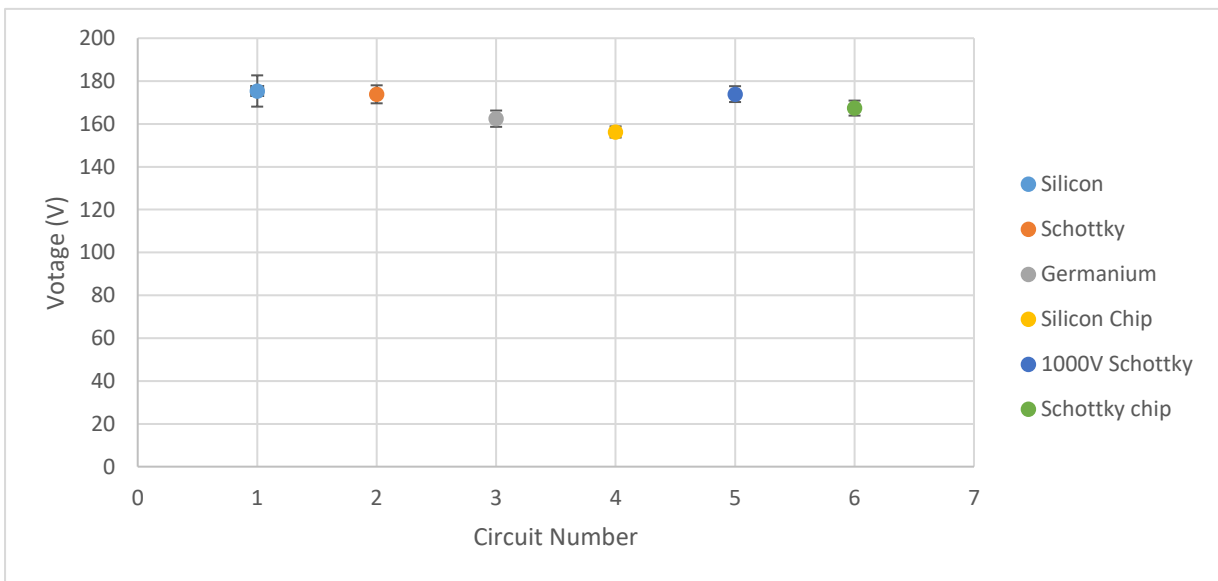


Figure 4-11 Peak 2 Open Circuit

4.4 Results: Full Wave Bridge Rectifier and Voltage Doubler Circuit with Storage Capacitor

Following the open circuit testing, the full-wave bridge rectifier and voltage doubler were then evaluated with two series capacitors. It is clear from the results that a voltage doubler

gives significantly lower output than a full-wave bridge rectifier, as shown in Table 4-4 and Figure 4-12. The results suggest that implementing a voltage doubler over the use of a full-wave bridge rectifier would result in a 67.2% reduction of the energy captured. Furthermore, the silicon signal diode rectifier has been found to store 8% more energy, when compared to the Schottky diode full-wave rectifier. This is attributed to the lower forward bias of these diodes and faster switching between positive and negative signals.

Table 4-4 Bridge and Doubler Results

Diode Type	Circuit	Actuations	Average Voltage (V)	Standard Deviation	Energy (µJ)	Difference (%)
Schottky	Bridge	157	3.06	0.16	23.44	67.39
Schottky	Doubler	101	1.75	0.04	7.65	
Germanium	Bridge	179	3.15	0.18	24.82	69.08
Germanium	Doubler	222	1.75	0.09	7.67	
Silicon	Bridge	104	3.18	0.16	25.34	65.17
Silicon	Doubler	144	1.88	0.14	8.82	

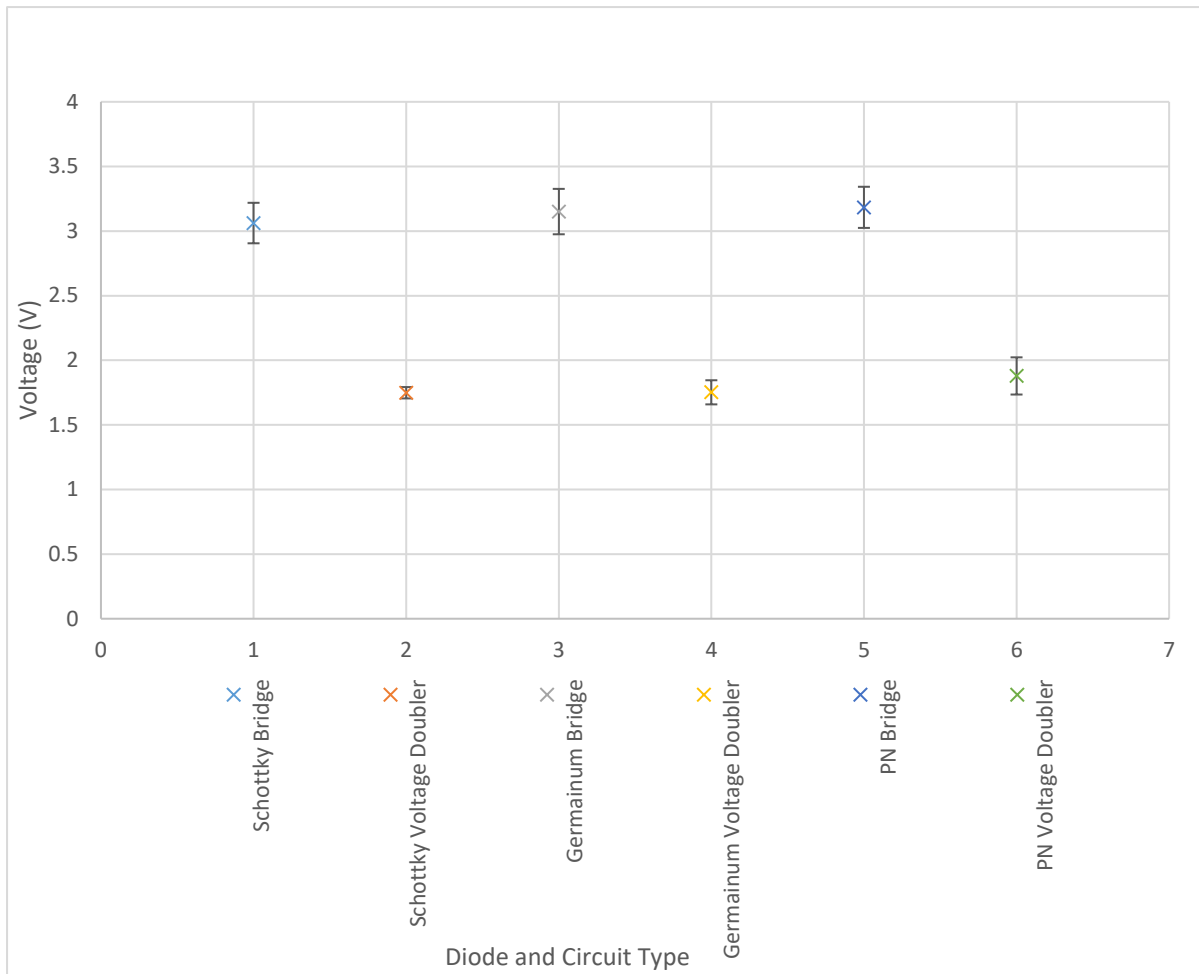


Figure 4-12 Bridge and voltage doubler comparison

Tantalum capacitors have been chosen for the storage capacitor for their low leakage properties, ensuring that the maximum amount of charge is stored, with minimal losses during signal capture and storage. Using the same experimental setup as before a buckling buzzer was actuated multiple times to reduce any statistical anomalies to produce reliable data. To identify the best storage system, capacitors of various sizes were tested. Results for $1\mu\text{F}$, $2.2\mu\text{F}$, $4.7\mu\text{F}$, $6.8\mu\text{F}$ and $10\mu\text{F}$ are displayed in Figure 4-13. Following this, the signal was captured and used to calculate the energy that is stored, shown in Table 4-5.

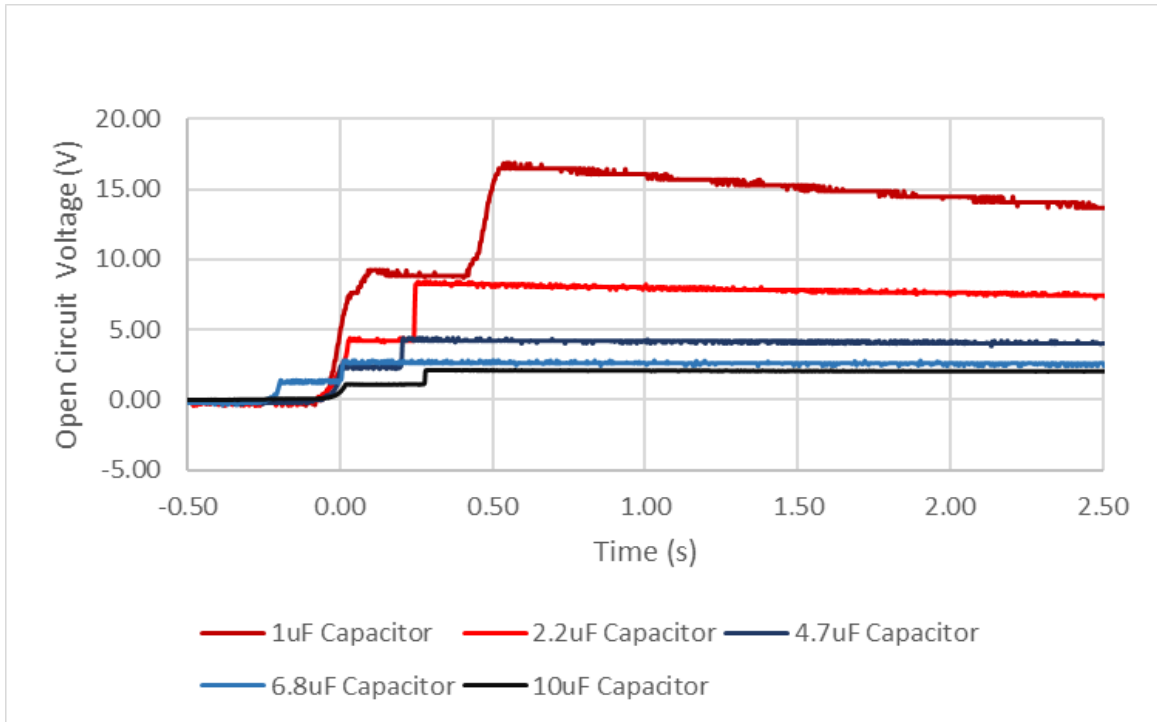


Figure 4-13 Storage Voltage

Table 4-5 Storage Energy

Capacitor Size (μF)	Average Voltage (V)	Average Energy (μ)
0.1	78.06 ± 1.727	304.668
0.34	41.58 ± 1.272	285.268
0.47	32.81 ± 1.051	252.977
1	17.5 ± 0.369	153.125
2.2	8.7 ± 0.198	83.259
4.7	4.35 ± 0.311	44.468
6.8	3.4 ± 0.0947	39.304
10	2.16 ± 0.0646	23.328

4.5 Discussion and Conclusion

It is clear from the results that using a full-wave bridge rectifier is the better technique for capturing energy from piezoelectric devices when compared to a voltage doubler. Initially, a voltage doubler appeared to be a more appropriate method of harvesting energy; this was attributed to the use of fewer diodes; furthermore, a larger voltage spike would allow for more energy to be stored into a capacitor. However, this was found not to be the case. The energy harvester output is approximately half that of the full-wave bridge rectifier.

In conclusion, a full-wave bridge rectifier using 1000V Schottky diodes should be used to improve the efficiency of an energy harvesting circuit. Furthermore, when characterising the samples produced, a more accurate assumption of the energy available can be achieved. However, there are still improvements that can be made to the testing circuit. This can be achieved using operation amplifiers (op-amp). The high impedance of an op-amp provides greater accuracy of the signal being produced from a piezoelectric device; these circuits can be made simply and adapted depending on input voltages they can also be purchased commercially.

Chapter 5 – Buckling Piezoelectric Elements

Summary

Within this chapter and investigation into the two methods of buckling for piezoelectric energy, harvesting has been performed. The first to be investigated is a pre-formed monostable piezoelectric energy harvester. The second is a preloaded energy harvester. Both methods have been shown to significantly increase efficiency of a commercially available piezoelectric transducer, creating an opportunity to produce low-cost power units for low power electronics. To validate the findings, three methods have been performed, numerical evaluation, simulation and experimental. A diaphragm structure can increase both efficiency and power output with an increase of efficiency from 0.522% to 3.765%. The observed power output increase from 191.686 μ J to 644.16 μ J. The findings for the preloaded structure demonstrate that efficiency can be increase from 0.522% to 16.813% while achieving a greater power output from 191.686 μ J to 208.577 μ J. Furthermore, this work identifies that a monostable structure as opposed to a bi or multi-stable structure can significantly produce higher power outputs, whilst achieving long life within a small compact area. This work contributes to a peer-reviewed paper **“Powering lights with Piezoelectric energy-harvesting floors” published in the journal Energy Technology.** [236]. One world patent **WO2020095064A1: Improvements in or relating to energy generation in a piezoelectric switch.** Published in May 2021 with a Priority date 09-11-2018.

5.1 Introduction

Recently, the demand for wireless sensors has gained significant interest from researchers; this has been attributed to development of the internet of things (IoT) [155]. A self-powering wireless switch is the most desired device as this will eliminate the need for regular maintenance yet collect information that can allow systems to be optimised [14, 155, 158]. Furthermore, a self-powering unit will allow for placement anywhere within the built environment without the need or restriction of electrical wiring [228, 229], thus, allowing buildings to become more versatile for disabled users. As a result, sensors have been developed that recharge batteries through the use of thermoelectric or photovoltaic modules [230, 231], however, batteries have a limited number of charge – recharge cycles [14, 232]. This is not ideal for long term use. Within this chapter, research has been performed on preformed and preloaded buckling piezoelectric transducers. This work pays attention to achieving a mono-stable structure that buckles under a low load. This is a highly desired characteristic for an energy harvester as this replicates a push-button, allowing for easy integration into existing systems. This has been broken down into seven sections that investigate numerical, simulation and experimental methods for both preformed and preloaded piezoelectric transducers.

5.2 Material identification

To ensure that the correct material properties are used throughout this work, the material properties of the metallic substrate and piezoelectric ceramic have been investigated.

A d_{33} meter is used to determine the amount of charge for a known force applied to the material. The charge is then measured, giving units in pC/N. The data from using a d_{33} meter, shown below (Figure 5-1), and the product specification for the piezoelectric ceramic was found to be PZT-5A ($350\text{pC/N} \pm 23$) [233].



Figure 5-1 D33 meter by Sinocera

The product specification states the material used for the substrate is brass. However, the properties of brass such as elastic modulus vary from 99GPa to 120GPa[234]. Through the use of a scanning electron microscope, the exact composition can be found. The images below (Figure 5-2) show the results of the test, using the rule of mixtures it was possible to identify

that the brass was made from 65% copper and 35% zinc. Using this data, the elastic modulus was found to be 112GPa and Poisson's ratio to be 0.34 [234].

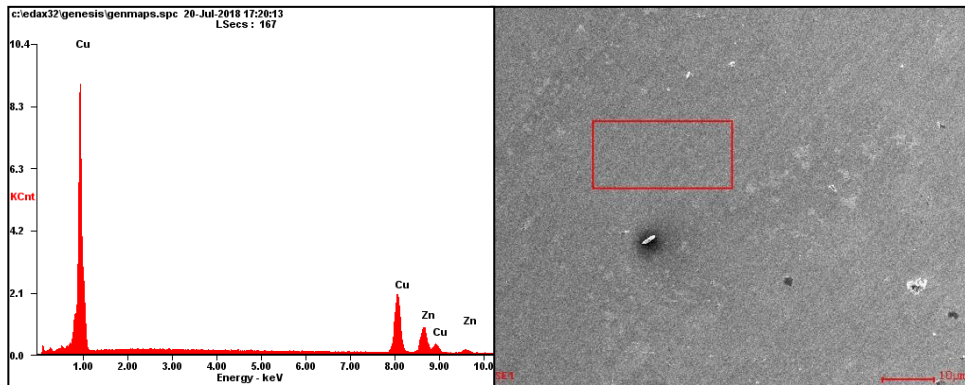


Figure 5-2 Scanning electron microscope image and material identification of brass substrate for the piezoelectric energy harvester

5.3 Manufacture

In this section of the chapter, the manufacture methods for the buckling piezoelectric elements are explained.

5.3.1 Preformed Piezoelectric Element

Through experimentation during the developments of described in the previous chapter 4 on electrical circuits, it was found that if a commercially available piezoelectric transducer's substrate was to buckle, a bistable structure could form. The result of this is a significant increase in the piezoelectric power output; however, this was at the cost to the lifetime of the piezoelectric ceramic. To gain a deeper understanding of this mechanism, the following work has been performed to identify how to achieve a mono-stable device that causes no damage to the ceramic.

To achieve a controlled preformed structure, the best method is to use a punch a die system that forms under uniform pressure. This is a common method of forming metals, most notably with vehicle bodywork such as car panels. To achieve the formation of the piezoelectric energy harvester, the piezoelectric transducer must be first placed into a die and clamped. Following this, a punch is used to compress the transducer into the die, shaping the structure. Commercially available piezoelectric transducers have been purchased from Rapid Electronics (product number: 51-7481). The dimensions have been displayed below in Figure 5-3 and listed in Table 5-1.

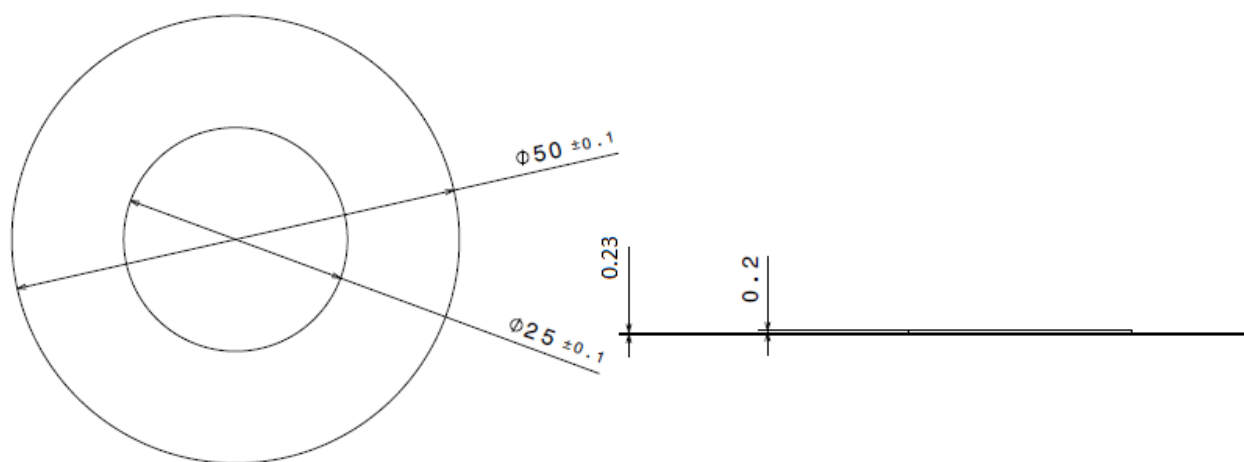


Figure 5-3 Piezoelectric transducer dimensions

Table 5-1 Piezoelectric Transducer Properties

Piezoelectric Transducer	
Substrate material	Brass
Substrate Diameter	50mm
Substrate Thickness	0.23mm
Piezoelectric Material	PZT (Lead Zirconate Titanate)
Piezo Diameter	25mm
Piezo Thickness	0.2mm
Capacitance	40±30% nF
Impedance	800Ω

The transducers have then been formed in a die shown in Figure 5-4, creating a buckling mono-stable structure shown in Figure 5-5. This structure amplifies the mechanical stresses within the PZT, thus, producing a significant increase in energy produced over a single actuation. The design allows for the structure to buckle, however, once the force has been removed it will return to its original state, allowing for the structure to be actuated multiple times without the need for complex mechanisms, once again reducing the cost of the product. Didomenico and Nussbaum suggested that the maximum poking force exerted by a human is 45.95N with a standard deviation of 17.8N [235]. Therefore, the mean force needed to actuate the switch will be 28.15N.

As discussed previously, the piezoelectric transducers have been formed using a punch and die, to achieve a mono-stable buckling structure. This is the most desired structure as it enables the structure to return to its original position after actuation, critically, the stresses associated with the structure's buckling are below the material limit of the ceramic. This means that the energy harvester can be actuated multiple times in comparison to a bi-stable system. It was found that a mechanically actuated bi-stable system's stresses are too significant to achieve repeated use without damage to piezoelectric ceramic.

Figure 5-4 shows the setup of the punch and die. It has been mounted on the tensile machine so that the forces and displacements can be monitored for the different parameters. A soft compressible surface is placed in the centre of the punch. This is to protect the piezoelectric ceramic from abrasion or doming. From over 500 tests, it was found that a maximum displacement of $2.0\text{mm} \pm 0.1\text{mm}$ and a minimum displacement of $0.6\text{mm} \pm 0.1\text{mm}$ would achieve a monostable buckling transducer, shown by Figure 5-5. The lower limit is important as anything less than this, and the stress is not enough to achieve plastic deformation of the flange.

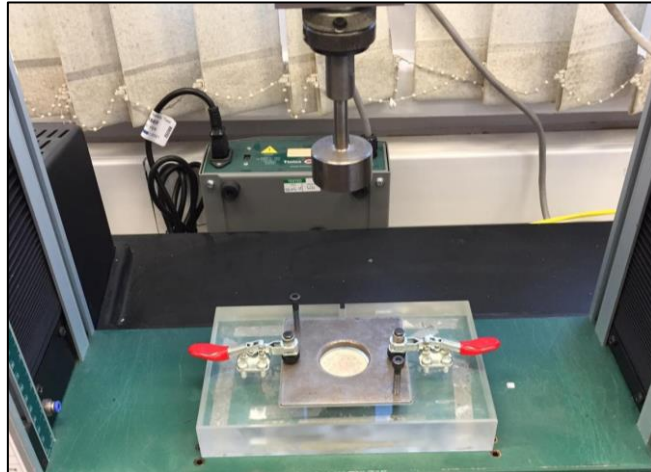


Figure 5-4 Punch and die setup

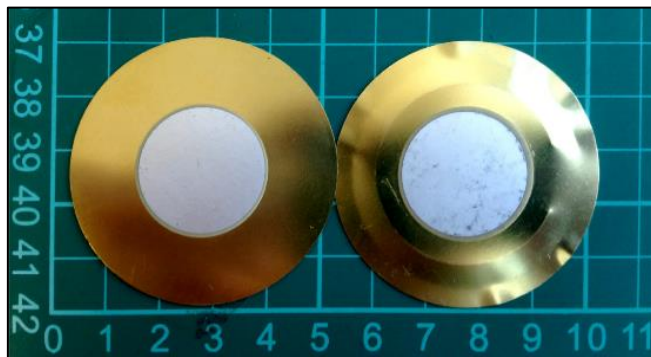


Figure 5-5 Before forming (left) and post-forming (right) piezoelectric element

5.3.2 Preloaded Piezoelectric Element

To manufacture a preloaded piezoelectric element the previous piezoelectric elements were used. However, to make them easier to clamp and smaller they were processed using a bespoke guillotine, creating uniform 25 by 25mm elements, this not only reduced the size of the elements making it easy to fit with other applications but also lighter. Figure 5-6 depicts the tooling used to produce such items.

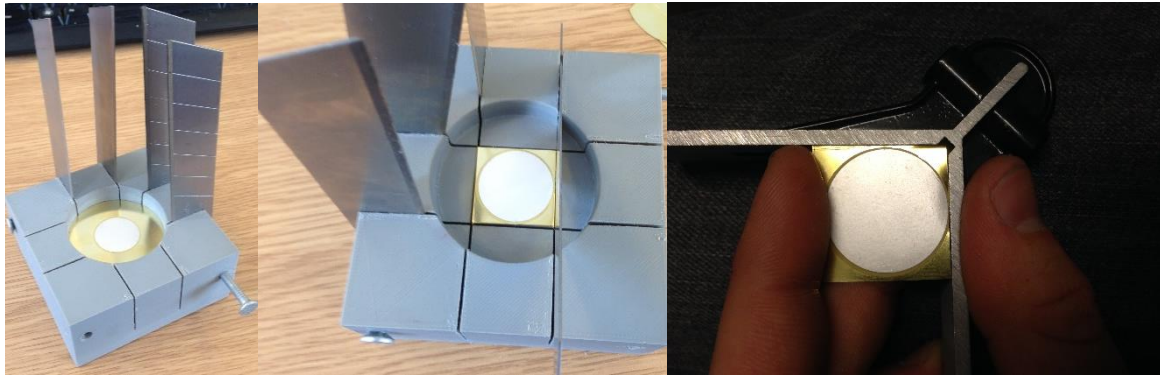


Figure 5-6 Manufacture of preloaded piezoelectric elements

Through further development of the monostable energy harvester, a new method of buckling was investigated, which involved simply supporting a piezoelectric transducer between two walls and applying a preload. This resulted in a significantly more times increase energy being extracted when the two methods are compared [236]. To achieve this, a flat piezoelectric transducer is placed between a moving wall and a fixed wall the distance between them can then be adjusted, which compresses the piezoelectric until it buckles. At this stage a curved piezoelectric transducer can be observed such as in Figure 5-7.

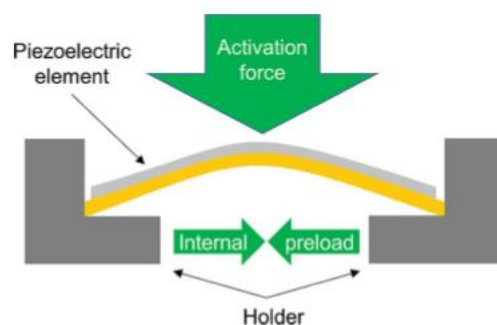


Figure 5-7 Preload piezoelectric element using solid walls to create a buckled transducer.

[236]

It was found that movement in the walls was essential for achieving a long last piezoelectric element. However, this movement caused the walls to fail due to large stresses associated with the buckling of the piezo. To avoid this, multiple iterations of the harvester were designed and tested, these can be observed in Figure 5-8 a and b.

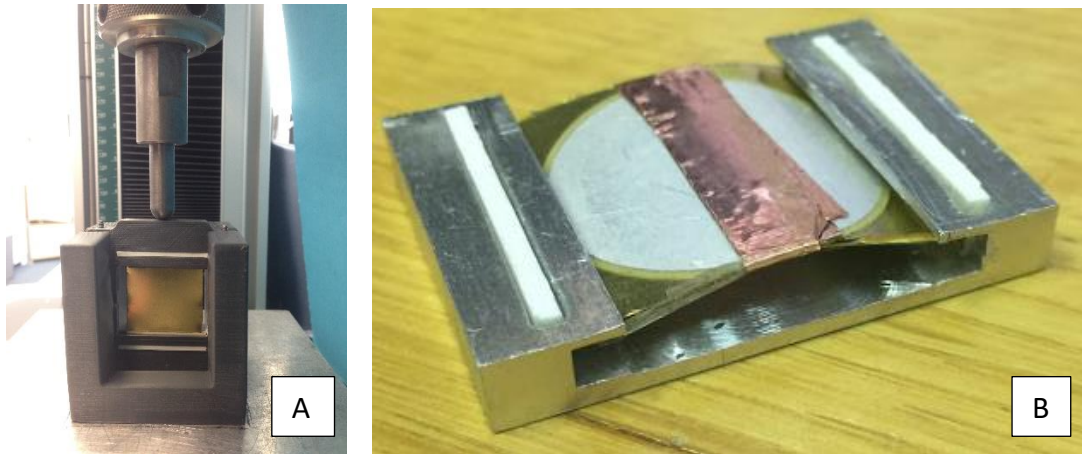


Figure 5-8 a. Buckling test equipment b. The power unit (25mm by 35mm and 3mm thick)

Figure 5-8 a. Shows a piece of bespoke equipment that was used to create the buckling structure and test for initial buckling forces. To achieve an optimised structure as shown by Figure 5-8 b. the bespoke clamp compresses the transducer using M1.8 bolts, which are threaded through the edges of the clamp to M1.8 nuts. This ensured that the piezo is mounted correctly that with a low pitch of 0.35mm excellent control of the walls can be achieved, meaning that one complete revolution of the bolt will result in the clamps moving 0.35mm. This provides accurate control over the curvature of the structure.

5.4 Theoretical Calculations

In this section of the chapter, numerical calculations have been performed to give a benchmark to validate both the simulation and experimental aspects of the work. Structural equations have been used to evaluate the buckling forces, forming forces and energy output.

5.4.1 Preformed Buckling Element

To ensure that the piezoelectric element does not break during the forming process the limiting drawing ratio (LDR) has been used. This is a ratio between the size of the work piece versus the size of the punch, shown in equation 5.1 [243, 244, 245].

$$LDR = \frac{d_0}{d_p} = \text{Steel } 2.7 \text{ and Brass } = 2.4 \quad 5.1$$

The substrate of the transducer is a copper alloy (Brass); therefore, an LDR of 2.4 will be used, to ensure that the substrate does not cause any failure. Further to this, the maximum punch force has been evaluated to ensure that during the forming process, the substrate is not damaged. This can be found using equation 5.2 [243, 244, 245].

$$F \approx \sigma_{yield} t \pi (d_0 - 0.7d_p) \quad 5.2$$

$$F \approx 2162.987N \quad 5.3$$

Therefore, to ensure the repeatability of the forming process, the punching force will not exceed 2162.987N a safety factor of 2 (1081.494N) will also be used to ensure that the structure is not close to the failure force.

To calculate the force needed to cause the structure to buckle, two methods have been investigated the first method investigated is Timoshenko's classic plate buckling theory [237], this forms the foundation of buckling diaphragms. The buckling shear force needed to achieve the buckling of a simply supported plate can be obtained using the below equation 5.4.

$$\tau_{cr} = \frac{k}{1} \times \frac{\pi^2 E}{12(1 - \nu^2)} \times \left(\frac{t}{h}\right)^2 \quad 5.4$$

Where

τ_{cr} is the critical shear force needed to achieve buckling

k is the buckling coefficient defined by the boundary conditions [238].

E is Young's modulus of the substrate

ν is Poisson's ratio for the substrate

t is this thickness of the panel

h is the web height of the panel

Completing the above equation 5.4, the buckling force of the diaphragm is found to be equal to 18.228N

The second method which has been investigated is Easley's buckling method [239, 240]. The most suitable method is the buckling for a simply supported diaphragm, which can be described by the below equation.

$$N_{cr} = k ((D_x)^{0.25} \times (D_y)^{0.75}) / b^2 \quad 5.5$$

$$D_x = \frac{Et^3l}{12s} \quad 5.6$$

$$D_y = \frac{EI_y}{l} \quad 5.7$$

Where

N_{cr} is the buckling shear load per unit length

l is the length of the diaphragm

s is the total length of the diaphragm

t is the thickness of the diaphragm

I_y is the Second moment of inertia/area of the diaphragm

E is Young's modulus of the substrate

The below Figure 5-9 can be used to visualise the design and geometry of the diaphragm. The labelled parameters have been then used to calculate s , l and I_y .

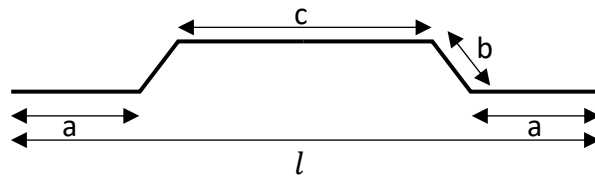


Figure 5-9 Simplified diaphragm design and geometry

The below equations 5.8 and 5.9 have been used to identify parameters for Easley's equation.

$$s = 2(a + b) + c = 50mm \quad 5.8$$

$$l = 48.8mm \quad 5.9$$

To complete the calculation of the buckling force, the second moment of area must be calculated. For this, the diaphragm was broken into six rectangular squares, where three are used due to symmetry of the structure depicted by Figure 5-10.

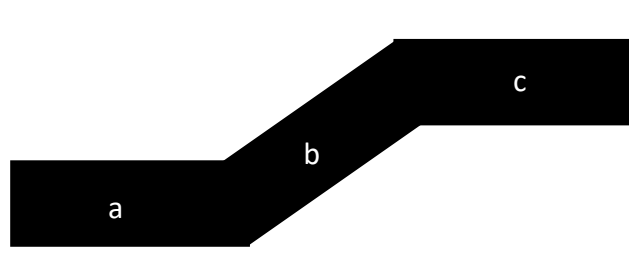


Figure 5-10 Diaphragm second moment of area assumption and breakdown

$$I_a = \frac{bd^3}{12} = \frac{3 \times 0.2^3}{12} \times 2 = 0.004mm^4 \quad 5.10$$

$$I_b = \left(\frac{ba}{12} \times (b^2 \cos^2 \theta + a^2 \sin^2 \theta) \right) \times 2 = 0.0146478mm^4 \quad 5.11$$

$$I_c = \frac{bd^3}{12} = \frac{38 \times 0.2^3}{12} = 0.0253mm^4 \quad 5.12$$

$$I_y = I_a + I_b + I_c = 0.0585956mm^4 \quad 5.13$$

With all unknowns calculated, it is now possible to calculate the buckling force for the diaphragm.

$$D_x = \frac{Et^3l}{12s} = 68.32 \quad 5.14$$

$$D_y = \frac{EI_y}{l} = 126.077 \quad 5.15$$

$$N_{cr} = k \frac{((D_x)^{0.25} \times (D_y)^{0.75})}{b^2} = \frac{973.546N}{50mm} = 19.471N \quad 5.16$$

A small difference can be observed between the Timoshenko method and Easley's method. This has been attributed to the increased stiffness that has been included in Easley's method. These findings will be used to verify the simulation model of the preformed buckling transducer, where the percentage error can be calculated. This identifies the error between the two methods the below equation has been used.

$$Error_{\%} = \frac{19.471 - 18.228}{18.228} \times 100 = 6.819\% \quad 5.17$$

The error observed between the two methods displays a good fit for both methods of modelling and evaluating the diaphragm model.

With the buckling force calculated, the below equation can be used to predict the voltage produced by piezoelectric material during buckling.

$$V = \frac{4 \times g_{33} \times F \times t}{\pi D^2} \quad 5.18$$

$$V_{Easley} = 60.7495V \quad 5.19$$

$$V_{Timo} = 56.8714V \quad 5.20$$

Where

F is the force acting over the whole element

t is the thickness of the piezoelectric element

g_{33} is the voltage constant for PZT-5A

Assuming that the piezoelectric element returns to its original position a half the energy is lost during this process can be increased by 1.5 providing a peak to peak voltage for Easley's and Timoshenko's methods of 91.124V and 85.307V, respectively.

To evaluate the energy that is being produced the below capacitor equation can then be implemented.

$$E = \frac{CV^2}{2} \quad 5.21$$

$$E_{Easley} = \frac{40nF \times 91.124^2}{2} = 166.072\mu J \quad 5.22$$

$$E_{Timo} = \frac{40nF \times 85.307^2}{2} = 145.546\mu J \quad 5.23$$

The result of the energy calculations highlights that a small difference in the actuation force can lead to approximately two times the error in the energy calculation. Therefore, any model developed to predict this behaviour much to be highly accurate.

5.4.2 Preloaded Buckling Element

To enhance the power output of a piezoelectric transducer, a curved structure must be produced. In the case of this research commercially available piezoelectric transducers have been purchased and cut to 25mm by 25mm squares around the piezoelectric material, using a bespoke punch and die set. To create a curved structure, a clamping force is applied to the plate. Initially, the structure is stable, however, when a critical force is achieved the structure buckles into its first mode, as shown by Figure 5-11 a), the second buckling mode by b) and the third c). To identify the critical force for the three different buckling modes, the Euler-Bernoulli's equation has been applied as shown by equation 5.28, where n is the mode number. It should be noted that other buckling modes can only be achieved through webs within the structure; therefore, this application will only focus on the first buckling mode for a simply supported, pinned-pinned beam.

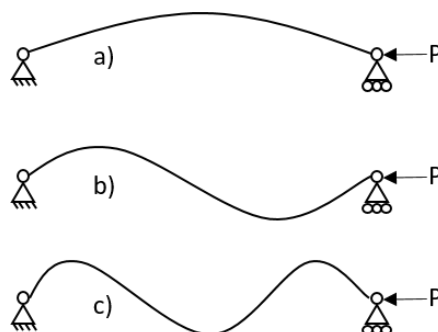


Figure 5-11 Buckling modes (1,2 and 3) for a perfect slender beam

Euler-Bernoulli's equation can be used if the beam is a slender beam. This can be identified using equation 5.24.

$$\frac{nL}{r} \geq \sqrt{\frac{\pi^2 E}{\sigma_y}} \quad 5.24$$

$$433.099 \geq 32.550 \quad 5.25$$

$$I = \frac{bd^3}{12} = 0.00235 \text{mm}^4 \quad 5.26$$

$$r = \sqrt{\frac{I}{A}} \quad 5.27$$

Where

k effective length factor that is determined by the clamping conditions

L is the length of the beam

b is the breath of the beam

d is the depth of the beam

I is the second moment of area

A is the cross-sectional area

r is the radius of gyration

E is the elastic modulus

σ_y is the yield stress

$$P_{cr} = \frac{n^2 \pi^2 EI}{(kl_0)^2} \quad 5.28$$

Where

k is the effective length factor that for a simply supported structure is equal to 1

l_0 is the original length of the beam.

To achieve the first buckling mode, a compressive force of 16.66N must achieve this which corresponds to $3.332 \frac{N}{mm^2}$. As the force increases, the different buckling modes can be observed at 66.64N and 149.94N. Although these buckling modes resemble the modes of buckling for the harvester, they are not applicable as the force is in-plane with the structure. This said, the clamping force must be between 16.66N and 66.64N, or with a stress of $3.332 \frac{N}{mm^2}$ and $13.328 \frac{N}{mm^2}$, respectively to achieve the correct shape for the higher output energy of the harvester.

Once an initial structure has been calculated the second stage of calculations can be performed to identify the force needed to buckle the structure. For this, Timoshenko's method has been used [237] shown by equation 5.29 and Figure 5-12.

$$P_{cr} = \frac{EI}{R^3} \left(\frac{4\pi^2}{\theta^2} - 1 \right)$$

5.29

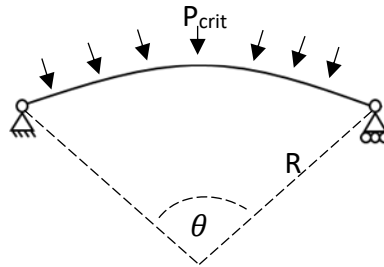


Figure 5-12 Hinged- Hinged shallow arch with uniformly distributed load

The below Table 5-2 has been used to identify the critical buckling force for a hinged-hinged arch the results of this shows the minimal change to the buckling force will be achieved from increasing the height of the arch's curvature. For additional comparison, this calculation has been calculated for fixed-fixed in-plane loading using equation 5.30 with results shown in Table 5-3.

.

Table 5-2 Hinged- hinged loading of a shallow arch with uniformly distributed load

Height of Arch (mm)	The radius of Arch (mm)	Width of Arch (mm)	Angle Arch (rad)	P_{crit} (N)
0.6	130.108	24.961	0.192	1.184
0.8	97.522	24.931	0.256	1.578
1	77.958	24.893	0.320	1.972
1.2	64.903	24.845	0.385	2.366
1.4	55.569	24.789	0.449	2.760
1.6	48.559	24.724	0.514	3.153

$$P_{cr} = \frac{EI}{R^3} (K^2 - 1) \quad [237]$$

5.30

$$K = 21.037 - 0.322439\theta + 0.0024401\theta^2 - 9.69329 \times 10^{-6}\theta^3 \quad [237]$$

$$+ 1.94155 \times 10^{-8}\theta^4 - 1.53892 \times 10^{-11}\theta^5 \quad 5.31$$

Table 5-3 Fixed-fixed in-plane loading of a shallow arch

Height of Arch (mm)	The radius of Arch (mm)	Angle Arch (rad)	K	Pcrit (N)
0.6	130.11	0.19	20.98	0.56
0.8	97.52	0.26	20.95	1.32
1	77.96	0.32	20.93	2.57
1.2	64.90	0.39	20.91	4.45
1.4	55.57	0.45	20.89	7.08
1.6	48.56	0.51	20.87	10.58

The results from Table 5-2 and Table 5-3 show that the buckling force for this structure is equal to 1.97N for a 1mm increase in height. From this buckling data shown and the equations 5.18 and 5.21 the energy output of this form of buckling energy harvester. Table 5-4 visualises visualises the power output of the system depending on the curvature of the harvester.

Table 5-4 Energy output of the preloaded buckling piezoelectric transducer

Height of Arc	Force Hinge-Hinge	Force	Voltage Hinge-Hinge	Voltage Fixed-Fixed	Energy Hinge-Hinge	Energy Fixed - Fixed
mm	N	N	V	V	Ⓜ	Ⓜ
0.6	1.184	0.555	2.012	28.314	0.081	16.034
0.8	1.578	1.317	4.774	37.750	0.456	28.501
1	1.972	2.573	9.327	47.178	1.740	44.516
1.2	2.366	4.450	16.131	56.603	5.204	64.078
1.4	2.760	7.077	25.654	66.021	13.162	87.174
1.6	3.153	10.584	38.366	75.431	29.439	113.796

5.5 Numerical Simulation

The use of computer-aided engineering tools has allowed engineering to technology to grow rapidly. To understand the need for this study, first, an understanding of finite element analysis (FEA) is needed. Using computer-aided design (CAD), a structure or geometry can be produced. This should be an accurate representation of the object or structure that is to be evaluated; this being said, the use of symmetries can be used to reduce the size of the component. This model can then be inputted into the solver. For this work, COMSOL

conditions for the system are defined. Following this, the mesh should be defined. Mesh is a critical aspect of any FEA study.

A mesh is made up of small domains. These domains are known as elements; these break a large object down into smaller parts and are used to approximate governing equations. The dependency of mesh is linked to the size of the elements used and their location with regards to the critical aspects of geometry. Increasing the size or number of elements increases the accuracy of the analysis. However, this comes at the expense of computational power and time. Therefore, particular attention should be paid to mesh when analysing and validating models. For this research, one simulation model has been produced, which uses two varying geometries. These have been evaluated with respect to the critical buckling force and the stress generated during the buckling phase. Using the results, it is possible to predict the power output of a piezoelectric energy harvester theoretically. The buckling force method can be used to calculate the actuation force. This is critical for applications involving human motion, such as finger actuation, as low forces are required to enable a broad spectrum of users. Previous studies have investigated the “snap-through” buckling of bi-stable systems. This method of energy harvesting generates a single pulse of energy and occurs due to the instability between the system switching phases. The scope of this work is to focus on the mono-stable region, in which, bi-stable buckling beams return to their original position. The use of this mono-stable region is an effective way to generate electrical power without damaging the piezoelectric element. The theory behind the mono-stable buckling is that two pulses of energy will be created equal to or greater than a bi-stable system. Furthermore, the

use of low buckling forces will ensure that the piezoelectric elements are not damaged, with the desire of ensuring that the harvesters have a long service life.

To ensure that the models provide accurate predictions for the buckling behaviours and stress, careful consideration of the geometry must be made. This includes; dimensions, the height of curvature, thickness, Young's modulus, Poisson's ratio, spring stiffness, clamping conditions, force application, mesh type and mesh size.

5.5.1 Preformed Piezoelectric Element

To create an accurate simulation model of the preformed piezoelectric element. CATIA V5 was used to draw the geometry used in the numerical evaluation of the preformed element. This was achieved through surface modelling. Surface modelling was selected over solid modelling for its ease of use when creating thin-skinned items such as the substrate of the element, plastic containers or objects with complex surface profiles. The profile of the diaphragm was modelled using lines and points (Figure 5-13). Following this, a revolve operation was used to create the completed model (Figure 5-14). This was then saved as a .stl file allowing it to be imported into COMSOL Multiphysics.

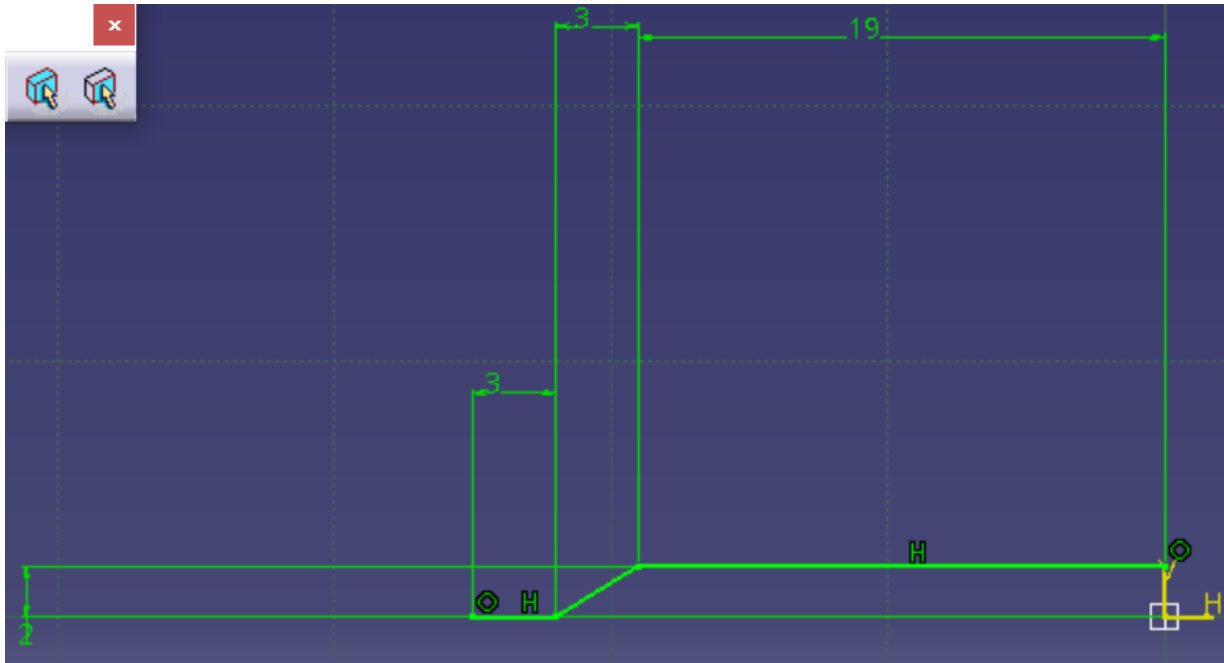


Figure 5-13 Points and lines for the buckling piezoelectric element

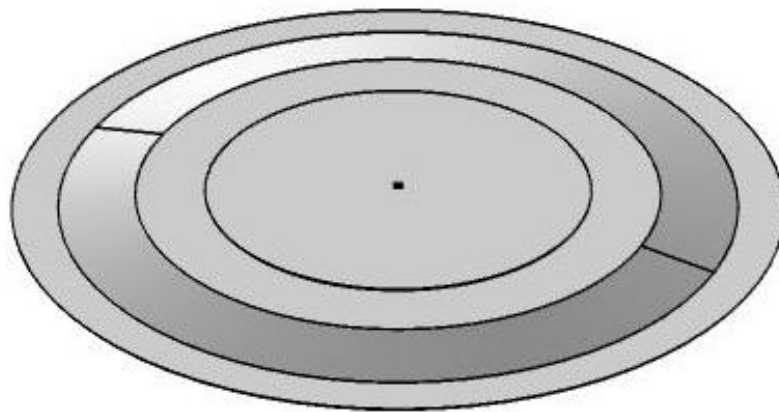


Figure 5-14 Full revolved model of a preformed buckling element

A linearized buckling study has been performed on this structure to identify the critical force needed to achieve the structure to buckle. This is a predefined study that is made of two steps. The First is a stationary solver where a load is applied to the centre of the diaphragm, and the second step is an eigensolver that is used to identify the critical buckling load.

This simulation works by solving for a stationary load known load (F) based on the stiffness of the structure. The following equation can be used to identify

$$K\mathbf{x} = (K_L + K_{NL})\mathbf{x} = \mathbf{F} \quad 5.32$$

Where

K is the total stiffness of the structure

K_L is the linear stiffness of the structure

K_{NL} is the nonlinear stiffness of the structure

A relationship between the linear and nonlinear stiffness shows it to be proportional to the stress in the structure due to an external load (F), therefore if the linear part is solved an initial value for F can be obtained. The nonlinear problem can then be written as

$$(K_L + \lambda K_{NL}(\mathbf{x}_0))\mathbf{x} = \lambda \mathbf{F}_0 \quad 5.33$$

Where

λ is the load multiplier

For the first step to be completed the equation must become singular, at this stage, the displacement tends toward infinity. The value of F at this value is then used in the second study step, where the eigenvalue problem can then be solved for λ .

$$(K_L + \lambda K_{NL}(x_0))x = 0$$

5.34

The output of this study shows a value for λ , which is a load multiplier for the load applied given the boundary conditions. This is a factor to find the critical buckling force of the structure. If λ is larger than 1 then the applied load is smaller than the buckling force; if the force is applied in the opposite direction λ will become negative. Simply multiply the applied load by λ will provide the critical buckling load for the structure.

Boundary conditions for the preformed harvester show simple support on the internal ring of the flange with a point load act in the negative Z-direction at the centre of the diaphragm shown by Figure 5-15.

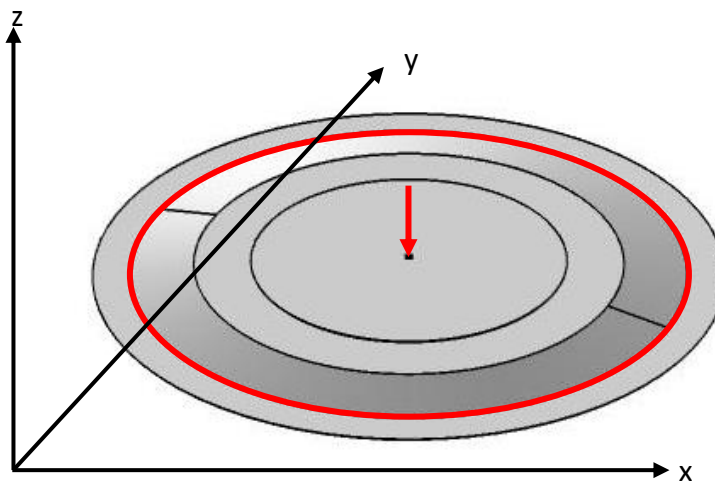


Figure 5-15 Boundary conditions for the preformed piezoelectric element

5.5.2 Preloaded Piezoelectric Element

Before gathering data and solving, computer-aided design (CAD) must be used to generate a structure that represents the structure of the piezoelectric transducer that is to be tested. In the case of this study, various geometries have been produced for two models of a piezoelectric transducer. Models for the 25mm by 25mm transducer have been generated in CATIA V5 using surface modelling.

Surface modelling is the most appropriate method of generating a reliable import file for COMSOL. As this system only uses point and lines, the resulting imported mesh is accurate, thus increasing the accuracy of the simulated model.

To create the geometry, a circle was drawn with a dependant radius. This is critical as the only known length is the original length of the piezoelectric transducer, which is equal to 25mm. From the centre point, three construction lines are added to the vertical drawing one, intersecting the circle and to that are mirrored either side of this axis (Figure 5-16). On these lines, points are added that coincide with both the circle and the mirror lines. From this, the outer part of the circle is removed, leaving only an arc. A horizontal line is now added to the drawing to measure the arc height. This will then be used to control the geometry for later designs.



Figure 5-16 CATIA V5 modelling of the arc with reference dimensions and controlled dimensions.

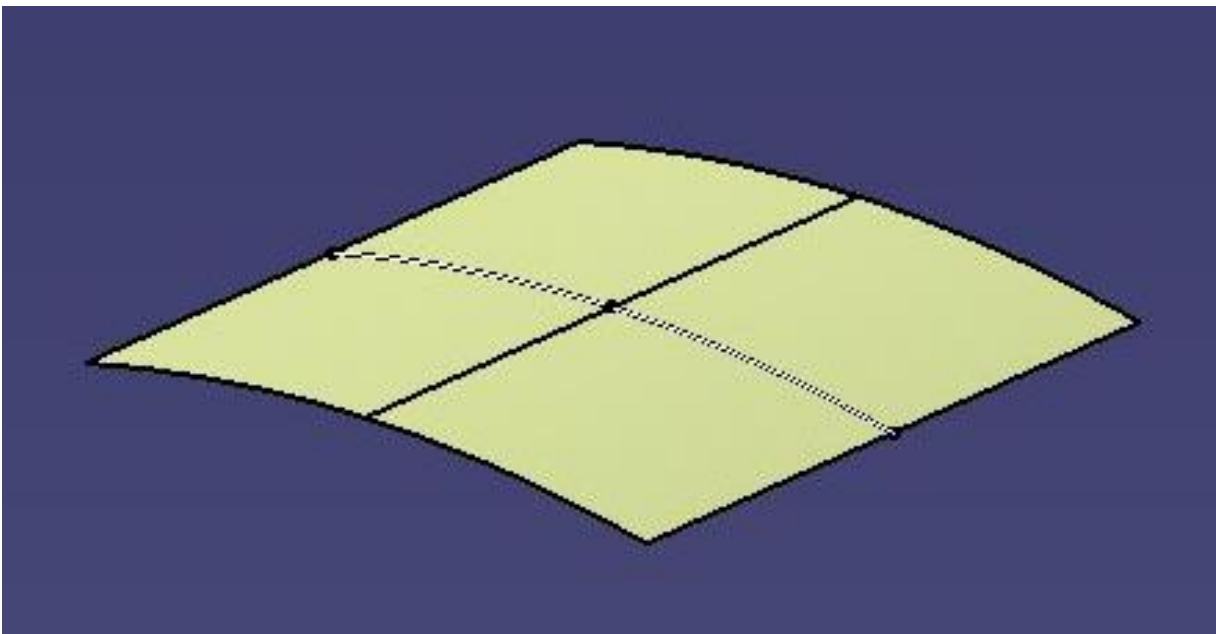


Figure 5-17 Extruded quarter model, creating a complete curved arch

This method of design has been chosen as it allows simple adaptation of geometry, furthermore, the desired modelling technique in COMSOL has used a shell structure that can only be generated in the generative shape design module of CATIA. Using this geometry, it is possible to ensure the length of the product does not change in keeping with a physical specimen, where one was limited to 25mm. The above figures; Figure 5-16, Figure 5-17 and Figure 5-18 demonstrate the geometry critical to the analysis. Various heights have been generated and saved as .stp files to ensure that they can be imported into COMSOL.

To solve a problem like this, a stationary study has been performed with a nonlinear solver. The solver selecting used damped Newtonian method. This can be written as

$$\mathbf{f}(\mathbf{U}) = 0 \quad 5.35$$

Where

$\mathbf{f}(\mathbf{U})$ is the residual vector

\mathbf{U} is the solution vector

This method works by selecting an initial solution for \mathbf{U}_0 . COMSOL then produces a linearized model using \mathbf{U}_0 as the linearized point. Giving the form of equation 5.36 for a Newton step of $\delta\mathbf{U}$.

$$\nabla \cdot \mathbf{f}(\mathbf{U}_0) \delta\mathbf{U} = -\mathbf{f}(\mathbf{U}_0) \quad 5.36$$

Following this, a second iteration is performed that introduces a damping factor

$$U_1 = U_0 + \lambda \delta U \quad 5.37$$

Where

λ is a damping factor between 0 and 1

The next step is then used to estimate the error from the new iteration in comparison to the previous. This is completed using the below equation 5.38

$$f(U_0)E = -f(U_1) \quad 5.38$$

Where E is the difference between the previous step, this enables a visualisation of the convergence of the solver. If the error calculated is larger than the error previously calculated the software continues to reduce the damping factor (λ) trending towards zero and recomputes for U_1 . This continues until a solution is smaller than the previous error or when the minimum damping factor is met. If the later is achieved termination of the computation will occur. If a smaller error is found, the computation moves on to the next Newtonian step.

Once imported into COMSOL, the boundary conditions for the simulation can be defined. This includes the clamping and test setup. To ensure repeatability, all tests have been performed under the same conditions. The below image depicts that original conditions where a point load is applied to the centre of the curved structure, which is also the highest point. The two-parallel edges are simply supported in the Z direction allowing for the structure to move in both the X and Y axis, however, due to the location and direction of the point load no movement can be observed in the X-direction, this setup can be observed from Figure 5-18.

A final condition represents the hyperelastic material, which for this simulation is Silicone

rubber. The purpose of this material is to behave like a spring, in which, resistance to travelling in the Y direction is achieved creating both the snap-through at a higher input force, more importantly, a snap-back motion desired for energy harvesting. It was found that if this material is too stiff or the structure is clamped, it becomes too stiff and prevents a snap-back motion that is most desired as shown by the below Figure 5-19, where the blue line shows that a reduction in force to approximately 1.3N will result in the snapback of the structure. However, with the orange line, a pulling action is needed of -0.5N is needed, meaning that no return will be observed.

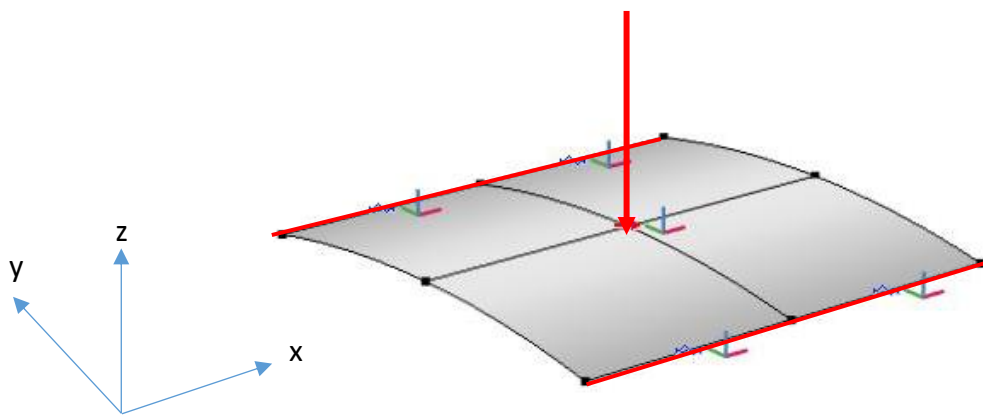


Figure 5-18 Imported model of buckling arc with boundary conditions applied

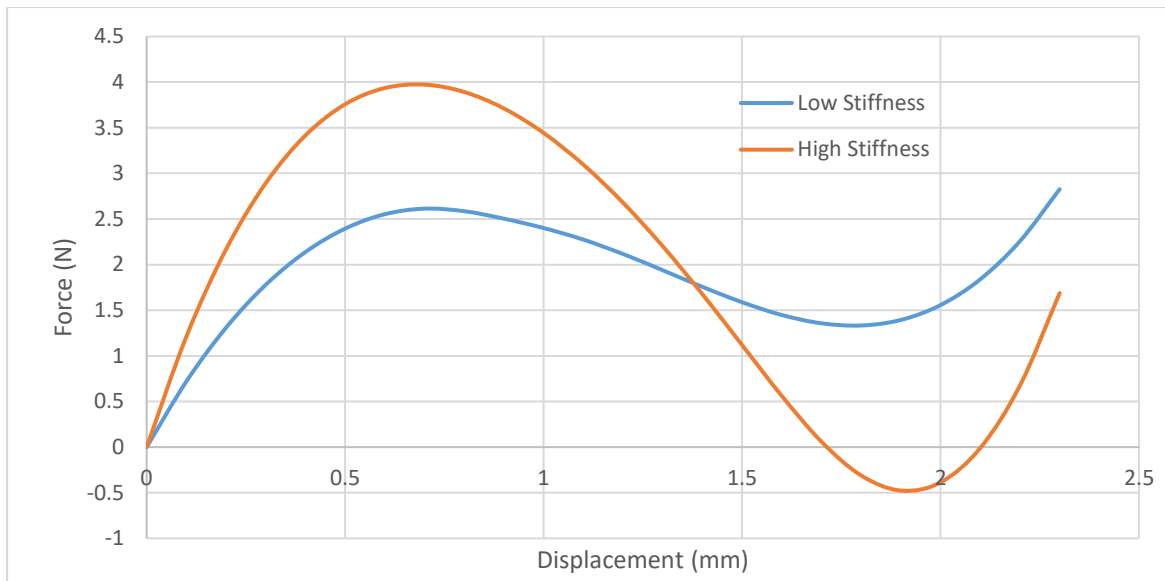


Figure 5-19 Demonstrates how buckling force related to the stiffness of the structure. High stiffness increased the buckling force, resulted in a bi-stable system, however with elastic walls simply support, system is transformed into a mono-stable system, this can be observed with the blue plot.

The simulation uses a 1mm curvature height 25 X 25mm piezoelectric transducer. Following the orange plot for which in this case is a ridged beam, it can be observed that the stiffness of the structure is increased, this is attributed to the increased gradient prior to the critical buckling force (0-0.5mm displacement). The first peak observed on the plot shows that critical buckling force for the structure. This can also be observed to be more significant when the stiffness is increased. Following this phase, a steep decline is observed (0.7-1.7mm displacement). This gradient shows that the rate of the snap-through of the beam. If this is too steep damage can occur in the piezoelectric element. The minimum point of the plots shows the force at which the snap-back of the beam will occur. If this point is greater than zero, enough energy is retained into the system for it to return to its original position,

however, if the force becomes negative a second stable state has been reached, causing the mono-stable region to cease to occur. To ensure that the stiffness is represented appropriately for the simulation model, experiments have been performed on Silicone rubber to identify the compressive properties which have then been used to inform the model correctly.

Through integrating (operator *intop1*) the centre point for the given displacement of the model it is then possible to identify the force being applied to the structure throughout each of the time steps and then generated a plot of the buckling behaviour.

The edges of the simply supported system were clamped along the edge, this then prevented any in-plane translation of the structure under load.

A nonlinear method for solving the problem has been applied. The method used is the Newton method. This was used for the highly nonlinear behaviour of the model. To control this method, three constants can be used; initial damping factor, minimum damping factor and restriction for the step-size update. The initial damping factor is the value used for the first Newton method. This was set to $1.0E-4$. The minimum damping factor is used to specify the smallest allowable damping factor that is was set to $1.0E-8$. Restriction of step-size update is used to limit how much the damping factor can change in an iteration and was set to 10. It should be noted that if the solver was to get stuck, resulting in no convergence of the system, a recovery damping factor should be used. This allows the solver to recover the damping

factor and continue to solve the equation with extra steps with the view of the solution converging; this was set to 0.75.

As stated previously, the mesh of any FEA is critical to the validity and accuracy of any results obtained. As a result, a mesh convergence study has been performed. A mesh convergence study involves reducing the mesh size until the results converge; it is then a matter of identifying a point where results are close while still maintaining a fast solution speed. This is a particularly effective method when using computers with low processing speeds.

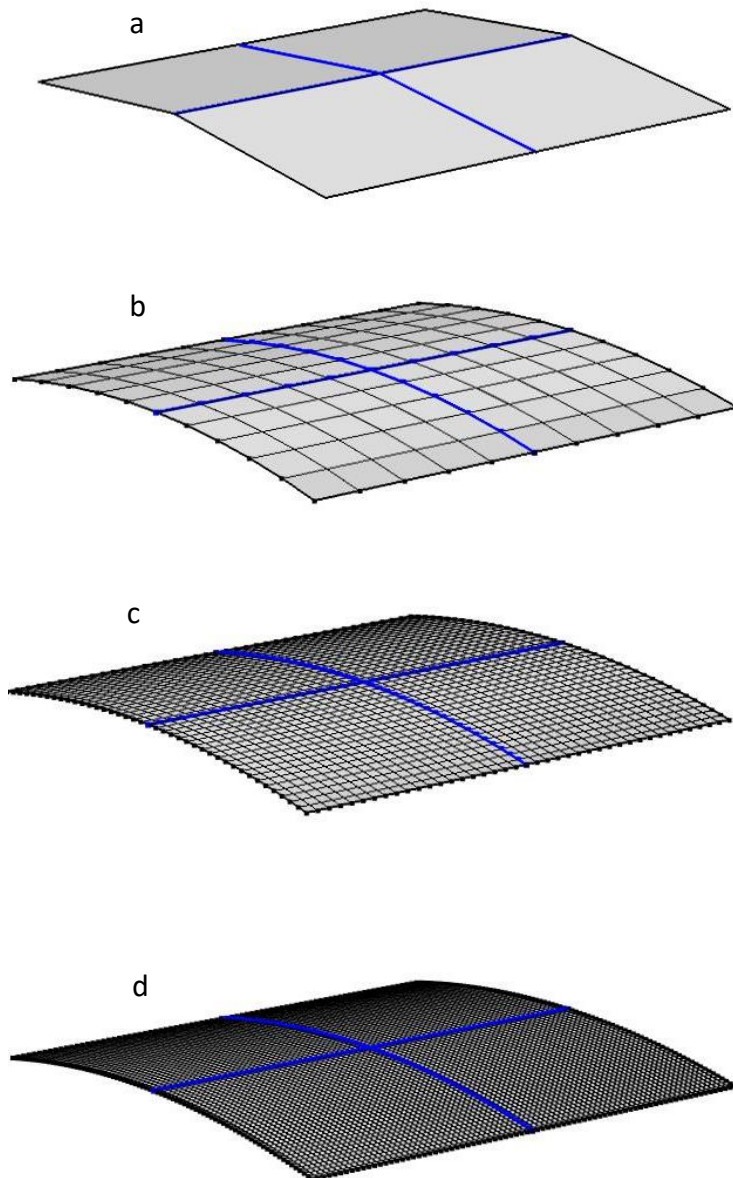


Figure 5-20 Mesh optimisation for buckling preloaded piezoelectric square element a. 12.5mm (4 elements) b. 2.5mm (100 elements) c. 0.625mm (160 elements) d. 0.4167mm (200 elements)

Using a 25mm model imported from CATIA V5 as a .stp file, a mesh convergence study was performed using mapped mesh, where a sweep from 4 to 200 elements in steps of 4 was

performed, this is equal to a maximum and minimum element size of 15.625mm² to 0.0625mm². A mapped mesh was chosen as the object; in this case, the curved structure is reasonably rectangular; it is a solid unit. Therefore, there was no need to change mesh around holes within the structure, the shape of each of the four domains are equal, and the use of a 2D shell model allows a fast and accurate prediction of the structure's behaviour under load. It can be observed in Figure 5-20 that as the number of elements increases as does the curvature of the structure, therefore, the higher the number of elements, the higher the accuracy of the analysis.

The results of the study have been displayed below (Figure 5-21). It can be observed that as the number of elements increases the closer the result, this is the convergence of the mesh. It has been identified that the most accurate and fastest mesh geometry is 1600 elements. Therefore, to ensure that reliability and repeatability of results, this is the number of elements that will be used throughout the further studies to be performed on the curved buckling beams.

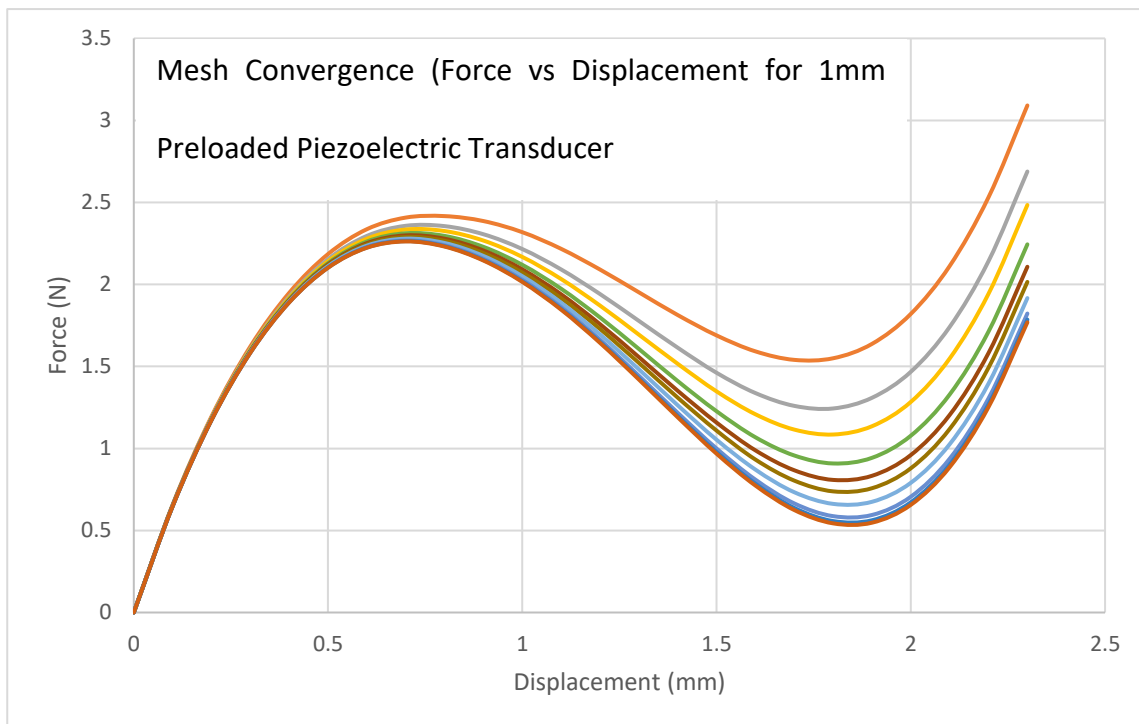


Figure 5-21 Mesh convergence study results for a buckling beam piezoelectric energy harvester.

5.6 Experimental – Introduction

To validate the numerical and simulated results, experiments have been performed that collect data on the performance of the buckling piezoelectric element. For this, a tensile machine and oscilloscope have been used to collect data relating to mechanical and electrical forces. The tensile machine that was used was a Tinius Olsen 25ST. This has an error of 5% during capture with sample rates at 20Hz. The Oscilloscope used to capture the voltage output of the piezoelectric transducer was from Keysight (Keysight MSOX3014T), due to the speed that the signals generate a high sample rate of 1GHz was used this ensured a smooth capture of the signal with minimal loss in the peak voltage due to sampling. Both pieces of equipment have been calibrated by the manufacture and were within date during use.

The setup for the system involved using the tensile machine in compression where a bespoke adapter was used to create the structures of the piezoelectric element and later actuate them to generate power. This can be observed in Figure 5-22.

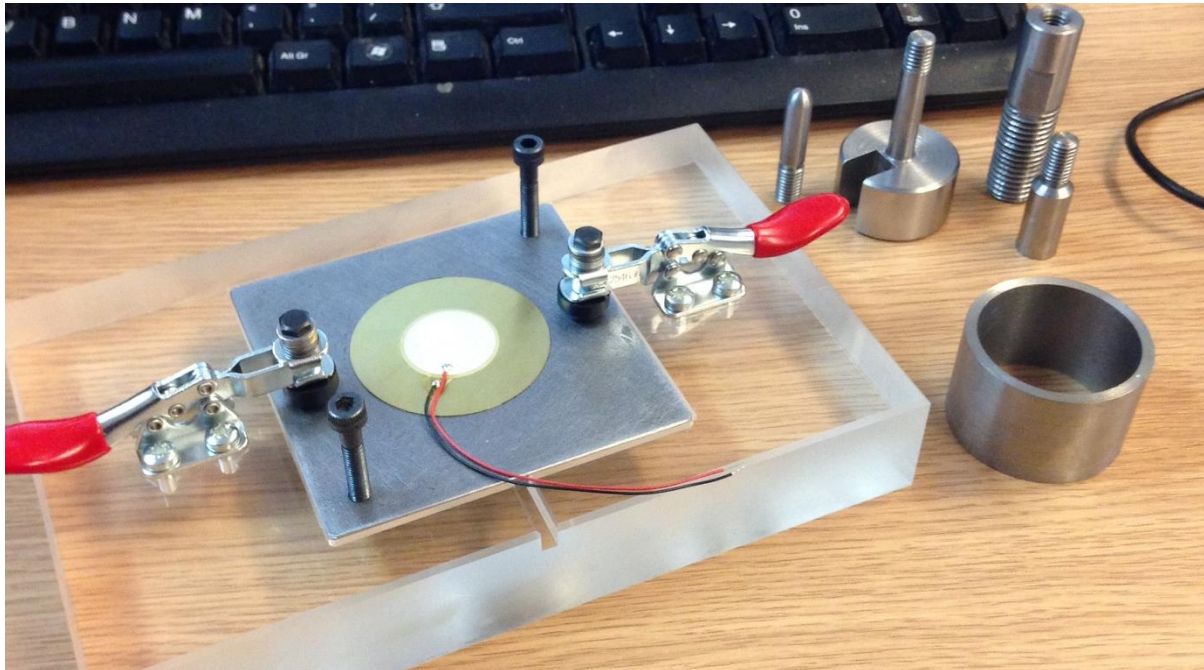


Figure 5-22 Tensile machine testing equipment

5.6.1 Preformed Piezoelectric Element

This section has been broken down into three subjects; the first is the experimental method that investigated the formation of the preformed piezoelectric element. The second is the data collection of the force needed to actuate the preformed piezoelectric element. The third is the data collection for the power output of the piezoelectric elements.

During the initial stages of this project, it was found that buckling piezoelectric harvesters produced significantly greater amounts of energy than commercially available counterparts.

However, most methods of creating a buckling structure are uncontrollable. Therefore, the manufacturing method of pressing has been investigated to produce repeatable and reproducible buckling structures that can be used commercially for energy harvesting. This initial involved designing a punch and die shown by the below Figure 5-23.

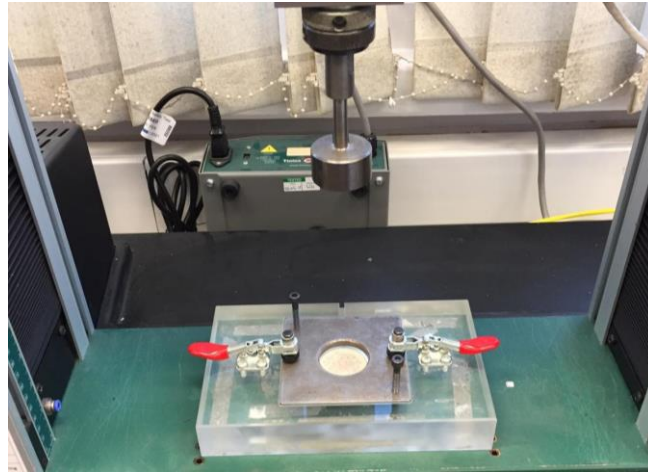


Figure 5-23 Punch and die set up on tensile machine ready for forming

To form the piezoelectric elements, the top plate is removed; following this, the element is placed ceramic side down into a milled hole with a tolerance of 0.1mm (Figure 5-24).

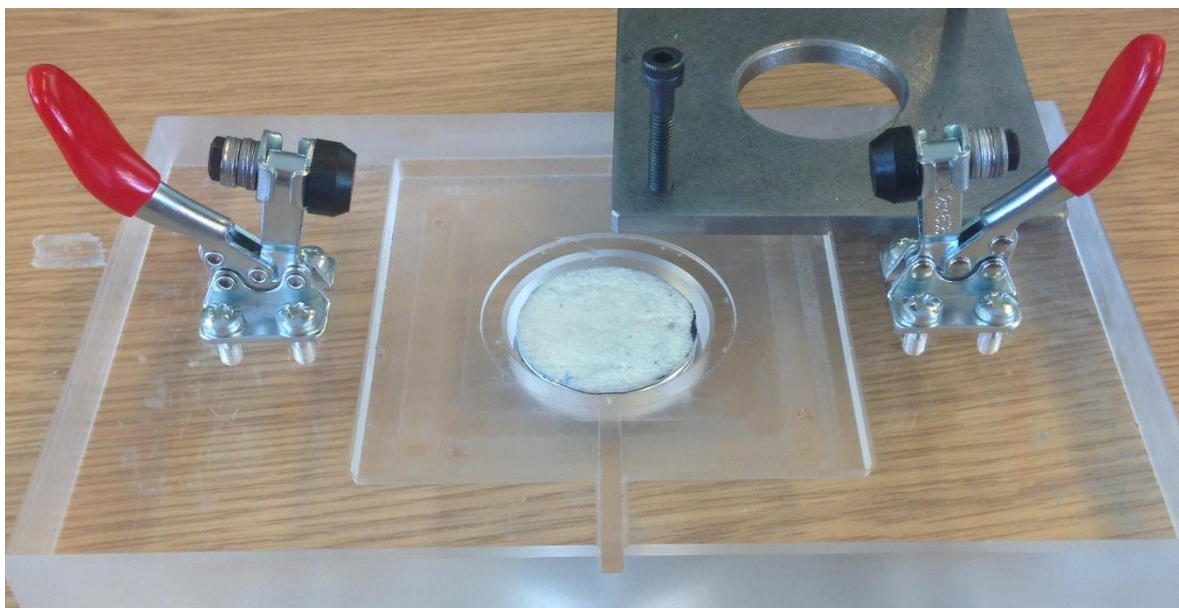


Figure 5-24 Die layout for clamping the piezoelectric element

Once secure, the top plate is returned to its original position. Toggle clamps are then applied, applying pressure to the element which prevents warping of the edges of the piezo. The below Figure 5-25 shows both a clamped and unclamped piezoelectric element, on the edges of the piezoelectric element wrinkling can be observed. This is due to a low clamping force of the flange during pressing.

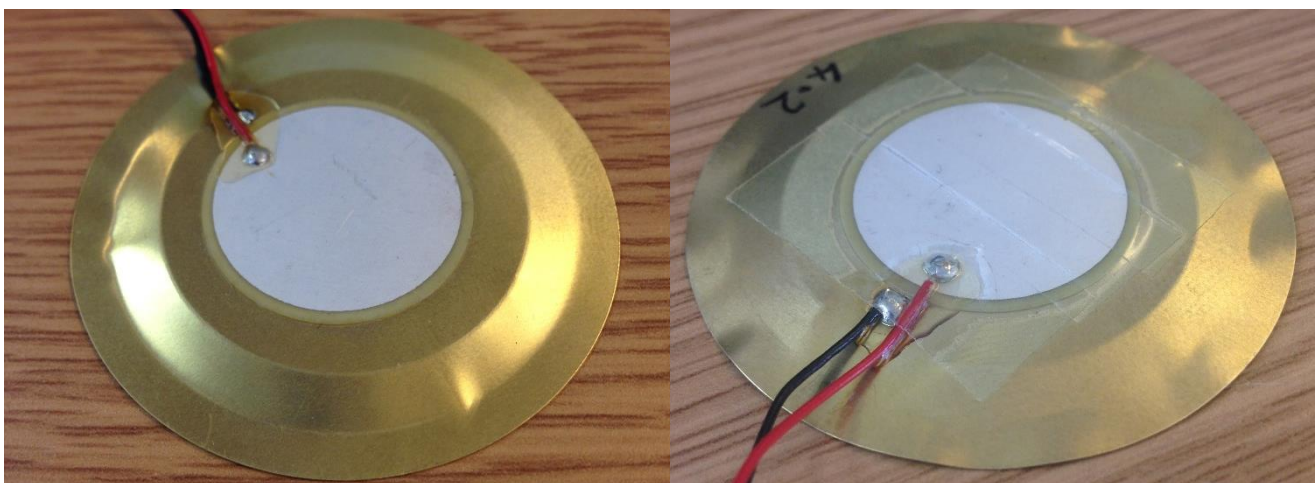


Figure 5-25 a. Clamped piezoelectric element b. unclamped piezoelectric element

The procedure used to evaluate the optimised structure of the preformed piezoelectric element involved pressing ten different elements to the same distance and rather than a target load. Due to the speed of the operation 10mm/min, it was found that the use of the micro switch set on the tensile machine would ensure safe and repeatable production of the elements. The below Table 5-5 displays the findings of this experiment.

Table 5-5 Preformed piezoelectric element diaphragm height and buckling behaviour

Displacement (mm)	Buckling method
0.2	NA
0.4	NA
0.6	NA
0.8	Monostable (minimal)
1.0	Monostable (minimal)
1.2	Monostable
1.4	Monostable
1.6	Monostable
1.8	Monostable (strong)
2.0	Monostable (strong)
2.2	Bistable
2.4	Bistable
2.6	Bistable
2.8	Bistable
3.0	Bistable (structure too stiff)

Findings from this experiment show that when the structure transitions from its monostable region into a bistable region, the energy store is significantly higher, this was observed from ceramic being shattered and thrown off the brass substrate. In contrast, the monostable region showed no signs of this even after 100 actuations.

To further test the setup and the structures being formed tests were done at an elevated temperature, using a heat gun and with various punch heads. The findings show temperature does not affect the structure through heating, and that symmetry or a-symmetry make no difference to the structures monostable region that has been formed. However, the use of a sloped punch head such as the one shown in Figure 5-26 e. created a larger monostable region; however, failure of the piezo was found to occur within 100 actuations.

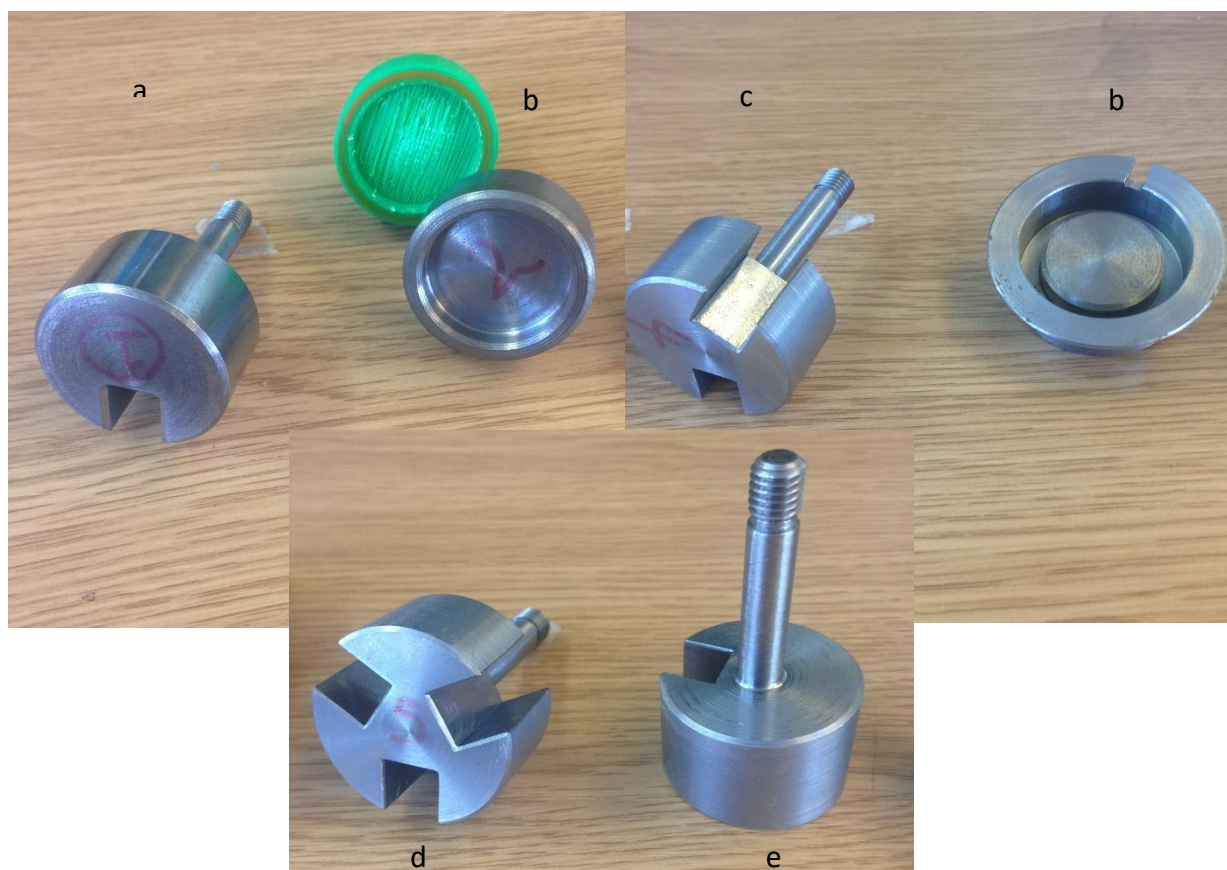


Figure 5-26 Punch heads used to press piezoelectric elements into monostable structures a. original punch head with a missing notch to prevent solder damage b. male and female forming cup c. two-notch symmetric punch head d. Three-notch symmetric punch head e. Sloped punch head

Having identified from Table 5-5 a region in which buckling can occur without damaging the piezoelectric ceramic the experimental method has moved to identify the force needed to actuate the buckling structure and the corresponding power output of the system.

During this stage the ten piezoelectric transducers were actuated 100 times each, this is to reduce any statistical anomalies that may occur during testing.

To produce this data, the die layout used in Figure 5-24 was adapted, where the steel plate was removed, allowing the element to buckle freely. To cause the element to buckle a point load that is electrically isolated from the tensile machine has been used. To replicate a scenario of someone actuating the piezoelectric element the speed of approach was set to be 700mm/min, once the system buckles the tensile machine then returns to its original position at a speed of 1200mm/min this ensures that the point load does not interfere with any data capture. At the same time as this, single capture and save had been set on the oscilloscope that captures the voltage being generated by the piezoelectric element allowing for the results to match the actuation force and the power output of the element.

5.6.2 Preloaded Piezoelectric Element

To produce a valid numerical and simulation model, experimental data has been gathered. This section has been once again broken down into three sections; the first is in the initial buckling force of the piezoelectric element, the second is on the actuation force for the preloaded element, and the third is on the power output of the piezoelectric element

To identify the initial buckling force of the piezoelectric element the tensile machine used in compression was used in conjunction with a bespoke grip that clamps the elements to ensure that stay vertical and are comparable to the numerical and simulation methods as they show in Figure 5-27. The tensile machine was used at 10mm/min, creating a quasi-static test to identify the forces needed to actuate the piezoelectric element. To ensure the reliability and repeatability, this was repeated 20 times, thus reducing any statistical fluctuations that may occur during testing.

The bespoke holder clamps the piezoelectric element vertically and uses two steel rods to guide the compression of the piezoelectric element. This experiment was repeated with and without silicone rubber (Figure 5-27), to show the effect of damping the silicone has on the initial buckling of the element. It was found that the buckling force did not change for the element; however, the displacement did. This has been attributed to the silicone compressing due to the pressure of the element.



Figure 5-27 Pinned-pinned initial buckling setup using a bespoke holder and point load

Once the initial buckling force was achieved, calibrated electronic callipers were used to identify the height of curvature compares to its original position. It was this distance that was controlled in later experiments that allowed for the identification of an optimised structure that produces large amounts of power at a low actuation force.

To identify the force needed to actuate and the power produced by the piezoelectric element, the below set up used. It is an adapted vice that bolts to the tensile machine (Figure 5-28). This ensures that the system stable, minimising and deflection in the holder. Through using only one bolt, complete control of the clamping conditions can be achieved. An M8 bolt has been used with a pitch of 1.25mm, meaning that per revolution the vice closes 1.25mm. A lock nut has also been used to mitigate any play in the system. The holder is made of aluminium with a slot insert for silicone rubber. This is used to store energy which enables a greater amount of energy to be harvested, it also minimises the amount of stress in the system, thus prolonging the lifetime of the element.

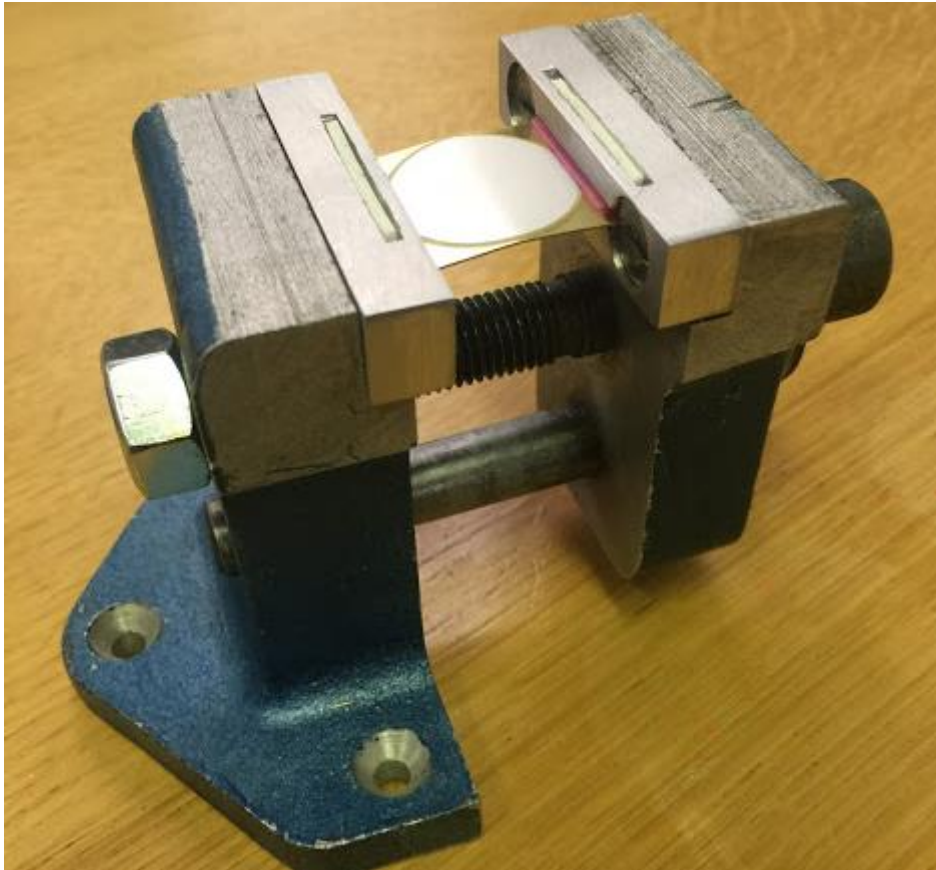


Figure 5-28 Preloaded piezoelectric element clamping device for evaluation of curvature on structural stiffness and power output.

The tensile machine was then used to identify the height of the flat piezoelectric element. This acted as the datum to evaluate the height of the arch, and this was found to be more reliable as the system did not move. Therefore the same systematic error was kept throughout the experiments to reduce any statistical errors this was repeated with 20 different piezoelectric elements. The below results shown in Table 5-6 the findings of the curvature test, highlighting the monostable region in which safe buckling can occur without damage to the piezoelectric element yet yield a high energy output.

Table 5-6 Preloaded buckling piezoelectric element parameter optimisation arch height

Arch Height (mm)	Buckling method
0.0	NA
0.2	NA
0.4	Monostable (minimal)
0.6	Monostable (minimal)
0.8	Monostable
1.0	Monostable
1.2	Monostable (strong snap-through)
1.4	Monostable (strong snap-through)
1.6	Bistable
1.8	Bistable
2.0	Bistable

To identify the power output of the piezoelectric element conductive copper tape was used instead of soldered joints this was to reduce stress concentrations on the ceramics surface, thus increasing the service life of the piezoelectric element.

5.7 Results

This section has been separated into four parts: Initial buckling force for preloaded shape generation, buckling force for the preformed and preloaded elements, the power output of flat, preformed and preloaded elements and power output into various capacitors.

5.7.1 Unmodified Piezoelectric Element

To understand the performance and efficiency of the new structures, an initial investigation was conducted on the performance of unmodified piezoelectric elements. This will act as a benchmark in which the other structures will be compared. This evaluation will justify the work that has been performed. In this section, the force versus displacement of unmodified piezoelectric elements has been explored. Using the same experimental setup as the preformed piezoelectric element, ten unmodified piezoelectric elements were actuated to achieve a target displacement of 1.6mm. This value was selected as it was found to be comparable to the energy needed to displace the preformed piezoelectric elements, thus providing a reliable prediction for the input energy. To identify the efficiency of the harvester, this input energy has been calculated by integrating the area under the curve using the trapezium rule this provides a more accurate prediction of the input energy to the system. Equation 5.39 can be referred to as Newton's method, and 5.40 is integral for force versus displacement.

$$E_{Mechanical}(J) = F (N) \times D (m) \quad 5.39$$

5.40

$$\int_0^{1.6} F dx$$

Where

F is equal the force applied to the transducer in Newtons

D is the displacement of the transducer in meters.

Both the force and the displacement of the input has been identified from the tensile machine's plots shown in Figure 5-29.

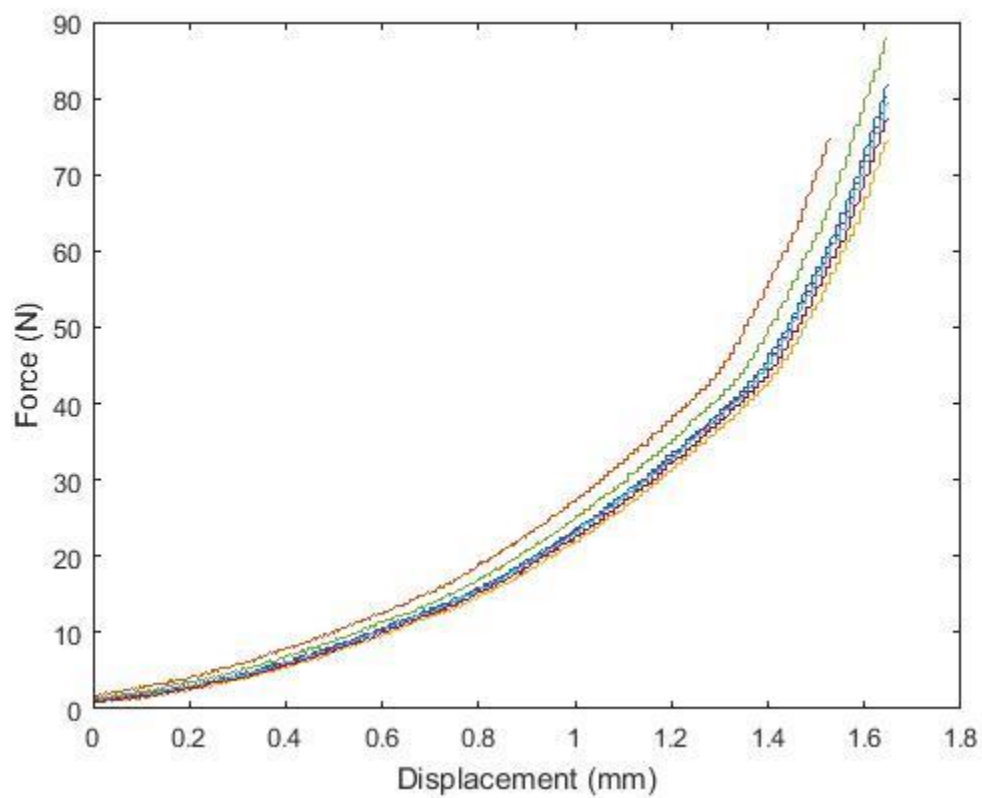


Figure 5-29 Flat piezoelectric element force vs displacement

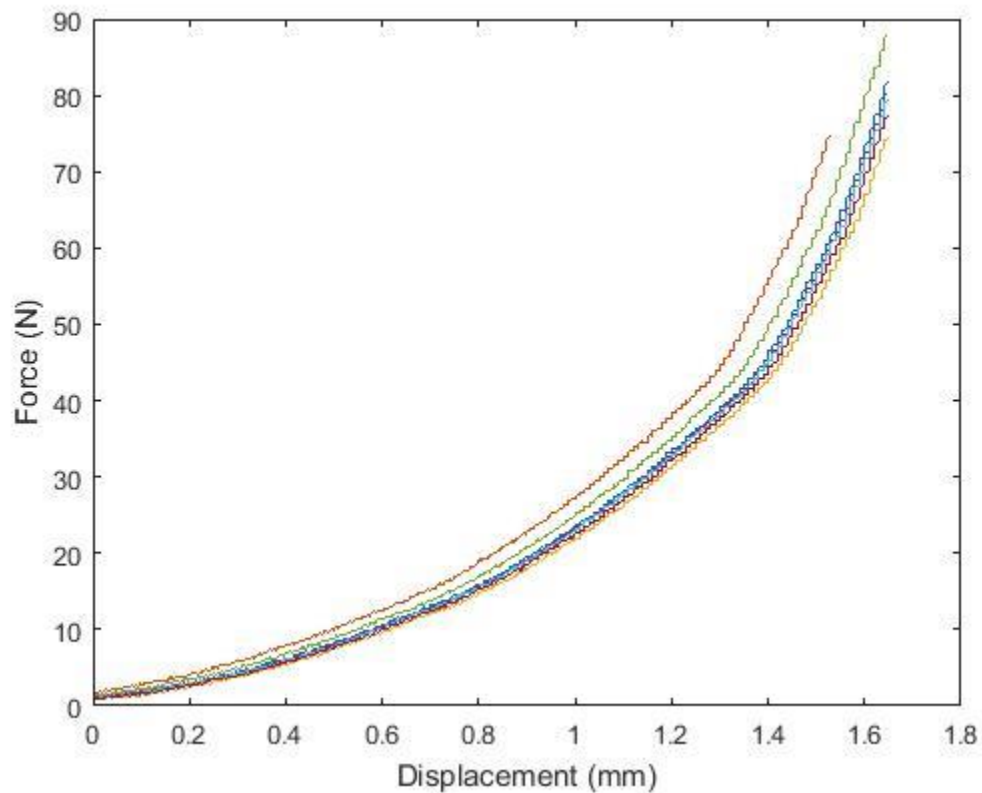


Figure 5-29, the average peak force of $79.38 \pm 6.15\text{N}$ and displacement of 1.65 ± 0.2 have been identified. Subsequently, the input energy was calculated using equation 5.40. It was found that the average input energy was found to be; 130mJ for the unmodified piezoelectric element.

$$E_{Trap\ in} = 36.6926\text{mJ} \quad 5.41$$

To confirm this finding, the data has been average and integrated finding the energy under the graph using the trapezium rule, which is equal to the energy in the system.

With the input energy identified, the study continues with the identification of the power output of the piezoelectric element. These readings were taken at the same time as the force versus displacement. Using the capacitor equations discussed in the previous section, it is possible to identify the amount of energy outputted by the unmodified piezoelectric elements. The below image portrays the average power output for ten unmodified piezoelectric elements. A very close voltage can be observed from this data showing repeatability and consistency during testing. An average peak to peak voltage of $106\text{V} \pm 2\text{V}$ was calculated from the data presented in Figure 5-30.

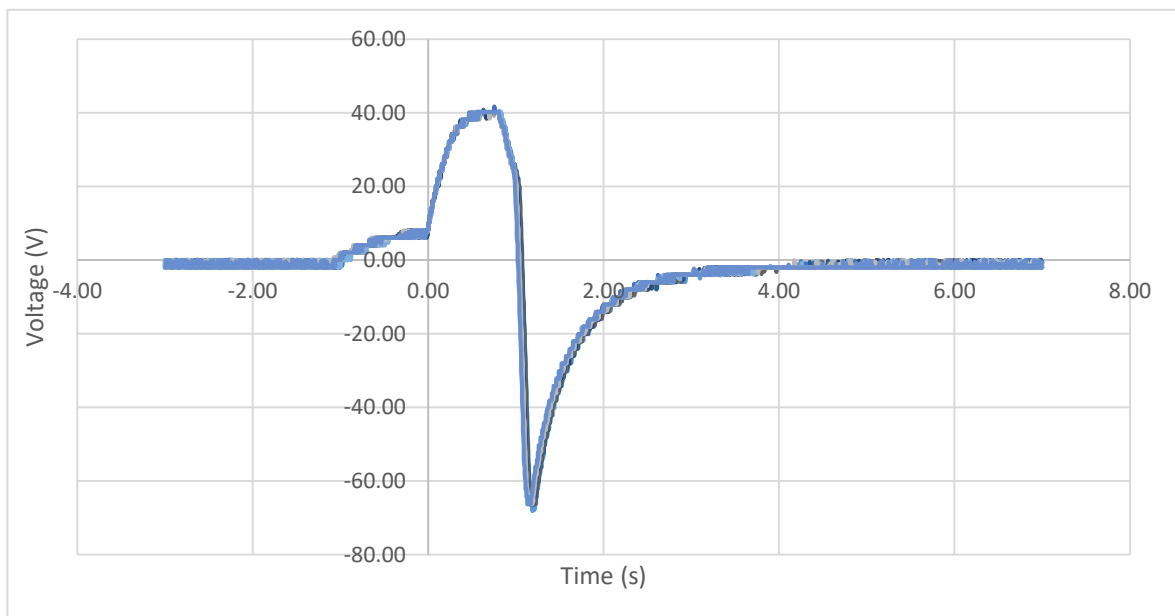


Figure 5-30 Open circuit voltage for ten unmodified piezoelectric elements

To calculate the power out the capacitance of the elements must be calculated; this was achieved through the use of a multimeter that was set to read the capacitance of the elements. Readings were taken at three different points on the element and averaged to provide an accurate prediction for the capacity. This can then be used for calculating the

energy output of the element. For the total number of unmodified elements tested an average capacitance of 34.12nF was found. This information will then be used in the next section to identify the energy output of the unmodified piezoelectric elements.

Using the equations in the numerical section, it is possible to identify the amount of energy produced by the unmodified piezoelectric elements.

$$E = \frac{CV^2}{2} = \frac{34.12nF \times 106^2}{2} = 191.686\mu J \quad 5.42$$

Completing the calculations, it can be observed that 191.686μJ of electricity is produced. To calculate the efficiency of the system the below equation 5.43 has been used.

$$\eta_{Trap} = \frac{W_{out}}{W_{in}} \times 100 = \frac{191.686\mu J}{36.6926mJ} \times 100 = 0.522\% \quad 5.43$$

It has been found that this system has an efficiency of 0.522%, meaning that 99.4% of the mechanical energy is lost. This is a very inefficiency system, and therefore any improvement to the efficiency will increase the likelihood of this technology being adopted into the industry.

5.7.2 Preformed Piezoelectric Element

The first structural modification that has been explored by this work has investigated the effect that a preformed diaphragm structure has of the actuation force for a piezoelectric

element. This has been broken into three sections, and the first is simulation predictions which have been made using COMSOL Multiphysics. The second part of this section is the experimental results for the actuation force needed to actuate the diaphragm. The final section is the comparison of the simulation, numerical and experimental results for the force needed to actuate the diaphragm. This is a critical piece of work as it identifies the amount of force needed to actuate a preformed piezoelectric element and the reliability of the numerical and simulated work.

Following the simulation setup described in the previous chapter, a preformed piezoelectric element with a 2mm height has been modelled, and simulated using CATIA V5 and COMSOL Multiphysics. A 2mm height has been selected as this is the region that is closed to a bistable system yet still in the monostable region. It is predicted that as the structure becomes more stiff, due to the increasing height, the more force needed to actuate increases. Therefore, for the largest yield of power, a preformed element closest to the bistable region will produce the largest amount of power. Within COMSOL a linear buckling study has been performed finding a critical buckling force of 20.487N is need for the structure to buckle. The image below (Figure 5-31) was taken from the study. It is clear from this image that the two clamping locations from the point load and boundary clamping conditions that this is the location of the highest stresses in the structure.

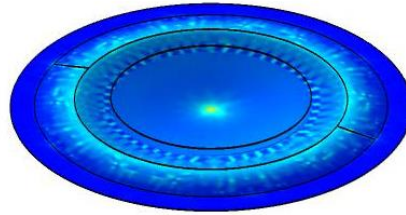


Figure 5-31 Linear buckling analysis of a preformed piezoelectric element

Within this section, the buckling force for the preformed piezoelectric element has been investigated. All testing has been performed under the previous section's experimental procedures. The results for the buckling force have been averaged out for each of the actuations finding a consistent buckling force of $20.6\text{N} \pm 0.4\text{N}$, shown by Figure 5-32. It can be concluded that from these results that the forming process is highly repeatable and consistent.

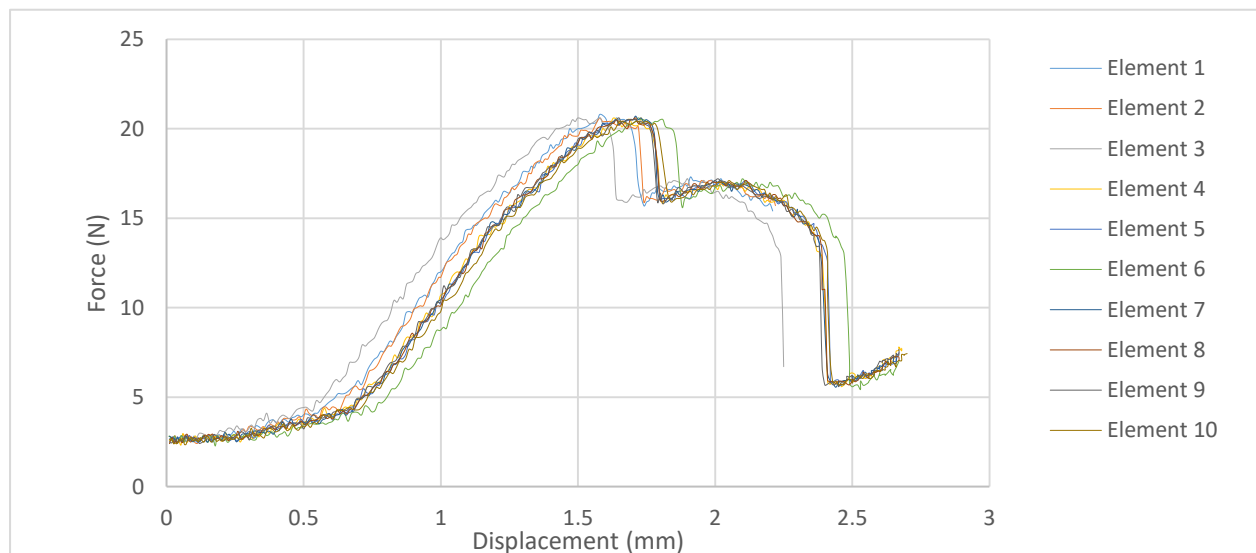


Figure 5-32 Buckling force for preformed piezoelectric elements

Further analysis of this work has been performed to identify the error between the methods used. The results for the buckling force have displayed good agreement between the

simulation and experimental method with an error of 0.55% (equation 5.44). This shows that the simulation model used it highly accurate at predicting the buckling force needed to accurately the preformed piezoelectric element.

$$\delta = \frac{v_a - v_e}{v_e} \times 100 = 0.55\% \quad 5.44$$

Further to this, the efficiency of the system has been calculated. This is to identify if by changing the structure of the piezoelectric element it is possible to improve the efficiency, thus producing an increase in the power output in relation to the input energy. To identify the input energy, equation 5.45 have been used. The results from the graph show a buckling force of $20.6 \pm 0.4\text{N}$ with an average displacement of $1.65 \pm 0.08\text{mm}$.

$$E_{trap\ in} = 17.1141\text{mJ} \quad 5.45$$

To verify this a second method shown by equation 5.45, which integrates the area under using the trapezium method. This method is more accurate as the graph is highly non-linear, and therefore a more accurate power prediction will be obtained.

During the capture of the buckling force, the voltage was also recorded where each element was actuated ten times. The overlaying results in Figure 5-33 show very good consistency; this once again shows the reliability of the manufacturing method for the preformed piezoelectric elements. In total, an average peak to peak voltage can be observed of $183.76\text{V} \pm 1.3\text{V}$.

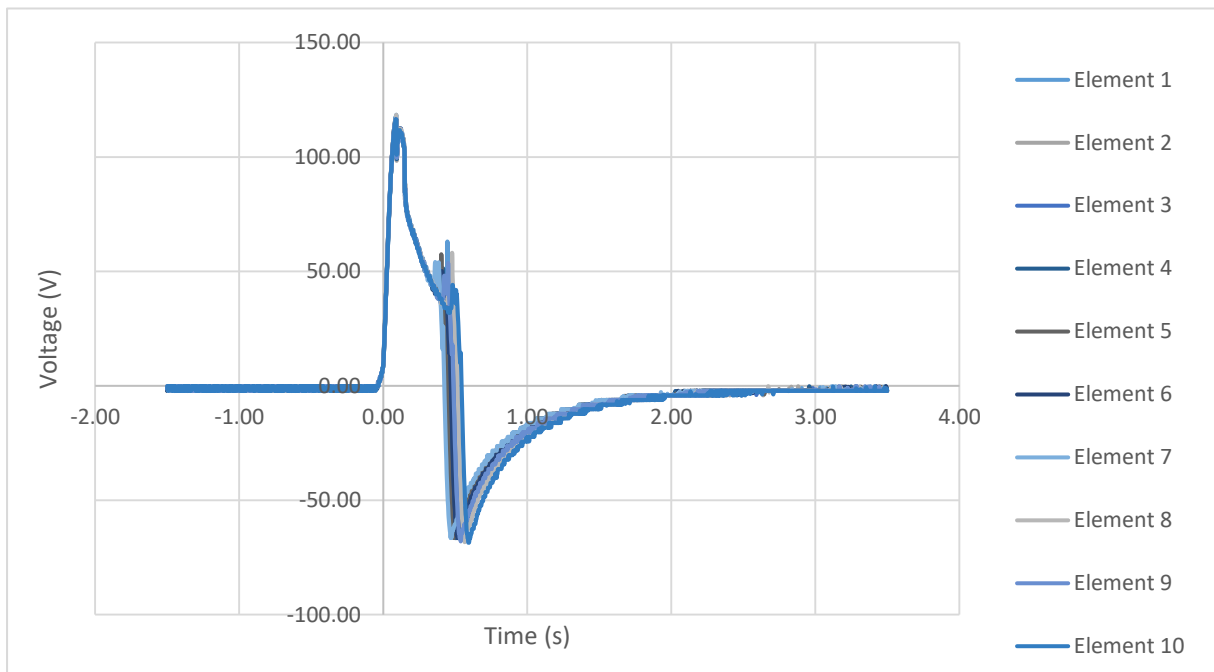


Figure 5-33 Open circuit voltage for the preformed piezoelectric elements

Using this data, it is then possible to calculate the energy output of the piezoelectric element shown by equation 5.46. Once again, a multimeter has been used in the same manner to measure the capacitance for the elements that have been preformed elements, finding the average capacitance to be 38.8nF.

$$E = \frac{CV^2}{2} = \frac{38.180nF \times 183.76^2}{2} = 644.416\mu J \quad 5.46$$

From this, the efficiency of the system can then be calculated using equation 5.47.

$$\eta = \frac{W_{out}}{W_{in}} \times 100 = \frac{644.416\mu J}{17.1141mJ} \times 100 = 3.765\% \quad 5.47$$

Through altering the structure to a preformed diaphragm, it is possible to increase the efficiency of the system to 3.765% from 0.522%. Furthermore, a significant increase in energy output can be observed from 191.686 μ J to 644.416 μ J. This means that for every preformed piezoelectric element, it would take three piezoelectric elements to achieve a comparable energy output. This is a significant step to achieving battery-less electronics.

5.7.3 Preloaded Piezoelectric Element

Within this section, the results and comparison to numerical calculations for the force needed to buckle the preloaded piezoelectric element into its curved shape are presented. Following the test procedures described in the previous section (experimental – preloaded piezoelectric element), the following results were collected. The findings show that after 20 tests with different elements, the initial buckling force of 16.533N can be observed with an error of \pm 1.14N. This can be found in the below Figure 5-34. The data was found to have an error of 6.89% this is acceptable due to the error associated with the load cell used on the tensile machine.

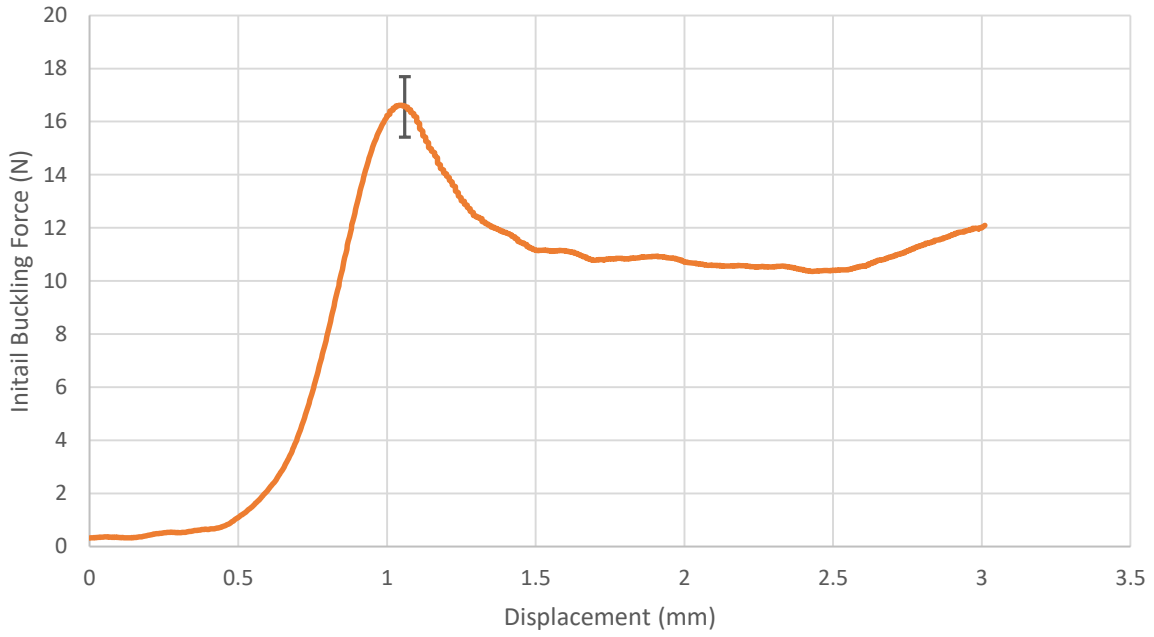


Figure 5-34 Initial buckling force averaged over 20 elements

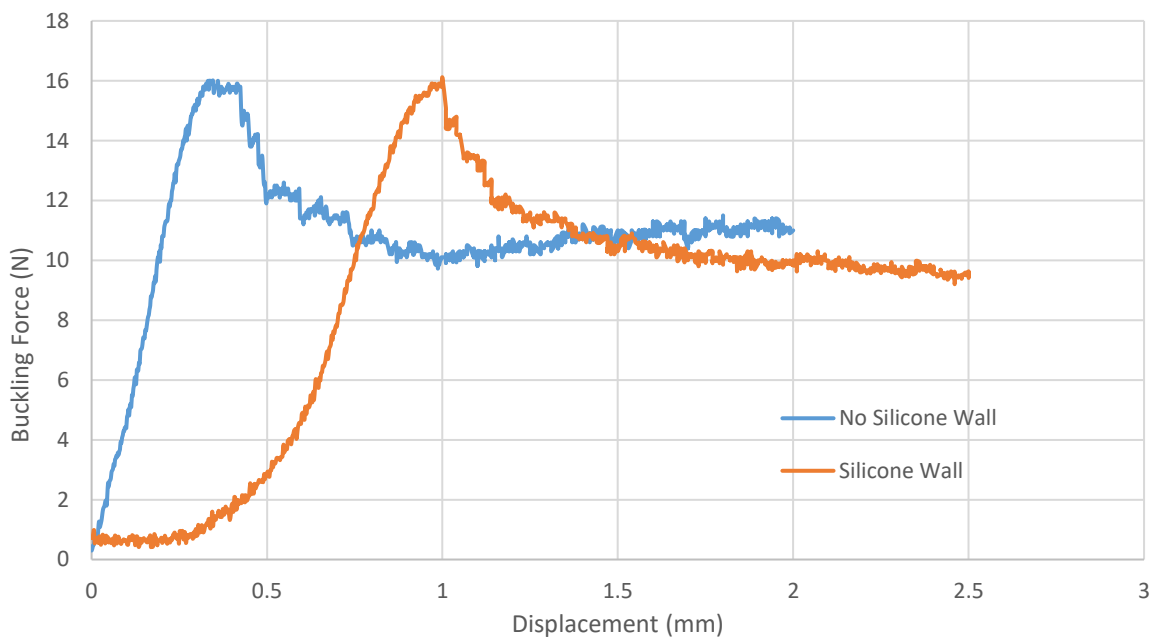


Figure 5-35 Comparison of initial buckling with and without silicone walls

It should also be noted that the buckling load of the element did not change between silicone and none silicone test setups. However, a change in the displacement data can be observed

due to the compression of the silicone depicted in Figure 5-35. Therefore, it can be concluded that silicone walls do not affect the buckling force associated with the structure; this is because it does not affect the element's stiffness.

To verify the work performed, a comparison of the experimental buckling force and numerical calculation has been completed. Using equation 5.48, the percentage error between the two values has been found. The results from this show excellent conformance with a calculated error of 0.762% between the numerical and experimental results

$$\delta = \frac{v_A - v_E}{v_E} \times 100 = -0.762\% \quad 5.48$$

Where

v_A is the observed value

v_E is the calculated value

δ is the percentage error between the two values

A simulation model of the preloaded piezoelectric energy harvester with an arch height of 0.8mm has been modelled within COMSOL Multiphysics the results have been shown in the below figure, Figure 5-36. The results show a very close fit between averaged testing and the simulated model. The maximum displacement point identifies the point of the graph there

the snapback occurs this has been marked to identify the maximum stress produced by the buckling structure shown by Figure 5-37.

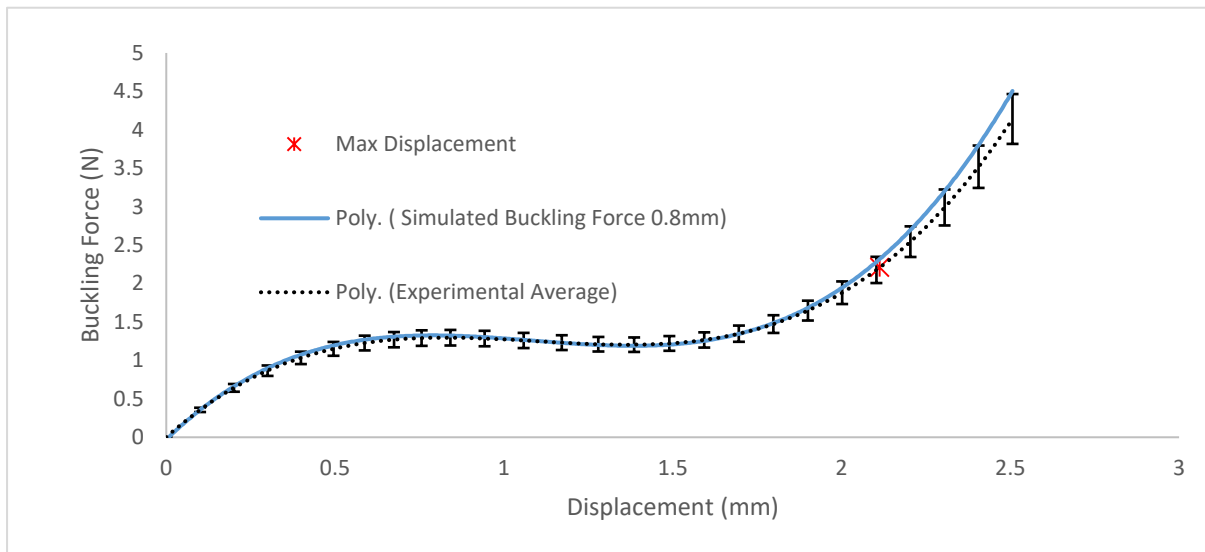


Figure 5-36 COMSOL Multiphysics results for 0.8mm arch preloaded piezoelectric element

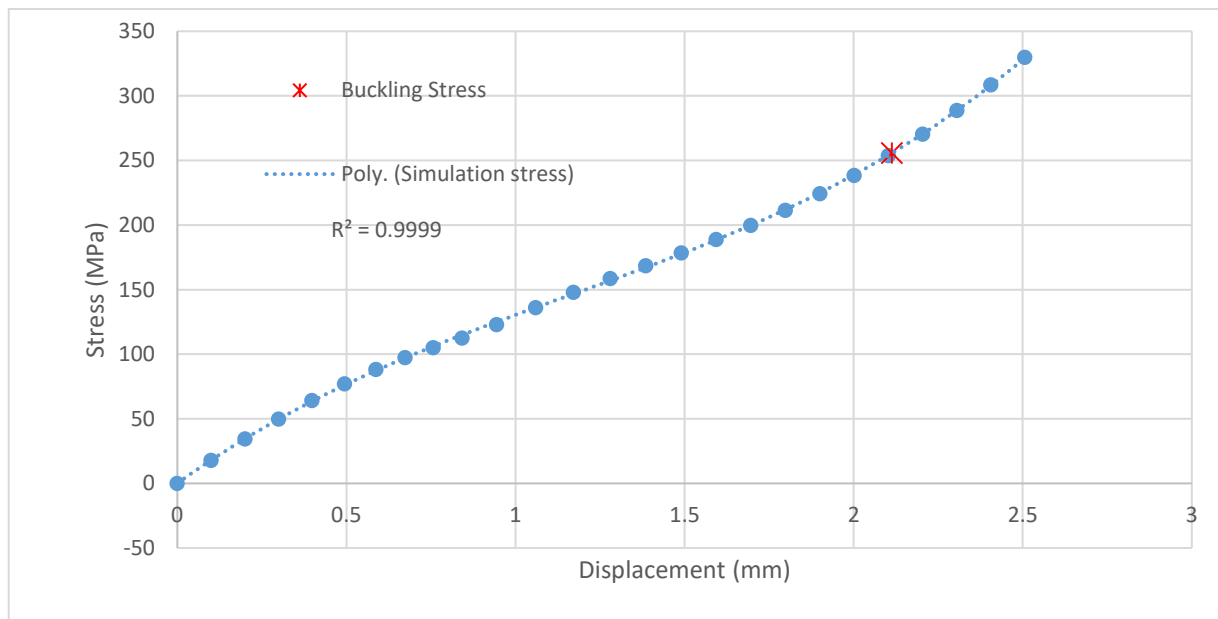


Figure 5-37 Buckling stress of a 0.8mm arch height preloaded piezoelectric element

The mono-stable buckling structure of the harvester generates significantly higher amounts of stress upon actuation compared to the force applied. Therefore, equation 5.18 can be used

to identify the voltage produced by the mono-stable buckling piezoelectric element, which considers the stress applied to the piezoelectric material rather than the force applied. The g_{33} constant has been taken from literature, which was found to be $24 \times 10^{-3} \text{ Vm/N}$ [241, 242]. The stress used for this calculation has been taken from the simulated stress vs displacement data shown in

Figure 5-37. A polynomial trend line has been fitted to the simulated data, equation 5.49, to identify the induced stress as a function of displacement equation.

$$\sigma = 23.231x^3 - 80.817x^2 + 188.04x - 0.0146 \quad 5.49$$

Where

x is the displacement of the preloaded piezoelectric element

σ is the stress-induced due to buckling to the piezoelectric material

The results displayed in Figure 5-36 shows that the maximum displacement occurs at 2.11mm, which corresponds to 255.699MPa of induced stress due to buckling. Therefore, the peak voltage was found to be 53.1 V for the initial peak of the mono-stable buckling element.

$$E_{Sim} = \frac{C \left(\frac{g_{33}}{1} \times \frac{\sigma}{t} \right)^2}{2} + 0.41486 \frac{C \left(\frac{g_{33}}{1} \times \frac{\sigma}{t} \right)^2}{2} \quad 5.50$$

Where

C is equal to the measured capacitance of the piezoelectric element.

t is equal to the thickness of the piezoelectric element

Through the application of equation 5.50, the estimated output energy of $112.87\mu\text{J}$ has been calculated. Simulations for 0.6mm, 0.8mm, 1.0mm and 1.2mm arches have been performed and compared to experimental results. The results of these simulations show good conformity for the buckling force needed to actuate the preloaded piezoelectric elements. This can be observed in Figure 5-38.

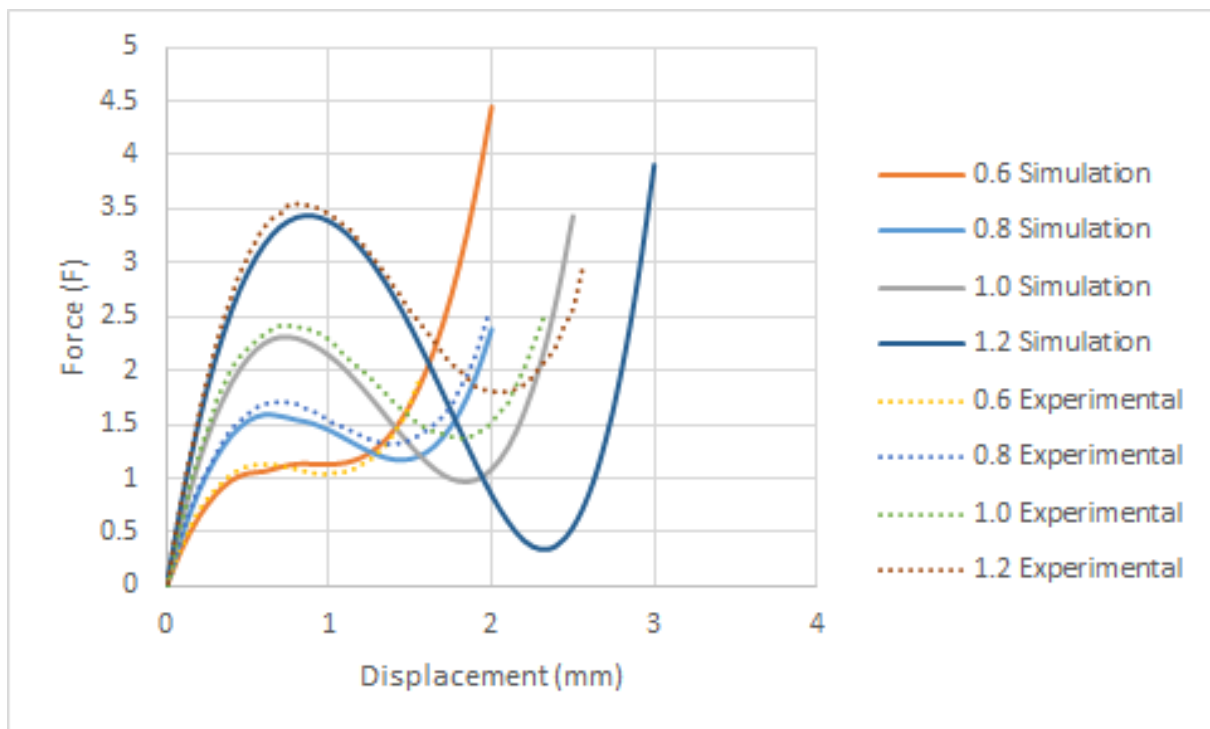


Figure 5-38 Simulation results compared to experimental results from COMSOL simulation of the preloaded piezoelectric element

Having identified the initial buckling conditions of the preloaded piezoelectric energy harvester, the force needed to actuate the structure has been investigated. Following the

procedures documented in the experimental section, the piezoelectric element was tested at 0.2mm intervals, starting 0.2mm and concluding at 1.4mm any further increase in arch height resulted in a bistable system and therefore was not of use for this study. The results from the testing can be observed in the below Figure 5-39. The 0.2mm arch can be seen with the blue dotted line, following the shape of this graph shows no instability with only a linear deflection of the beam. The 0.4mm shown to be a solid orange line shows a slight instability; this can be seen due to a plateauing behaviour seen between 0.4mm and 1 mm displacement. This can also be said for 0.6mm. At 0.8mm arch height, clear buckling behaviour can be observed this is the same until 1.4mm where the graph trend changes again, a significant force reduction can be observed tending towards a negative force. It is at this crossing point that a bistable system can be observed. In addition, the initial loading is nonlinear; this is due to the silicone walls absorbing the energy being applied to the system, allowing more energy to be stored and reducing the stress on the piezoelectric ceramic.

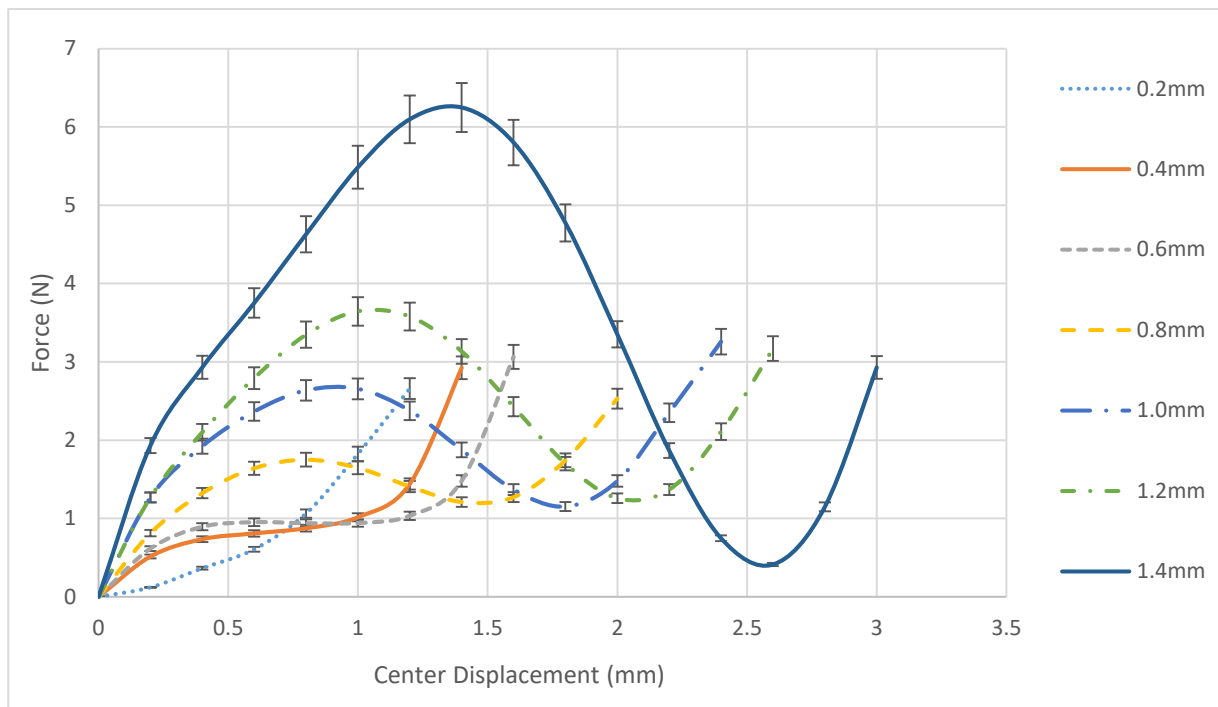


Figure 5-39 Experimental force vs displacement data of mono-stable buckling structures with different arch heights

Using this empirical data, a theoretical model can be developed to estimate the energy output for a given arch height for the energy harvester. This behaviour can be seen in Figure 5-39, which shows the effect of arch height on force vs displacement characteristics of the buckling structure. In order to predict the buckling load accurately, the following empirical relationship has been developed. This relationship is nonlinear due to the use of hyper elastic silicone walls. These walls deflect and change the profile of the graph. However, it does not change the buckling force needed to actuate the structure. For this reason, a third-order polynomial can be used to describe the buckling force of the preloaded piezoelectric elements. This can be observed in equation 5.51, where the constants are equal to equations 5.52, 5.53, and 5.54.

$$F = Ax^3 + Bx^2 + C \quad 5.51$$

$$A = -11.483h^4 + 43.691h^3 - 58.238h^2 + 30.953h - 3.0729 \quad 5.52$$

$$B = 16.575h^4 - 71.066h^3 + 105.1h^2 - 67.438h + 9.7827 \quad 5.53$$

$$C = 5.7706h^4 - 6.7593h^3 - 4.3901h^2 + 14.874h - 2.027 \quad 5.54$$

Where

x is the displacement at the centre of the buckling harvester

h is the arch height of the harvester

Using the above equations and the appropriate values of constants A, B and C has been calculated and plotted in Figure 5-40. From this work, it is possible to predict the buckling force (i.e. the actuation force) needed for the preloaded piezoelectric element to buckle as shown.

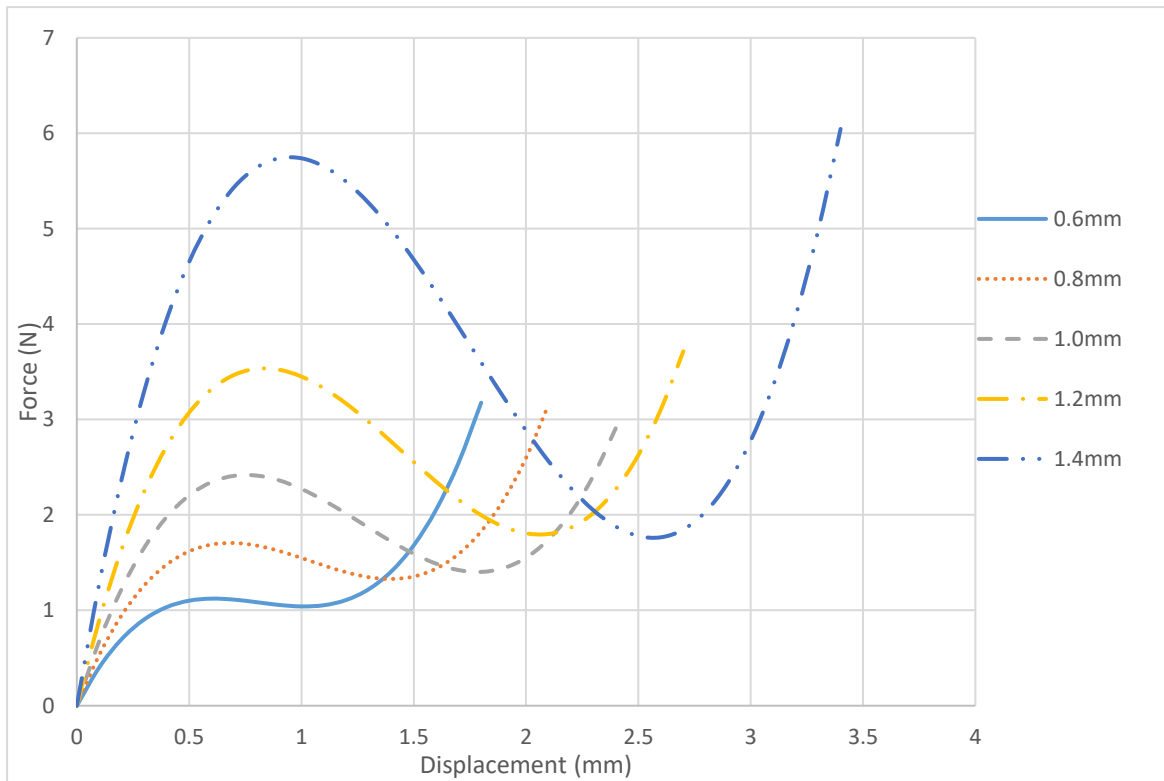


Figure 5-40 Predicted force vs displacement of preloaded piezoelectric element buckling structures with different arch heights

Differentiating equation 5.51 yields the following expression

$$y = 3Ax^2 + 2Bx + C \quad 5.55$$

By finding the roots of it is possible to find the maxima and minima of the force vs displacement graph which correspond to the critical buckling and return force of the preloaded buckling structure, respectively. The points at which the lines cross the x-axis signify the real roots. The below Figure 5-41 displays the first derivative of the buckling data.

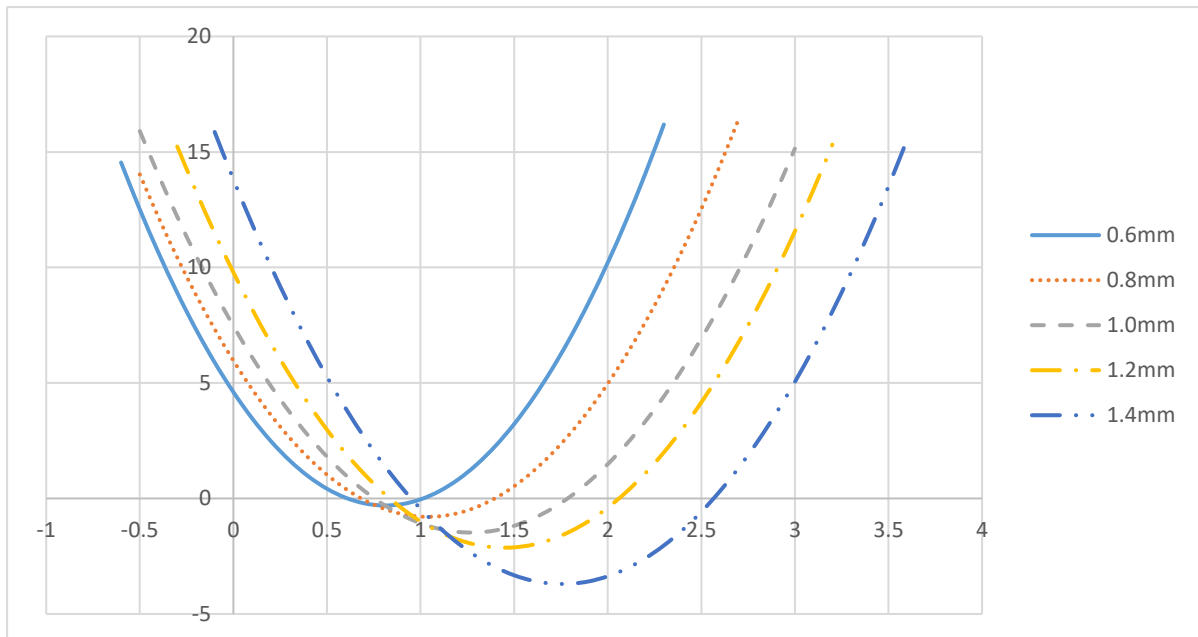


Figure 5-41 Plots of force vs displacement 1st derivative for mono-stable buckling structures with different arch heights

The real roots of the mono-stable preloaded structure of different arch heights have been identified and listed in Table 5-7. Using the information obtained from the roots, it is possible to calculate the buckling and return forces using equations 5.55, as shown in Table 5-7.

Table 5-7 Buckling and return force calculations for the preloaded buckling element with different arch heights

Arc Height (h) (mm)	Displacement (roots)		Buckling Load (N)	Return Force (N)
	+(mm)	-(mm)		
0.5	0.607	0.811	0.872	0.861
0.6	0.609	1.014	1.122	1.040
0.8	0.683	1.396	1.705	1.328
1.0	0.753	1.785	2.418	1.401
1.2	0.835	2.060	3.535	1.794
1.4	0.949	2.565	5.749	1.759
1.5	1.006	3.384	7.616	-3.445
1.6	1.049	6.156	10.228	-60.769

Table 5-8 compares the measured and predicted buckling and return forces. Although the percentage error for the arch height of 0.60mm is 10%, it remains within $\pm 5\%$ for other arch heights which confirms the validity of the predictive model.

Table 5-8 Comparison of the predicted and measured buckling and return forces

Number this equation 6.8 and 6.9

Arc	New Model		Experimental		Error	
	Buckling	Return	Buckling	Return	Buckling	Return
Height	Load	Force	Load	Force	Load	Force
(mm)	(N)	(N)	(N)	(N)	%	%
0.60	1.122	1.040	0.960	0.933	-14.455	-10.280
0.80	1.705	1.328	1.688	1.288	-1.017	-2.992
1.00	2.418	1.401	2.406	1.449	-0.465	3.422
1.20	3.535	1.794	3.395	1.699	-3.971	-5.285
1.40	5.749	1.759	5.770	1.779	0.367	1.114

The results from this work show accurate predictions for the buckling force of a preloaded piezoelectric energy harvester. This information is vital for developing commercial power units as it allows the manufacturer to develop technology for the user's needs.

To identify the efficiency of the system the input energy has to be computed, this is done by taking the distance to the peak buckling force shown by equation finding the roots following this it has been verified by integrating using equation 5.41 results shown in Table 5-9 depict the input energy using both methods for the various arch heights.

Table 5-9 Input energy calculations for preloaded piezoelectric elements of varying arch heights

Arch height	Trapezium rule
(mm)	(mJ)
0.6	0.4113
0.8	0.7612
1.0	1.2406
1.2	2.0090
1.4	3.6922

To calculate the energy output of the piezoelectric energy harvester voltage data was collected at the same time as that of the force data. This was repeated ten times per element, with the averaged results displayed in Figure 5-42.

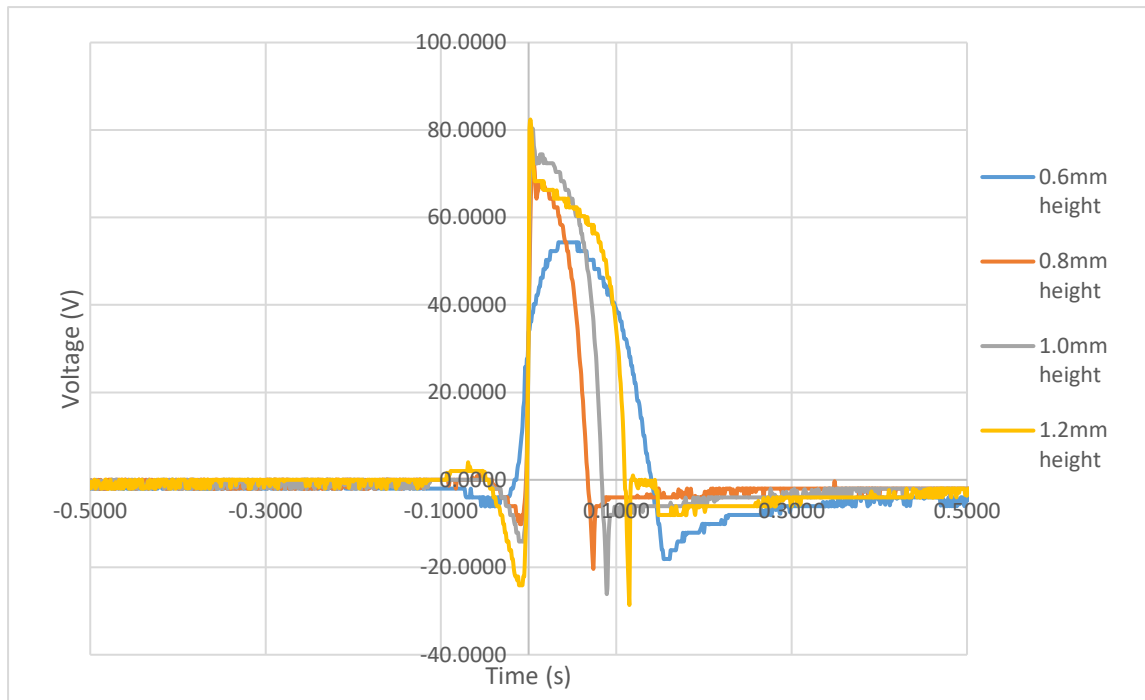


Figure 5-42 Voltage output of different arch heights for a preloaded piezoelectric element

To create a predictive model for the power output for the preloaded buckling piezoelectric elements, the following empirical correlations have been derived to predict the maximum and minimum output voltages.

$$V_{max} = 85.993h^3 - 330.39h^2 + 426.12h - 101.94 \quad 5.56$$

$$V_{min} = 18h + 6.9 \quad 5.57$$

Where

h is the height of the arch between 0.4 and 1.8mm

Using the above equations, it is possible to predict the power output of a mono-stable buckling preloaded piezoelectric element as a function of arch height.

In Table 5-10, below the peak to peak voltages and error can also be observed for the differing arch heights. Before testing a multimeter has been used to measure the average capacitance of all ten elements, the findings show an average of 38.2nF this will be used to calculate the output energy of the preloaded structure.

Table 5-10 Preloaded piezoelectric element voltage and energy output

Arch height	Peak to peak voltage	Error	Output energy
(mm)	(V)	(V)	(μJ)
0.6	70.4	1.2	94.663
0.8	94.5	2.2	170.568
1.0	104.5	1.4	208.577
1.2	108.8	3.6	226.095

Using the information in Table 5-10, the efficiency of the system can be computed. Once again, this will be completed using equation 5.45. The results for the efficiency of the system have been listed in the below Table 5-11.

Table 5-11 Preloaded piezoelectric element energy efficiency

Arch height	Efficiency Trap
(mm)	(%)
0.6	23.016
0.8	22.408
1.0	16.813
1.2	7.206

The results show that through using a preloaded piezoelectric element with a silicone wall the efficiency of the energy harvester can be significantly improved through this a combination of the low buckling force need and the increased power caused by increase stress due to buckling.

The below Table 5-12 has been used to compare experimental results from the work that has been performed.

Table 5-12 System efficiency and power output

	Unmodified	Preformed	Preloaded			
			0.6	0.8	1.0	1.2
Trapezium rule (η) (%)	0.522	3.765	23.016	22.408	16.813	7.206
Energy Output (μJ)	191.686	644.416	94.663	170.568	208.577	226.095

Chapter 6 – Conclusion

Summary

This chapter presents concluding remarks regarding the work that has been performed to further the area of knowledge regarding piezoelectric energy harvesting and buckling structures which increase the power output of low-cost commercial piezoelectric elements.

6.1 Concluding remarks

Throughout this project, an in-depth literature review has been performed, to develop and understand the unique ideas, applications and developments within the field of piezoelectricity. This review commences with an outline of the history of piezoelectricity, giving an insight into major contributors since its discovery in the 18th century until the late 1990s. Following this, the review investigates the properties of piezoelectric materials where an understanding of constitutive equations has been outlined, laying a foundation of knowledge to the enhancement of piezoelectric energy harvesting (PEH) outputs. To further develop upon this knowledge, an investigation into recent developments for PEH was performed, identifying bi-stable systems as an excellent method for enhancing the power output of a PEH through the use of buckling. This knowledge has led to the investigation and development of the knowledge that a mono-stable buckling piezoelectric element is capable of producing large amounts of energy without the need for push back actuation, increasing the efficiency of the system.

This work initiated with the development of a preformed buckling structure. This was found to generate large amounts of stress, thus increased power output. It was found that the diaphragm shaped preformed energy harvester was able to create a mono-stable system that produces three times the power of commercially available piezoelectric transducers. However, it was found that this novel method of energy harvesting had a critical buckling load that was high, reducing its industrial application. Further to this initial force, a significant noise is generated that would not be desirable for most applications. On the other hand, this work

demonstrated that increased efficiency could be achieved from 0.552% energy conversion of an unmodified piezoelectric element to 3.765% for the preformed piezoelectric transducer. This increased efficiency has resulted in enough power to enable wireless communication using radio signals.

Following the development of a preformed buckling harvester, a novel piezoelectric preloaded piezoelectric element was produced. It was identified from work performed previously and the literature that a preloaded element would involve little modification to the piezoelectric transducers. Further to this, significantly more energy can be generated at lower buckling forces and without damaging the piezoelectric ceramic. Further investigation into this method of energy harvesting identified that the arch height plays a significant role in the generation of energy and return snap for the mono-stable preloaded structure. An arch that is too high generates a bi-stable system which requires a push back mechanism. In contrast, a low arch causes the system to behave like a cantilever. Using the obtained experimental data, it was possible to develop two equations that can be used to predict the buckling force of a preloaded element and the power output of the buckling energy harvester. The theoretical models have been verified using both experimental and numerical results. Through the use of COMSOL, it was possible to generate a finite element model for a 25mm square. These models were then run using various arch heights, giving an accurate prediction of the buckling force and stresses generated in the mono-stable buckling structure. Using established equations, it was then possible to predict the power output of a given geometry. A single preloaded piezoelectric energy harvester has been shown to increase the efficiency from

0.522% to 22.408%. Furthermore, it is possible to stack the elements, enabling higher power output and efficiency.

A critical part of any energy harvester is the circuit used to harvest, rectify and store energy. This work has investigated different circuits that can be used to convert the alternating current to direct current. Through a review of existing work, it was determined that the use of passive components would ensure that the circuits are simple and therefore easy to implement into existing products and structures. Two circuits were identified; a full-wave bridge rectifier and a voltage doubler. The tests performed identified that a full-wave bridge rectifier allowed more energy to be captured.

Moreover, an investigation into the diodes used for this circuit was performed, once again this was to ensure that the optimal amount of energy could be harvested from a single actuation. It was found that Schottky diodes achieved this; this was attributed to the high switching speed and low forward bias. Finally, storage capacitors were investigated. The size and composition play a major part in how much energy can be captured and the time that it is stored for. It was found that as the capacitance of the capacitor reduces more energy can be stored; however, the time that it can be stored for also reduces. Furthermore, the composition of the component changes these characteristics. From testing, it was identified that a Tantalum capacitor stored energy for the longest period of time and size between $2\mu\text{F}$ and $10\mu\text{F}$ provides a good trade-off for discharge and energy.

Finally, through the course of this research, a patent has been developed and applied for. This shows the novelty of the work performed and one published paper. **“Powering lights with piezoelectric energy-harvesting floors” published in Energy Technology [236]** and one world patent **WO2020095064A1: Improvements in or relating to energy generation in a piezoelectric switch**. Published in May 2021 with a Priority date 09-11-2018.

Chapter 7 – Recommendations

The presented research work has opened new avenues into piezoelectric energy harvesting, which provides an opportunity to replace disposable batteries within low power electronics. To continue this research, optimisation of the hyperelastic wall can be performed. The purpose of this work is to relate the wall stiffness to the curvature of the harvester. It was identified during simulation that the wall stiffness is closely linked to the buckling force and power output, thus the energy in the system.

During the development of the patent and the preformed piezoelectric harvesters, it was found that stacking piezoelectric transducers generated significantly more energy. Simulation and experimental work can be performed on multilayer stacked piezoelectric transducers, coupled to the electrostatics module of COMSOL. The behaviour such as buckling force and power output can be identified for various arch heights, geometries and hyperelastic materials.

Finally, an investigation into an ultra-low energy radio transmitter circuit can be performed to develop a battery-less transmitter where a human interaction such as a finger press can generate significant amounts of energy for smart home devices.

References

1. Howe, J.P., *This is nature; this is un-nature: Reading the keeling curve*. Environmental History, 2015. **20**(2): p. 286-293.
2. Oecd.org. *Carbon dioxide emissions embodied in international trade - OECD*. 2019 26/01/2020]; Available from: <https://www.oecd.org/sti/ind/carbondioxideemissionsembodiedininternationaltrade.htm>.
3. Crowley, T.J., *Causes of Climate Change over the past 1000 Years*. Science, 2000. **289**(5477): p. 270-277.
4. Mitchell, J.F., et al., *Extreme events due to human-induced climate change*. Philosophical Transactions of the Royal Society of London A: Mathematical, Physical and Engineering Sciences, 2006. **364**(1845): p. 2117-2133.
5. Patz, J.A., et al., *Impact of regional climate change on human health*. Nature, 2005. **438**(7066): p. 310-317.
6. Donner, S.D., T.R. Knutson, and M. Oppenheimer, *Model-based assessment of the role of human-induced climate change in the 2005 Caribbean coral bleaching event*. Proceedings of the National Academy of Sciences, 2007. **104**(13): p. 5483-5488.
7. Jamieson, D., *Ethics, public policy, and global warming*. Global Bioethics, 1992. **5**(1): p. 31-42.
8. Parliament, U., *Climate change act 2008*. London, UK, 2008.
9. Ricardon-AEA, O.f.N.S., *2013 UK Greenhouse Gas Emissions, Final Figures*, D.o.E.C. Change, Editor. 2015, National Statistics London.
10. Government, U.K., *The Promotion of the Use of Energy from Renewable Sources Regulations 2011*, D.o.E.a.C. Change, Editor. 2011: London.

11. Protocol, K., *United Nations framework convention on climate change*. Kyoto Protocol, Kyoto, 1997. **19**.
12. Tahvonen, O., *Fossil Fuels, Stock Externalities, and Backstop Technology*. The Canadian Journal of Economics / Revue canadienne d'Economique, 1997. **30**(4a): p. 855-874.
13. Knight, C., J. Davidson, and S. Behrens, *Energy options for wireless sensor nodes*. Sensors, 2008. **8**(12): p. 8037-8066.
14. Paradiso, J.A. and T. Starner, *Energy scavenging for mobile and wireless electronics*. IEEE Pervasive computing, 2005. **4**(1): p. 18-27.
15. Wang, W., et al., *Magnetic-spring based energy harvesting from human motions: Design, modeling and experiments*. Energy Conversion and Management, 2017. **132**: p. 189-197.
16. Siddique, A.R.M., S. Mahmud, and B.V. Heyst, *A comprehensive review on vibration based micro power generators using electromagnetic and piezoelectric transducer mechanisms*. Energy Conversion and Management, 2015. **106**: p. 728-747.
17. Saadon, S. and O. Sidek, *A review of vibration-based MEMS piezoelectric energy harvesters*. Energy Conversion and Management, 2011. **52**(1): p. 500-504.
18. Zou, H.-X., et al., *Design and experimental investigation of a magnetically coupled vibration energy harvester using two inverted piezoelectric cantilever beams for rotational motion*. Energy Conversion and Management, 2017. **148**: p. 1391-1398.
19. Pan, D. and F. Dai, *Design and analysis of a broadband vibratory energy harvester using bi-stable piezoelectric composite laminate*. Energy Conversion and Management, 2018. **169**: p. 149-160.

20. Fan, K., et al., *Design and development of a multipurpose piezoelectric energy harvester*. Energy Conversion and Management, 2015. **96**: p. 430-439.
21. Liu, H., et al., *Piezoelectric MEMS-based wideband energy harvesting systems using a frequency-up-conversion cantilever stopper*. Sensors and Actuators A: Physical, 2012. **186**: p. 242-248.
22. Firoozy, P., S.E. Khadem, and S.M. Pourkiaee, *Power enhancement of broadband piezoelectric energy harvesting using a proof mass and nonlinearities in curvature and inertia*. International Journal of Mechanical Sciences, 2017. **133**: p. 227-239.
23. Yang, Z., et al., *Introducing arc-shaped piezoelectric elements into energy harvesters*. Energy Conversion and Management, 2017. **148**: p. 260-266.
24. Febbo, M., et al., *An out-of-plane rotational energy harvesting system for low frequency environments*. Energy Conversion and Management, 2017. **152**: p. 166-175.
25. Jiang, X.-Y., H.-X. Zou, and W.-M. Zhang, *Design and analysis of a multi-step piezoelectric energy harvester using buckled beam driven by magnetic excitation*. Energy Conversion and Management, 2017. **145**: p. 129-137.
26. Guan, M. and W.-H. Liao, *Design and analysis of a piezoelectric energy harvester for rotational motion system*. Energy Conversion and Management, 2016. **111**: p. 239-244.
27. Jing, B.Y. and K.S. Leong, *Parametric Studies on Resonance Frequency Variation for Piezoelectric Energy Harvesting With Varying Proof Mass and Cantilever Length*. Journal of Telecommunication, Electronic and Computer Engineering (JTEC), 2016. **8(5)**: p. 119-123.

28. He, X., et al., *Modeling and experimental verification of an impact-based piezoelectric vibration energy harvester with a rolling proof mass*. Sensors and Actuators A: Physical, 2017. **259**: p. 171-179.
29. Jia, Y. and A.A. Seshia, *Power optimization by mass tuning for MEMS piezoelectric cantilever vibration energy harvesting*. Journal of Microelectromechanical Systems, 2016. **25**(1): p. 108-117.
30. Xie, X., et al., *Energy harvesting from high-rise buildings by a piezoelectric coupled cantilever with a proof mass*. International Journal of Engineering Science, 2013. **72**: p. 98-106.
31. Choi, W., et al., *Energy harvesting MEMS device based on thin film piezoelectric cantilevers*. Journal of Electroceramics, 2006. **17**(2): p. 543-548.
32. Shen, D., et al., *The design, fabrication and evaluation of a MEMS PZT cantilever with an integrated Si proof mass for vibration energy harvesting*. Journal of Micromechanics and Microengineering, 2008. **18**(5): p. 055017.
33. Ferrari, M., et al., *Improved energy harvesting from wideband vibrations by nonlinear piezoelectric converters*. Sensors and Actuators A: Physical, 2010. **162**(2): p. 425-431.
34. Erturk, A., J. Hoffmann, and D. Inman, *A piezomagnetoelastic structure for broadband vibration energy harvesting*. Applied Physics Letters, 2009. **94**(25): p. 254102.
35. De Paula, A.S., D.J. Inman, and M.A. Savi, *Energy harvesting in a nonlinear piezomagnetoelastic beam subjected to random excitation*. Mechanical Systems and Signal Processing, 2015. **54**: p. 405-416.
36. Cottone, F., H. Vocca, and L. Gammaitoni, *Nonlinear energy harvesting*. Physical Review Letters, 2009. **102**(8): p. 080601.

37. Cao, J., et al., *Nonlinear time-varying potential bistable energy harvesting from human motion*. Applied Physics Letters, 2015. **107**(14): p. 143904.
38. Zhu, Y. and J.W. Zu, *Enhanced buckled-beam piezoelectric energy harvesting using midpoint magnetic force*. Applied Physics Letters, 2013. **103**(4): p. 041905.
39. Xu, C., et al., *Bi-stable energy harvesting based on a simply supported piezoelectric buckled beam*. Journal of Applied Physics, 2013. **114**(11): p. 114507.
40. Eltanany, A.M., et al., *Development of piezoelectric bistable energy harvester based on buckled beam with axially constrained end condition for human motion*. Japanese journal of applied physics, 2017. **56**(10S): p. 10PD02.
41. Cottone, F., et al., *Effect of boundary conditions on piezoelectric buckled beams for vibrational noise harvesting*. The European Physical Journal Special Topics, 2015. **224**(14-15): p. 2855-2866.
42. Litak, G., M.I. Friswell, and S. Adhikari, *Regular and chaotic vibration in a piezoelectric energy harvester*. Meccanica, 2016. **51**(5): p. 1017-1025.
43. Lan, C., W. Qin, and W. Deng, *Energy harvesting by dynamic instability and internal resonance for piezoelectric beam*. Applied Physics Letters, 2015. **107**(9): p. 093902.
44. Halvorsen, E. and G. Litak, *Statistics of a noise-driven elastic inverted pendulum*. The European Physical Journal Applied Physics, 2015. **70**(1): p. 10901.
45. Solar Energy Research, I. and P. Solar Technical Information, *Wind energy technical information guide*. 1989, Golden, Colo. : Washington, D.C.: The Institute ; For sale by the Supt. of Docs., U.S. G.P.O. viii, 116 p.
46. Moyer, R.H. and S.A. Everett, *Windmills are going around again*. Science Scope, 2011. **34**(7): p. 8-15.

47. Theophrastus, O.S., *Introduction, Greek Text, English Translation, and Commentary*, Earle R. Caley and John FC Richards, Columbus, Ohio, 1956.
48. Lang, S.B., *Pyroelectricity: from ancient curiosity to modern imaging tool*. *Physics Today*, 2005. **58**(8): p. 31-36.
49. Matthew, T., *Kelvin and piezoelectricity*. *European Journal of Physics*, 2003. **24**(5): p. 535.
50. Ballato, A. *Piezoelectricity: history and new thrusts*. in *Ultrasonics Symposium, 1996. Proceedings., 1996 IEEE*. 1996.
51. Katzir, S., *The Discovery of the Piezoelectric Effect*. *Archive for History of Exact Sciences*, 2003. **57**(1): p. 61-91.
52. Curie, J. and P. Curie, *Développement, par pression, de l'électricité polaire dans les cristaux hémihédres à faces inclinées*. *Comptes Rendus*, 1880. **91**: p. 294-295.
53. Moheimani, S.R. and A.J. Fleming, *Piezoelectric transducers for vibration control and damping*. 2006: Springer Science & Business Media.
54. Katzir, S., *Who knew piezoelectricity? Rutherford and Langevin on submarine detection and the invention of sonar*. *Notes and Records of the Royal Society*, 2012. **66**(2): p. 141-157.
55. Jaffe, B., W.R. Cook, and H.L. Jaffe. *Piezoelectric ceramics*. 1971; Available from: <http://site.ebrary.com/id/10693893>.
56. Cady, W.G., *Piezoelectricity: An introduction to the theory and application of electromechanical phenomena in crystals*. 1946: McGraw-Hill.

57. Fukada, E., *History and recent progress in piezoelectric polymers*. Ultrasonics, Ferroelectrics, and Frequency Control, IEEE Transactions on, 2000. **47**(6): p. 1277-1290.
58. Hsu, C. and P. Geil, *Morphology-structure-property relationships in ultraquenched poly (vinylidene fluoride)*. Journal of Applied Physics, 1984. **56**(9): p. 2404-2411.
59. Yang, D. and Y. Chen, *β -phase formation of poly (vinylidene fluoride) from the melt induced by quenching*. Journal of materials science letters, 1987. **6**(5): p. 599-603.
60. Song, D., D. Yang, and Z. Feng, *Formation of β -phase microcrystals from the melt of PVF2-PMMA blends induced by quenching*. Journal of Materials Science, 1990. **25**(1): p. 57-64.
61. Satyanarayana, K.C., et al., *Analysis of the torsion angle distribution of poly (vinylidene fluoride) in the melt*. Polymer, 2012. **53**(5): p. 1109-1114.
62. Sharma, M., G. Madras, and S. Bose, *Process induced electroactive β -polymorph in PVDF: effect on dielectric and ferroelectric properties*. Physical Chemistry Chemical Physics, 2014. **16**(28): p. 14792-14799.
63. Sajkiewicz, P., A. Wasiak, and Z. Goćłowski, *Phase transitions during stretching of poly(vinylidene fluoride)*. European Polymer Journal, 1999. **35**(3): p. 423-429.
64. Ye, H.-J., et al., *Effect of electroactive phase transformation on electron structure and dielectric properties of uniaxial stretching poly (vinylidene fluoride) films*. RSC Advances, 2013. **3**(45): p. 23730-23736.
65. Gregorio, R. and D.S. Borges, *Effect of crystallization rate on the formation of the polymorphs of solution cast poly (vinylidene fluoride)*. Polymer, 2008. **49**(18): p. 4009-4016.

66. Gregorio Jr, R. and E. Ueno, *Effect of crystalline phase, orientation and temperature on the dielectric properties of poly (vinylidene fluoride)(PVDF)*. Journal of Materials Science, 1999. **34**(18): p. 4489-4500.
67. Zhang, M., et al., *Polymorphism in porous poly (vinylidene fluoride) membranes formed via immersion precipitation process*. Journal of Membrane Science, 2008. **319**(1): p. 169-175.
68. Tiwari, V. and G. Srivastava, *Effect of thermal processing conditions on the structure and dielectric properties of PVDF films*. Journal of Polymer Research, 2014. **21**(11): p. 1-8.
69. Ma, W., et al., *β -Phase of poly (vinylidene fluoride) formation in poly (vinylidene fluoride)/poly (methyl methacrylate) blend from solutions*. Applied Surface Science, 2008. **254**(17): p. 5635-5642.
70. Kumar, A. and M.M. Periman, *Simultaneous stretching and corona poling of PVDF and P(VDF-TriFE) films. II*. Journal of Physics D: Applied Physics, 1993. **26**(3): p. 469.
71. Jee, T., et al., *Effect of microstructures of PVDF on surface adhesive forces*. Tribology Letters, 2007. **26**(2): p. 125-130.
72. Dhakras, D., et al., *Enhanced piezoresponse of electrospun PVDF mats with a touch of nickel chloride hexahydrate salt*. Nanoscale, 2012. **4**(3): p. 752-756.
73. Prabhakaran, T. and J. Hemalatha, *Ferroelectric and magnetic studies on unpoled Poly (vinylidene Fluoride)/Fe₃O₄ magnetoelectric nanocomposite structures*. Materials Chemistry and Physics, 2013. **137**(3): p. 781-787.

74. Soin, N., et al., *High performance triboelectric nanogenerators based on phase-inversion piezoelectric membranes of poly (vinylidene fluoride)-zinc stannate (PVDF-ZnSnO₃) and polyamide-6 (PA6)*. *Nano Energy*, 2016. **30**: p. 470-480.
75. Soin, N., et al., *Exclusive self-aligned β -phase PVDF films with abnormal piezoelectric coefficient prepared via phase inversion*. *Chemical Communications*, 2015. **51**(39): p. 8257-8260.
76. Oka, Y. and N. Koizumi, *Formation of Unoriented Form I Poly (vinylidene fluoride) by High-Rate Quenching and its Electrical Properties (Commemoration Issue Dedicated to Professor Naokazu Koizumi on the Occasion of his Retirement)*. 1985.
77. Maji, S., et al., *Self-oriented β -crystalline phase in the polyvinylidene fluoride ferroelectric and piezo-sensitive ultrathin Langmuir–Schaefer film*. *Physical Chemistry Chemical Physics*, 2015. **17**(12): p. 8159-8165.
78. Chen, S., et al., *Self-polarized ferroelectric PVDF homopolymer ultra-thin films derived from Langmuir–Blodgett deposition*. *Polymer*, 2012. **53**(6): p. 1404-1408.
79. Jiang, Y., et al., *A study on ferroelectric PVDF ultrathin films prepared by LB technique*. *Integrated Ferroelectrics*, 2007. **88**(1): p. 21-26.
80. Kliem, H. and R. Tadros-Morgane, *Extrinsic versus intrinsic ferroelectric switching: experimental investigations using ultra-thin PVDF Langmuir–Blodgett films*. *Journal of Physics D: Applied Physics*, 2005. **38**(12): p. 1860.
81. Zhu, H., et al., *Ferroelectricity of poly (vinylidene fluoride) homopolymer Langmuir–Blodgett nanofilms*. *Journal of Materials Chemistry C*, 2014. **2**(33): p. 6727-6731.

82. Rodriguez, B.J., et al., *Nanoscale polarization manipulation and imaging of ferroelectric Langmuir-Blodgett polymer films*. Applied physics letters, 2007. **90**(12): p. 122904.
83. Wu, Z., et al., *Fabrication of PVDF-based blend membrane with a thin hydrophilic deposition layer and a network structure supporting layer via the thermally induced phase separation followed by non-solvent induced phase separation process*. Applied Surface Science, 2017.
84. Jung, J.T., et al., *Understanding the non-solvent induced phase separation (NIPS) effect during the fabrication of microporous PVDF membranes via thermally induced phase separation (TIPS)*. Journal of Membrane Science, 2016. **514**: p. 250-263.
85. Cardoso, V.F., G. Botelho, and S. Lanceros-Méndez, *Nonsolvent induced phase separation preparation of poly (vinylidene fluoride-co-chlorotrifluoroethylene) membranes with tailored morphology, piezoelectric phase content and mechanical properties*. Materials & Design, 2015. **88**: p. 390-397.
86. Wang, B., J. Ji, and K. Li, *Crystal nuclei templated nanostructured membranes prepared by solvent crystallization and polymer migration*. Nature Communications, 2016. **7**.
87. Kim, J.F., et al., *Microporous PVDF membranes via thermally induced phase separation (TIPS) and stretching methods*. Journal of Membrane Science, 2016. **509**: p. 94-104.
88. Rajabzadeh, S., et al., *Preparation of PVDF/PMMA blend hollow fiber membrane via thermally induced phase separation (TIPS) method*. Separation and Purification Technology, 2009. **66**(1): p. 76-83.
89. Xiao, T., et al., *Fabrication and characterization of novel asymmetric polyvinylidene fluoride (PVDF) membranes by the nonsolvent thermally induced phase separation*

- (NTIPS) method for membrane distillation applications*. Journal of Membrane Science, 2015. **489**: p. 160-174.
90. Ike, I.A., et al., *Effects of dissolution conditions on the properties of PVDF ultrafiltration membranes*. Ultrasonics Sonochemistry, 2017.
91. Liu, F., M.-m. Tao, and L.-x. Xue, *PVDF membranes with inter-connected pores prepared via a Nat-ips process*. Desalination, 2012. **298**: p. 99-105.
92. Rajabzadeh, S., et al., *Preparation of PVDF hollow fiber membrane from a ternary polymer/solvent/nonsolvent system via thermally induced phase separation (TIPS) method*. Separation and Purification Technology, 2008. **63**(2): p. 415-423.
93. Mago, G., D.M. Kalyon, and F.T. Fisher, *Membranes of polyvinylidene fluoride and PVDF nanocomposites with carbon nanotubes via immersion precipitation*. Journal of Nanomaterials, 2008. **2008**: p. 17.
94. Correa, D., et al., *Nanostructured Conjugated Polymers in Chemical Sensors: Synthesis, Properties and Applications*. Journal of Nanoscience and Nanotechnology, 2014. **14**.
95. Benz, M. and W.B. Euler, *Determination of the crystalline phases of poly (vinylidene fluoride) under different preparation conditions using differential scanning calorimetry and infrared spectroscopy*. Journal of Applied Polymer Science, 2003. **89**(4): p. 1093-1100.
96. El Mohajir, B.-E. and N. Heymans, *Changes in structural and mechanical behaviour of PVDF with processing and thermomechanical treatments. 1. Change in structure*. Polymer, 2001. **42**(13): p. 5661-5667.
97. ELmezayyen, A.S., et al., *Significantly enhanced electroactive β phase crystallization and UV-shielding properties in PVDF nanocomposites flexible films through loading of*

- ATO nanoparticles: Synthesis and formation mechanism*. European Polymer Journal, 2017. **90**: p. 195-208.
98. Kumar, C. and P. Viswanath, *Solvent driven polymorphism in Langmuir and Langmuir Schaefer film of poly (vinylidene fluoride)*. European Polymer Journal, 2017. **86**: p. 132-142.
99. Jia, N., et al., *Crystallization behavior and electroactive properties of PVDF, P (VDF-TrFE) and their blend films*. Polymer Testing, 2017. **57**: p. 302-306.
100. Sencadas, V., R. Gregorio Filho, and S. Lanceros-Mendez, *Processing and characterization of a novel nonporous poly (vinylidene fluoride) films in the β phase*. Journal of Non-Crystalline Solids, 2006. **352**(21): p. 2226-2229.
101. Wang, B., et al., *Critical Composition of the β Form of Poly (vinylidene fluoride) in Miscible Crystalline/Crystalline Blends*. The Journal of Physical Chemistry B, 2015. **119**(44): p. 14303-14308.
102. Garain, S., et al., *Self-Poled Transparent and Flexible UV Light-Emitting Cerium Complex–PVDF Composite: A High-Performance Nanogenerator*. ACS Applied Materials & Interfaces, 2015. **7**(2): p. 1298-1307.
103. Benz, M., W.B. Euler, and O.J. Gregory, *The role of solution phase water on the deposition of thin films of poly (vinylidene fluoride)*. Macromolecules, 2002. **35**(7): p. 2682-2688.
104. Gregorio, R., *Determination of the α , β , and γ crystalline phases of poly (vinylidene fluoride) films prepared at different conditions*. Journal of Applied Polymer Science, 2006. **100**(4): p. 3272-3279.

105. Cui, Z., et al., *Poly (vinylidene fluoride) membrane preparation with an environmental diluent via thermally induced phase separation*. Journal of Membrane Science, 2013. **444**: p. 223-236.
106. Wang, X., et al., *Piezoelectric properties, densification behavior and microstructural evolution of low temperature sintered PZT ceramics with sintering aids*. Journal of the European Ceramic Society, 2001. **21**(10-11): p. 1367-1370.
107. Agrawal, D.K., *Microwave processing of ceramics*. Current Opinion in Solid State and Materials Science, 1998. **3**(5): p. 480-485.
108. Choy, J.-H., Y.-S. Han, and J.-T. Kim, *Hydroxide coprecipitation route to the piezoelectric oxide Pb (Zr, Ti) O₃ (PZT)*. Journal of Materials Chemistry, 1995. **5**(1): p. 65-69.
109. Rao, K.R.M., A.P. Rao, and S. Komarneni, *Reactive PZT precursor powder by coprecipitation*. Materials Letters, 1996. **28**(4-6): p. 463-467.
110. Xu, G., et al., *Low temperature synthesis of lead zirconate titanate powder by hydroxide co-precipitation*. Microelectronic engineering, 2003. **66**(1-4): p. 568-573.
111. Wang, Z., et al., *Dense PZT thick films derived from sol-gel based nanocomposite process*. Materials Science and Engineering: B, 2003. **99**(1): p. 56-62.
112. Nashimoto, K. and S. Nakamura, *Preparation and characterization of sol-gel derived epitaxial and oriented Pb (Zr_{0.52}Ti_{0.48}) O₃ thin films*. Japanese journal of applied physics, 1994. **33**(9S): p. 5147.
113. Muralt, P., *Ferroelectric thin films for micro-sensors and actuators: a review*. Journal of Micromechanics and Microengineering, 2000. **10**(2): p. 136-146.

114. Hayashi, T., T. Inoue, and Y. Akiyama, *Low temperature sintering of PZT powders coated with Pb5Ge3O11 by sol–Gel method*. Journal of the European Ceramic Society, 1999. **19**(6-7): p. 999-1002.
115. Guo, D., et al., *Gelcasting of PZT*. Ceramics International, 2003. **29**(4): p. 403-406.
116. Dey, S., K.D. Budd, and D.A. Payne, *Thin-film ferroelectrics of PZT of sol-gel processing*. IEEE transactions on ultrasonics, ferroelectrics, and frequency control, 1988. **35**(1): p. 80-81.
117. Omatete, O.O., M.A. Janney, and R.A. Strehlow, *Gelcasting: a new ceramic forming process*. American Ceramic Society Bulletin, 1991. **70**(10): p. 1641-1649.
118. Medesi, A., et al., *Low Temperature Sintering of PZT*. Journal of Physics: Conference Series, 2014. **557**: p. 012132.
119. Panda, P. and B. Sahoo, *PZT to Lead Free Piezo Ceramics: A Review*. Ferroelectrics, 2015. **474**(1): p. 128-143.
120. Koga, K. and H. Ohigashi, *Piezoelectricity and related properties of vinylidene fluoride and trifluoroethylene copolymers*. Journal of Applied Physics, 1986. **59**(6): p. 2142-2150.
121. Tajitsu, Y., et al., *Investigation of switching characteristics of vinylidene fluoride/trifluoroethylene copolymers in relation to their structures*. Japanese journal of applied physics, 1987. **26**(4R): p. 554.
122. Won, S.S., et al., *Piezoelectric poly (vinylidene fluoride trifluoroethylene) thin film-based power generators using paper substrates for wearable device applications*. Applied Physics Letters, 2015. **107**(20): p. 202901.

123. Yu, H., et al., *Enhanced power output of an electrospun PVDF/MWCNTs-based nanogenerator by tuning its conductivity*. *Nanotechnology*, 2013. **24**(40): p. 405401.
124. Li, B., et al., *Sensitivity of Pressure Sensors Enhanced by Doping Silver Nanowires*. *Sensors*, 2014. **14**(6): p. 9889-9899.
125. Rödel, J., et al., *Perspective on the Development of Lead-free Piezoceramics*. *Journal of the American Ceramic Society*, 2009. **92**(6): p. 1153-1177.
126. Torretta, V., et al., *Management of waste electrical and electronic equipment in two EU countries: A comparison*. *Waste Management*, 2013. **33**(1): p. 117-122.
127. Liu, W. and X. Ren, *Large piezoelectric effect in Pb-free ceramics*. *Physical Review Letters*, 2009. **103**(25): p. 257602.
128. Bai, Y., et al., *(Ba, Ca)(Zr, Ti) O₃ lead-free piezoelectric ceramics—The critical role of processing on properties*. *Journal of the European Ceramic Society*, 2015. **35**(13): p. 3445-3456.
129. Bai, W., et al., *Phase transition behavior and enhanced electromechanical properties in (Ba_{0.85}Ca_{0.15})(Zr_xTi_{1-x}) O₃ lead-free piezoceramics*. *Ceramics International*, 2015.
130. Tian, Y., et al., *Phase Transition Behavior and Large Piezoelectricity Near the Morphotropic Phase Boundary of Lead-Free (Ba_{0.85}Ca_{0.15})(Zr_{0.1}Ti_{0.9}) O₃ Ceramics*. *Journal of the American Ceramic Society*, 2013. **96**(2): p. 496-502.
131. Fu, H. and R.E. Cohen, *Polarization rotation mechanism for ultrahigh electromechanical response in single-crystal piezoelectrics*. *Nature*, 2000. **403**(6767): p. 281-283.

132. Ahart, M., et al., *Origin of morphotropic phase boundaries in ferroelectrics*. Nature, 2008. **451**(7178): p. 545-548.
133. Sang, Y., et al., *A vibration-based hybrid energy harvester for wireless sensor systems*. Magnetics, IEEE Transactions on, 2012. **48**(11): p. 4495-4498.
134. Choi, D., et al., *Piezoelectric touch-sensitive flexible hybrid energy harvesting nanoarchitectures*. Nanotechnology, 2010. **21**(40): p. 405503.
135. Yang, Y., et al., *Flexible hybrid energy cell for simultaneously harvesting thermal, mechanical, and solar energies*. ACS nano, 2012. **7**(1): p. 785-790.
136. Moro, L. and D. Benasciutti, *Harvested power and sensitivity analysis of vibrating shoe-mounted piezoelectric cantilevers*. Smart Materials and Structures, 2010. **19**(11): p. 115011.
137. Sharpes, N., D. Vučković, and S. Priya, *Floor Tile Energy Harvester for Self-Powered Wireless Occupancy Sensing*. Energy Harvesting and Systems, 2016. **3**(1): p. 43-60.
138. González, J.L., A. Rubio, and F. Moll, *Human powered piezoelectric batteries to supply power to wearable electronic devices*. International journal of the Society of Materials Engineering for Resources, 2002. **10**(1): p. 34-40.
139. Paradiso, J.A. and T. Starner, *Energy scavenging for mobile and wireless electronics*. Pervasive Computing, IEEE, 2005. **4**(1): p. 18-27.
140. Mateu, L. and F. Moll, *Optimum piezoelectric bending beam structures for energy harvesting using shoe inserts*. Journal of Intelligent Material Systems and Structures, 2005. **16**(10): p. 835-845.

141. Niu, P., et al. *Evaluation of motions and actuation methods for biomechanical energy harvesting*. in *Power Electronics Specialists Conference, 2004. PESC 04. 2004 IEEE 35th Annual*. 2004. IEEE.
142. Xie, L. and M. Cai, *Increased piezoelectric energy harvesting from human footstep motion by using an amplification mechanism*. *Applied Physics Letters*, 2014. **105**(14): p. 143901.
143. Shenck, N.S. and J.A. Paradiso, *Energy scavenging with shoe-mounted piezoelectrics*. *Micro*, IEEE, 2001. **21**(3): p. 30-42.
144. Gupta, A. and A. Sharma, *Piezoelectric Energy Harvesting via Shoe Sole*.
145. Alghisi, D., et al., *Triaxial ball-impact piezoelectric converter for autonomous sensors exploiting energy harvesting from vibrations and human motion*. *Sensors and Actuators A: Physical*, 2015. **233**: p. 569-581.
146. Bobby, K., et al., *Footstep Power Generation Using Piezo Electric Transducers*. *International Journal of Engineering and Innovative Technology (IJEIT)*, 2014. **3**(10).
147. Li, X. and V. Strezov, *Modelling piezoelectric energy harvesting potential in an educational building*. *Energy Conversion and Management*, 2014. **85**: p. 435-442.
148. Ghosh, S.K. and D. Mandal, *Efficient natural piezoelectric nanogenerator: Electricity generation from fish swim bladder*. *Nano Energy*, 2016. **28**: p. 356-365.
149. Starner, T., *Human-powered wearable computing*. *IBM Systems Journal*, 1996. **35**(3.4): p. 618-629.
150. Howells, C.A., *Piezoelectric energy harvesting*. *Energy Conversion and Management*, 2009. **50**(7): p. 1847-1850.

151. Chen, H., et al., *Low-power circuits for the bidirectional wireless monitoring system of the orthopedic implants*. IEEE transactions on biomedical circuits and systems, 2009. **3**(6): p. 437-443.
152. Pillatsch, P., E.M. Yeatman, and A.S. Holmes, *A piezoelectric frequency up-converting energy harvester with rotating proof mass for human body applications*. Sensors and Actuators A: Physical, 2014. **206**: p. 178-185.
153. Song, S. and K.-S. Yun, *Design and characterization of scalable woven piezoelectric energy harvester for wearable applications*. Smart Materials and Structures, 2015. **24**(4): p. 045008.
154. Yoon, S. and Y.-H. Cho. *A skin-attachable flexible piezoelectric pulse wave energy harvester*. in *Journal of Physics: Conference Series*. 2014. IOP Publishing.
155. Yang, J., et al. *A 2.5-V, 160- μ J-output piezoelectric energy harvester and power management IC for Batteryless Wireless Switch (BWS) applications*. in *VLSI Circuits (VLSI Circuits), 2015 Symposium on*. 2015. IEEE.
156. Jeong, S.Y., et al., *Design of a multi-array piezoelectric energy harvester for a wireless switch*. International Journal of Hydrogen Energy, 2016. **41**(29): p. 12696-12703.
157. Tan, Y., K. Hoe, and S. Panda. *Energy harvesting using piezoelectric igniter for self-powered radio frequency (RF) wireless sensors*. in *Industrial Technology, 2006. ICIT 2006. IEEE International Conference on*. 2006. IEEE.
158. Ferrari, M., et al., *An autonomous battery-less sensor module powered by piezoelectric energy harvesting with RF transmission of multiple measurement signals*. Smart materials and Structures, 2009. **18**(8): p. 085023.

159. Paradiso, J. and M. Feldmeier. *A compact, wireless, self-powered pushbutton controller*. in *Ubicomp 2001: Ubiquitous Computing*. 2001. Springer.
160. Almouahed, S., et al., *The use of piezoceramics as electrical energy harvesters within instrumented knee implant during walking*. IEEE/ASME Transactions on Mechatronics, 2011. **16**(5): p. 799-807.
161. Platt, S.R., et al., *The use of piezoelectric ceramics for electric power generation within orthopedic implants*. IEEE/ASME Transactions on Mechatronics, 2005. **10**(4): p. 455-461.
162. Mercier, P.P., et al., *Energy extraction from the biologic battery in the inner ear*. Nature biotechnology, 2012. **30**(12): p. 1240-1243.
163. Zhang, H., et al., *A flexible and implantable piezoelectric generator harvesting energy from the pulsation of ascending aorta: in vitro and in vivo studies*. Nano Energy, 2015. **12**: p. 296-304.
164. Lewandowski, B., K. Kilgore, and K. Gustafson, *Design considerations for an implantable, muscle powered piezoelectric system for generating electrical power*. Annals of biomedical engineering, 2007. **35**(4): p. 631-641.
165. Häslér, E., L. Stein, and G. Harbauer, *Implantable physiological power supply with PVDF film*. Ferroelectrics, 1984. **60**(1): p. 277-282.
166. Deterre, M., et al. *Energy harvesting system for cardiac implant applications*. in *Design, Test, Integration and Packaging of MEMS/MOEMS (DTIP), 2011 Symposium on*. 2011. IEEE.

167. Karami, M.A. and D.J. Inman, *Powering pacemakers from heartbeat vibrations using linear and nonlinear energy harvesters*. Applied Physics Letters, 2012. **100**(4): p. 042901.
168. Zheng, Q., et al., *In Vivo Powering of Pacemaker by Breathing-Driven Implanted Triboelectric Nanogenerator*. Advanced Materials, 2014. **26**(33): p. 5851-5856.
169. Deterre, M., et al. *Micromachined piezoelectric spirals and ultra-compliant packaging for blood pressure energy harvesters powering medical implants*. in *Micro Electro Mechanical Systems (MEMS), 2013 IEEE 26th International Conference on*. 2013. IEEE.
170. Lu, B., et al., *Ultra-Flexible Piezoelectric Devices Integrated With Heart to Harvest the Biomechanical Energy*. Scientific reports, 2015. **5**.
171. Potkay, J.A. and K. Brooks. *An arterial cuff energy scavenger for implanted microsystems*. in *Bioinformatics and Biomedical Engineering, 2008. ICBBE 2008. The 2nd International Conference on*. 2008. IEEE.
172. Mathieu, A., et al., *Powering Pacemakers from Heart Pressure Variation with Piezoelectric Energy Harvesters*. World Academy of Science, Engineering and Technology, International Journal of Medical, Health, Biomedical, Bioengineering and Pharmaceutical Engineering, 2016. **8**(9): p. 694-697.
173. Goto, H., et al., *Feasibility of using the automatic generating system for quartz watches as a leadless pacemaker power source*. Medical & biological engineering & computing, 1999. **37**(3): p. 377-380.
174. Simona, R., et al., *ANALYSIS OF PIEZOELECTRIC MATERIALS FOR IMPLANTABLE DEVICES*. Scientific Proceedings Faculty of Mechanical Engineering STU in Bratislava, 2013. **21**(1): p. 1-6.

175. Sun, C., et al., *PVDF microbelts for harvesting energy from respiration*. Energy & Environmental Science, 2011. **4**(11): p. 4508-4512.
176. Granstrom, J., et al., *Energy harvesting from a backpack instrumented with piezoelectric shoulder straps*. Smart Materials and Structures, 2007. **16**(5): p. 1810.
177. Ramsay, M.J. and W.W. Clark. *Piezoelectric energy harvesting for bio-MEMS applications*. in *SPIE's 8th Annual International Symposium on Smart Structures and Materials*. 2001. International Society for Optics and Photonics.
178. Qi, Y., et al., *Piezoelectric ribbons printed onto rubber for flexible energy conversion*. Nano letters, 2010. **10**(2): p. 524-528.
179. Dagdeviren, C., et al., *Conformal piezoelectric energy harvesting and storage from motions of the heart, lung, and diaphragm*. Proceedings of the National Academy of Sciences, 2014. **111**(5): p. 1927-1932.
180. Ansari, M. and M.A. Karami. *Piezoelectric energy harvesting from heartbeat vibrations for leadless pacemakers*. in *Journal of Physics: Conference Series*. 2015. IOP Publishing.
181. Dutoit, N.E., B.L. Wardle, and S.-G. Kim, *Design considerations for MEMS-scale piezoelectric mechanical vibration energy harvesters*. Integrated ferroelectrics, 2005. **71**(1): p. 121-160.
182. Roundy, S., P.K. Wright, and J. Rabaey, *A study of low level vibrations as a power source for wireless sensor nodes*. Computer communications, 2003. **26**(11): p. 1131-1144.
183. Challa, V.R., et al., *A vibration energy harvesting device with bidirectional resonance frequency tunability*. Smart Materials and Structures, 2008. **17**(1): p. 015035.
184. Hu, Y., H. Xue, and H. Hu, *A piezoelectric power harvester with adjustable frequency through axial preloads*. Smart materials and structures, 2007. **16**(5): p. 1961.

185. Leland, E.S. and P.K. Wright, *Resonance tuning of piezoelectric vibration energy scavenging generators using compressive axial preload*. Smart Materials and Structures, 2006. **15**(5): p. 1413.
186. Harne, R.L. and K. Wang, *A review of the recent research on vibration energy harvesting via bistable systems*. Smart materials and structures, 2013. **22**(2): p. 023001.
187. Li, S., et al., *Bi-resonant structure with piezoelectric PVDF films for energy harvesting from random vibration sources at low frequency*. Sensors and Actuators A: Physical, 2016. **247**: p. 547-554.
188. Lallart, M., S.R. Anton, and D.J. Inman, *Frequency self-tuning scheme for broadband vibration energy harvesting*. Journal of Intelligent Material Systems and Structures, 2010. **21**(9): p. 897-906.
189. Zhao, L., S.C. Conlon, and F. Semperlotti, *Broadband energy harvesting using acoustic black hole structural tailoring*. Smart materials and structures, 2014. **23**(6): p. 065021.
190. Zhao, D., et al., *Analysis of broadband characteristics of two degree of freedom bistable piezoelectric energy harvester*. Materials Research Express, 2018. **5**(8): p. 085704.
191. Wang, G., et al., *Dynamic and energetic characteristics of a bistable piezoelectric vibration energy harvester with an elastic magnifier*. Mechanical Systems and Signal Processing, 2018. **105**: p. 427-446.
192. Dasgupta, S.S., V. Rajamohan, and A.K. Jha, *Dynamic characterization of a bistable energy harvester under gaussian white noise for larger time constant*. Arabian Journal for Science and Engineering, 2019. **44**(2): p. 721-730.

193. Zhou, Z., W. Qin, and P. Zhu, *Harvesting performance of quad-stable piezoelectric energy harvester: modeling and experiment*. Mechanical Systems and Signal Processing, 2018. **110**: p. 260-272.
194. Zhou, S., et al., *Numerical analysis and experimental verification of broadband tristable energy harvesters*. Tm-Technisches Messen, 2018. **85**(9): p. 521-532.
195. Yan, B., S. Zhou, and G. Litak, *Nonlinear analysis of the tristable energy harvester with a resonant circuit for performance enhancement*. International Journal of Bifurcation and Chaos, 2018. **28**(07): p. 1850092.
196. Li, H., W. Qin, and W. Deng, *Coherence resonance of a magnet-induced buckled piezoelectric energy harvester under stochastic parametric excitation*. Journal of Intelligent Material Systems and Structures, 2017: p. 1045389X17742732.
197. Green, P.L., E. Papatheou, and N.D. Sims, *Energy harvesting from human motion and bridge vibrations: An evaluation of current nonlinear energy harvesting solutions*. Journal of Intelligent Material Systems and Structures, 2013. **24**(12): p. 1494-1505.
198. Arrieta, A., et al., *A piezoelectric bistable plate for nonlinear broadband energy harvesting*. Applied Physics Letters, 2010. **97**(10): p. 104102.
199. Tang, Q., Y. Yang, and X. Li, *Bi-stable frequency up-conversion piezoelectric energy harvester driven by non-contact magnetic repulsion*. Smart Materials and Structures, 2011. **20**(12): p. 125011.
200. Mann, B. and B. Owens, *Investigations of a nonlinear energy harvester with a bistable potential well*. Journal of Sound and Vibration, 2010. **329**(9): p. 1215-1226.

201. Erturk, A. and D.J. Inman, *Broadband piezoelectric power generation on high-energy orbits of the bistable Duffing oscillator with electromechanical coupling*. Journal of Sound and Vibration, 2011. **330**(10): p. 2339-2353.
202. Tehrani, M.G. and S.J. Elliott, *Extending the dynamic range of an energy harvester using nonlinear damping*. Journal of Sound and Vibration, 2014. **333**(3): p. 623-629.
203. Zhou, S., et al., *Exploitation of a tristable nonlinear oscillator for improving broadband vibration energy harvesting*. The European Physical Journal-Applied Physics, 2014. **67**(3).
204. Zhou, S., et al., *Enhanced broadband piezoelectric energy harvesting using rotatable magnets*. Applied physics letters, 2013. **102**(17): p. 173901.
205. Jung, J., et al., *Nonlinear dynamic and energetic characteristics of piezoelectric energy harvester with two rotatable external magnets*. International Journal of Mechanical Sciences, 2015. **92**: p. 206-222.
206. Leadenham, S. and A. Erturk, *M-shaped asymmetric nonlinear oscillator for broadband vibration energy harvesting: Harmonic balance analysis and experimental validation*. Journal of Sound and Vibration, 2014. **333**(23): p. 6209-6223.
207. Baker, J., S. Roundy, and P. Wright. *Alternative geometries for increasing power density in vibration energy scavenging for wireless sensor networks*. in *3rd international energy conversion engineering conference*. 2005.
208. Masana, R. and M.F. Daqaq, *Electromechanical modeling and nonlinear analysis of axially loaded energy harvesters*. Journal of vibration and acoustics, 2011. **133**(1).
209. Masana, R. and M.F. Daqaq, *Energy harvesting in the super-harmonic frequency region of a twin-well oscillator*. Journal of Applied Physics, 2012. **111**(4): p. 044501.

210. Betts, D.N., et al., *Optimal configurations of bistable piezo-composites for energy harvesting*. Applied Physics Letters, 2012. **100**(11): p. 114104.
211. Friswell, M.I., et al., *Non-linear piezoelectric vibration energy harvesting from a vertical cantilever beam with tip mass*. Journal of Intelligent Material Systems and Structures, 2012. **23**(13): p. 1505-1521.
212. Jung, S.-M. and K.-S. Yun. *A wideband energy harvesting device using snap-through buckling for mechanical frequency-up conversion*. in *2010 IEEE 23rd International Conference on Micro Electro Mechanical Systems (MEMS)*. 2010. IEEE.
213. Jung, S.-M. and K.-S. Yun, *Energy-harvesting device with mechanical frequency-up conversion mechanism for increased power efficiency and wideband operation*. Applied Physics Letters, 2010. **96**(11): p. 111906.
214. Sebald, G., et al., *Simulation of a Duffing oscillator for broadband piezoelectric energy harvesting*. Smart Materials and Structures, 2011. **20**(7): p. 075022.
215. Naseer, R., et al., *Piezomagnetoelastic energy harvesting from vortex-induced vibrations using monostable characteristics*. Applied Energy, 2017. **203**: p. 142-153.
216. Wang, W., et al., *Comparison of harmonic balance and multi-scale method in characterizing the response of monostable energy harvesters*. Mechanical Systems and Signal Processing, 2018. **108**: p. 252-261.
217. Lan, C., L. Tang, and W. Qin, *Obtaining high-energy responses of nonlinear piezoelectric energy harvester by voltage impulse perturbations*. The European Physical Journal Applied Physics, 2017. **79**(2): p. 20902.
218. Fan, K., et al., *A monostable piezoelectric energy harvester for broadband low-level excitations*. Applied Physics Letters, 2018. **112**(12): p. 123901.

219. Priya, S., et al., *A review on piezoelectric energy harvesting: materials, methods, and circuits*. Energy Harvesting and Systems, 2019. **4**(1): p. 3-39.
220. Kong, N., et al., *Resistive impedance matching circuit for piezoelectric energy harvesting*. Journal of Intelligent Material Systems and Structures, 2010. **21**(13): p. 1293-1302.
221. Kong, N., T.S. Deyerle, and D.S. Ha. *Universal power management IC for small-scale energy harvesting with adaptive impedance matching*. in *2011 IEEE Energy Conversion Congress and Exposition*. 2011. IEEE.
222. Sze, S.M., *Semiconductor devices: physics and technology*. 2008: John Wiley & Sons.
223. Rodov, V. and A.L. Ankoudinov, *Super barrier rectifier—a new generation of power diode*. IEEE Transactions on Industry Applications, 2008. **44**(1): p. 234-237.
224. APC.International.Ltd, *Direction of Forces Affecting a Piezoelectric Element*, Figure1_6, Editor.
225. Vijaya, M.S., *Piezoelectric Materials and Devices: Applications in Engineering and Medical Sciences*. Vol. 1. 2012, GB: CRC Press.
226. Bing, K.L., T. Li, and H.H. Hng, *Waste Energy Harvesting : Mechanical and Thermal Energies*. 2014, Springer: Berlin/Heidelberg.
227. Briscoe, J. and S. Dunn, *Piezoelectric nanogenerators – a review of nanostructured piezoelectric energy harvesters*. Nano Energy, 2015. **14**(Supplement C): p. 15-29.
228. Song, Y., et al., *Road energy harvester designed as a macro-power source using the piezoelectric effect*. International Journal of Hydrogen Energy, 2016. **41**(29): p. 12563-12568.

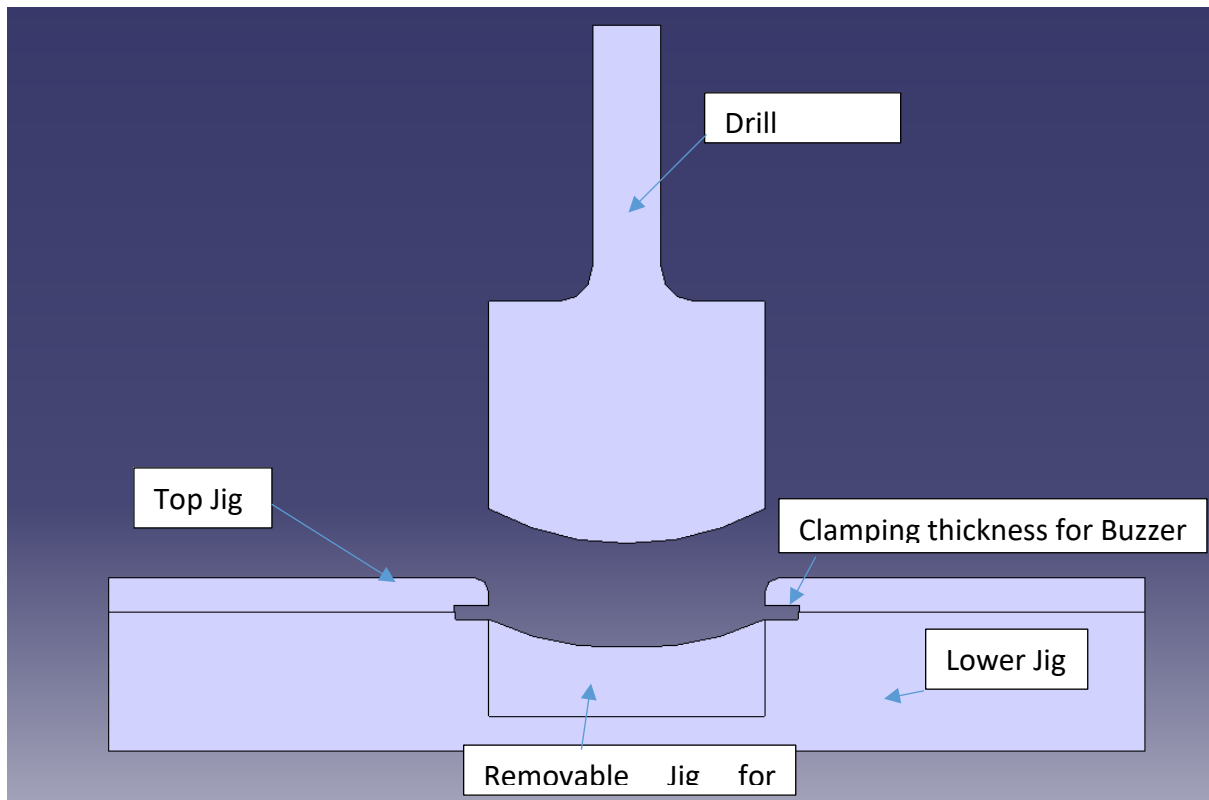
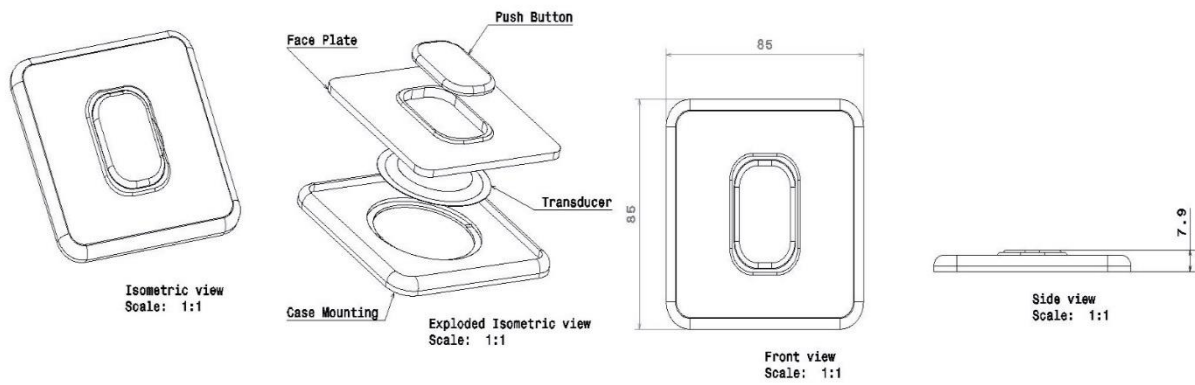
229. Yu, A., P. Jiang, and Z. Lin Wang, *Nanogenerator as self-powered vibration sensor*. Nano Energy, 2012. **1**(3): p. 418-423.
230. Gorji, N.E., et al., *Transition and recombination rates in intermediate band solar cells*. Scientia Iranica, 2012. **19**(3): p. 806-811.
231. Ratlamwala, T. and I. Dincer, *Comparative energy and exergy analyses of two solar-based integrated hydrogen production systems*. International Journal of Hydrogen Energy, 2015. **40**(24): p. 7568-7578.
232. Strba, A. *Operating system design challenges for wireless embedded systems powered by energy harvesters*. in *Applied Machine Intelligence and Informatics, 2009. SAMI 2009. 7th International Symposium on*. 2009. IEEE.
233. Hooker, M.W., *Properties of PZT-based piezoelectric ceramics between-150 and 250 C*. 1998.
234. MatWeb, L., *Material property data*. MatWeb,[Online]. Available: <http://www.matweb.com>, 2016.
235. Didomenico, A. and M.A. Nussbaum, *Measurement and prediction of single and multi-digit finger strength*. Ergonomics, 2003. **46**(15): p. 1531-1548.
236. Puscasu, O., et al., *Powering Lights with Piezoelectric Energy-Harvesting Floors*. Energy Technology, 2018. **6**(5): p. 906-916.
237. Timoshenko, S.P. and J.M. Gere, *Theory of elastic stability*. 2009: Courier Corporation.
238. Gil, H., et al., *Shear buckling strength of trapezoidally corrugated steel webs for bridges*. J Transport Res Board, 2005: p. 473-80.
239. Easley, J.T. and D.E. McFarland, *Buckling of light-gage corrugated metal shear diaphragms*. Journal of the Structural Division, 1969. **95**(7): p. 1497-1516.

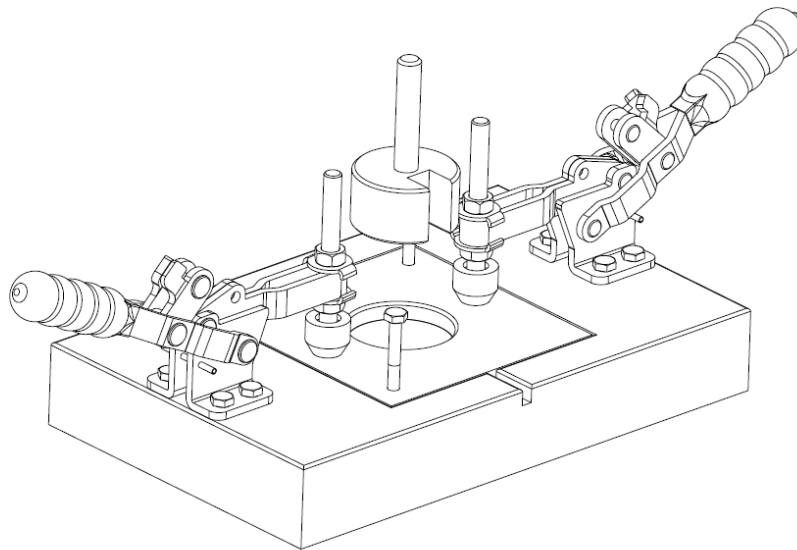
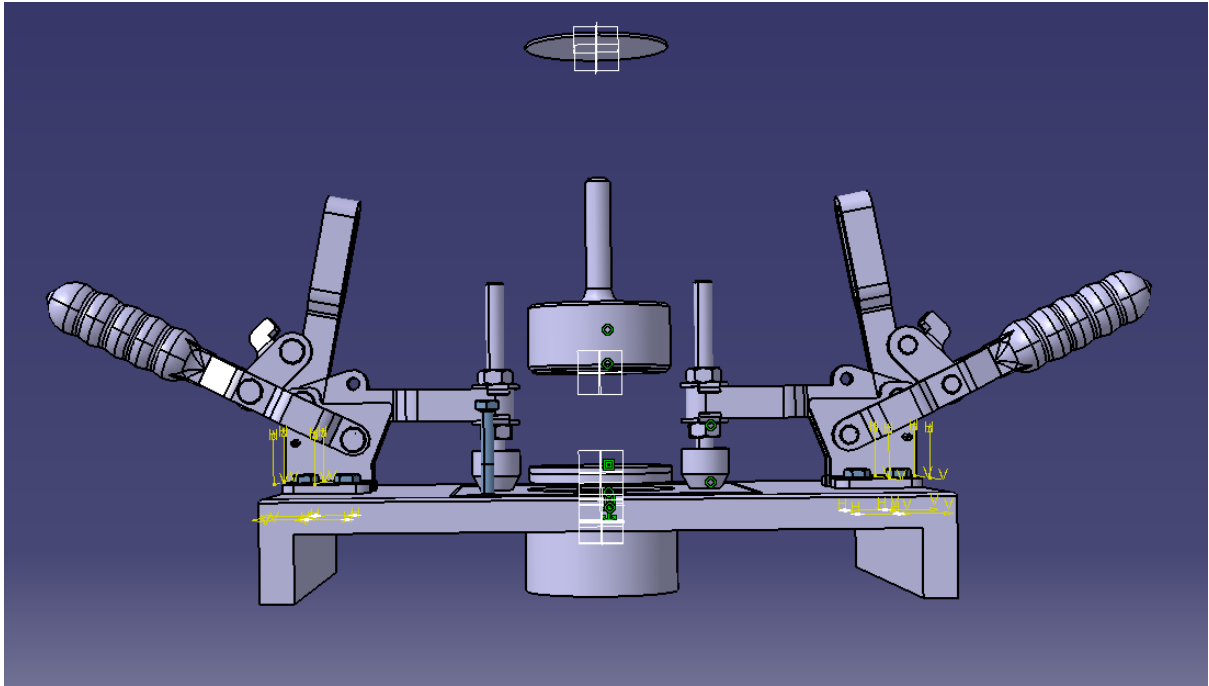
240. Yi, J., et al., *Interactive shear buckling behavior of trapezoidally corrugated steel webs*. Engineering structures, 2008. **30**(6): p. 1659-1666.
241. Butt, Z., et al., *Generation of electrical energy using lead zirconate titanate (PZT-5A) piezoelectric material: Analytical, numerical and experimental verifications*. Journal of Mechanical Science and Technology, 2016. **30**(8): p. 3553-3558.
242. Butt, Z., et al., *Investigation of electrical properties & mechanical quality factor of piezoelectric material (PZT-4A)*. Journal of Electrical Engineering & Technology, 2017. **12**(2): p. 846-851.
243. Faraji G, Mashhadi MM, Hashemi R. Using the finite element method for achieving an extra high limiting drawing ratio (LDR) of 9 for cylindrical components. CIRP Journal of Manufacturing Science and Technology. 2010 Jan 1;3(4):262-7.
244. Reddy AS, Rajesham S, Reddy PR. Evaluation of limiting drawing ratio (LDR) in deep drawing by rapid determination method. International Journal of Current Engineering and Technology. 2014;4(2):757-62.
245. Lee DN. Relation between limiting drawing ratio and plastic strain ratio. Journal of materials science letters. 1984 Aug 1;3(8):677-80.
246. Hajati A, Kim SG. Ultra-wide bandwidth piezoelectric energy harvesting. Applied Physics Letters. 2011 Aug 22;99(8):083105.
247. Lallart M, Guyomar D. An optimized self-powered switching circuit for non-linear energy harvesting with low voltage output. Smart Materials and Structures. 2008 May 6;17(3):035030.
248. Ottman GK, Hofmann HF, Lesieutre GA. Optimized piezoelectric energy harvesting circuit using step-down converter in discontinuous conduction mode. IEEE Transactions on power electronics. 2003 Mar 26;18(2):696-703.
249. Guan MJ, Liao WH. On the efficiencies of piezoelectric energy harvesting circuits towards storage device voltages. Smart Materials and Structures. 2007 Mar 2;16(2):498.

250. Erturk, A.; Inman, D.J. 11.2 Two-Stage Energy Harvesting Circuits: DC-DC Conversion for Impedance Matching. In *Piezoelectric Energy Harvesting*, 1st ed.; JohnWiley & Sons: Hoboken, NJ, USA, 2011; pp. 331–336.
251. Covaci C, Gontean A. Piezoelectric energy harvesting solutions: A review. *Sensors*. 2020 Jan;20(12):3512.
252. Liu H, Hua R, Lu Y, Wang Y, Salman E, Liang J. Boosting the efficiency of a footstep piezoelectric-stack energy harvester using the synchronized switch technology. *Journal of intelligent material systems and structures*. 2019 Apr;30(6):813-22.
253. Jung SM, Yun KS. Energy-harvesting device with mechanical frequency-up conversion mechanism for increased power efficiency and wideband operation. *Applied Physics Letters*. 2010 Mar 15;96(11):111906.
254. Han D, Yun KS. Piezoelectric energy harvester using mechanical frequency up conversion for operation at low-level accelerations and low-frequency vibration. *Microsystem Technologies*. 2015 Aug;21(8):1669-76.
255. Andò B, Baglio S, Bulsara AR, Marletta V, Pistorio A. Investigation of a nonlinear energy harvester. *IEEE Transactions on Instrumentation and Measurement*. 2017 Feb 17;66(5):1067-75.
256. Ando B, Baglio S, Marletta V, Pistorio A, Bulsara AR. Performance investigation of a nonlinear energy harvester with random vibrations and subthreshold deterministic signals. *IEEE Transactions on Instrumentation and Measurement*. 2017 Jan 31;66(5):992-1001.
257. Ajitsaria J, Choe SY, Shen D, Kim DJ. Modeling and analysis of a bimorph piezoelectric cantilever beam for voltage generation. *Smart Materials and Structures*. 2007 Feb 14;16(2):447.
258. Dietl JM, Wickenheiser AM, Garcia E. A Timoshenko beam model for cantilevered piezoelectric energy harvesters. *Smart Materials and Structures*. 2010 Mar 31;19(5):055018.
259. Ly R, Rguiti M, D'astorg S, Hajjaji A, Courtois C, Leriche A. Modeling and characterization of piezoelectric cantilever bending sensor for energy harvesting. *Sensors and Actuators A: Physical*. 2011 Jul 1;168(1):95-100.

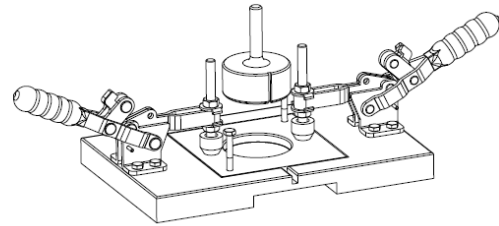
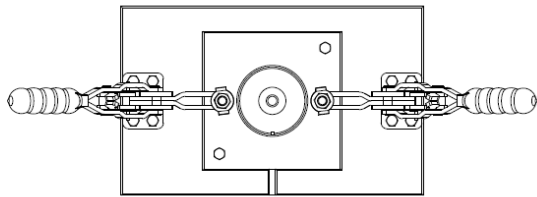
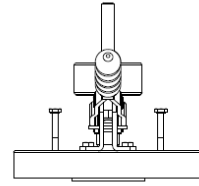
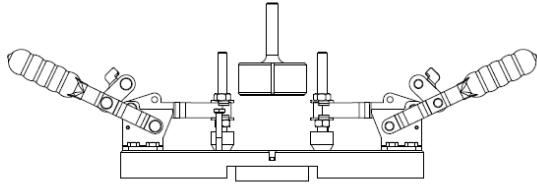
260. Wang G. Analysis of bimorph piezoelectric beam energy harvesters using Timoshenko and Euler–Bernoulli beam theory. *Journal of Intelligent Material Systems and Structures*. 2013 Jan;24(2):226-39.
261. Maurini C, Pouget J, Dell'Isola F. Extension of the Euler–Bernoulli model of piezoelectric laminates to include 3D effects via a mixed approach. *Computers & structures*. 2006 Sep 1;84(22-23):1438-58.
262. Erturk A. Assumed-modes modeling of piezoelectric energy harvesters: Euler–Bernoulli, Rayleigh, and Timoshenko models with axial deformations. *Computers & Structures*. 2012 Sep 1;106:214-27.
263. Liang X, Hu S, Shen S. Effects of surface and flexoelectricity on a piezoelectric nanobeam. *Smart materials and structures*. 2014 Feb 14;23(3):035020.
264. Shen J, Wang H, Zheng S. Size-dependent pull-in analysis of a composite laminated micro-beam actuated by electrostatic and piezoelectric forces: Generalized differential quadrature method. *International Journal of Mechanical Sciences*. 2018 Jan 1;135:353-61.
265. Hajheidari P, Stiharu I, Bhat R. Performance of tapered cantilever piezoelectric energy harvester based on Euler–Bernoulli and Timoshenko Beam theories. *Journal of Intelligent Material Systems and Structures*. 2020 Mar;31(4):487-502.
266. She GL, Shu X, Ren YR. Thermal buckling and postbuckling analysis of piezoelectric FGM beams based on high-order shear deformation theory. *Journal of Thermal Stresses*. 2017 Jun 3;40(6):783-97.
267. Li HT, Qin WY, Zu J, Yang Z. Modeling and experimental validation of a buckled compressive-mode piezoelectric energy harvester. *Nonlinear Dynamics*. 2018 Jun;92(4):1761-80.
268. Liang C, Zhang C, Chen W, Yang J. Static buckling of piezoelectric semiconductor fibers. *Materials Research Express*. 2020 Jan 10;6(12):125919.
269. Roy R, Garg A, Dwivedy SK. Dynamic Analysis of Parametrically Excited Coupled Beam-Based Piezoelectric Energy Harvester. In *Recent Advances in Mechanical Engineering 2021* (pp. 631-642). Springer, Singapore.
270. Li X, Luo Y. Size-dependent postbuckling of piezoelectric microbeams based on a modified couple stress theory. *International Journal of Applied Mechanics*. 2017 Jun 12;9(04):1750053.

Appendices

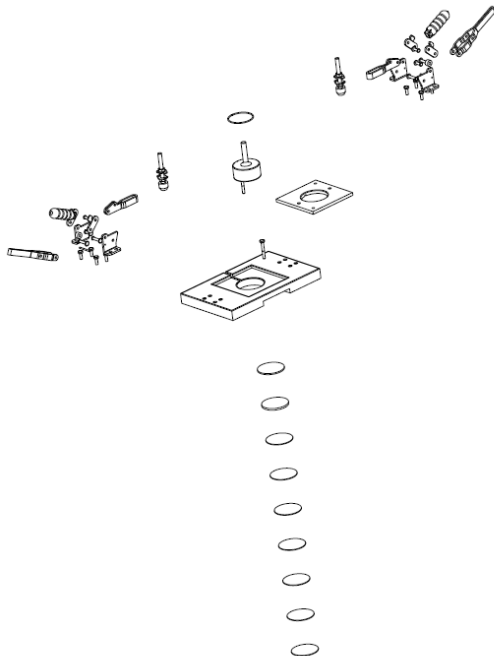




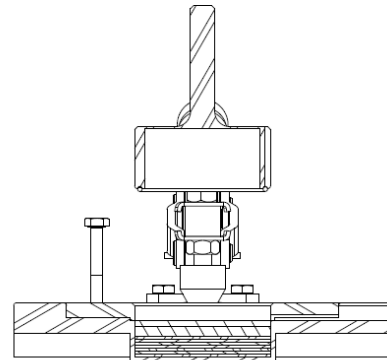
DESIGNED BY: Nathan Counsell		I	-
Isometric View		H	-
Scale: 1:1		G	-
DATE: XXX		F	-
DATE: XXX		E	-
SIZE: A3		D	-
SCALE: 1:1	XXX	C	-
		B	-
UNIVERSITY OF HERTFORDSHIRE		Buzzer Jig Design	
Isometric View		1/1	



Bistable Jig for RS Component 622-1584 (Buzzer)		University of Hertfordshire		
		Bistable Buzzer Jig		
DRAWN BY Nathan Counsell	DATE 23/11/2015	SIZE A3	DRAWING NUMBER Assembly of Jig	REV X
CHECKED BY XXX	DATE XXX	SCALE 1:2	WEIGHT (kg) 0.47	SHEET 1/1
DESIGNED BY XXX	DATE XXX			

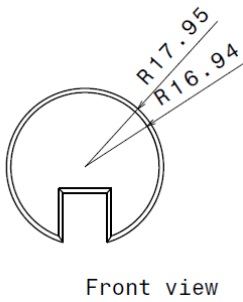
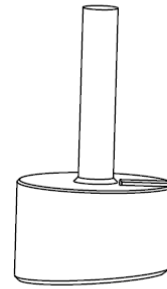
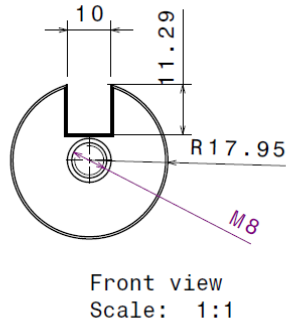
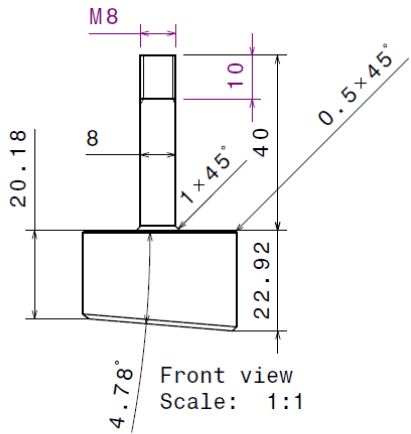


Isometric view
Scale: 1:5

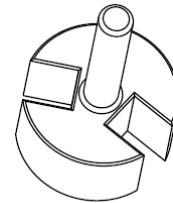
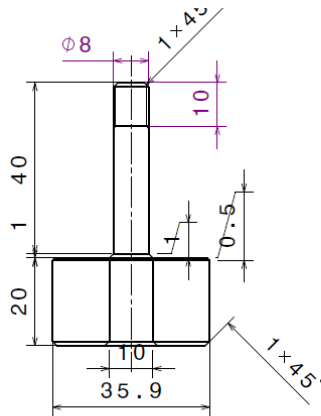
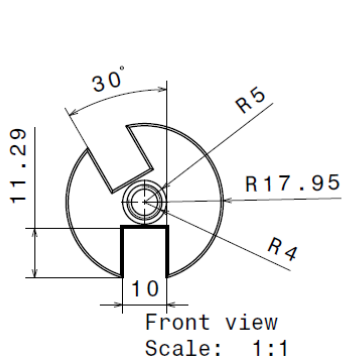


Section view A-A
Scale: 1:1

Bistable Jig for RS Component 622-1584 (Buzzer)		University of Hertfordshire		
		Bistable Buzzer Jig		
DRAWN BY Nathan Counsell	DATE 23/11/2015	SIZE A3	DRAWING NUMBER Assembly of Jig	REV X
CHECKED BY XXX	DATE XXX	SCALE 1:2	WEIGHT (kg) 0.47	SHEET 1/1
DESIGNED BY XXX	DATE XXX			

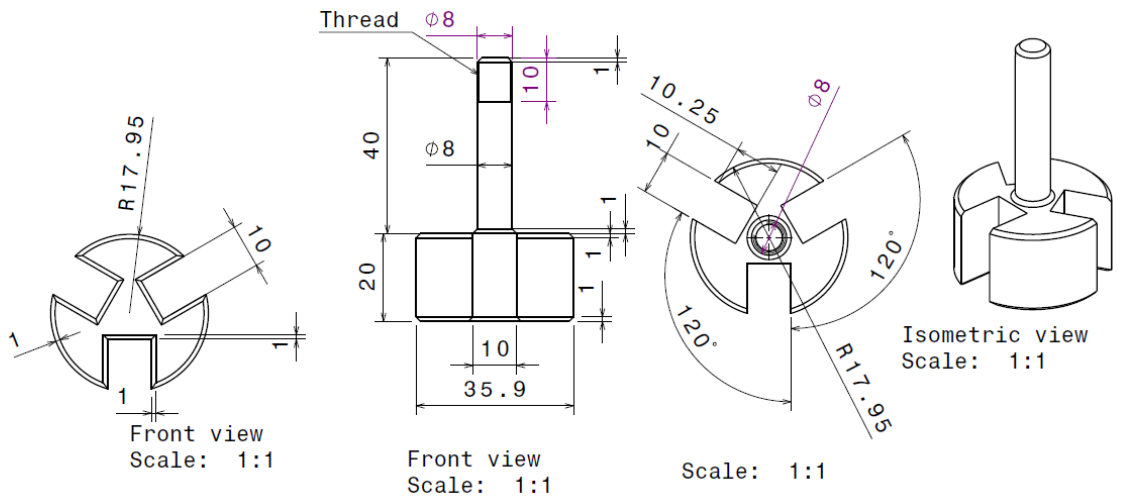


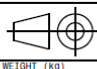
DESIGNED BY: Nathan Counsell				I	-
DATE: 14/03/2016				H	-
CHECKED BY: XXX				G	-
DATE: XXX				F	-
SIZE: A4		University of Hertfordshire		E	-
SCALE: 1:1		DRAWING NUMBER: Stamp Slope		D	-
WEIGHT (KG): 0.02		SHEET: 1/1		C	-
				B	-



DESIGNED BY: Nathan Counsell				I	-
DATE: 10/03/2016		Two Hole Punch 150 Degrees off set		H	-
CHECKED BY: XXX				G	-
DATE: XXX				F	-
SIZE: A4		Univeristy of Hertforshire		E	-
SCALE: 1:1		DRAWING NUMBER: Stamp Two Hole		D	-
WEIGHT (KG): 0.02		SHEET: 1/1		C	-
				B	-
				A	-

This drawing is our property; it can't be reproduced or communicated without our written agreement.



DESIGNED BY: Nathan Counsell		Three Point Buzzer Press	I	-
DATE: 09/03/2016			H	-
CHECKED BY: XXX		University of Hertfordshire	G	-
DATE: XXX			F	-
SIZE: A4		E	-	
SCALE: 1:1	WEIGHT (kg): 0.02	D	-	
DRAWING NUMBER: Stamp 2		C	-	
SHEET: 1/1		B	-	



Powering Lights with Piezoelectric Energy-Harvesting Floors

Onoriu Puscasu,^{*,[a], [b]} Nathan Counsell,^[a] Mohammad R. Herfatmanesh,^[a] Richard Peace,^[b] John Patsavellas,^[b] and Rodney Day^[a]

The present work introduces a new technology for converting energy from steps into electricity. It starts with a study of the mechanical energy available from steps in a busy corridor. The subsequent development efforts and devices are presented, with an iterative approach to prototyping. Methods for enhancing the piezoelectric conversion efficiency have been determined as a part of the process and are introduced in the present article. Capitalizing on these findings, we have fabricated energy-harvesting devices for stairs that

power embedded emergency lighting. The typical working unit comprises an energy-harvesting stair nosing, a power management circuit, and an embedded light-emitting diode that lights the tread in front of the user with an illuminance corresponding to emergency standards. The stair nosing generates up to 17.7 mJ of useful electrical energy per activation to provide up to 10.6 seconds of light. The corresponding energy density is 0.49 J per meter square and per step, with an 8.5 mm thick active layer.

Introduction

Harvesting energy from steps is an exciting and equally challenging scientific and technological undertaking. Several efforts have been made by the scientific community and companies, leading to energy-harvesting devices with various form factors and power outputs. Work has been performed using two main approaches: inserting energy-harvesting components into floors or shoes. Some authors proposed devices that can be attached to human limbs. In the present project, we focused on generating energy from steps by using active floors as a joint effort between academic research and a floor covering manufacturer.

Research into energy generation with steps has led to the development of several techniques, with heel-strike energy harvesting being the most common. In 1996 Starner proposed one of the first estimations of the mechanical power available from heel strikes.^[1] It is calculated that 67 W of power are generated by a person walking at a pace of 2 steps per second, with the possibility of extracting 5 W by using piezoelectric shoe inserts. Niu et al. estimate the useful energy available at 0.4–1 J step⁻¹.^[2] They predict that the maximal electrical power extracted from heel strikes would be 2 W for a user walking at 2 steps per second. Shenck and Paradiso have developed energy-harvesting soles based on polyvinylidene fluoride (PVDF) and lead zirconate titanate (PZT) piezoelectric materials.^[3] The test results show that the PVDF sole generates approximately 1.3 mW of power for a strike frequency of 0.9 Hz, whereas the PZT design produced 8.4 mW. In both cases the generated power is dissipated in resistors. The authors have also tested storing the energy to power a radio frequency identification (RFID) transmitter circuit embedded in the shoe.

Various other shoe- or limb-mounted devices have been designed, exploring different force transmission techniques.


Howells investigated a mechanism with lead screw and cam that activated piezoelectric cantilevers,^[4] while Alghisi explored the activation of piezoelectric membranes with a metal ball that was free to move in a cavity.^[5] Xie designed a device that used an amplification mechanism with sliders to generate high strain in piezoelectric bimorphs.^[6] Studies on nonlinear techniques for piezoelectric energy harvesting from human motion have previously been proposed by Green^[7] and Cao.^[8]

Investigations on energy-harvesting floors have been conducted by researchers from academia and companies. Sharpes designed a tile based on PZT cymbal transducers capable of powering wireless signal transmissions,^[9] and Bischur proposed using PVDF-based modules.^[10] Notable efforts have been conducted in developing electromagnetic energy-harvesting tiles.^[11] For energy-harvesting stairs, a study has been proposed by Puspitarini.^[12] It is focused on collecting information on the user's needs to define a sustainable stairway concept.

Our research efforts have been focused on developing an energy-harvesting floor based on piezoelectric technology.^[13]

[a] Dr. O. Puscasu, N. Counsell, Dr. M. R. Herfatmanesh, Dr. R. Day
School of Engineering
University of Hertfordshire
College Lane, AL10 9AB, Hatfield (UK)
E-mail: onoriu.puscasu@gmail.com

[b] Dr. O. Puscasu, Dr. R. Peace, J. Patsavellas
Altro Ltd
Works Road, SG61 1NW, Letchworth (UK)

 This publication is part of a Special Issue on "Ferroelectric Devices for Energy Harvesting and Storage". To view the complete issue, visit: <http://dx.doi.org/10.1002/ente.v6.5>.

This choice is due to the readily available materials and the thin form factor that piezoelectrics allow.

As our goal is to convert the mechanical energy from a walking person into electrical energy, we started our research by evaluating the former. In parallel, we built our first devices and evaluated the electrical energy recovered using PZT-based piezoelectric materials. Once aware of the gap between the available and recovered energy, we started a process of enhancement that allowed us to increase significantly the power output and efficiency.

The technological choices during the development journey and the reasoning behind them are described in the following sections.

Results

Mechanical energy per step

Previous work^[14] shows that while stepping a person develops a vertical force pattern that resembles the letter M. Our own gait analysis recordings confirm this, as reflected in Figure 1. The two peaks correspond to precise moments of the gait cycle. The first peak is reached when the foot finishes landing and is in full contact with the floor. It comes at the end of the gait phase also known as the heel rocker, when the foot revolves around the heel.^[14] A valley follows, with the force diminishing generally to approximately 50% of the peak, while the other foot swings forward. The subsequent increase in force culminating with the second peak is due to the acceleration of the foot in preparation for “take-off”. The second peak is reached just before the heel starts rising. This is the end of the phase called the “ankle rocker” when the dominant movement is the rotation of the leg around the ankle.

In the measurements presented in Figure 1, the average peak force is 1143 N for a subject weighing 87 kg. This is 33.9% greater than the body weight. The average local minimum in the valley is 44% of the peak. These ratios are close to data found in the literature.^[14]

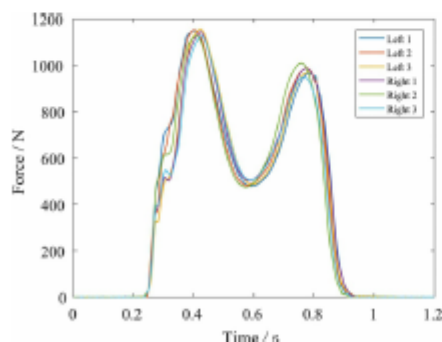


Figure 1. Forces developed during stepping. Measurements for the left and right foot of the subject are presented, respectively, as recorded using a force plate. The subject weight was 87 kg.

The peak forces while walking are generally 20–30% greater than the bodyweight, this being the first input into the calculation of the mechanical energy that is generated. The second input should be the displacement induced in the floor surface. While a person walks the flooring is subjected to some degree of deformation. Simple physics shows that the mechanical energy stored in an object depends on its deflection and the forces involved. The same can be applied to the portion of flooring on which a user steps:

$$E_m = \int F \cdot dz$$

in which E_m represents the mechanical energy, F the vertical force exerted on the floor, and z the average deflection under the foot.

As precise force versus deflection measurements are not trivial, we chose to make an estimation of the energy by assuming a linear increase. With this in mind, the peak mechanical energy becomes:

$$E_{max} = \frac{1}{2} \cdot F_{max} \cdot d_{max}$$

in which F_{max} is the peak force and d_{max} is the peak deflection.

In the case of an energy-harvesting floor, the maximal deflection will be the one allowed by design. Indeed, we would want to protect the active piezoelectric elements by limiting the amount of strain subjected to them. This allows estimating the mechanical energy that one can generate per step in a typical case:

$$E_m = \frac{1}{2} \cdot m \cdot g \cdot d_{max} = 0.47 \text{ J}$$

for a typical weight of 76.5 kg and 1 mm floor deflection.

Without surprise, the higher the force involved, the higher the mechanical energy that can be converted into electricity. Roughly 0.5 J of mechanical energy is generated by an average person on a floor that allows 1 mm of deflection. This amount will increase to 1.41 J for 3 mm deflection, and to 2.35 J for 5 mm. Although this is an estimation relying on the assumption of a linear variation of force with deflection, it gives a good understanding of the order of magnitude of the energy that can be generated while walking. Therefore, it is safe to say that this order of magnitude is of 1 J per step.

The contribution of the deflection to the energy is worth a more detailed analysis. According to the expression above, a floor that deflects more will store more energy than a floor that hardly deforms, for the same user. In the second case the energy will be stored elsewhere: shoes, legs, joints of the user, or vibrations of the substrate, and will be dissipated through thermal effects. Therefore, to maximize energy generation we will have to allow for some deflection, enough to harvest the desired amount without compromising the comfort of the user or reaching the strain limits of the flooring

materials. This conclusion is valid independent of the energy conversion technology employed. The latter will determine the amount of electrical energy in the output by its efficiency.

Energy in a busy corridor

The next step of the study is calculating the amount of energy that can be generated per day in a busy corridor inside a public building. This will give an idea of the upper limits of energy harvesting from steps as a solution for powering lights and building systems.

We used optical counting to monitor the number of users in a portion of a busy university corridor. A camera connected to a data processing system was installed in a corridor with high traffic, and counted the number of users over 3 months' time. The complete statistics are shown in Figure 2.

One can notice the weekly cycles, with maxima reached during working days, and low traffic during weekends and the winter break. The maximum traffic on the portion of the corridor under study was 4613 users per day. Considering that the average stride length of a person is 76 cm, an energy-harvesting floor with the same length will harvest 4613 steps per day. If this flooring allowed 5 mm deflection, the users would generate 11500 J per day, or 3.2 Wh. Supposing a harvesting technology with 50% mechanical–electrical conversion efficiency, 1.6 Wh will be stored as electrical energy for use. This would amount to 210 Wh per day with 100 m length of active flooring, or 77 kWh per year with sustained high traffic every day.

Knowing the price per kilowatt-hour of electrical energy it is easy to determine that energy-harvesting flooring will probably not be a cost-effective solution for powering the primary lights or other building systems such as heating or air conditioning, even in a busy corridor.

The main conclusion of this study is that energy harvesting from steps is more suitable for low-power applications. One can cite building monitoring and safety: place and forget environmental sensors, intrusion detection, requiring just one alert per event, or low-level lighting. The latter, and more precisely powering emergency lighting, is our application of choice that we decided to develop further, as described in the next sections.

Design of an energy-harvesting tile

We built our first step energy-harvesting devices using commercially available piezoelectric membranes. Elements such as the one presented in Figure 2a were employed. They have an outer diameter of 50 mm. The first representative prototype consists of an 8 × 7 matrix of circular piezoelectric membranes, connected to the same output through conductive paths (Figure 3b).

Conductive tape was used to collect the charge generated by the piezoelectrics. All of the elements in the matrix were connected electrically in parallel. Conductive paths below the membranes were in contact with the ground electrodes and a second set of paths run above the top electrode (Figure 3c). Each set of paths was then directed towards the common output. An air gap was left below each piezoelectric (not shown in Figure 3) through an incision into the substrate. This allowed each piezoelectric element to deflect by 1 mm upon actuation. The surface supporting the assembly acted as a mechanical stop to limit the deflection of the membranes. A spacer was placed at the center of each piezoelectric element to transmit the effort coming from the foot of the user.

A rigid top plate was used to distribute the walker's force across the piezoelectric matrix. Here we used a 0.9 mm steel sheet. To complete the assembly, the entire device was covered with a slip resistant flooring layer and two light-emitting

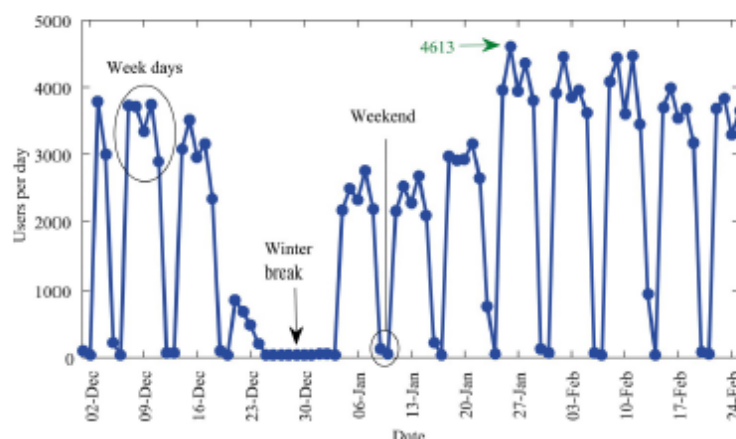


Figure 2. Traffic in a busy university corridor, as recorded using an optical counting system.

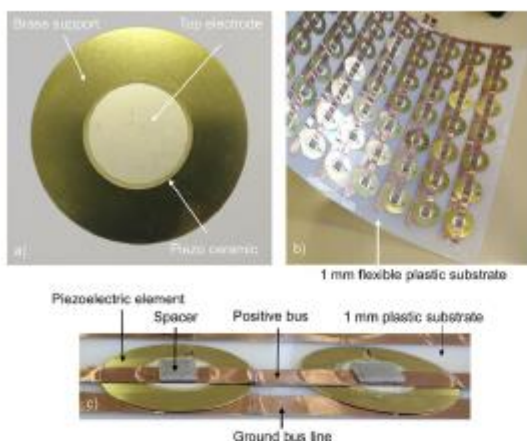


Figure 3. Structure of the energy-harvesting tile active layer: a) commercially available piezoelectric element as used in the assembly; b) active matrix of 8×7 elements on a flexible substrate; c) structural detail. Spacers are used for actuation purposes. Air gaps are left below the piezoelectric membranes to allow for deflection (not shown).

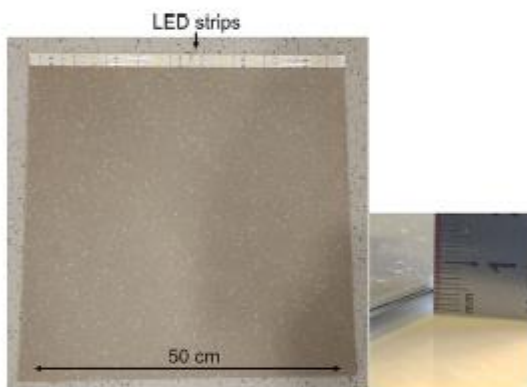


Figure 4. $50 \times 50 \text{ cm}^2$ energy-harvesting tile with embedded LED strips. The total thickness, including the slip resistant upper layer, is 7 mm.

diode (LED) strips were applied onto the edge, to be powered by the prototype (Figure 4).

Performance of the energy-harvesting tile

The energy-harvesting tile was tested under real conditions, with consecutive steps taken on it. The output signal is presented in Figure 5a, as measured with a $10 \text{ M}\Omega$ probe. The average voltage rise for each peak was approximately 50 V. The shift in the signal is due to charge flow through the probe, as its impedance is not infinite and it does not ensure open-circuit conditions.

To store the generated energy, we connected the tile to a diode bridge and a $10 \mu\text{F}$ capacitor. The result is presented in Figure 5b and shows that the capacitor charged in two stages

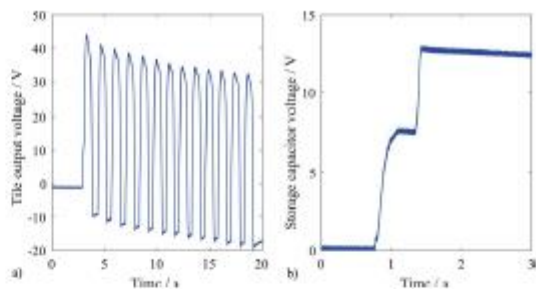


Figure 5. a) Output signal of the $50 \times 50 \text{ cm}^2$ tile as measured using a $10 \text{ M}\Omega$ probe; b) Charging of a $10 \mu\text{F}$ capacitor with one step through a diode bridge.

up to 13 V upon taking one step on the tile. The initial rise was due to the user stepping on the tile and the second was due to the foot being lifted.

We estimate the stored electrical energy using the capacitor formula:

$$E_{\text{el}} = \frac{CV^2}{2} = 0.84 \text{ mJ}$$

The electrical energy generated with one step is thus slightly below 1 mJ. An electrolytic capacitor rated at 63 V was used for the experiment. The main reason behind this choice is the large storage voltage limit, allowing for comparison between various energy-harvesting modules.

As confirmed by visual observations, not all of the piezoelectric elements were well deflected in this configuration. The thin steel sheet bent on the edges, and failed to actuate as required for peripheral membranes. To enhance the actuation, an 18 mm thick wooden tile was added to the sandwich, under the steel sheet, as presented in Figure 6. The new total thickness was 25 mm, with the active layer accounting for 4 mm.



Figure 6. Energy-harvesting tile with an additional 18 mm wooden slab.

Measurements were performed once again under similar conditions. The output signal, and the capacitor loading are shown in Figure 7. The average voltage rise for a peak was 82 V, significantly higher than in the previous case. As for the storage voltage on the same capacitor, it rose to 22 V per step. This corresponds to 2.44 mJ of electrical energy, a threefold increase compared to the previous configuration.

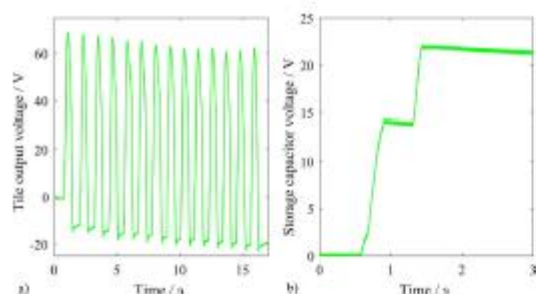


Figure 7. a) Signal of the tile after inserting an 18 mm wooden slab for more efficient actuation; b) 10 μF capacitor charging through a diode bridge.

This study shows the importance of transmitting the force efficiently to the active elements. It was visible with the naked eye that peripheral piezoelectrics in the tile had minimal deflection when the user stepped on the center. Therefore, increasing the thickness of the actuation layer has proven to be an efficient approach to address that. When activated at a pace of 1 step per second this configuration would produce 2.44 mW of power.

Fatigue study

A useful piece of information that flooring manufacturers collect is the fatigue behavior of their products for quality and warranty purposes. Slip-resistant flooring must show resilience in heavy traffic areas, and therefore manufacturers perform tests upon production to ensure a suitable quality. Usual tests involve performing 1 million walking cycles on a sample of flooring and observing the changes in texture and color.

Within this in mind, we conducted a study on the fatigue behavior of the piezoelectric elements used in the energy-harvesting tile. A membrane was mounted onto a rigid frame and actuated with a cylindrical head for a large number of cycles. The test machine used was the Instron ElectroPulse E3000 system. The main elements of the setup are shown in Figure 8.

Up to 10 million repetitive compression cycles were performed on the piezoelectric element with a 10 Hz actuation frequency. The deflection at the center was set to 1 mm, as in the tile itself, and the open-circuit signal was recorded. A sample signal is shown in Figure 9, with maxima reaching 64 V and minima -43 V, for a peak-to-peak amplitude of 107 V.

The evolution of the signal maxima and minima is presented in Figure 10. The results of the first and last half of a million cycles out of 10 million are included. Little variation in the value of the peaks was observed. Indeed, the initial peak-to-peak signal amplitude was 109 V and the end amplitude was 110 V. A slight floating of the peak values was also observed, and it was most likely due to changes in the ambient temperature of the test room, for the duration (several days) of the tests.

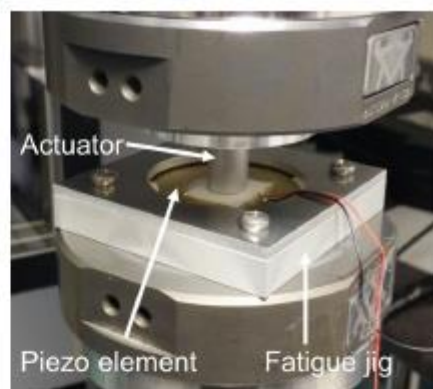


Figure 8. Compression fatigue test setup.

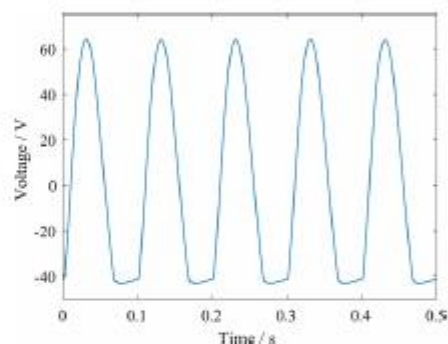


Figure 9. Sample piezoelectric signal during fatigue testing.

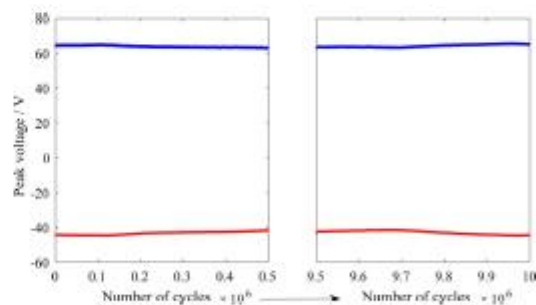


Figure 10. Evolution of the positive and negative piezoelectric peaks over 10 million fatigue cycles. The first and last halves of one million cycles are presented. Little variation in the signal is observed, with a slight floating, most probably due to ambient temperature variation.

These results are highly encouraging for our technology because they prove the reliability of the piezoelectric elements well above 1 million fatigue cycles, the usual mark in the flooring industry.

Intermediate discussion

These results conclude the first part of the study. To summarize, an estimation of the energy that can be recovered in a busy corridor has been provided, and an energy-harvesting tile with commercially available piezoelectric elements has been fabricated and tested. Also, fatigue tests were performed.

We have concluded from the busy corridor study that harvesting energy from steps is not an optimal solution for powering building systems, such as main lighting, heating, or air conditioning. Building monitoring applications with low-power sensors and powering low-level lighting are suitable due to their lower energy requirements. In this context, energy-harvesting flooring will bring the benefit of autonomy, without the need for wiring to the main electrical supply of the building. Thus, it will become possible to power devices in situations where the mains electricity fails, is too expensive to connect to, or is not available at all.

Aiming at providing a benefit to the user through energy harvesting from steps is a more reasonable approach than aiming at generating energy for use at will. Rather than connecting energy-harvesting floors to the grid, one would benefit from powering applications with low energy requirements, tailored to the generation capabilities of the flooring.

By using commercially available piezoelectric elements assembled into a $50 \times 50 \text{ cm}^2$ tile, we generate a few millijoules of electrical energy per step. This is sufficient for powering RF transmitters and allowing for the use of the energy-harvesting floor as part of a presence detection/alarm system, for example. Additionally, this study shows that the rigid tile format is desirable. Moreover, the thicker the top actuating plate, the higher the energy output.

With these conclusions in mind, it was decided to direct the research towards devices for staircases, to power emergency lighting. This is to capitalize on the tile format, while providing a benefit in an area that is critical for the user. To address the new use case, we decided to start by improving the efficiency of the piezoelectric elements. This was necessary to achieve compact devices that can provide enough power for emergency lighting.

Enhancing the power output with bistable piezoelectric elements

It has previously been observed that when a piezoelectric disc is subjected to high deflection, it reaches a state of plastic deformation. Initially the authors investigated this behavior and its impact on the performance as a damaging mechanism. After a series of trials it was found that under special forming conditions a piezoelectric disc reaches a bistable behavior, similar to that of a push button.

An example of bistable piezoelectric membrane is shown in Figure 11. A concave shape is reached through controlled loading causing permanent deformation. Contrary to expectations, it was found that the output signal was significantly increased with respect to a flat disc operating in the elastic

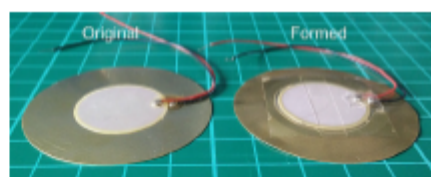


Figure 11. Piezoelectric disc in its original shape and formed disc showing bistable behavior similar to a push button.

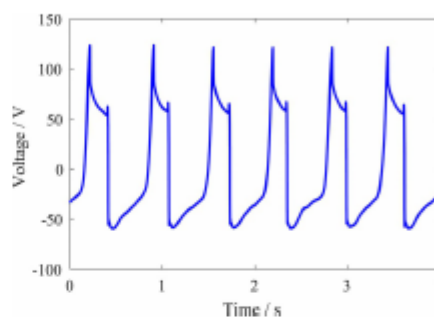


Figure 12. Signal of a bistable piezoelectric element.

zone. An example is presented in Figure 12. Here the actuation frequency is approximately 1.5 Hz, with a negative peak value down to -60 V and a positive peak value up to 124 V . The resulting peak-to-peak voltage amplitude was 184 V , which is significantly higher than the signal of the flat piezoelectric membrane (107 V). The abrupt rise in voltage at each cycle corresponds to snap action. The actuation force required is 19 N , as measured with a mechanical testing machine. This is similar to the force applied on a flat element to reach 1 mm deflection.

Far from being damaging, the forming process yielded piezoelectric elements with increased voltage for a force similar to that applied to a flat element. The signal was also repeatable, making it possible to integrate formed piezoelectrics into energy-harvesting devices for stairs.

Design and performance of a device for stairs

When a person walks on stairs, they tend to step on the edges of the stair treads. Usually these edges are protected or at least highlighted with a stair nosing. Typically they come as L-shaped profiles that wrap around the edges, which can be made of metal, plastic, or a combination of the two.

The stair nosing has the role of providing slip resistance, visual contrast for the user, and protecting the edge of the tread. As users tend to step on the edge of the treads, we decided to design a device that fits perfectly in this area.

We used a metal holding plate with circular slots, in which we placed bistable piezoelectric elements, realizing that it was possible to stack them for increased power output. Fourteen piezoelectric elements were used to build the device

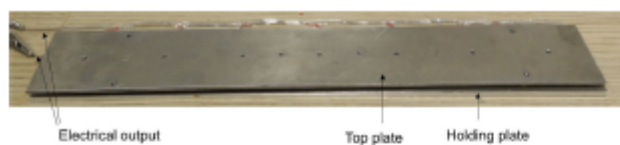


Figure 13. Energy-harvesting device for stair nosings (40 cm × 6 cm × 1.2 cm).

presented in Figure 13. They were placed on seven slots, each containing two stacked piezoelectrics with an actuator on top. The array is covered by a steel top plate that transmits the force from the user's foot across the whole surface.

The resulting device had a size of 40 cm × 6 cm × 1.2 cm; having a thin profile, only 12 mm thick, it could be easily placed under existing stair coverings. Capacitor loading tests were performed to assess the electrical output. As previously for the energy-harvesting tile, a circuit consisting of a diode bridge and a 10 μ F storage capacitor was used. A screenshot of the capacitor loading with one step is presented in Figure 14.

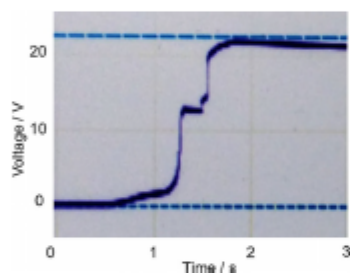


Figure 14. 10 μ F capacitor loading per step with the stair nosing device.

The voltage reached was 22.5 V, corresponding to 2.53 mJ of electrical energy. This is slightly higher than the energy supplied by the energy-harvesting tile with a wooden slab on top, and a total thickness of 25 mm. Moreover, the surface area of the stair nosing device was 10 times smaller, and only 14 piezoelectric elements were used, as opposed to 56 for the tile. This corresponds to an increase in energy per piezoelectric by a factor 4, proving the advantage of forming piezoelectric membranes.

Integration into a staircase to power emergency lighting

The new device is ideal for integration into a staircase. To capitalize on its thin form factor, it was fitted to a set of steps built for this purpose, as presented in Figure 15.

The demonstrator was composed of two steps and an additional riser (Figure 15a). The energy-harvesting nosing was placed at the edge of the first step (Figure 15b). A power-management circuit was placed close to the next riser. It was composed of a bridge rectifier connected to a capacitor followed by a direct current (DC)—DC converter. A voltage

regulator allowed setting the output to the desired level. The power-management circuit rectified the signal coming from the harvester to power the component of our choice. Here, we used a 5000 K white LED, with an adapted resistor. The LED was chosen for its high efficiency, and it was placed at the top of the last riser, as shown in Figure 15a.

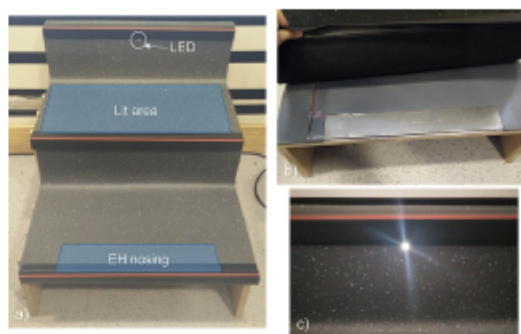


Figure 15. a) Staircase with embedded energy-harvesting nosing and a high-efficiency LED; b) energy-harvesting device placed under the stair covering; c) light generated with one step.

Polyvinyl chloride (PVC) stair coverings were placed on top of the steps. They provided slip resistance and concealed the energy-harvesting system.

When the user steps on the first tread, the LED turns on and lights the second one. The light output is shown in Figure 15c. With this particular energy-harvesting device, 0.9 s of light were generated per step. The illuminance created was approximately 1 lux, which corresponds to the level required for emergency lighting on staircases.^[15]

This is the first complete demonstration, containing all the parts required for an energy-harvesting system. It is capable of providing a benefit to the user, one step being sufficient to trigger emergency lighting.

Although the functionality of the system and of the formed piezoelectrics has been proven, we decided to improve the energy output further. This next step involves minimizing the passive area of the piezoelectric elements.

Preloading piezoelectrics to improve performance

The authors decided to reduce the passive brass area that surrounds the active piezoelectric ceramics. To do so, square patterns were cut around the latter, keeping the brass surface close to the necessary minimum, as depicted in Figure 16. This allowed for an overall decrease in surface area by a factor of 3.14.

As forming is not practical for the new elements, it was decided to preload the membranes laterally to provide them with a 3D shape. This was achieved by clamping square elements on the sides and applying lateral force inside a



Figure 16. From left to right: flat, formed, and pre-cut piezoelectric elements.

custom-made thin holder. It has been observed that under these conditions the piezoelectric element buckles, as presented in Figure 17. By doing so, it becomes bistable, thus allowing multiple actuations, each followed by self-return to the initial position. In short, the pre-loaded square elements exhibit similar behavior to the formed elements, with the added benefit of much reduced surface area and mechanical noise. Indeed, the snapping of the formed membranes was accompanied by a clicking sound, whereas under the new conditions the sound was not perceptible anymore.

Having the new configuration in place, we measured the energy generated per piezoelectric element, and we compared it to the previous cases. As before, the comparison was achieved by observing the loading of a $10\ \mu\text{F}$ capacitor with one actuation. The results are summarized in Figure 18.

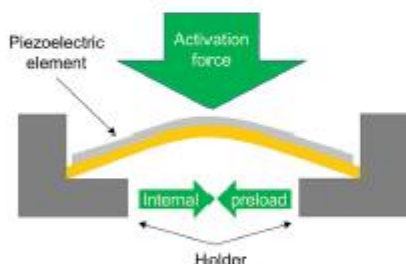


Figure 17. Schematic section of a preloaded piezoelectric. An internal preloading mechanism induces buckling in the initially flat square element. In use, the actuation force is transmitted from the top.

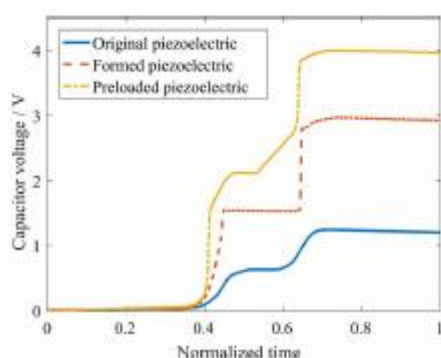


Figure 18. Capacitor loading with one press for 3 types of piezoelectrics.

The original piezoelectric loaded the capacitor to 1.2 V level, and the preformed device to 3.0 V. In terms of stored energy this is a 5.7 times increase. The preloaded piezoelectric charged the capacitor to 4.0 V, which is an increase of 10.3 times that of the original element. Given that the surface area of the preloaded piezoelectric is 3.14 times smaller, this translates into an increase in energy of 32 times per unit area and per activation. This design was then investigated further to fabricate a new generation of energy-harvesting devices for stairs.

Upgraded energy-harvesting devices for stairs

A new design for energy-harvesting devices was then proposed for using preloaded piezoelectrics. Fifty-six piezoelectric elements were assembled together onto a machined aluminum holding plate. They were separated into two parallel lines, each one preloaded laterally before use. The resulting device is presented in Figure 19. A commercially available aluminum stair nosing was used as a top plate to actuate the piezoelectric elements. It was covered with white plastic strips for slip resistance and visual contrast purposes. End caps were used to hold all the parts together and stabilize the structure.

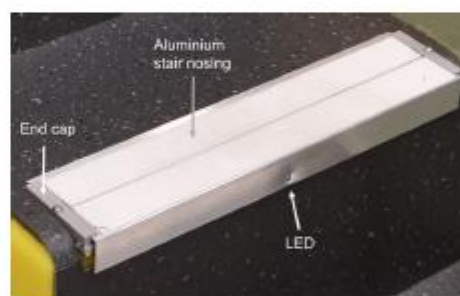


Figure 19. Energy-harvesting stair nosing mounted on a step. The aluminum stair nosing actuates preloaded piezoelectrics placed underneath (not visible on the image). End caps stabilize the structure.

The overall dimensions of the prototype were $40\ \text{cm} \times 9\ \text{cm} \times 1.35\ \text{cm}$. The 1.35 cm total fitted thickness is composed of the thickness of the active part (8.5 mm) and top aluminum nosing thickness (5 mm). The nosing riser is 32 mm high, and contains the LED in the middle. The latter lights the step below when the device is activated.

Capacitor loading through a diode bridge with the new prototype is shown in Figure 20. Given the increase in generated energy, a $47\ \mu\text{F}$ storage capacitor was used. The voltage on it reached 27.5 V per activation, which corresponds to 17.7 mJ of electrical energy. This is a 7.3 times increase compared to the $50 \times 50\ \text{cm}^2$ tile with a wooden slab actuator incorporating the same number of piezoelectrics. The energy density per unit area also increased by 51 times, reaching $0.49\ \text{Jm}^{-2}$.

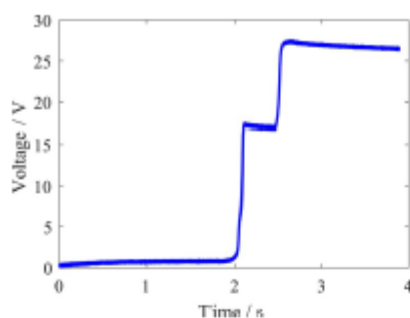


Figure 20. Charging a 47 μF capacitor with a device based on preloaded piezoelectrics. A storage voltage of 27.5 V was reached, corresponding to 17.7 mJ of electrical energy.

The emergency light output was tested with the new device. To do so, it was connected to the white LED presented previously through the power management circuit and a series resistor of 1.2 k Ω . The output voltage of the circuit was regulated to 3 V, with the nominal threshold voltage of the LED being 2.5 V. As a result, 10.6 seconds of light at emergency levels were generated per activation, as depicted in Figure 21 a. A photograph of the light beam during use is shown in in Figure 21 b.

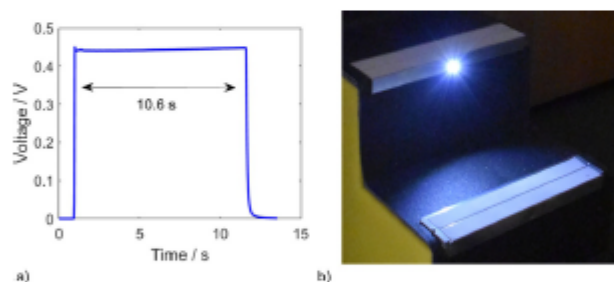


Figure 21. Light output with an enhanced stair nosing; a) voltage on the series resistor of the LED after one activation of the energy-harvesting stair nosing. The square pulse corresponds to 10.6 s of current and thus light output; b) photograph of the light beam as observed in a dark environment.

As the current intensity is the same as that observed for the demonstrator based on formed piezoelectrics, it is safe to say that we observed an increase of 12 times in lighting duration, up from 0.9 s recorded previously.

Work has also been conducted on a multistep system capable of tracking the user and lighting the necessary treads in front of them. Details on this system will be revealed at a later stage.

Discussion

The demonstrators and results presented here prove the viability of energy-harvesting stair treads as a solution to power

emergency lighting. To achieve this, it was necessary to improve the power output and energy density of the existing piezoelectrics by forming or preloading. A design of experiments process was conducted at each stage to determine the best conditions for the performance of the active elements. Each of the two kinds of stair nosing prototypes is the product of an iterative design process aimed at increasing the energy output while reducing complexity and cost.

The final device design, as presented in Figure 19, is composed of parts that can be manufactured by extrusion, nearly identical to the ubiquitous aluminum stair nosings. Therefore, adapting the devices to the width of a given set of stairs is as easy as cutting to size. Internal electrical interconnections are scalable as well, the only varying parameters with size being the number of piezoelectric elements and the assembly time.

Further optimization steps are possible to enhance the latter. Indeed, the 56 piezoelectrics used have been integrated individually into the assembly. To decrease this number, longer shapes could be fabricated for our particular use.

The piezoelectric elements used in the present work have an affordable cost that can be further reduced through the economy of scale. They are approximately 30 times cheaper than the state-of-the-art piezoelectric ceramics used for actuation in precision applications. In their unchanged flat disc shape, the piezoelectric elements used in the present work show a conversion efficiency of a few percent. State-of-the-art ceramics are expected to have efficiencies of up to 14%, based on their coupling factors, but are penalized by the high cost and some degree of fragility. The optimization methods used in the present work allowed the efficiency of our piezoelectrics to be increased without having the negative impact of increased cost. It is estimated that forming alone can increase efficiency by up to 11%, thus reducing the gap with state of the art materials.

As mentioned previously, the energy-harvesting modules are connected to a power-management circuit that includes a rectifier and a voltage regulator. As in every case the active energy-harvesting layer will be surrounded with an underlay for thickness matching, the power-management circuit can be conveniently housed inside the latter.

It is worth mentioning here that the energy our devices recover from steps is available for use immediately. As they do not rely on inertial phenomena for temporary energy storage, the electrical energy builds up on the storage capacitor simultaneously with the user's steps on the tread.

Also, any force applied to our active nosings will result in energy generation. This means that the present devices cater for a large number of users. There are however good reasons to have a threshold force required to obtain light output. The power management circuit consumes a part of the charge to become operational, and the threshold force required to achieve this must be measured and added to the operational parameters of the devices. As it stands, an aver-

age user generates enough energy to trigger an LED with ease, which indicates that the threshold force is rather low.

As compared to existing electromagnetic energy-harvesting tiles, the devices developed in the present work are much thinner: 1.35 cm total thickness, as opposed to 7–10 cm for devices available on the market. Although not verified by the authors, the efficiency is expected to be higher for the latter, given the use of electromagnetic conversion.

An advantage of the demonstrations developed here is that they do not use mechanical aids to help the piezoelectric components return to the initial position after step pressure is released. This is performed through boundary condition control, which simplifies the device design, thereby reducing the number of parts and failure sources.

It is worth noting that the devices are to be subjected to fatigue testing. The flat piezoelectrics used initially exhibit excellent fatigue resistance, as presented previously. Similar tests must be performed on the latest devices to monitor the behavior of preloaded piezoelectrics and validate them for a large number of cycles. Validation for a small number of cycles has been performed though, with no detectable change in performance over 500 activations.

Another discussion point is regarding the units and quantities used in the present work. Energy is preferred to power because user's steps are discrete events, as is apparent for the energy-harvesting devices. Indeed, there is no predefined step frequency at which a harvester will be actuated, because local foot traffic can vary in a large interval, as shown in the busy corridor study. This motivates the authors to analyze individual events and the potential uses of the energy generated per event. In case the reader would like to estimate the power production for comparison purposes, it is enough to picture an environment and multiply the energy generated per step by the frequency of steps. For example, on a staircase fitted with the latest devices a user will generate 17.7 mJ per step. If they walk at a pace of one step per second, the resulting power will be 17.7 mW.

Conclusions

The present article describes the research journey towards the fabrication of stair devices capable of harvesting energy from steps to power emergency lighting. The first demonstrator was a 50 × 50 cm² energy-harvesting tile, capable of generating up to 2.4 mJ of electrical energy per step when fitted with a rigid top. It incorporates commercially available circular piezoelectric elements. These show excellent fatigue resistance, reaching 10 million compression cycles without decay in performance. It was observed that forming the circular piezoelectrics under controlled conditions improved the energy output by 5.7 times.

A new device was built to capitalize on this. It is a 40 cm × 6 cm rectangular harvester, to be placed under a stair nosing. The device was fitted into a demonstration staircase with two steps and an additional riser with an embedded LED. The harvested energy was fed into a custom-made power management circuit that produces a regulated voltage for the

LED. The harvester generated 0.9 s of light at emergency levels upon activation.

Further optimization was performed on the piezoelectric elements by cutting out the active part and subjecting the resulting shapes to lateral loading. This increased the output energy 10.3 times compared to the initial circular elements. As the surface area of the new shapes is 3.14 times smaller, this translates into an increase of energy density per unit area by a factor of 32.

An additional new device was built using this finding. It was composed of an active layer containing preloaded piezoelectric elements, activated by a commercially available stair nosing placed on top. An LED was embedded in the middle of the nosing riser to light the surface below. The footprint of the device was 40 cm × 9 cm, for a total thickness of 13.5 mm, with 8.5 mm for the active layer. This device generated 10.6 s of light per actuation under the same conditions as the previous prototype, bringing a factor of 12 increase in light output.

Future developments for the present technology include the optimization for quicker assembly, fatigue testing, and live deployment.

Experimental Section

Throughout the present work care was taken to measure the piezoelectric signals or voltage on the capacitors being charged using high-impedance probes. This is necessary because of the high output impedance of the piezoelectric elements or assemblies. To minimize the impact on the measurements, 10 MΩ probes were used in all experiments.

A buffer circuit was also tested for lossless measurements. Although the circuit has a very high input impedance, it does not allow high input voltage, and thus was not used for the measurements presented here. This is a suitable tool for observing the pyroelectric effect, which is outside the scope of the present work. Fatigue testing was performed in a room with controlled ambient temperature dedicated to mechanical tests. The piezoelectric output signal was recorded using a Pico series oscilloscope, allowing waveforms to be stored for a large number of cycles. In the test procedure, the piezoelectric membrane is initially actuated to a deflection of 0.5 mm. Cyclic deflection with an amplitude of 0.5 mm was then performed around this point, for a peak-to-peak center deflection of 1 mm. The data sampling rate was adjusted to 400 samples per second: this is the minimum required for a correct reading of the peak-to-peak voltage amplitude, to decrease the amount of recorded data points and increase the number of recorded cycles.

Measurements of force during gait were performed using an force plate (AMTI). The user under observation was given enough space to reach their normal walking speed before stepping onto the force plate. They were also allowed to take a few additional steps afterwards, before slowing to a stop. A series of several tens of measurements were performed for the left and right foot, respectively, with representative samples shown in Figure 1.

People counting in a busy corridor was performed using an Axis M30 network connected camera, and the data were stored on a personal computer. The camera was installed in the ceiling on a highly used, straight portion of a university corridor.

Acknowledgements

This research was supported by Innovate UK through the Knowledge Transfer Partnerships programme (KTP nr. 009704).

Conflict of interest

The authors declare no conflict of interest.

Keywords: building integration • light-emitting diodes • energy harvesting • piezoelectrics • smart electronics

- [1] T. Starner, *IBM Syst. J.* **1996**, *35*, 618–629.
- [2] P. Niu, P. Chapman, R. Riemer, X. Zhang, in *Power Electronics Specialists Conference, 2004. PESC 04. 2004 IEEE 35th Annual*, Vol. 3, IEEE, **2004**, pp. 2100–2106.
- [3] N. S. Shenck, J. A. Paradiso, *IEEE Micro* **2001**, *21*, 30–42.
- [4] C. A. Howells, *Energy Convers. Manage.* **2009**, *50*, 1847–1850.

- [5] D. Alghisi, S. Dalola, M. Ferrari, V. Ferrari, *Sens. Actuators A* **2015**, *233*, 569–581.
- [6] L. Xie, M. Cai, *Appl. Phys. Lett.* **2014**, *105*, 143901.
- [7] P. L. Green, E. Papatheou, N. D. Sims, *J. Intell. Mater. Syst. Struct.* **2013**, *24*, 1494–1505.
- [8] J. Cao, W. Wang, S. Zhou, D. J. Inman, J. Lin, *Appl. Phys. Lett.* **2015**, *107*, 143904.
- [9] N. Sharpes, D. Vučković, S. Priya, *Energy Harvesting Syst.* **2016**, *3*, 43–60.
- [10] E. Bischur, N. Schwesinger, *Adv. Mater. Res.* **2012**, *433–440*, 5848–5853.
- [11] L. Kembhall-Cook (Pavegen Systems Ltd.), U.S. Pat. No. 8736088 B2, **2014**.
- [12] D. Puspitarini, A. Suzianfi, H. Al Rasyid, *Procedia Soc. Behav. Sci.* **2016**, *216*, 938–947.
- [13] R. Peace, B. Hall, I. Patsavellas, (Altro Ltd.), EP 3121950 A1, **2017**.
- [14] C. Fowle, *SATRA Bulletin*, **2015**, March, 32–36.
- [15] Approved document K, 2013 edition: Protection from falling, collision and impact, The Building Regulations 2010, UK, **2013**.

Manuscript received: September 9, 2017
Revised manuscript received: October 4, 2017
Version of record online: March 6, 2018

(12) INTERNATIONAL APPLICATION PUBLISHED UNDER THE PATENT COOPERATION TREATY (PCT)

(19) World Intellectual Property
Organization
International Bureau

(43) International Publication Date
14 May 2020 (14.05.2020)



(10) International Publication Number
WO 2020/095064 A1

- (51) **International Patent Classification:**
H01L 41/04 (2006.01) H01L 41/193 (2006.01)
H01L 41/113 (2006.01) H02N2/18 (2006.01)
- (21) **International Application Number:**
PCT/GB20 19/053 173
- (22) **International Filing Date:**
08 November 2019 (08.11.2019)
- (25) **Filing Language:** English
- (26) **Publication Language:** English
- (30) **Priority Data:**
1818294.9 09 November 2018 (09.11.2018) GB
- (71) **Applicant: UNIVERSITY OF HERTFORDSHIRE HIGHER EDUCATION CORPORATION** [GB/GB];
College Lane, Hatfield Hertfordshire AL10 9AB (GB).
- (72) **Inventors: HERFATMANESH, Mohammad Reza;** *c/o* University of Hertfordshire Higher Education Corporation, College Lane, Hatfield Hertfordshire AL10 9AB (GB). **COUNSELL, Nathan;** *c/o* University of Hertfordshire Higher Education Corporation, College Lane, Hatfield Hertfordshire AL10 9AB (GB).
- (74) **Agent: CSY HERTS;** Helios Court, 1 Bishop Square, Hatfield Hertfordshire AL10 9NE (GB).

- (81) **Designated States** (unless otherwise indicated, for every kind of national protection available): AE, AG, AL, AM, AO, AT, AU, AZ, BA, BB, BG, BH, BN, BR, BW, BY, BZ, CA, CH, CL, CN, CO, CR, CU, CZ, DE, DJ, DK, DM, DO, DZ, EC, EE, EG, ES, FI, GB, GD, GE, GH, GM, GT, HN, HR, HU, ID, IL, IN, IR, IS, JO, JP, KE, KG, KH, KN, KP, KR, KW, KZ, LA, LC, LK, LR, LS, LU, LY, MA, MD, ME, MG, MK, MN, MW, MX, MY, MZ, NA, NG, NI, NO, NZ, OM, PA, PE, PG, PH, PL, PT, QA, RO, RS, RU, RW, SA, SC, SD, SE, SG, SK, SL, SM, ST, SV, SY, TH, TJ, TM, TN, TR, TT, TZ, UA, UG, US, UZ, VC, VN, ZA, ZM, ZW.
- (84) **Designated States** (unless otherwise indicated, for every kind of regional protection available): ARIPO (BW, GH, GM, KE, LR, LS, MW, MZ, NA, RW, SD, SL, ST, SZ, TZ, UG, ZM, ZW), Eurasian (AM, AZ, BY, KG, KZ, RU, TJ, TM), European (AL, AT, BE, BG, CH, CY, CZ, DE, DK, EE, ES, FI, FR, GB, GR, HR, HU, IE, IS, IT, LT, LU, LV, MC, MK, MT, NL, NO, PL, PT, RO, RS, SE, SI, SK, SM, TR), OAPI (BF, BJ, CF, CG, CI, CM, GA, GN, GQ, GW, KM, ML, MR, NE, SN, TD, TG).

Published:
— with international search report (Art. 21(3))

(54) **Title: IMPROVEMENTS IN OR RELATING TO ENERGY GENERATION IN A PIEZOELECTRIC SWITCH**

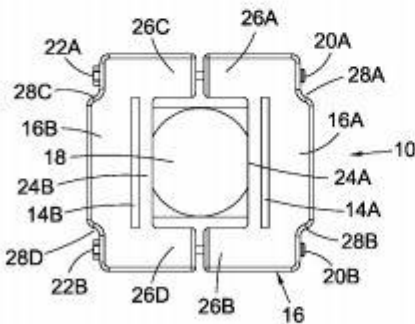


Fig. 1

(57) **Abstract:** The present invention provides an energy harvesting system that removes the need for batteries for sensing and actuating purposes through the use of energy harvesting materials such as piezoelectric transducers. The present invention particularly provides clamping and actuation mechanisms for energy harvesting applications including energy harvesting switches, more particularly energy harvesting wireless switches. The present invention is designed to produce sufficient instantaneous energy to power low-power circuits such as radio transmitters, allowing for seamless integration with existing smart devices. In addition, the system benefits from battery less operation, eliminating the need for regular battery maintenance and replacement as well as end of life recycling. An energy harvesting system is provided comprising: a) an energy harvesting material which generates energy when deformed or moved from a first position to a second position; and b) an energy generator support which has first and second mounting supports between which the energy harvesting material is mounted in the first position wherein the first and second mounting supports each have an internal surface and the internal surfaces are each provided with a layer of a resilient material and a layer of a non-resilient material wherein the layer of the non-resilient material engages the energy harvesting material.

WO 2020/095064 A1